Synthetic lethality driven by *N*-Myristoyltransferase inhibition in MYC deregulated cancers.

Gregor Alexander Lueg

Imperial College London

and

The Francis Crick Institute

PhD Supervisor:

Prof Ed W. Tate, Dr Dinis P. Calado, Prof Alan Armstrong

A thesis submitted for the degree of

Doctor of Philosophy

Imperial College London

January 2020

Declaration of originality

I, Gregor Alexander Lueg, confirm that the work presented in this thesis is my own. Where information has been derived from other sources, I confirm that this has been indicated in the thesis.

Declaration of copyright

Abstract

N-myristoylation is the irreversible attachment of myristate (a C_{14} fatty acid) to the N-terminal glycine of a given substrate. The enzyme responsible for this reaction is *N*-myristoyl transferase (NMT), a protein shown to be essential for many organisms, ranging from eukaryotes, plants, fungi, to infectious parasites. Initially, the NMTs of the fungi and infectious parasites sparked the interest of researchers in drug discovery to target these pathogens. However, the question remained whether one could target NMT in cancer. While early studies suggested potential upregulation of NMT1 in some early stage cancers, it remained unclear which cancer types to target and for which mechanistical reason.

In this study, data from pharmacogenomics screens across hundreds of cancer cell lines, treated with three different NMT inhibitors, were analysed. Haematological malignancies were amongst the most responsive cell lines; however, also cancers originating from other tissues were sensitive, indicating a more complicated picture. Detailed phenotypical and omics-based analysis of the effects of NMT inhibition in an example cancer cell line from the haematological malignancies, and an unbiased bioinformatics approach across the pharmacogenomics data hinted at the same protooncogene: MYC. Two different isogenic system with inducible MYC confirmed that MYC deregulated cells are highly dependent on myristoylation.

This newly uncovered synthetic lethality has potentially wide implications as MYC, a key transcription factor, is commonly deregulated in cancer and involved in most of the hallmarks of cancer. Targeting MYC or its downstream program attracted wide attention of the field; however, to date no drug has been approved to specifically target either. Novel approaches to target MYC, in the context of cancer, are urgently needed, and this study identified a potential new one.

Acknowledgement

'Transformation is a process, and as life happens there are tons of ups and downs. It's a journey of discovery – there are moments on mountaintops and moments in deep valleys of despair' – Rick Warren

In the end, the journey leading to this thesis was a transformation with its ups and downs, from a (medicinal) chemist to a chemical and cancer biologist. When I started, I had not touched any tissue culture, had not the slightest clue about most omics techniques (outside of reading about them in papers), had never heard about flow cytometry, lacked knowledge about immunology, and my background was basically (medicinal) chemistry.

Dinis and Ed took me under their supervision, trusting that I will learn all of these unknowns during the journey of this PhD. I need to thank both of them very much for this trust, the guidance and support over the years, the scientific discussions in person or in seemingly endless emails, and that they let me pursue my ideas.

I was in the very fortunate situation to be 'shared' between two labs, thus, I had the opportunity to meet a lot of great people and scientists over the years of this PhD. They helped in teaching me new techniques, bounce off ideas, explain me things which were trivial to them (not to me…), and collaborate on the science. A big thanks to current and former members of the Tate group and the Immunity and Cancer lab! In alphabetical order, I would like to thank especially the following people because they played a special role in this journey, be it as friends, collaborators, teachers, proof readers of this thesis, and/or great discussion partners for science or everything else (over a beer or two): Amparo, Ana, Andrea, Andy, Anja, Julia, Magda, Marc, Monica, Nik, Rita, Roman, Scott, Tom, Tony and Wouter.

I am also particularly grateful to all the core facilities and the technical support I got over the years in the Crick. Specifically, I would like to thank the Advanced Sequencing facility, the FACS, the Bioinformatics core, the Proteomics and the High-Throughput Screening labs, Cell Services and the BRF. I would like to thank the following people for their support, knowledge, patience with all my questions and enquiries, and their pivotal roles in some of the work: Aaron, Andrew, Bobbi, Claire, Greg, Hefin, Joana, Julie, Mike, Miriam, Ok-Ryul, Probir and Sukhveer. Thanks to

the funders of the Crick Institute, and the institute itself, which made all of this possible. Additionally, a special thanks goes to my thesis committee, Alan, Peter (Parker) and Peter (Van Loo), who monitored my progress over the years and were very helpful in various thesis committees.

Lastly, I would like to thank family and friends who over the years supported and distracted me in some of the lows, one inevitably experiences in a PhD–be it in London, or when I travelled back to France and Germany (sometimes on a sailing boat). Thanks to my parents for being there for me with all the trust, support and love I got from you. And thanks to the following people: Chloe, Eike, Friedemann, Felix, Jonas, Kai, Nerea, Phil, Stephan, Sebastian and Yves. All of you made a difference in this journey, and I am truly grateful for this!

Table of Contents

Table of figures

List of tables

Abbreviations

ABC DLBCL	Activated B cell like DLBCL
ABHD	α/β-hydrolase domain
AMBIC	Ammonium bicarbonate
AML	Acute myeloid leukaemia
AR	Androgen receptor
AUC	Area-under-curve
bHLHZip	Basic helix-loop-helix leucine zipper
BID	BH3 interacting-domain death antagonist
BL	Burkitt's lymphoma
CCLE	Cancer Cell Line Encyclopaedia
CDK	Cyclin-dependent kinase
CFE	Cancer functional event
CI	Combination index
CML	Chronic myeloid leukaemia
CN	Copy number
CoA	Coenzyme A
COSMIC	Catalogue of Somatic Mutations in Cancer
CoTMyr	Co-translational myristoylation
DBA	Dibenzylideneacetone
DepMap	Cancer dependency map
DHHC	Aspartate-histidine-histidine-cysteine motif
DLBCL	Diffuse large B cell lymphoma
DMSO	Dimethyl sulfoxide
DTT	Dithiothreitol
eBL	Endemic Burkitt's lymphoma
ER	Estrogen receptor
ESC	Embryonic stem cells
FACS	Fluorescence-activated cell sorting
FDA	Food and Drug Administration
FTase	Farnesyl transferase
G2A	Glycine to alanine mutations

GC	Germinal centre
GCB DLBCL	Germinal centre B cell like DLBCL
GDP	Guanosine diphosphate
GDSC	Genomics of Drug Sensitivity in Cancer
GNAT	GCN5-related N-acetyl transferases
GOF	Gain-of-function
GPI	Glycosylphosphatidylinositol
GSEA	Gene Set Enrichment Analysis
GTP	Guanosine triphosphate
Hhat	Hedgehog acyltransferase
HSC	Haemopoietic stem cell
IAA	Iodoacetamide
IpA	Intronic polyadenylation
iPSC	Induced pluripotent stem cell
K_D	Equilibrium dissociation constants
LOF	Loss-of-function
MetAP	Methionine amino peptidases
MFI	Median fluorescence intensity
MM	Multiple myeloma
MOFA	Multi-omics factor analysis
MOMP	Mitochondrial outer membrane permeabilization
MRC	Medical Research Council
MSigDB	Molecular Signature Data Base
MXD	MAX dimerisation proteins
NaPyr	Sodium pyruvate
NB	Neuroblastoma
ncRNAs	Non-coding RNAs
NES	Normalised enrichment score
NMD	Nonsense-mediated decay
NMT	*N*-Myristoyl transferase
NSCLC	Non-small-cell lung cancer
OV	Ovarian serous carcinoma
PAS	Poly adenylation sites
PAT	Palmitoyl-acyltransferase

PDX	Patient derived xenografts
Pen/Strep	Penicillin/streptomycin
PFA	Paraformaldehyde
PMN	Proximal MYC network
PPI	Protein-protein interactions
PPT	Palmitoyl-protein thioesterase
PRC2	Polycomb repressive complex 2
PTMyr	Post-translational myristoylation
RACS	Recurrently abnormal copy number segment
RMA	Robust multiarray average
RNAi	RNA interference
rNMT1	Recombinant NMT1
RT	Room temperature
SAR	Structure activity relationship
sBL	Sporadic Burkitt's lymphoma
scRNA	Single-cell RNAseq
SDS	Sodium dodecyl sulphate
SFK	SRC family kinases
sgRNA	Short guide RNA
snRNA	Small nuclear RNA
SrtA	Sortase A
STR	Short tandem repeat
tBID	Truncated BID
TBTA	Tris(benzyltriazolylmethyl)amine
TCA	Tricarboxylic acid cycle
TCEP	Tris(2-carboxyethyl)phosphine
TCGA	The Cancer Genome Atlas
TCR	T cell receptor
TEAB	Tetraethylammonium bromide
TFA	Trifluoroacetic acid
UPS	Ubiquitin-proteasome system
YnMyr	Alkyne myristate

Chapter 1. Introduction

1.1 Myristoylation

This subchapter will introduce myristoylation in the context of other lipid modifications of proteins (in this thesis myristoylation refers to *N*-myristoylation if not otherwise specified); the enzyme responsible for myristoylation, *N*-myristoyl transferase (NMT) and the two different types of myristoylation: co-translational (CoTMyr) and post-translational (PTMyr). Moreover, it will briefly introduce the chemical biology tools which allowed to identify substrates at unprecedented rates and explore the biology of myristoylation. Lastly, it will give an overview into the different NMT substrates, their biological significance and what is known about the impact of the attached myristate (a C_{14}-fatty acid).

1.1.1 Lipidations

Lipids are the key component of cellular membranes: the barriers between the cellular content and the outside world. These natural barriers necessitate mechanisms to allow for sensing outside signals (e.g., growth factors or nutrients), membrane trafficking and cell-to-cell communication in multicellular organisms. Proteins can either have specific domains tethering them into the membrane; or lipid modifications on the proteins control for membrane-protein interactions, but also protein-protein interactions. These modifications typically occur on nucleophilic amino acids, such as cysteine, serine or lysine, or the N-terminal amino group. Some modifications, such as cholesterol esterification and GPI (glycosylphosphatidylinositol) anchoring occur on the C-termini of proteins; others, such as glycine myristoylation, occurs on the N-terminus of proteins. Several different enzymes catalyse the attachment of those lipids to the respective proteins (Jiang et al., 2018; Lanyon-Hogg et al., 2017) (see Figure 1-1 for the different lipidations). These enzyme caught the attention as potential drug targets in cancer and other diseases, due to the broad biological role of the different lipidations (Jiang et al., 2018).

A particular interest into prenylation, more specifically farnesylation, was sparked due to the fact that all the isoforms of the oncogene RAS are farnesylated and this

lipidation is required for the transformative capacity of the oncogene (Berndt et al., 2011; Palsuledesai and Distefano, 2015). More than 30% of all cancers show activating mutations in one of the RAS isoforms (Resh, 2012). Thus, targeting farnesylation was considered a possible way to shut down oncogenic RAS signalling and highly specific inhibitors, such as Tipifarnib, for farnesyl transferases (FTase) were developed (End et al., 2001). While preclinical data in cancer cell lines and mouse models looked promising, the following evaluation of different FTase inhibitors in 75 clinical trials showed no or only a very modest clinical benefit, and mostly independent of RAS mutation status (Berndt et al., 2011). The RAS isoforms are farnesylated, but upon inhibition of this process, they can be geranylgeranylated, still leading to their membrane anchoring and activity (Wang and Casey, 2016). This farnesylation to geranylgenerylation switch was recently shown via chemical proteomics and the use of two different metabolic tags (Storck et al., 2019).

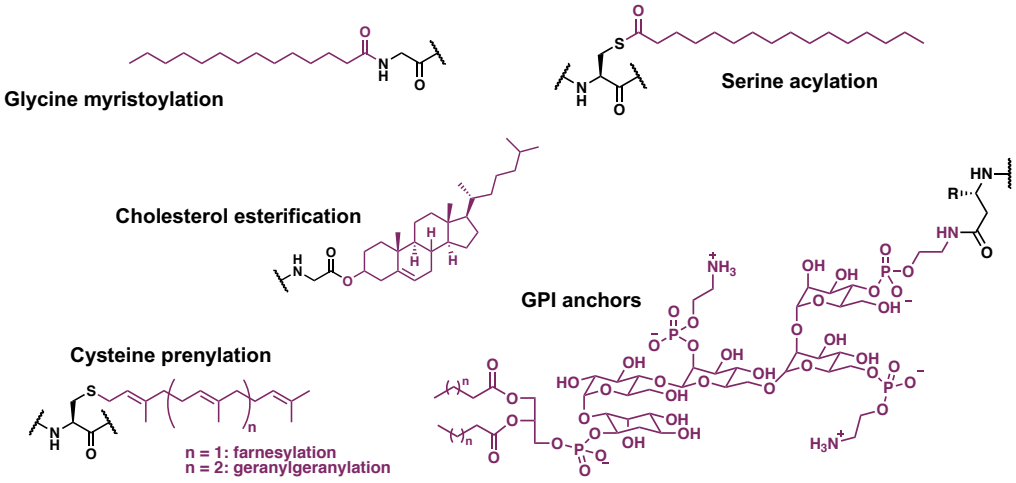

Figure 1-1: Lipidation on proteins.

Structures of different lipid modifications on proteins.

Protein palmitoylation is the reversible addition of a C_{16} fatty acid (palmitoyl) to cysteine residues, and is mediated by the palmitoyl-acyltransferases (PAT), consisting of 23 members. The PATs have a conserved aspartate-histidine-histidine-cysteine (DHHC) motif, located in a cysteine-rich, zinc finger-like domain, thus are named zDHHCs (Tabaczar et al., 2017). The enzymes responsible for depalmitoylation are palmitoyl-protein thioesterases (PPT) that contain α/β-hydrolase domains, hence are called ABHD proteins (Globa and Bamji, 2017). A number of synaptic proteins have been shown to be palmitoylated dynamically in neurons in response to synaptic activity. Also, palmitoylation has been associated

with schizophrenia, Huntington's and Alzheimer's disease, leading to a research focus of the palmitoylation field on neurons and other brain cells (Globa and Bamji, 2017). Additionally, mutations in different PATs are observed in cancer, and thought to alter the ability of PATs to function as oncogenes or tumour suppressors, leading to investigations of the role of palmitoylation in cancer and its potential druggability (Resh, 2017). To date, over 2500 proteins have been described to be palmitoylated in humans (Blanc et al., 2015). The substrate specificity of the PATs and PPTs remains controversial and difficult to assess due to redundancies between different PATs and PPTs (Tabaczar et al., 2017). A limiting factor to identify the exact role of different PATs is the lack of specific inhibitors for a given zDHHC. The commonly used lipid-based inhibitors such as 2-bromopalmitate are highly unspecific, and interfere with proteases, lipid transport and lipid metabolism (Chavda et al., 2014; Davda et al., 2013; Lanyon-Hogg et al., 2017). The exception is the Hedgehog acyltransferase (Hhat) which is essential for hedgehog signalling. Specific inhibitors for Hhat could be identified (Rodgers et al., 2016).

Lysine acylation has been proposed to occur for interleukin 1α (Stevenson et al., 1993). As a potential deacylating enzyme SIRT2 has been put forward as an 'eraser' of this lysine-myristoylation (Liu et al., 2015); however, little is known about potential enzymes driving lysine myristoylation, and it remains to date poorly defined and the data is suggestive (Lanyon-Hogg et al., 2017).

To conclude, the different lipid modifications are highly relevant for cellular function and the enzymes catalysing these lipidations have already been in extensive focus for drug discovery and development, particularly for prenylation. The focus of this work is on the *N*-terminal glycine myristoylation and the application of inhibitors in cancer, which will be introduced in the following sections.

1.1.2 Myristoylation, a tale from two types of myristoylation and two enzymes

Myristoylation is the typically irreversible attachment of myristate to the *N*-terminal glycine of the respective substrates via a thioester bond. Myristoylation usually occurs in a co-translational manner: methionine aminopeptidases (MetAP) expose, after cleavage of the initiator methionine, the N-terminal glycine, which can

be subsequently irreversibly myristoylated (see Figure 1-2 A) (Jiang et al., 2018; Wright et al., 2010).

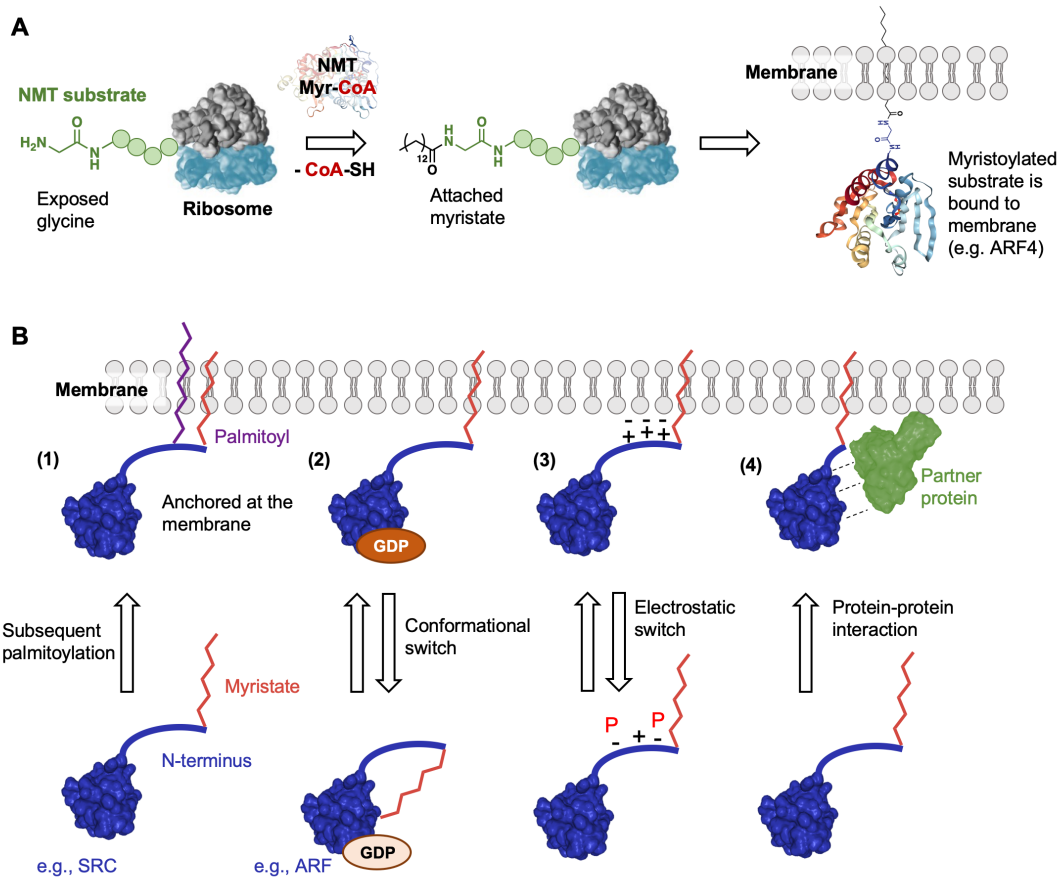

Figure 1-2: Co-translational myristoylation and dynamic regulation of membrane association.

[A] During peptide elongation at the ribosome, the N-terminal glycine is exposed after cleavage of the initiator methionine. NMT catalyses the attachment of myristate at the glycine, using the cofactor myristate-coenzyme A (CoA). After further protein maturation, the myristate mediates e.g. membrane tethering of e.g. the ARF4, which then can activate signalling pathways (the structures of ARF4 and NMT1 were generated with NGL viewer (Rose et al., 2018) using the deposited structures of NMT1 – PDB ID: 3IU1 and ARF4 – PDB ID: 1Z6X). **[B]** (1) For SRC the irreversible membrane anchoring is achieved through a subsequent palmitoylation, following the initial CoTMyr (Koegl et al., 1994). (2) A conformational switch was identified in the members of the ARF family. Upon binding of GDP, the myristate is 'hidden' in a lipophilic pocket. If GTP binds, the myristate is exposed and can mediate membrane binding (Goldberg, 1998). (3) The electrostatic switch is based on additional positive charges from respective amino acid residues, facilitating membrane anchoring. These positive charges can be neutralised by e.g. phosphorylation events, causing displacement from the membrane (Resh, 2006). (4) Protein-protein interactions with another membrane bound partner protein can promote the membrane binding (Resh, 1999).

While eukaryotic cells lack the capacity, i.e. enzymes to hydrolyse the thioester bond between glycine and myristate, thus reverse myristoylation, it has been shown that bacterial enzymes can actually hydrolyse the bond and remove the myristate from their host's NMT substrates. This is observed for e.g., the pathogen *Shigella flexneri* (Burnaevskiy et al., 2013; Burnaevskiy et al., 2015).

Myristoylation is involved, amongst other things, in trafficking of proteins to and from the membranes and this process is dynamically regulated (see Figure 1-2 B) (Resh, 1999; Resh, 2006; Wright et al., 2010). For example several members of the SFK family are additionally palmitoylated at their N-termini to irreversibly anchor them to the membrane (Koegl et al., 1994). There are also several dynamic switches, such as for the ARF family for which upon binding of guanosine diphosphate (GDP) or guanosine triphosphate (GTP), the N-terminus with the myristate is exposed or not. Another dynamic switch is based on electrostatic interactions, where the N-terminus of the given substrate is negatively charged, thus facilitates membrane binding. These charges can be controlled by phosphorylation, or binding of other proteins (Resh, 2006). Additionally, interactions with other membrane bound proteins can reinforce the interaction of the NMT substrate with the membrane (Resh, 1999).

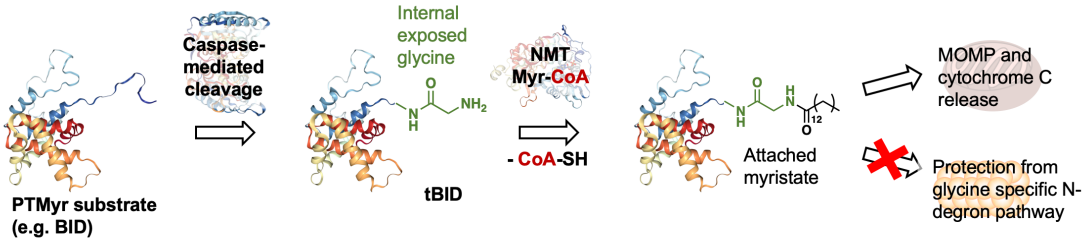

Figure 1-3: Post-translational myristoylation.

Internal glycines can be exposed through caspase-mediated endoproteolysis, as shown for BID here. These internal glycines can be subsequently myristoylated in a post-translational manner, and can cause for example for BID a change of localisation to the mitochondrial membrane, causing MOMP and cytochrome C release (Zha et al., 2000), or in general protect the PTMyr substrate from subsequent degradation by the UPS (Timms et al., 2019) (the structures of ARF4 and NMT1 were generated with NGL viewer (Rose et al., 2018) using the deposited structures of NMT1 – PDB ID: 3IU1, caspase 3 – PDB ID: 1QX3 and BID – PDB ID: 2BID).

While myristoylation occurs usually in a co-translational manner, post-translational myristoylation is also observed, specifically in the case of apoptosis and the involved caspase-mediated endoproteolysis (Martin et al., 2011; Thinon et al., 2014). Other caspase-mediated cell deaths, such as pyroptosis are known (Shi et al., 2017), but the extent of PTMyr has not yet been defined in these cases. Caspases cleave

proteins, exposing internal glycines, which can be subsequently myristoylated (see Figure 1-3) (Martin et al., 2011; Thinon et al., 2014). One of the first proteins for which this process was described is the apoptotic protein BID. Upon caspase-mediated cleavage, the truncated version of BID (tBID) is myristoylated, directed to the mitochondria, and being involved in cytochrome C release (Zha et al., 2000). This subsequently leads to further caspase activation and mitochondrial outer membrane permeabilization (MOMP) (Green, 2005). Interesting in this context is the recently described glycine specific N-degron pathway: of the ~1800 known caspase cleavage sites, a third would result in exposure of an N-terminal glycine, a potent degron. However, myristoylation is a regulator of this degron pathway, potentially implying that PTMyr protects its substrates from further degradation by the ubiquitin-proteasome system (UPS) (Timms et al., 2019).

The enzyme responsible for myristoylation is *N*-myristoyl transferase (NMT), a member of the GCN5-related N-acetyl transferases (GNAT) (Dyda et al., 2000). NMTs exist across a large number of species (Boutin, 1997), indicating that this lipidation is a conserved protein modification across evolution. Furthermore, myristoylation has been identified as essential in *Candida albicans* (Weinberg et al., 1995), *Plasmodium falciparum* (Gunaratne et al., 2000), mice (Yang et al., 2005), kinetoplastid parasites such as *Leishmania* and *Trypanosoma brucei* (Price et al., 2003), and for optimal proliferation of human (cancer) cells (Meyers et al., 2017; Reddy et al., 2017; Wang et al., 2015a). A second paralog has been identified in humans (Giang and Cravatt, 1998). The two isoforms, hsNMT1 and hsNMT2, share 77% sequence similarity (Thinon, 2013), and do not have altered substrate specificity in peptide-based assays (Castrec et al., 2018; Martinez et al., 2008). A key difference is the N-terminal ribosomal binding domain present on NMT1, suggesting that it might be responsible for CoTMyr (Glover et al., 1997). This would fit with the observation that NMT1 is essential for optimal proliferation in different human (cancer) cell lines, but not NMT2 (further discussed in subchapter 1.2.3) (Meyers et al., 2017; Reddy et al., 2017; Wang et al., 2015a), raising the question of which biological role hsNMT2 plays.

NMT1 is overall higher expressed than NMT2 across all the tested tissues in humans, potentially underlying the increased relevance of the former isoform. Lower NMT1 expression, compared to other tissues, is observed in endocrine tissues, muscle, male and adipose/soft tissue; NMT2 expression is lower in the muscle and

adipose/soft tissue (see Figure 1-4 A) (Uhlen et al., 2015). The subcellular localisation for both isoforms is cytoplasm and plasma membrane–NMT2 additionally localises at the Golgi (Thul et al., 2017). These data indicate that NMT inhibition (which will be further introduced in subchapter 1.2) would likely affect all tissues (assuming inhibitors with good blood-brain barrier permeability), as the targets are expressed across all of them.

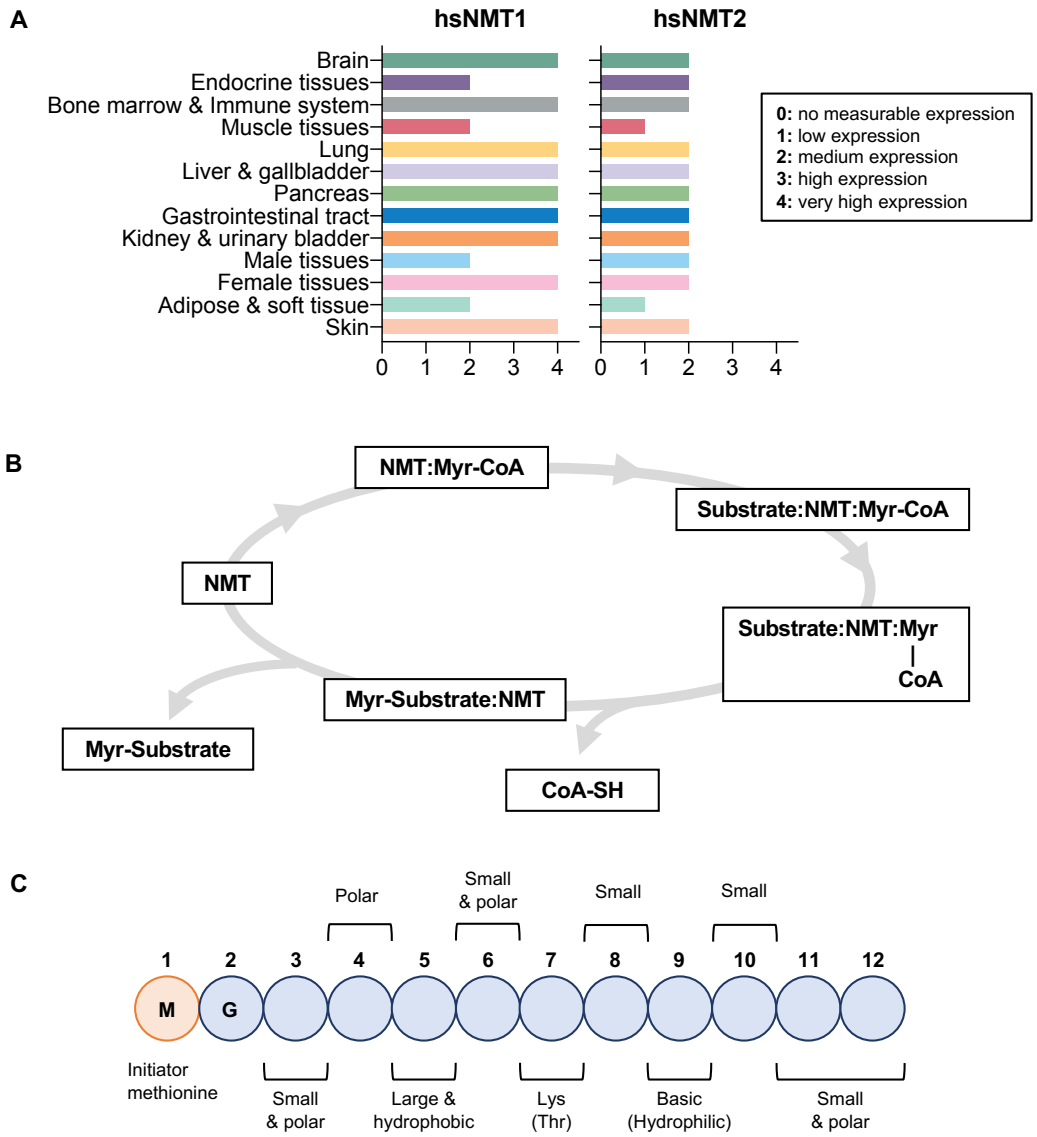

Figure 1-4: Catalytic cycle of myristoylation, preferred peptide sequence and tissue distribution.

[A] Shows the Bi-Bi mechanism of NMT (Adapted from (Rudnick et al., 1991)). **[B]** hsNMT1 peptide sequence preference for substrates. **[C]** Tissue distribution of hsNMT1 and hsNMT2; data extracted from (Uhlen et al., 2015).

The structure of scNMT1, the NMT of *Saccharomces cerevisiae*, has been described (Bhatnagar et al., 1998), and several structures of hsNMT1, bound to myristoyl-CoA or different NMT inhibitors have been deposited into the protein data bank (PDB) (Berman et al., 2000), 18 different structures to date. The catalytic cycle of NMT, firstly identified in scNMT1, follows a Bi-Bi mechanism: two substrates and two products are involved in the enzymatic reaction (Rudnick et al., 1991) (see Figure 1-4 B). Kinetic studies revealed the same Bi-Bi mechanism applies also for hsNMT1 (Rocque et al., 1993).

Bioinformatical analysis of sequence motifs that are preferred by NMT revealed three motif regions: positions 2 to 7 fitting in the peptide pocket; positions 8 to 12 interacting with the surface of NMT at the catalytic pocket; and positions 13 to 18 comprising of a hydrophobic linker (Maurer-Stroh et al., 2002b) (see Figure 1-4 C).

The N-terminal glycine, following the initiator methionine is absolutely essential for myristoylation (Maurer-Stroh et al., 2002b). Glycine to alanine mutations (G2A) are thus typically used to disrupt myristoylation on a given NMT substrate. Based on the preferred sequence motifs, two online tools have been developed to assess the likelihood of a given protein to be myristoylated: ‘Myr predictor’ (Maurer-Stroh et al., 2002a) and ‘Myristoylater’ (Bologna et al., 2004).

Alternative splicing variants of NMT1 are observed in humans and rats, but the exact function of these alternative isoforms remains unknown (McIlhinney et al., 1998). It has been proposed that NMT might be regulated through phosphorylation by some of members of the SRC family kinases (SFK); however, any functional differences between the differentially phosphorylated NMT enzymes have not been shown and only the first 416 residues of NMT1 were expressed in this study (Rajala et al., 2001). To date, there is no clear consensus or strong evidence on what regulates myristoylation (Wright et al., 2010).

1.1.3 Chemical proteomics to explore myristoylation

Initial research into myristoylated proteins was limited: the lipids themselves have poor antigenicity, making the generation of specific antibodies almost impossible. At the time the only alternative left to study myristoylation was the use of radioactive labelled version of the myristate, followed by autoradiography. This work

was laborious, took several weeks, and there was an inherent hazard due to the radioactive materials used. This situation changed with the development of chemical proteomics and metabolic tags (Heal et al., 2011; Storck et al., 2013; Tate, 2008). The Tate laboratory specialises in the development of new chemical tools and chemical proteomics strategies for lipidation, amongst them myristoylation.

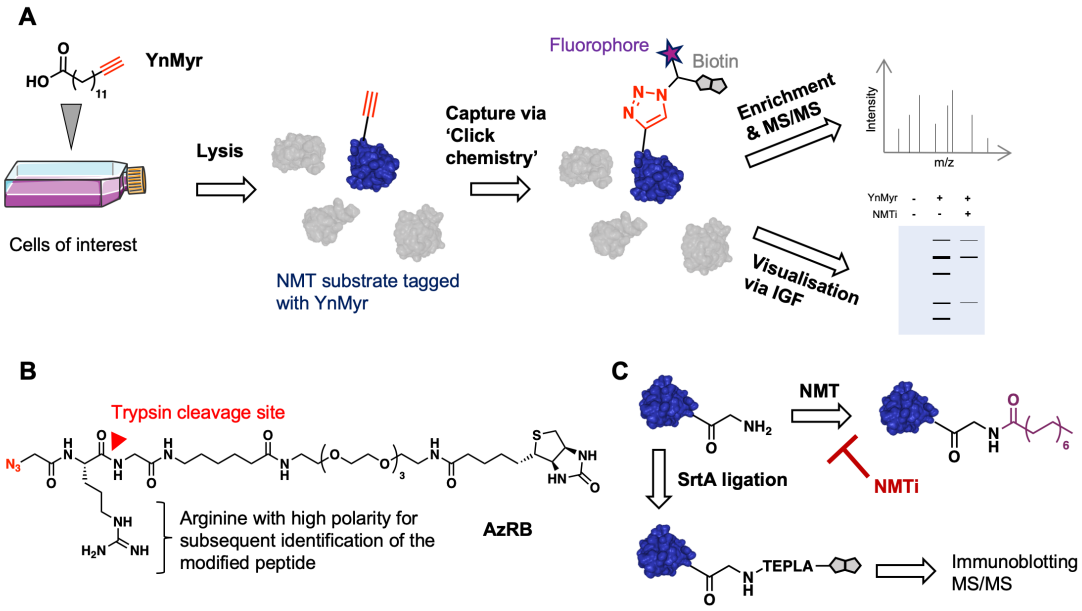

Figure 1-5: Different chemical proteomics approaches to identify NMT substrates and the inhibition thereof.

[A] Chemical proteomics workflow, utilising metabolic tagging with an alkyne modified myristate analogue (YnMyr). Cells are incubated with YnMyr and then lysed, yielding in a mixture of tagged and untagged proteins. The former can be captured via 'click chemistry' and multifunctional capture reagents for subsequent visualisation on gel; or, after enrichment and digest, for identification via MS/MS. **[B]** Structure of AzRB, a capture reagent, specifically designed to have a trypsin digest side (red triangle) after arginine. Arginine is easily ionised in mass spectrometry, hence allows for the identification of the modified peptides. **[C]** Label-free approach to identify NMT substrates that, due to NMT inhibition, have free N-terminal glycines. These can be tagged via a SrtA-mediated enzyme reaction with a small peptide sequence and biotin. For light NMT substrates the mass shift can be visualised via immunoblotting; or the biotin can be used for subsequent enrichment and MS/MS.

These tools and experimental approaches were used to identify NMT substrates in the parasites *Plasmodium falciparum* (Wright et al., 2014) and *Leishmania donovani* (Wright et al., 2015), human (cancer) cells (Thinon et al., 2014), zebrafish (Broncel et al., 2015), and the common cold virus (Mousnier et al., 2018). Crucial for these

workflows is the so-called ‘click chemistry’, which allows for biorthogonal reaction of alkyne and azide groups through copper mediated catalysis (Debets et al., 2010). The experimental workflow, using an alkyne myristate analogue (YnMyr), is shown in Figure 1-5 A. The cells of interest are incubated with YnMyr for a given time and, if desired, with a suitable NMT inhibitor. The cells incorporate YnMyr onto their NMT substrates. After cell lysis, the alkyne handle can be used for the previously mentioned ‘click chemistry’ to capture the proteins of interest with multifunctional capture reagents. These capture reagents can have fluorophores for subsequent visualisation with in-gel fluorescence and/or biotin handles that allow for enrichment on Streptavidin/Neutravidin beads and analysis via mass spectrometry. Importantly, the combination with specific NMT inhibitors (Thinon et al., 2014), or the use of specially designed capture reagents (see Figure 1-5 B for an example) (Broncel et al., 2015) allow for high levels of confidence in the identified NMT substrates. The capture reagents have specifically designed trypsin cleavage sides that are followed by an arginine. After tryptic digest the peptide, tagged with YnMyr and AzRB, is highly polar, thus, can be identified by mass spectrometry (Broncel et al., 2015). Additionally, within the Tate group a label-free approach was developed to observe NMT inhibition on a subset of NMT substrates, using sortase A (SrtA) mediated ligation. In the case of NMT inhibition, only the free N-terminal glycine will be amenable for ligation to a peptide-biotin moiety, which can be visualised via a mass-shift in immunoblotting or be used for enrichment with subsequent mass spectrometry analysis (Goya Grocin et al., 2019) (see Figure 1-5 C). This approach has been extensively used in the (in)validation of different chemical probes for NMT (Kallemeijn et al., 2019). The herein described chemical proteomics approaches are of course not limited to myristoylation and have been modified to study other lipid modifications (Lanyon-Hogg et al., 2017; Rodgers et al., 2016; Storck et al., 2019). To conclude, chemical proteomics revolutionised the identification of NMT substrates and follow dynamics of the substrates across a large number. The next subchapter will discuss what is known about the effect of myristate on different NMT substrates.

1.1.4 Significance of myristoylation on its substrates

As described earlier, myristoylation is considered as an essential process for optimal proliferation in eukaryotic cells, more specifically in cancer cell line proliferation in various CRISPR whole genome essentiality screens (Behan et al., 2019; Meyers et al., 2017; Wang et al., 2015a). To assess the importance of a given gene for optimal proliferation across various cell lines, the cells are transfected with an inducible Cas9-protein, an enzyme responsible for nicking of the DNA, and a lentiviral short guide RNA (sgRNA) library to guide Cas9 to the desired gene target. Deep sequencing compares the initial abundance of sgRNAs in the population with the abundance of sgRNAs after the induction of the Cas9 protein and several passages of the cancer cell lines. Depletion of the sgRNA indicates importance for optimal proliferation of the respective gene, whereas increase of the sgRNA abundance indicates an anti-proliferative role of the respective gene (Wang et al., 2014). These abundance changes of sgRNAs need to be corrected for copy number amplifications, and serve as a readout for how important or essential a given gene is for optimal proliferation in a given cell line, e.g. the CERES score by the Broad institute (Meyers et al., 2017). A potential question is which NMT substrates are needed *per se* for optimal cell proliferation hinting at potentially important substrates for the phenotype of NMT inhibition (the gene KO might phenocopy a loss-of-function situation due to the lack of the myristate).

The five NMT substrates most essential for cell proliferation, measured by the CERES score (also known as gene effect score in the Broad DepMap), are CHMP6, TOMM40, PSMC1, ARF4 and DDX46, across a large number of cancer cells (Meyers et al., 2017). Their function and the potential role of the myristate are shown in Table 1-1. Additionally, a range of gene scores (a different name for the previously mentioned CERES score) of NMT1 for proliferation is observed in these screens, from very dependent cell lines to less dependent cell lines (Meyers et al., 2017). This leads to the question if gene scores of any NMT substrate might correlate with this observed gene scores for NMT1, potentially hinting at substrates driving the phenotype of NMT inhibition.

Table 1-1: The five most essential NMT substrates, and the (potential) function of the myristoylation.

Gene	Function	Function of the myristoylation?
CHMP6	Considered a core component of the endosomal sorting machinery. It coordinates the vesicular transport between the trans-Golgi network, the plasma membrane and the lysosome (Yorikawa et al., 2005).	The N-terminus of CHMP6 binds to CHMP4b and EAP20, parts of the ESCRT-II complex. However, no G2A mutations were conducted, leaving it unclear if the myristate is important for this binding (Yorikawa et al., 2005).
TOMM40	Channel-forming protein, important for protein precursor import into the mitochondria (Hill et al., 1998).	Myristoylation is interestingly not considered essential for membrane targeting of TOMM40 (Utsumi et al., 2018). It might be however important in the recognition of the protein precursors.
PSMC1	Component of the 26S proteasome, involved in protein homeostasis via degradation of proteins (Coux et al., 1996).	Evidence in yeast, that lack of myristoylation changes the localisation of the proteasome. This seems to cause severe growth defects when protein misfolding is caused with e.g. unnatural amino acids or changes in temperature (Kimura et al., 2012).
ARF4	Part of the ARF family, involved in the regulation of membrane trafficking and organelle structure. ARF4 is involved in the trans-Golgi network (Donaldson and Jackson, 2011).	The myristate is key in the regulation of ARF GTPase through the GTP-Myristoyl switching (Goldberg, 1998).
DDX46	RNA helicase, involved in the pre-mRNA splicing machinery, and part of the complex A of the spliceosome (Will et al., 2002b). Also implicated in the antiviral response (Zheng et al., 2017).	Unknown.

Figure 1-6 A shows an overview of the gene scores of 128 CoTMyr substrates identified as myristoylated using proteomics and/or other biochemical assays (Broncel et al., 2015; Kallemeijn et al., 2019; Thinon et al., 2014; Utsumi et al., 2018).

Several NMT substrates have been annotated on UniProt by sequence similarity as NMT substrates (Consortium, 2019). However, e.g. in the case of ARL1 and ARL2, despite sequence similarity and the former being myristoylated (Thinon et al., 2014), ARL2 is not myristoylated (Chen et al., 2016; Sharer et al., 2002). This indicates that a more cautious approach is warranted to ensure a protein is indeed myristoylated.

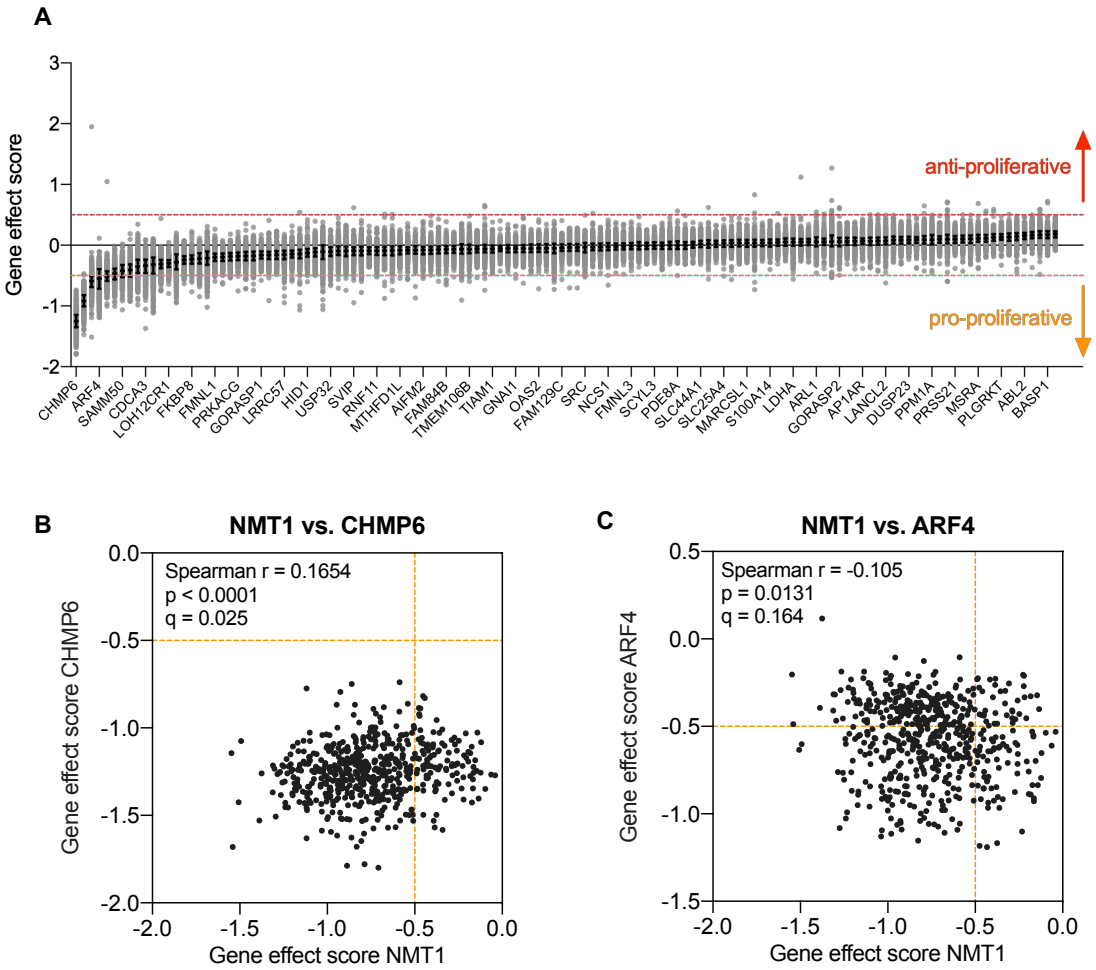

Figure 1-6: NMT substrates essentiality in 550+ cell lines and its correlation to dependence to NMT1.

[A] The gene effect scores from the Broad Institute DepMap project (Meyers et al., 2017; Tsherniak et al., 2017) for CoTMyr NMT substrates (N = 128). **[B]** Correlation of dependence on the core-essential NMT substrate CHMP6, compared to the dependence of NMT1. **[C]** Correlation of the dependence of the core-essential NMT substrate ARF4 and the dependence of NMT1. (orange lines: cut-off for a gene to be considered essential (Gene effect score < -0.5); p-values: Spearman correlation test; q-values: Benjamini and Hochberg FDR)

Interestingly, none of the NMT substrates cause an increase of sgRNA abundance, that is an increase of the gene effect score, upon genetic knockout (as observed for anti-proliferative genes such as PTEN or TP53) in a larger number of cancer cell

lines. The essentiality of an NMT substrate does not necessarily indicate importance of the myristate *per se*; however, as mentioned previously, one can attempt to correlate the gene effect score of an NMT substrate with the gene effect score of NMT1 in itself, which could hint at NMT substrates that play a major role in the toxic effects of NMT1 KO.

To identify these co-dependencies, the Spearman correlations for the gene effect score of NMT1 and the gene effect scores of the respective NMT substrate were calculated. To correct for multiple hypothesis testing, a Benjamini-Hochberg FDR correction was utilised. Within the essential NMT substrates (that is that have at least 50% of all cell lines with a gene essentiality score of below -0.5), only the gene score of to two NMT substrates correlated with dependence to NMT1: CHMP6 (shown in Figure 1-6 B) and ARF4 (shown in Figure 1-6 C). In the case of the former, there seems to be a significant trend that cells dependent on CHMP6 are also dependent on NMT1 for optimal proliferation. For the latter, there is a trend that cells dependent on ARF4 are actually less dependent on NMT1, that did not reach statistical significance after multiple hypothesis correction. These data could indicate that the toxicity of NMT1 KO might be driven by interfering with CHMP6, whereas ARF4 might play less of a role for the toxicity of an NMT1 KO. However, this is a reductive approach to the problem, and likely the toxic effect of loss of NMT1 is mediated by various NMT substrates in combination. This is also apparent, as myristoylation and NMT substrates have been implicated in various biological processes.

The role of myristoylation in T cell activation, differentiation and proliferation has been more extensively researched. Complete loss of NMT1/2 in T cells (Lck-Cre mediated) suppresses differentiation and proliferation, likely through defective T cell receptor (TCR) signalling, due to mis-localisation of LCK (Rampoldi et al., 2015). The same group observed an increase of $\gamma\delta$ T cells, upon genetic knockout of NMT1/2 (Rampoldi et al., 2017); however, they only compared to a WT mouse, lacking Lck-Cre, known to cause a shift towards $\gamma\delta$ T cells on its own. This renders an exact distinction of the effect of Cre on its own and the loss of NMT1/2 difficult (Carow et al., 2016) Interestingly, reduced levels of NMT1 have been implicated with impaired activation of the energy sensor AMPK (an NMT substrate) and on promoting pathogenesis of T cells in the context of rheumatoid arthritis. However, the authors utilise YnMyr in flow cytometry as quantification method for myristoylation, and without any further validation, this might not be a good readout of actual ongoing

myristoylation. Importantly, YnMyr can also be integrated in membranes and in GPI anchors (Thinon et al., 2014; Wen et al., 2019). Myristoylation of AMPK is also important for mitophagy and clearance of defective mitochondria (Liang et al., 2015). Myristoylation of SRC has been shown to regulate its membrane binding, stability and activity (Patwardhan and Resh, 2010). Interestingly, overexpression of G2A mutant SRC and LYN causes delocalisation of the kinases to the nucleus and can mediate chromosome missegregation (Honda et al., 2016). This work shows that NMT substrates might be subject to gain- or change-of-function situations upon impaired myristoylation. Myristoylation on the phosphatases PPM1A and PPM1B has been shown to be essential for substrate recognition (Patwardhan and Resh, 2010) and G2A overexpression of PPM1A causes localisation changes within the cell (Zhu et al., 2018). In the context of post-translational myristoylation, the effect on BID was already discussed, but many more proteins are myristoylated upon caspase cleavage (Martin et al., 2011; Thinon et al., 2014) (see section 1.1.2). Interesting in this context is the recent discovery of a glycine specific N-degron pathway: N-terminal glycines can act as powerful degron signals and one third of the ~1800 known caspase cleavage sides are followed by a glycine. The authors show that *N*-terminal myristoylation stabilises proteins, potentially indicating that PTMyr protects a subset of proteins from degradation, after caspase mediated endoproteolysis (Timms et al., 2019). Why cells would have a need for this mechanism remains to be explored. A potential reason could be to avoid the earlier mentioned toxic GOF of non-myristoylated substrates, such as SRC and LYN (Honda et al., 2016).
In summary, myristoylation is involved in a plethora of different biological functions and dependently of cellular or tissue context can have varied effects on the cells. Several NMT substrates are essential for optimal proliferation on their own; however, this is not sufficient to imply that the myristate is absolutely necessary for correct protein function.

1.2 NMT as a drug target – from fungal and infectious diseases to cancer

This subchapter will give a brief time-line and overview of the drug discovery programs, and the respective inhibitors that attempt to target NMT in different

disease contexts. Those programmes range from anti-fungal drug programs to infectious disease to targeting cancer. Initially, the drug discovery programs focussed on infectious pathogens, exploiting potential selectivity over the human NMT to avoid host toxicity. While NMT was proposed as a potential anti-cancer target, it is not clear if genetic markers correlate with increased or decreased responsiveness.

1.2.1 The early antifungal programs

The initial drug discovery programs against NMT were focussed on developing new anti-fungal drugs. Two reasons drove the initial excitement for NMT as an anti-fungal target. Firstly, it was shown that NMT is essential for *Candida albicans* (Weinberg et al., 1995) and *Cryptococcus neoformans* (Lodge et al., 1994) and secondly, a research group showed that it is indeed possible to generate peptide-based inhibitors that were selective towards the *C. albicans* NMT over hsNMT1 (Devadas et al., 1995).

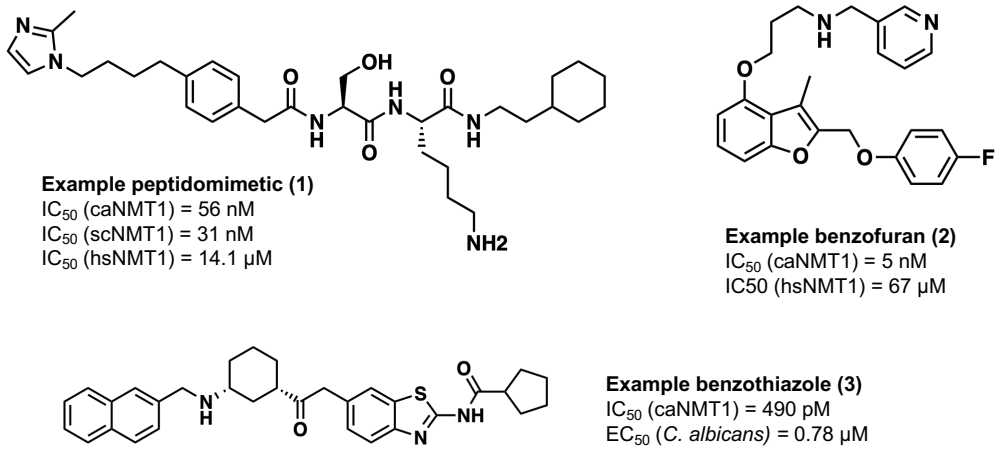

Figure 1-7: Structure of different anti-fungal NMT inhibitors.

Further development yielded in different series of peptidomimetics, developed by Searle (an example is shown with **1** in Figure 1-7) (Devadas et al., 1997). However, the peptidomimetics lacked *in vitro* efficacy, likely due to problems to penetrate membranes (Taha et al., 2011). Another series was based on benzofurans (Masubuchi et al., 2001): an example of this series is shown with **2** in Figure 1-7; **2** has high potency against the caNMT1, the NMT of *Candida albicans*, with a selectivity window of over 10,000-fold compared to hsNMT1 (Ebiike et al., 2002). However, the series lacked efficacy against a range of systemic fungal pathogens

(Masubuchi et al., 2003). Another example are the benzothiazoles (Yamazaki et al., 2005), such as **3** in Figure 1-7. This inhibitor also suffered from poor translation of its high enzymatic potency into cellular potency, likely due to similar membrane permeability issues as the peptidomimetics (Ebara et al., 2005). Still, academic research groups expanded the structure activity relationship (SAR) of different series and potentially created a new generation of NMT antifungal drugs, with better properties than the previous series (Sheng et al., 2010).

1.2.2 Targeting different (tropical) infectious diseases

As myristoylation was identified as essential for the parasite *T. brucei*, the cause of sleeping sickness (Price et al., 2003), a high throughput screening was initiated to identify potential chemical scaffolds to target tbNMT. This led to the identification of pyrazole sulphonamide compounds (Frearson et al., 2010). Further modification of the initial hits, led to the development of DDD100097 (**4** in Figure 1-8), an inhibitor with good blood-brain barrier permeability. To note is the little difference in enzymatic potency between tbNMT and hsNMT1, which could cause unwanted host toxicity. However, there was a 1000-fold difference in toxicity between *Trypanosoma brucei* and human MRC5 cell line (Brand et al., 2014). Another high throughput screening, conducted in a collaboration between Imperial College London and the Medical Research Council (MRC), identified quinolines (see **5** as an example in Figure 1-8) as potential starting point to develop NMT inhibitors against *Plasmodium vivax* (Goncalves et al., 2012). In yet another collaboration between Imperial College London and Pfizer, several additional chemical scaffolds were identified with potency against different protozoan NMTs (Bell et al., 2012). Optimisation of one of those initial scaffolds, based on benzothiophene, led to potent anti-malarial drugs (see **6** in Figure 1-8) and were used, amongst a member of the pyrazole sulphonamides, to validate NMT as a drug target in malaria (Wright et al., 2014). Further modification, away from a benzofuran scaffold to a monocyclic scaffold increased drastically the potency towards the NMT of *Leishmania Donovani* (see **7** in Figure 1-8). However, those inhibitors lacked efficacy against *Leishmania Donovani* amastigotes *ex vivo* with an EC_{50} of >50 μM (Wright et al., 2015).

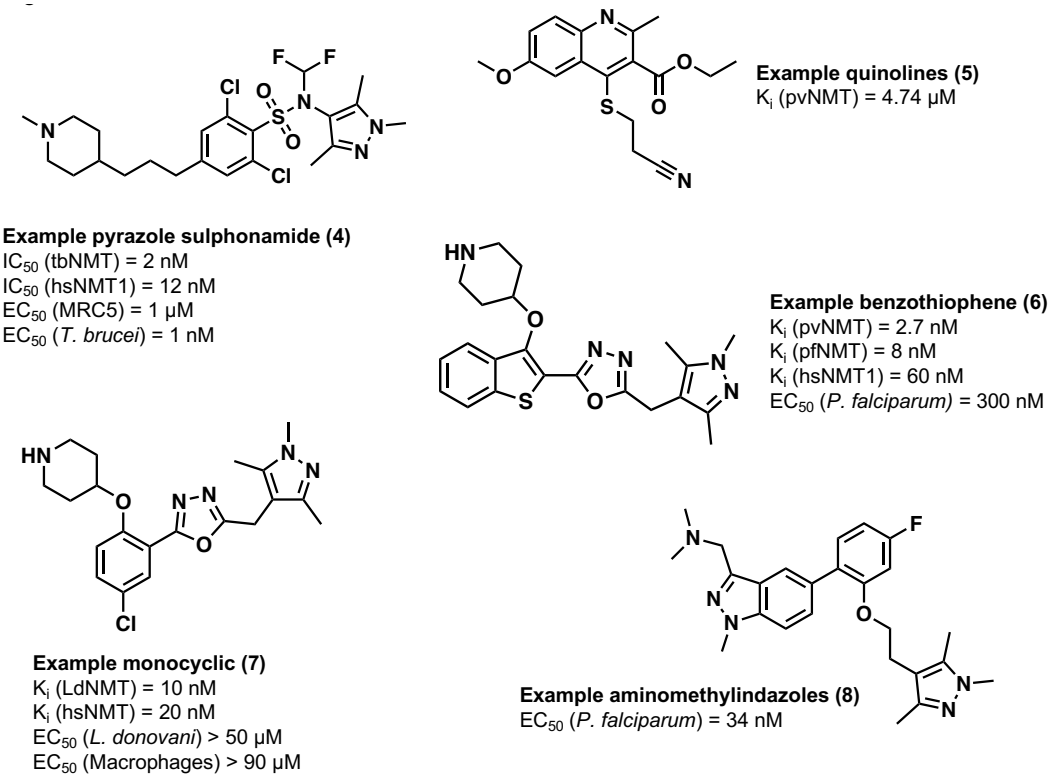

Figure 1-8: Structures of example NMT inhibitors against various infectious diseases.

Lastly, the Imperial/Pfizer screen identified an aminomethylindazole scaffold that was further optimised to yield a new series of exceptionally potent NMT inhibitors (Bell et al., 2017; Mousnier et al., 2018) (see **8** in Figure 1-8). One inhibitor of this series, IMP1002, has been recently disclosed as a highly potent antimalarial agent and a potential resistance mechanism through gatekeeper mutations in the enzyme have been uncovered in the comparison of IMP1002 and an example of the pyrazole sulphonamides series (Schlott et al., 2019).

In conclusion, several highly potent small molecule inhibitors have been developed against different infectious pathogens; however, in all of these cases the aim is to create a high selectivity over the human NMTs. But could one target human NMT as a new way to treat cancer?

1.2.3 Myristoylation as a drug target in cancer

Targeting NMT in cancer has been already proposed in the 1990s (Felsted et al., 1995). However, due to its essentiality in mammals (Yang et al., 2005), the question remains whether one can achieve a therapeutic window. Transient inhibition of the human NMT, to block the replication of the common cold virus was shown to be feasible, and proofs that shorter periods of inhibition do not seem to cause any toxicity in human cells, at least in the cell line HeLa (Mousnier et al., 2018). As mentioned in section 1.1.2, NMT1 has been identified as essential for cancer cell line proliferation (pro-proliferative) in the first CRISPR gene essentiality screens (Wang et al., 2015a), and has now been confirmed in a large number of cancer cell lines (Meyers et al., 2017). Interestingly, NMT2 is not necessary for optimal proliferation in the cancer cells, nor does it act as an anti-proliferative gene, in the sense that a gene knockout increases the sgRNA abundance (see Figure 1-9 A). However, its expression levels are negatively correlated with the gene effect score of NMT1, indicating that NMT2 can compensate to some extent for loss of NMT1. This would be relevant in the context of specific NMT1 inhibitors; however, most inhibitors are equipotent against NMT1 and NMT2, and as shown in subchapter 2.2.2, neither NMT1 nor NMT2 expression predicts sensitivity of a cancer cell line to a dual NMT1/2 inhibitor.

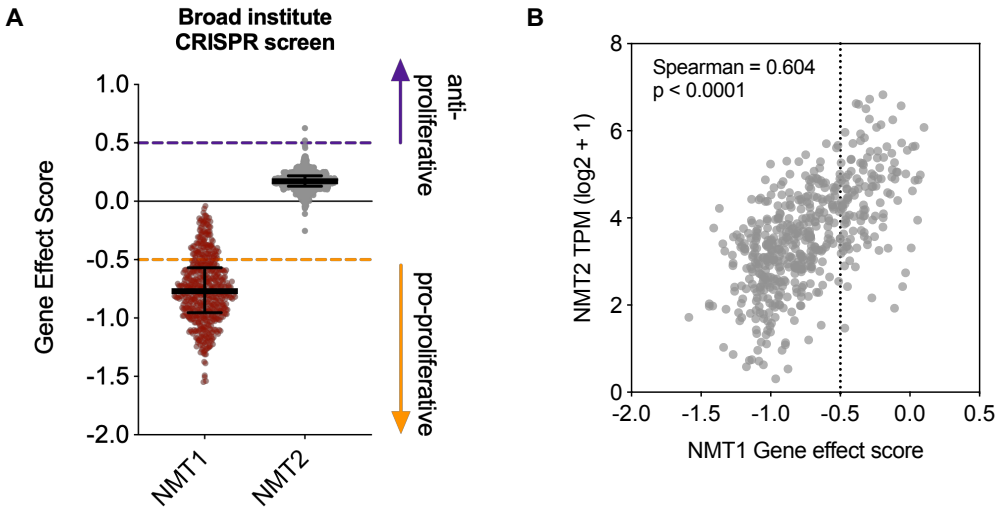

Figure 1-9: Essentiality of NMT1 in different cancer cell lines, and the NMT2 compensatory capacity.

[A] Gene effect scores for the human NMT1 and NMT2 in over 550 cancer cell lines. **[B]** Correlation of NMT2 expression and gene effect score of NMT1.

Initially, Tris dibenzylideneacetone (DBA) dipalladium (see **9** in Figure 1-10), usually associated with Suzuki couplings in synthetic chemistry (Kudo et al., 2006), was reported as a specific NMT1 inhibitor through downregulation of NMT1 mRNA (Bhandarkar et al., 2008) and effective as a treatment for melanoma. Subsequently, further publications described the efficacy of Tris DBA in chronic lymphocytic leukaemia (CLL), multiple myeloma and pancreatic cancer (de la Puente et al., 2016; Diaz et al., 2016; Kay et al., 2016). Furthermore, nanoparticles of Tris DBA have been described as efficient in the treatment of advanced melanoma *in vivo* (Elsey et al., 2019). Recently, also B13 (see **10** Figure 1-10) was described as an NMT inhibitor, although it was initially described as a ceramidase inhibitor (Bielawska et al., 1996), suppressing prostate cancer progression through SRC inhibition (Kim et al., 2017). However, the Tate and Calado laboratory showed (the author of this thesis was one of the two lead scientists in this project) via the use of different enzymatic, cellular and chemical proteomics tools, that neither Tris DBA or B13 are *bona fide* NMT inhibitor and warn against their use as NMT inhibitors (Kallemeijn et al., 2019). This indicates that the toxicity against cancer cells in these reports is not mediated by NMT inhibition. On the other hand, IMP1088 (see **11** in Figure 1-10) and IMP366 (see **12** Figure 1-10) were validated as *bona fide* NMT inhibitors. In fact, the latter was shown to induce ER stress and cell cycle arrest in cancer cells (Thinon et al., 2016).

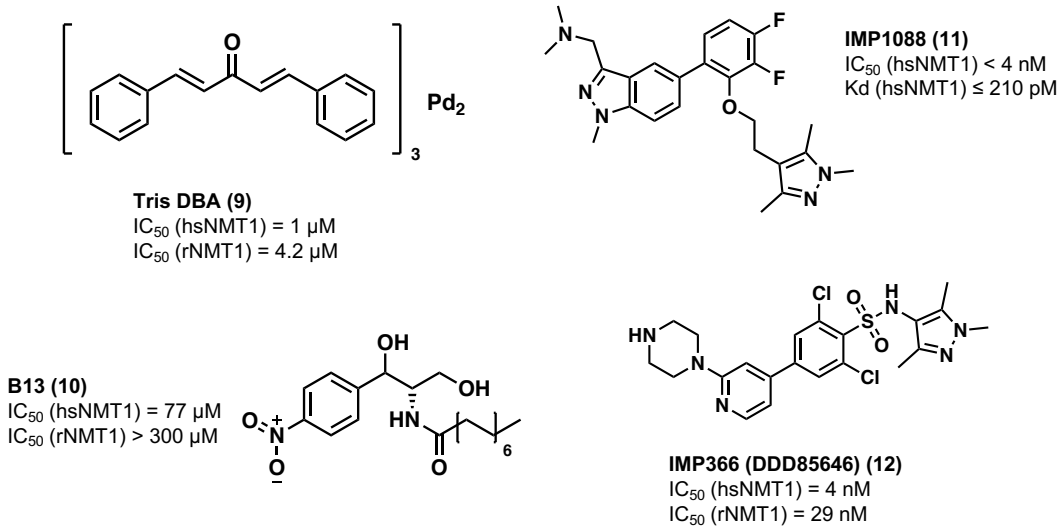

Figure 1-10: Structures of claimed and commonly applied human NMT inhibitors, used against cancer.

Early literature described that RNA interference (RNAi) of both NMT1 and NMT2 causes apoptosis in cancer cells; in this study NMT2 knockdown caused increased apoptosis compared to NMT1 knockdown (Ducker et al., 2005). However, the recent CRISPR gene essentiality screens, conducted by various groups across large numbers of different cancer cell lines, question those findings, particularly concerning the role of hsNMT2 (Behan et al., 2019; Meyers et al., 2017; Reddy et al., 2017; Wang et al., 2015a). shRNA mediated knockdown of NMT1 modulates breast cancer progression, by blocking cancer initiation, growth and metastasis (Deng et al., 2018). Additionally, overexpression of NMT1 has been observed in colon cancer, gallbladder carcinoma, and brain tumours, reviewed here: (Selvakumar et al., 2007), potentially indicating a role of myristoylation in these cancers. However, it is not clear to date which cancer type to target. Is there a particular molecular phenotype in a given cancer that predicts sensitivity or resistance towards NMT inhibition? This question is highly important in terms of therapeutic window. If a molecular or genetic marker could be identified, it could be used for subsequent patient stratification, in the case NMT inhibitors reach clinical trials as a novel therapy in oncology.

To summarise, due to NMT's enzymatic and thus druggable nature, several NMT inhibitors have been developed, initially focussing on targeting pathogens, while sparing the host NMT. These efforts resulted in a number of highly potent NMT inhibitors with different applications. Some of these inhibitors have very good selectivity for the pathogen NMT over the human NMT. A different approach to target the common cold virus (or any other virus that hijacks the host myristoylation machinery) is the transient inhibition of the host NMT with exceptionally potent hsNMT1/2 inhibitors (Mousnier et al., 2018).

To date, no NMT inhibitor has reached clinical stage. In the case of cancer, the picture remains complex: it is unclear which cancers to target and why these particular cancer cells would be more sensitive (or resistant) to NMT inhibition? In light of the essential nature of myristoylation for cells themselves, identifying patients that might benefit (or not) from NMT inhibition to target their respective malignancy is crucial. Previous work from the Tate laboratory identified, in collaboration with the Sanger institute, that Burkitt's lymphoma (BL) cancer cell lines, a germinal centre (GC) derived B cell malignancy (Schmitz et al., 2014), are particularly responsive to NMT inhibition (Lim, 2016); however, a mechanistical explanation for this increased sensitivity is lacking and/or a genetic marker/hypothesis that could identify sensitive

cancer cell lines beyond BL (Lim, 2016). This thesis identified such a potential marker (discussed in Chapter 4), which leads to the introduction of the very (in)famous protooncogene in the next subchapter: MYC.

1.3 MYC, the "gas pedal"[1] of the cell…

Initially, identified as a viral oncogene v-myc (Bishop, 1983; Payne et al., 1982), c-Myc (MYC) was revealed over the next decades of research to be key transcription factor involved in cellular proliferation, cell growth, biosynthesis, metabolic reprogramming, apoptosis, transcription and effects on its micro-environment, with wide implications in oncology. Myc biology has been extensively reviewed (Conacci-Sorrell et al., 2014; Dang, 2012; Meyer and Penn, 2008; Soucek and Evan, 2010; Stine et al., 2015), thus, the next subchapters will only give a brief introduction and summary into some seminal findings of Myc biology.

1.3.1 Structure of the MYC paralogs

The Myc paralogs, MYC, MYCN and MYCL1, are evolutionary conversed basic helix-loop-helix leucine zipper (bHLHZip) transcription factors, with a transactivation domain (TAD) at the N-terminus; a central region containing a PEST–a peptide sequence rich in proline (P), glutamic acid (E), serine (S) and threonine (T), associated with short half-life of the respective protein (Rogers et al., 1986)–and a nuclear localisation signal (NLS); lastly, a basic region (BR) for DNA binding and a bHLH-LZ domain at the C-terminus for protein-protein interactions (PPI) (see Figure 1-11). The conserved so-called MYC homology boxes I and II are within the TAD domain, whereas the MYC homology boxes IIIa, IIIb and IV are within the central region (to note is that IIIa is conserved for MYC and MYCN, but not for MYCL1). Two phosphorylation sites on MYC homology box I play a crucial role in the stability of MYC: phosphorylation of T58 (mediated by GSK3-β) marks MYC for degradation by the proteasome, whereas phosphorylation of S62 (downstream of the MAPK/ERK signalling pathway) stabilises the protein (Farrell and Sears, 2014; Vervoorts et al.,

[1] This term for MYC was used by Andreas Trumpp at a seminar given at the Crick in March 2017, titled 'Stem Cell Function During Normal Physiology, Cancer and Drug Resistance'.

2006). The importance of these phosphorylations in regulating MYC protein levels will be discussed later.

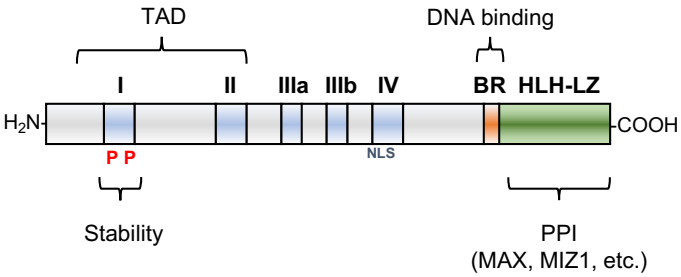

Figure 1-11: MYC protein domains and their functions.
(Adopted from (Meyer and Penn, 2008))

The C-terminus is critical for DNA binding via the BR domain and the HLH-LZ domain is needed for PPIs with MYC interactors. It was shown that MYC dimerises with MAX at the so-called E-Box motifs CACGTG (Blackwood and Eisenman, 1991), and this dimerization is crucial for MYC's transformative capacity (Amati et al., 1993). The heterodimer recruits TRRAP, which subsequently recruits more chromatin modifying proteins, leading to chromatin remodelling at the target genes (McMahon et al., 2000). However, MYC can also interact with different proteins, e.g., to serve as a transcriptional repressor, as shown in its interactions with MIZ1 (Wanzel et al., 2003). The next sections will describe the many functions of MYC, which are summarised in Figure 1-12.

1.3.2 Between life and death

From the three paralogs, MYC, MYCN and MYCL, the former two were shown to be essential in mice; the knockout of either paralog caused death in the embryonic stage between 10 to 11 days through multiple organ failure (Charron et al., 1992; Davis et al., 1993). On the other hand, Mycl-deficient mice develop normally (Hatton et al., 1996).

MYC plays a crucial role in cell cycle progression through controlling the expression of different cell cycle cyclin-dependent kinases (CDKs) and cyclins (Bouchard et al., 1999; Perez-Roger et al., 1999; Santoni-Rugiu et al., 2000), and in contrast to *Drosophila dmyc* mutants, mice with reduced levels of MYC protein suffer from hypoplasia and not from hypertrophy, showing the clear role of MYC in proliferation

in mammals (Trumpp et al., 2001). On the other hand, MYC overexpression induces apoptosis in different cells (Evan et al., 1992; Shi et al., 1992). This apoptosis induction was shown to be p53-dependent (Hermeking and Eick, 1994; Wagner et al., 1994). This paradoxical function of MYC as an inducer of apoptosis, while simultaneously acting as a key cell cycle driver and essential gene, has strong implications for its role as an oncogene and malignant transformation, which will be discussed in subchapter 1.4.

1.3.3 MYC drives increased protein synthesis, is involved in DNA replication, reprograms metabolism, and causes dedifferentiation

Within the last two decades, it became apparent that MYC was involved in many more biological functions than initially appreciated. Besides its role in Pol II mediated transcription through recruitment of Pol II and CDK9 (Cowling and Cole, 2007), MYC is also involved in RNA pol I (Grandori et al., 2005) and RNA pol III-transcription (Gomez-Roman et al., 2003). Due to this involvement in the transcription of ribosomal mRNA and rRNA, MYC also drives indirectly increased protein synthesis through increased ribosomal biogenesis (Dai and Lu, 2008). Moreover, MYC is also involved in mRNA cap methylation, a process in which the 5'-end is capped with a specifically altered nucleotide: a guanine, methylated on the 7 position (m^7-cap). This process increases the stability and translational efficacy of the respective mRNA. In numbers MYC caused an increase of 1.8-fold in the amount of total RNA; it increased however the m^7-capped mRNA by 4.9-fold in fibroblasts (Cowling and Cole, 2010).

A seminal paper also showed the role of MYC in the pre-replication complex, where it acts in a non-transcriptional manner. Additionally, overexpression of MYC causes increased number of replication forks and checkpoint activation (Dominguez-Sola et al., 2007). MYC also rewires the metabolism towards increased glucose and glutamine uptake and increases lipid synthesis, the so-called Warburg metabolism (Dang, 2010, 2013; Stine et al., 2015).

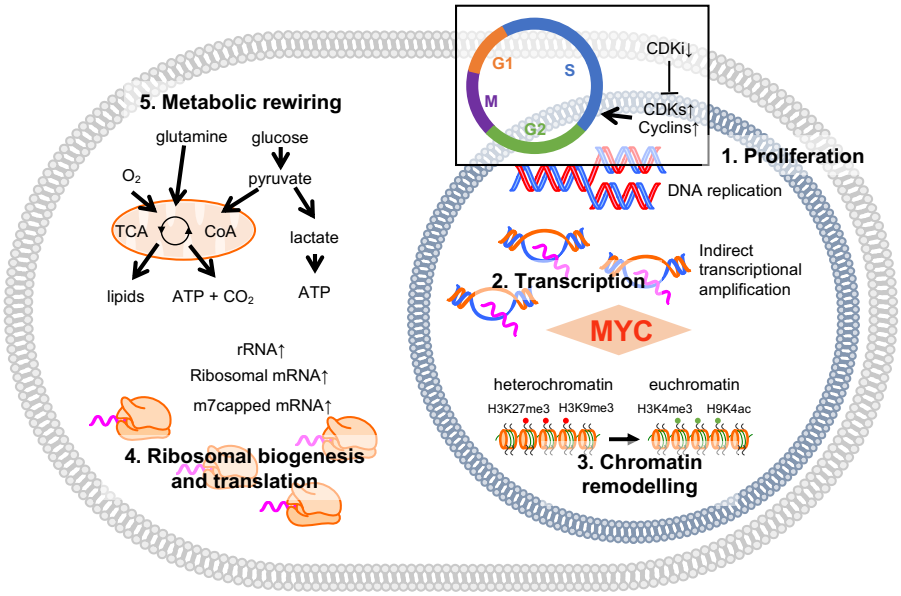

Figure 1-12: MYC's involvement in most major cellular functions.

(1) MYC has direct implications in the proliferation of cells, by increasing the expression of cyclins and cell cycle related CDKs (Bouchard et al., 1999; Perez-Roger et al., 1999; Santoni-Rugiu et al., 2000), while transcriptionally repressing together with MIZ1 with the expression of cell cycle inhibitors (Wanzel et al., 2003). Additionally, it binds to several proteins of the pre-replicative complex for DNA replication (Dominguez-Sola et al., 2007). **(2)** MYC recruits Pol II and CDK9 to its target genes (Cowling and Cole, 2007), and can indirectly amplify the transcription of all accessible chromatin, particularly in the case of an oncogenic overexpression (Sabo et al., 2014; Walz et al., 2014). **(3)** MYC can also remodel the chromatin, usually causing the transition from heterochromatin, defined by repressive chromatin marks (such as H3K27me3 or H3K9me3) to euchromatin, defined by activating chromatin marks (such as H3K4me3 or H3K9ac) (McMahon et al., 2000). On the other hand, it can also repress transcription through interaction with MIZ1 or recruiting the PRC2 complex; this is thought to be important in MYCs ability to cause dedifferentiation and a stem cell-like state (Fagnocchi et al., 2016; Fagnocchi and Zippo, 2017; Takahashi et al., 2007). **(4)** MYC also increases the production of rRNA through recruiting Pol I (Grandori et al., 2005) and Pol III (Gomez-Roman et al., 2003), increased mRNA expression of ribosomal proteins and translation initiators and additionally is involved in mRNA capping, increasing translation efficacy (Cole and Cowling, 2008; Cowling and Cole, 2010; Dai and Lu, 2008). **(5)** MYC can also cause a rewiring of the metabolism to a Warburg-like metabolism, utilising increased glycolysis, and increasing the demand for glutamine (Dang, 2010, 2013; Stine et al., 2015).

To add to the multiple functions of MYC, it is also a Yamanaka factor, and can, if combined with OCT3/4, SOX, and KLF4, dedifferentiate human dermal fibroblasts back into induced pluripotent stem cells (iPSC) (Takahashi et al., 2007). It is however possible to generate iPSCs without MYC. Interestingly, these lack the capacity to form tumours, again emphasising the importance of MYC as a protooncogene (Nakagawa et al., 2008). MYC controls in pluripotent stem cells several regulatory

networks, through non-coding RNAs (ncRNAs) or potentiating Wnt/β-catenin signalling through recruiting the polycomb repressive complex 2 (PRC2) complex directly to Wnt antagonists (Fagnocchi et al., 2016; Fagnocchi and Zippo, 2017). These same mechanisms are also hijacked in e.g. breast cancer to induce a stem cell-like state in the cancer cells (Poli et al., 2018).

1.3.4 MYC, a transcriptional amplifier?

In an attempt to understand the pleiotropic effects of MYC expression, different research teams aimed at identifying MYC target genes. However, their conclusions were that instead of binding a particular subset of genes, MYC acts as a transcriptional amplifier of a given cell's transcriptional profile: it accumulates in the promoter regions of active genes (usually marked by histone acetylation, such as H3K27ac) and causes increased production of the respective mRNAs, thus 'just' amplifying transcription of active genes. Those experiments were conducted in different cancer cell lines, a B cell line with inducible MYC levels, lymphocytes and embryonic stem cells (Lin et al., 2012; Nie et al., 2012). However, different explanations of these observations were proposed following those initial claims. Firstly, Sabo A., et. al. proposed a model in which MYC controls indeed a subset of genes, which drive changes in cellular states and by increased proliferation, protein synthesis, metabolic reprogramming. This cellular state changes then subsequently can cause the observed transcriptional amplification. Additionally, they warned against equating promotor invasion with productive engagement (Sabo et al., 2014). Secondly, Walz S., et. al. argue that physiological levels of MYC bind to canonical E-boxes (CACGTG), whereas oncogenic levels invade areas with non-canonical E-boxes (CANNTG). Additionally, they showed that the interaction of MYC with MIZ1 represses a particular subset of genes (Walz et al., 2014). The transcriptional repression effect can also be observed in medulloblastoma: the abrogation of the MYC-MIZ1 interaction causes differential medulloblastoma subgroup identities (Vo et al., 2016), indicating that MYC must have specific target genes, at least on the level of transcriptional repression.

To summarise, MYC is involved in most major cellular function, ranging from driving proliferation and transcription, remodelling the chromatin, increasing ribosomal

biogenesis, thus cell mass, and reprogramming the metabolism towards a more Warburg-like metabolism (see Figure 1-12). It is therefore unsurprising that MYC, as a key node between various biological functions, plays a pivotal role in cancer and its hallmarks (Hanahan and Weinberg, 2011). Deregulation of MYC expression, by different means, is commonly observed in cancer–the topic of the next subchapter.

1.4 … and thus, a key protooncogene

As discussed in the previous chapter, MYC is a key regulator of many cellular functions ranging from increasing proliferation and translation, causing dedifferentiation and increasing 'stemness' of the cells. Thus, MYC plays a key role in tumour initiation and maintenance (Dang, 2012). This chapter will discuss firstly, the stringent control mechanisms to regulate MYC levels in a physiological context to avoid its transformative effects, and how cancer cells utilise different means to avoid exactly those control mechanisms.

1.4.1 Physiological control of MYC

Due to its tumorigenic capacity, MYC expression is tightly controlled by different signalling pathways, and has additional feedback mechanisms. The MYC protein is very unstable with a half-life of 20 to 30 minutes (Gregory and Hann, 2000). Upon mitogenic signalling through receptor tyrosine kinases, the RAS/MEK pathway is activated, causing phosphorylation of MYC at S62, stabilising it. Additionally, PI3K can inhibit GSK3β, which would usually phosphorylate MYC at T58 after S62 phosphorylation, marking it for proteasomal degradation (Farrell and Sears, 2014; Vervoorts et al., 2006) (see Figure 1-13 A, left). An additional pathway, shown to increase MYC mRNA expression is WNT signalling, particularly important during embryonic development. Cytosolic β-catenin is usually phosphorylated and marked for proteasomal degradation by a complex between APC, Axin and GSK3β. Upon WNT signalling, Axin and GSK3β are recruiting to the plasma membrane, and β-catenin can accumulate in the nucleus and activate the transcription of its target genes, amongst them MYC (MacDonald et al., 2009) (see Figure 1-13 A, right). These signalling mechanisms ensure that the MYC levels are only elevated in the

presence of growth signals. Thus, these signalling pathways are commonly mutated in cancer through e.g. activating mutation which will be further discussed in section 1.4.2. Additionally, an ARF/P53 feedback loop blocks the proliferative capacity of MYC, the reason why development of tumours upon forced MYC expression in mice has a latency period (Eischen et al., 1999). If MYC levels rise further, p53-dependent apoptosis is induced (Hermeking and Eick, 1994; Murphy et al., 2008; Wagner et al., 1994) (see Figure 1-13 B). Interestingly, the activation of the p53-dependent apoptosis is regulated by the distinct levels of MYC: low levels of MYC deregulation, thus increased expression, are well-tolerated and drive ectopic proliferation of cells and cause subsequently oncogenesis; however, high oncogenic levels activate the ARF/p53 checkpoint and cause programmed cell death (Murphy et al., 2008). An additional layer of regulatory control comes from the members of the MXD family. Their interactions with MAX is thought to negatively regulate MYC (Conacci-Sorrell et al., 2014), and shallow deletions of MXD members are observed in some cancers (Schaub et al., 2018).

1.4.2 Deregulation in cancer

The first observation of MYC deregulation in human cancer was the translocation of MYC into the immunoglobulin locus in BL (Burkitt, 1958), from chromosome 8 to chromosome 2, 14 or 22 (Dalla-Favera et al., 1982). These translocations are also observed in other lymphomas, such as diffuse large B cell lymphoma (DLBCL) or plasmablastic lymphoma, however as secondary oncogenic hits (Ott et al., 2013). Additionally, in multiple myeloma (MM), a plasma cell tumour, MYC translocations can also occur in the later stages of the disease (Mikulasova et al., 2017; Wardell et al., 2013). Over the following decades it became apparent that amplifications of MYC were among the most common events in various cancers within the TCGA data sets (Beroukhim et al., 2010; Sanchez-Vega et al., 2018). Recent studies, under the project of the Pan-Cancer Atlas, identified that 28% of all cancers in the TCGA data set show amplification of at least one Myc paralog, with MYC alone being responsible for 21% of the total amplifications. Interesting to note is the difference in frequency of alterations (that is mutations and/or amplifications) within the proximal MYC network (PMN), that is the MYC paralogs themselves, MAX

and negative regulators of the MAX dimerization protein (MXD) family, in different cancer subtypes: in the case of the ovarian serous carcinoma (OV) study, more than 95% of all patients showed alterations in the PMN; on the other hand, less than 10% of the patients in the thyroid carcinoma (THCA) group had alterations.

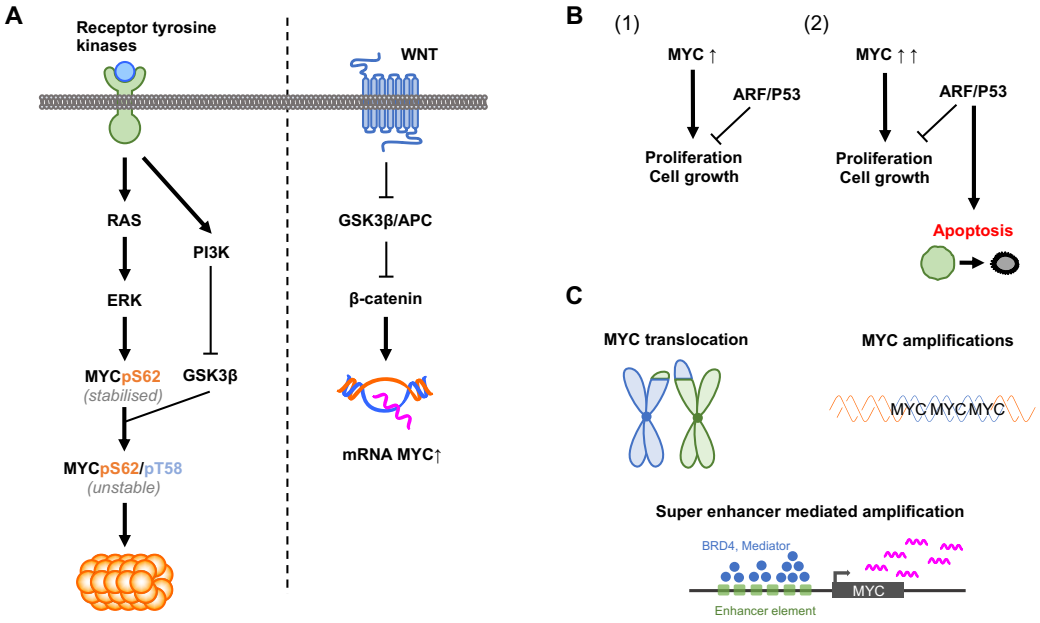

Figure 1-13: MYC regulation, feedback loops, and structural alterations causing deregulation in cancer.

[A] Left: Mitogenic signalling through various receptor tyrosine kinases can activate on the one hand downstream RAS signalling. RAS activates the ERK pathway, which can phosphorylate MYC on the S62, causing a stabilisation of the MYC protein. On the other hand, signalling through PI3K/AKT signalling can inhibit GSK3β, which would phosphorylate T58 on MYC. This recruits PP2A to dephosphorylate p-S62, and marking MYC for subsequent proteasomal degradation (Dang, 2012; Farrell and Sears, 2014; Vervoorts et al., 2006). Right: In embryonic development, Wnt signalling blocks the activity of GSK3β and APC, which would induce the proteasomal degradation of β-catenin. Upon Wnt signalling, β-catenin is not degraded anymore and can localise to the nucleus and enhance MYC mRNA expression (Dang, 2012; MacDonald et al., 2009). **[B]** The proliferative capacity of MYC is kept in check by the tumour suppressors ARF and p53 (Eischen et al., 1999). If MYC expression increases beyond a certain threshold, the p53 dependent apoptosis is triggered (Evan et al., 1992; Hermeking and Eick, 1994; Shi et al., 1992; Wagner et al., 1994). **[C]** MYC can be deregulated on the genetic level through e.g. translocations; this causes ectopic expression through the use of different enhancer elements. These are often observed in haematological malignancies (Dalla-Favera et al., 1982; Mikulasova et al., 2017; Ott et al., 2013; Wardell et al., 2013). MYC amplifications are another mean to increase MYC mRNA expression, and it is amongst the most observed amplifications in two different studies (Beroukhim et al., 2010; Schaub et al., 2018). Additionally, upregulation of MYC can occur through altered SEs, that recruit BRD4 and the mediator complex to increase MYC mRNA levels (Chapuy et al., 2013; Loven et al., 2013). These alterations are e.g., aberrant loss of DNA methylation at enhancers (Heyn et al., 2016) or focal amplifications of enhancers themselves (Zhang et al., 2016).

The effect of alterations in the *MYC* (or *MYCN*) loci seems to be broadly speaking increased levels of MYC (or MYCN) mRNA and protein (Schaub et al., 2018). A third way for cancer cells to increase the levels of MYC is through deregulating super-enhancer (SE) elements. In DLBCL and multiple myeloma SEs cause increased expression of key oncogenes, such as MYC, through aberrant recruitment of the bromodomain family member BRD4 and the mediator complex (Chapuy et al., 2013; Loven et al., 2013). BRD4 inhibition was proposed as a potential way to target MYC indirectly, which will be further discussed in section 1.5.2. The deregulation of SE elements can occur due to e.g., aberrant DNA methylation in cancer at enhancers (Heyn et al., 2016), or the direct amplifications of the enhancer (Zhang et al., 2016). These three means for cancer cells to increase elevated levels of MYC mRNA are shown in Figure 1-13 C.

As previously mentioned, pathways, such as RAS, PI3K, and WNT signalling can increase the levels of MYC, through either increasing expression itself or stabilising the protein. Activating mutations in kinases or LOF of inhibitors in these signalling pathways are commonly observed in cancer (Sanchez-Vega et al., 2018). The signalling pathways of RTK/RAS and PI3K, both known to stabilise MYC are altered in 46% and 33% respectively of all TCGA patients; the WNT pathway is altered in 15% (Sanchez-Vega et al., 2018). To illustrate this with an example: colorectal cancer has commonly mutations in APC, a negative regulator of Wnt signalling, which would increase MYC mRNA expression. Additionally, KRAS mutations are common, which would stabilise the MYC protein. Furthermore, TP53 mutations are also often observed; the inactivation of TP53 blocks the MYC-induced apoptosis. A sequential model of first the inactivation of APC, followed by activating KRAS mutations, followed by inactivation of TP53 was proposed along the disease progression from pre-malignant to malignant tissue (Fearon and Vogelstein, 1990); however, this sequence of oncogenic events is controversial, as the actual co-occurrence between these three oncogenic hits in colorectal cancer is low (6.6%). This indicates that firstly, this sequence of oncogenic hits only occurs in a minority of patients and secondly, that there are likely multiple genetic pathways in the development of colorectal cancer (Smith et al., 2002).

Independently of the controversy around the sequential order of oncogenic events in colorectal cancer, MYC activation and deregulation is considered a hallmark of cancer initiation and maintenance (Gabay et al., 2014; Kalkat et al., 2017).

1.4.3 Consequences of MYC deregulation in cancer

Due to its involvement in a plethora of biological functions, aberrant MYC expression is involved in most of the cancer hallmarks, such as evading growth suppression, sustained proliferation, increasing the 'stemness' of the cancer, and rewiring cellular energetics (Hanahan and Weinberg, 2011). It additionally plays a major role in many cell autonomous effects which were discussed previous sections. Thus, this last part will focus firstly, how cancers use mechanisms to avoid the initially toxic effects of MYC overexpression. Secondly, it will discuss the non-cell autonomous effects of MYC in the context of cancer. Lastly, it will discuss the prognostic effect of high MYC expression in the clinic.

Oncogenic MYC activation on its own causes apoptosis and engages the ARF/p53 checkpoints, as discussed in section 1.3.2; hence, there is a need for a second oncogenic event to counteract these effects, such as introduction of oncogenic RAS to fully transform primary embryo fibroblasts (Land et al., 1983). Deregulated Myc expression, driven by immunoglobulin enhancer, can induce malignancies in transgenic mice, the so-called Eμ-myc model (Adams et al., 1985). However combination with the anti-apoptotic BCL2 shows strong synergistic effects, reducing tumour latency time, likely through counteracting the pro-apoptotic effects of MYC (Strasser et al., 1990). Disruption of the ARF/p53 checkpoint, through ARF knockout, drastically accelerates the demise of the Eμ-myc mice (Eischen et al., 1999). The link between MYC and p53 is also observed in the cluster of TCGA cases, defined by MYC amplifications; these patients had also recurrently mutations in p53 (Ciriello et al., 2013).

In addition to its cell-autonomous effects, MYC also has effects on the micro-environment of the tumours, thus, plays also a role in the emerging hallmarks of cancer, namely in avoiding immune destruction and causing tumour-promoting inflammation (Hanahan and Weinberg, 2011). A first hint of these effects came from the observation that $CD4^+$ T cells are needed for sustained regression of the tumours upon oncogene inactivation (Rakhra et al., 2010). Additionally, MYC was shown to

cooperate with $KRAS^{G12D}$ in a remodelling of the stroma of the tumour. Influx of macrophages, increased angiogenesis with a subsequent change from hypoxia to normoxia, and expulsion of T, B, and NK cells are observed if both oncogenes are combined (Kortlever et al., 2017).

Thus, once MYC oncogenic potential is unchecked, its capacity to drive proliferation (Bouchard et al., 1999; Perez-Roger et al., 1999), induce cell growth (Cole and Cowling, 2008), increase the 'stemness' in cancer cells (Poli et al., 2018), and to remodel the tumour microenvironment towards a tumour favourable environment (Kortlever et al., 2017), makes high expression of MYC a negative prognostic marker for renal cancer, urothelial cancer and ovarian cancer (Uhlen et al., 2017). High expression or translocations of MYC in DLBLC, combined with BCL2 overexpression or translocations, are defined as so called 'double hit' DLBCL. Patients with 'double hit' DLBCL have worse clinical outcome (Riedell and Smith, 2018). Furthermore, in MM increased protein or expression level are also correlated with worse patient outcome (Chng et al., 2011). Furthermore, in breast cancer high MYC expression and amplifications are associated with the basal type breast cancer, considered the most aggressive subtype (Xu et al., 2010). MYC's paralog MYCN is also often associated with worse patient outcome: MYCN amplifications are observed in neuroblastoma (NB) and a sign of more aggressive disease (Huang and Weiss, 2013). MYCN is also involved in other malignancies of the nervous system, such as medulloblastoma, retinoblastoma and glioblastoma multiforme, but also in non-neuronal tumours, such as acute myeloid leukaemia (AML), prostate cancer and pancreatic cancer, and is often associated again with more aggressive disease and worse clinical outcome (Rickman et al., 2018).

In conclusion, MYC might be one of the key oncogenes (Dang, 2012; Gabay et al., 2014), with deregulation through various means observed in most cancer subtypes (Kalkat et al., 2017). It is considered to be potentially 'the' weak point (Sodir and Evan, 2011) in cancer, and is in addition associated with worse clinical outcome across different types of cancer. Unsurprisingly, targeting MYC has become a major effort of the drug discovery field, be it in academic or industrial settings–the topic of the next subchapter.

1.5 The 'holy grail' of cancer drug discovery?

Due to its vast implication in cancer the following questions arise: could we treat cancer if MYC or the MYC driven oncogenic program are targeted? Is there a therapeutic window for MYC inhibition? Conditional ablation of MYC causes cancer regression through apoptosis, differentiation and growth arrest, in various mouse models (Arvanitis and Felsher, 2006). Omomyc, a protein-based inhibitor, can efficiently suppress the dimerization of MYC and MAX (Soucek et al., 1998), enhancing MYC driven apoptosis in vitro, and in vivo (Soucek et al., 2004). Systemic, transient expression of Omomyc effectively blocks formation and maintenance of a $KRAS^{G12D}$-driven lung cancer model. It also causes regression in established lung tumours, and while it affects negatively healthy tissue, these degenerative phenotypes are reversible upon restoration of MYC function (Soucek et al., 2008). The same observations were made with a mouse model of glioma, a highly aggressive brain cancer (Annibali et al., 2014). This led to the idea that targeting MYC could be a viable strategy to combat cancer (Sodir and Evan, 2011). Three different methods have been applied over the years: direct targeting, usually aiming at disrupting the interaction between MYC and MAX; reduction of MYC levels through targeting transcription or translation; or uncovering synthetic lethalities due to high expression of MYC.

1.5.1 Direct targeting: the problem of small molecules

An initial report described two small molecule inhibitors of the MYC-MAX interaction: 10058-F4 (**13** in Figure 1-14) and 10074-A4 (**14** in Figure 1-14) (Yin et al., 2003). To note is the large concentrations needed to inhibit the growth in mammalian fibroblasts in this report: 64 μM for 10058-F4 and 39 μM for 10074-A4. Other publications which also used these inhibitors, tend to incubate the cells with very high concentrations, ranging from 50 μM for 10058-F4 in ESCs (Rahl et al., 2010) to 75 μM to disrupt the MYCN-MAX inhibition in a NB cell line (Zirath et al., 2013). The high concentrations needed make off-target effects quite likely, and make these inhibitors not suitable for the clinic.

Recently, a research group used a virtual screen to identify potentially optimised MYC-MAX inhibitors. They identified PKUMDL-YC-1205 (**15** in Figure 1-14) as the

best binder. In cellular assays, it proved to be less potent than 10074-A4 and to have a similar potency to 10058-F4 (however, again in the micromolar range) (Yu et al., 2016). So far, (potent) small molecule inhibition of the MYC-MAX interaction has proven very difficult due to its intrinsic disordered nature of MYC. Most approaches utilising different scaffolds have failed, with many scaffolds being annotated as so-called PAINS (pan-assay interference compounds) (McKeown and Bradner, 2014). Recently, it was shown that Omomyc has an intrinsic cell-penetrating capacity, which makes targeting of a $KRAS^{G12D}$ driven lung cancer model via direct pulmonary administration possible (Beaulieu et al., 2019). It remains to be seen, if other administration routes are feasible, upon further modification of Omomyc.

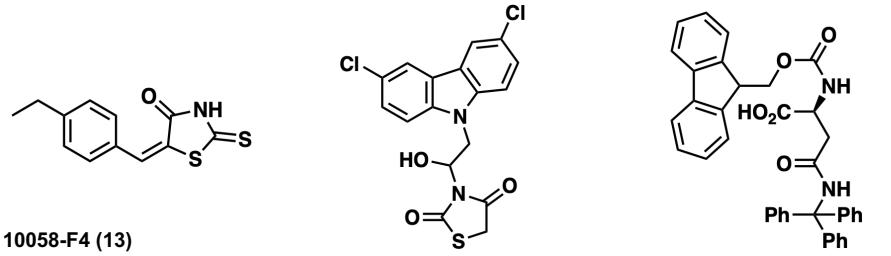

Figure 1-14: Example inhibitors of MYC-MAX interaction
Equilibrium dissociation constants (K_D) extracted from the (Yu et al., 2016)

1.5.2 Reduction of MYC copies through targeting transcription, translation and stability

In 2011 two papers described the dependency of leukaemia and lymphoma cell lines to BRD4, utilising a shRNA for chromatin modifying proteins and the BRD2/3/4 specific inhibitor JQ1 (Filippakopoulos et al., 2010; Mertz et al., 2011; Zuber et al., 2011). Both papers show that the BRD4 inhibition causes reduction in MYC levels and collapse of the MYC-driven transcriptional program (Mertz et al., 2011; Zuber et al., 2011). Mechanistical studies into this sensitivity towards BRD4 inhibition linked the effects to the disruption of SE elements, with large accumulation of BRD4 on the SE of key oncogenes (Chapuy et al., 2013; Loven et al., 2013). Also, CDK7i can disrupt in a similar fashion SEs in MYCN amplified neuroblastoma (Chipumuro et al., 2014). Those effects are, however, not MYC-specific and different cancers with 'transcriptional addiction' (a term used to describe the specific

dependence of cancer, due to specific gene expression deregulation, to certain regulators of transcription such as BRD4 (Bradner et al., 2017)), such as triple negative breast cancer (Wang et al., 2015b) or T cell acute lymphoblastic leukaemia (ALL) (Kwiatkowski et al., 2014) can be, in theory, targeted with CDK7 inhibition. CDK9 inhibition also disproportionally yields in a reduction of MYC transcripts, through likely similar mechanisms (Garcia-Cuellar et al., 2014).

Instead of disrupting MYC transcription, it was proposed to alternatively target MYC protein levels through, on the one hand, targeting its translation via mTOR/AKT inhibition (Frost et al., 2004; Yu et al., 2001) or, in general, via disruption of translation (Manier et al., 2017). On the other hand, MYC protein levels can also be targeted by reducing its stability. It has been shown that the deubiquitination of MYCN via USP7 stabilises the protein and that small molecule inhibition or RNAi mediated knockdown causes MYCN level reduction and reduced tumour growth. USP7 is also a marker of poor prognosis in neuroblastoma, through potentially this mechanism (Tavana et al., 2016). The clinical state of those different approaches will be discussed in section 1.5.4.

1.5.3 Concepts of synthetic lethality

The last concept to target MYC is through exploiting vulnerabilities, coming from aberrant activation of the MYC program: in short, uncovering synthetic lethalities with deregulated MYC expression. One of those approaches is to target CDK1, master regulator of the cell cycle progression (Malumbres, 2014). It was previously described that pan-CDKi (more specifically targeting CDK1, 2, 5 and 9) is more toxic in MYC driven triple negative breast cancer (Horiuchi et al., 2012). Further studies in breast cancer identified CDK1 as the mediator, within the cell cycle CDKs, to drive this synthetic lethality (Kang et al., 2014).

Another approach aims at exploiting MYC induced replication stress and amplify it. CHK1 was identified in an RNAi screen, specifically targeting kinases, as a therapeutic target in neuroblastoma (Cole et al., 2011). Loss of ATR (upstream of CHK1) delayed disease progression in the Eμ-myc mouse model, and CHK1 inhibition was shown to specifically kill a MYC driven pancreas mouse model, but not cause increased replication stress in a $KRAS^{G12V}$ pancreas mouse model (Murga et

al., 2011). Supporting this hypothesis, murine lymphoma cells, driven by ectopic MYC expression, were responsive to CHK1 inhibition (Ferrao et al., 2012).

In a synthetic lethality screen to identify genes that were lethal upon knockdown, comparing MYC normal and MYC overexpressing human mammary epithelial cells, BUD31, part of the core spliceosome, was identified. The dependency of MYC high cells on the spliceosome was confirmed with the RNAi of several core spliceosome proteins, such as SF3B1, U2AF1 and SNRPF (Hsu et al., 2015). Supporting the increased sensitivity of MYC high cells to disturbance of the splicing machinery, homozygous loss of Prmt5, also part of the spliceosome, in the background of the Eμ-myc model delayed lymphomagenesis. Additionally, PRMT5 KD was shown to reduce the proliferative capacity of human BL cell lines (Koh et al., 2015). These data are interesting in the light of a recently published, orally bioavailable, splicing modulator H3B-8800, initially developed against spliceosome mutant cancers (Seiler et al., 2018b).

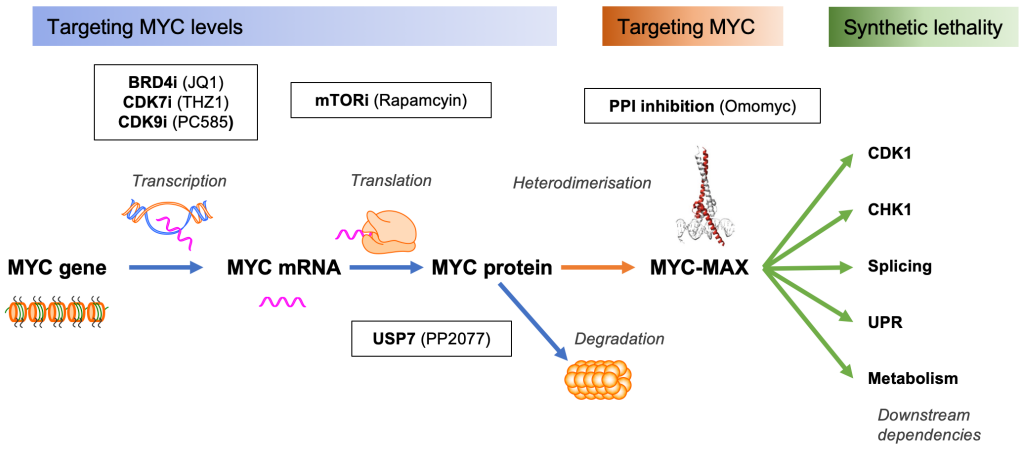

Figure 1-15: Targeting MYC

Approaches to target MYC are based on three methods: firstly, targeting the levels, through either inhibiting the transcription via BRD4, CDK7 or CDK9 inhibition; reducing its protein levels through targeting translation via e.g. mTOR inhibition; or reducing its protein levels through manipulating its stability, with e.g. targeting specific deubiquitination enzymes, such as USP7 for MYCN. Secondly, directly targeting its activity, usually by blocking the protein-protein interaction with MAX, with e.g. Omomyc. The third approach is based on targeting increased dependencies due to high levels of MYC, such as targeting CDK1 for the cell cycle, CHK1 for increased replication stress, the splicing machinery, components of the unfolded protein response (UPR), or different proteins involved in the MYC rewired metabolism.

Targeting two out of the three arms of the unfolded protein response (UPR) (Hetz, 2012) has recently been shown to be a potential viable strategy against MYC-driven cancers. Chemical and genetic inhibition of XBP1 in isogenic models with inducible MYC and MYCN and in BL cell lines showed a synthetic lethality (Xie et al., 2018). Targeting the same IREα/XBP1 arm, showed increased dependence of the MYC-driven breast cancer on the upstream RNAse IRE1 (Zhao et al., 2018). Additionally, targeting the PERK arm of the UPR through genetic ablation of ATF4 or small molecule inhibition of PERK delays tumour progression of MYC driven models (Tameire et al., 2019).

It has been shown that MYC alters the metabolic program of the cells, so that they become glutamine-addicted. This led to the idea that one could potentially target this increased demand on glutamine (Wise et al., 2008). Additionally, MYC also regulates different essential amino acid transporter, and knockdown of two of them, SLC7A5 and SLC43A1, reduces growth of MYC-driven models (Yue et al., 2017). This indicates that one could potentially exploit this rewired metabolism and target it (Wise and Thompson, 2010). A summary of the different approaches to target MYC is shown in Figure 1-15.

1.5.4 Where do we stand in the clinic?

The initial excitement of bromodomain inhibition was dampened after the results of the first clinical trials showing limited efficacy and high toxicity of different bromodomain inhibitors that reached the clinic. Current approaches are aiming at combination of the bromodomain inhibitors with other anti-cancer agents (Doroshow et al., 2017; Pervaiz et al., 2018). CDK7 inhibition is being evaluated against different transcriptionally addicted cancers, with a focus on solid tumours, with SY-1365 (Hu et al., 2019) and ICEC0942 (Patel et al., 2018b) being now tested in phase I clinical trials (SY-1365, ClinicalTrials.gov identifier: NCT03134638; ICEC0942, also known as CT7001, ClinicalTrials.gov identifier: NCT03363893). Various other CDK inhibitors reached the clinic, and two pan CDK inhibitors, Dinaciclib and AT7519, are currently being evaluated in clinical trials (Whittaker et al., 2017). Some AKT and mTOR inhibitors have been approved by the Food and Drug Administration (FDA) against haematological malignancies and renal carcinoma; however, not specifically

against MYC deregulated cancers (Song et al., 2019). Despite its attractiveness as a drug treat cancer (Sodir and Evan, 2011), there is not a single approved drug targeting specifically MYC deregulated cancers. There is a clear unmet clinical need to identify further and innovative strategies to target this protooncogene thought to be deregulated through different means in over 50% of all human cancers (Gabay et al., 2014).

Chapter 2. Pharmacogenomics screens identify haematological malignancies as highly responsive to NMT inhibition

2.1 Introduction

Traditionally, until the end of the 20th century cancer treatment was based on three pillars: cytotoxic chemotherapy, radiation therapy and surgical removal. Recent developments in drug discovery in oncology added two new pillars: targeted therapies, aiming at exploiting genetic vulnerabilities of cancer cells; and more recently, the use of the patients' immune system, to fight the cancer, in form of e.g., checkpoint inhibition and genetically modified T cells (Marshall and Djamgoz, 2018; Oiseth and Aziz, 2017; Tang et al., 2018). The immuno-oncology landscape has rapidly expanded in recent years (Tang et al., 2018); nonetheless, targeted therapies, designed to exploit the genetic program of cancer cells to reduce harm to normal tissue, are still the standard-of-care for several cancer types in the clinic: with the early discoveries of the beneficial effects of Tamoxifen administration to estrogen receptor (ER) positive breast cancer patients (Clemons et al., 2002), depriving androgen receptor (AR) dependent prostate cancer from its crucial hormone (Taplin and Balk, 2004), targeting specifically the 'Philadelphia' chromosome in chronic myeloid leukaemia (CML) (An et al., 2010), to PARP inhibition against BRAC1/2-deficient breast cancer (Fong et al., 2009), treating EGFR mutant non-small-cell lung cancer (NSCLC) with specifically designed drugs (Lee, 2017; Sridhar et al., 2003), BRAF inhibition in V600E mutant melanoma (Sosman et al., 2012), or recently approved CDK4/6 inhibitors in hormone receptor positive (RB wild type) breast cancer (Goel et al., 2018). Approaches to target the spliceosome in spliceosome-mutant cancers, that is cancers with mutations in some spliceosome subunits, which have been shown to be highly responsive to splicing modulation, is another example that might reach soon clinical trials (Seiler et al., 2018b), and many more drugs are currently in different stages of the drug discovery pipeline (Patterson et al., 2016). However, for approved and new experimental drugs genetic markers which allow for more personalised treatments are often not known. As an example, PARP inhibitors were initially developed to sensitise cancer cells to typical DNA damaging therapy,

and it was only later appreciated that they can work as single-agents in BRCA-deficient breast and ovarian cancers (Drew, 2015). One approach to identify genetic markers or transcriptional profiles correlating with outcome is pharmacogenomics screening in immortalised cancer cell lines: dozen to hundreds of different (anti-cancer) drugs are screened against large numbers of immortalised cancer cell lines, from e.g. the Catalogue of Somatic Mutations in Cancer (COSMIC) project. The results are linked back to sequencing data from those cancer cell lines, to test if certain mutations, chromosomal rearrangements, epigenetics, copy number (CN) gains or losses in a given gene render a cancer cell line more sensitive (or resistant) against the respective drug. Research teams from the Broad Institute within the Cancer Cell Line Encyclopaedia (CCLE) project (Barretina et al., 2012) and the Sanger Institute within the Genomics of Drug Sensitivity in Cancer (GDSC) project (Garnett et al., 2012; Yang et al., 2013) applied this approach to a large number of commonly used immortalised cancer cell lines with different (anti-cancer) drugs. Those large screening efforts identified known genomic markers for certain drugs (e.g. TP53 WT vs mutant for MDM2 inhibitors such as Nutlin-3a) validating the approach.

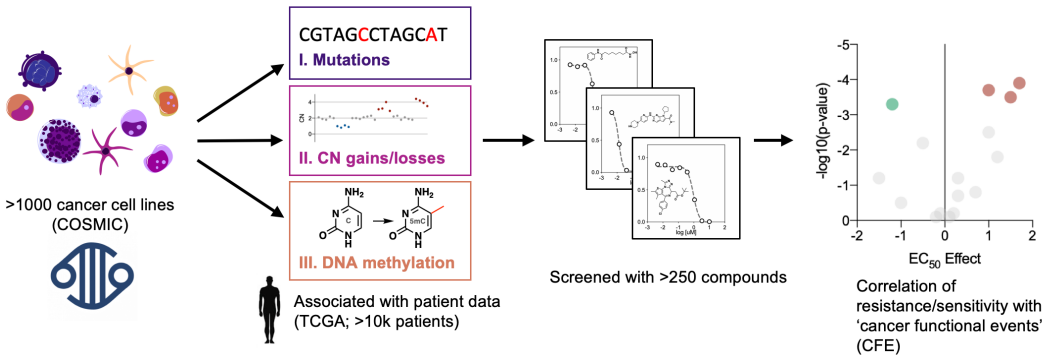

Figure 2-1: Principle of the pharmacogenomic screening of drugs.

The >1000 cancer cell lines, encompassing the COSMIC project, were subjected to sequencing to call mutations, CN gains/losses and DNA methylation. These data were correlated with the sequencing data from patients, to identify overlaps between the patients and cancer cell lines. Additionally, gene expression profiling was conducted on all of the cell lines. >250 different chemical compounds were screened against the cancer cell lines (median screened cell lines: 878; range: 366 to 935) and ANOVA tests were used to identify if any CFEs correlate with sensitivity or resistance. See (Iorio et al., 2016)

Novel correlations were also identified, such as that plasma cell-related tumours are more responsive to IGF1 receptor inhibitors; or that EWS-FLI1 rearrangement sensitises cells to PARP inhibitors (Barretina et al., 2012; Garnett et al., 2012). More recently, the Sanger Institute combined this approach with patient sequencing data, such as from The Cancer Genome Atlas (TCGA) (Lawrence et al., 2013; Zack et al., 2013) to obtain more clinically relevant information about which 'cancer functional events' (CFEs) observed actually in patients, correlated with resistance/sensitivity to a given drug (see Figure 2-1). The research team also analysed to what extent the repertoire of commonly used cancer cell lines represents the clinical reality in terms of the landscape of CFEs. In addition, they assessed in this study the predictive ability of gene expression, tissue origin, methylation on CpG islands, recurrently abnormal copy number segments (RACS) and mutations to determine the sensitivity to a given cancer drug, with gene expression and tissue origin being the most predictive ones (Iorio et al., 2016). While pharmacogenomics screens, in immortalised cancer cell lines, are a powerful tool, there have been controversies about reproducibility between screens conducted at different institutes (Cancer Cell Line Encyclopedia and Genomics of Drug Sensitivity in Cancer, 2015; Haibe-Kains et al., 2013; Haverty et al., 2016). This could be potentially due to genetic and transcriptional discrepancies between the supposedly same cancer cell lines, used in different institutes and research centres (Ben-David et al., 2018; Liu et al., 2019). Nevertheless, such screening remains an initially very powerful tool to identify genetic markers for drug sensitivity and resistance, especially for drugs for which little is known about their underlying mode of action or which did not reach yet clinical trials, hence lack patient data. Thus, the Tate laboratory collaborated with the Sanger Institute to screen three different NMT inhibitors, from two structurally different series: two are based on the aminomethylindazole scaffold and one is based on the pyrazole sulphonamide (see section 1.2.2). The results of these screens are presented in this chapter, as well as the implication for NMT inhibition as a novel target in cancer.

2.2 Results

2.2.1 Comparison of the previously reported data and the newly published data for IMP366

Initially, the Tate laboratory collaborated with the Sanger Institute to screen IMP366, also known as DDD85646 (Frearson et al., 2010) or in the GDSC data as ICL1100013 (Iorio et al., 2016) (see Figure 1-10 for the structure), in >900 cancer cell lines and this initial (unpublished) data set was analysed by a former PhD student, Siak Gee Lim (Lim, 2016). The potency values were generated using a Bayesian sigmoid model (Garnett et al., 2012). However, the Sanger Institute changed their methodology of modelling the EC_{50}s of a given drug since the initial publication in 2012 (Garnett et al., 2012), utilising now a multilevel fixed effects model (Vis et al., 2016), and published the new values on their portal: www.cancerrxgene.org (Yang et al., 2013).

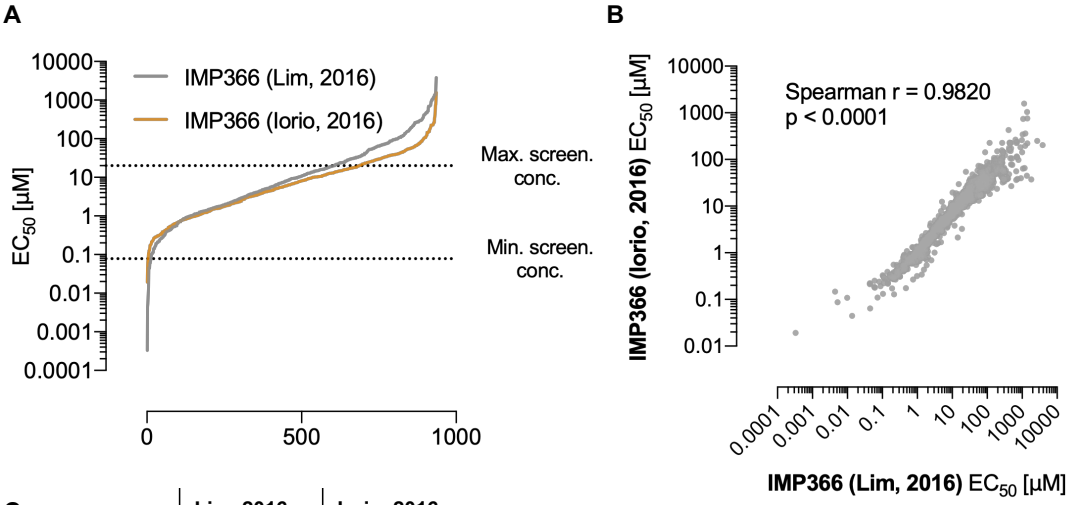

C

	Lim, 2016	Iorio, 2016
Median	9.30 µM	6.73 µM
Max	3834 µM	1570 µM
Minimum	3 pM	19.3 nM
Range	$1.16 \cdot 10^7$	$8.13 \cdot 10^4$

Figure 2-2: Differences between the two models used by the Sanger for IMP366.

[A] Range of the EC_{50}s of the previously analysed, unpublished 'Lim, 2016' data set and the now published 'Iorio, 2016' data set, within the screened concentrations. **[B]** Correlation between 'Lim, 2016' data set and the 'Iorio, 2016' data set. **[C]** Table with the reported median, maximum, minimal and range of the EC_{50}s.

The initially reported and unpublished (referred to as 'Lim, 2016' based on the Bayesian sigmoid model) and now officially published EC_{50}s on the GDSC portal (referred to as 'Iorio, 2016', based on the multilevel fixed effects model) differ in dynamic range (see Figure 2-2 A), however they correlate with high statistical significance (see Figure 2-2 B).

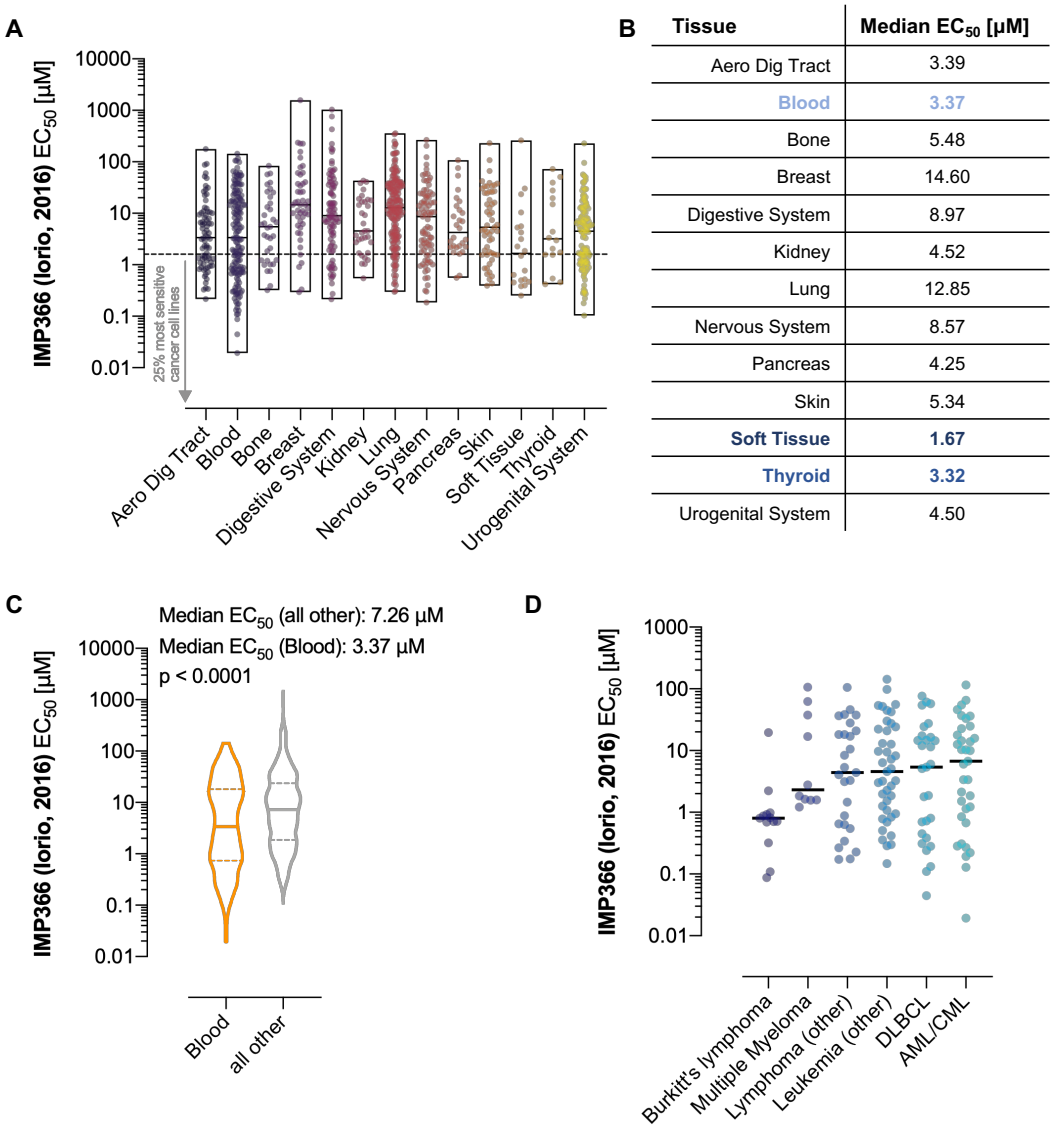

Figure 2-3: Cancer cell lines of the tissue subgroup Blood, in particular Burkitt's lymphoma, are enriched for the most responsive cell lines to IMP366.

[A] Distribution of the reported EC_{50}s across the different tissue groups. **[B]** Median EC_{50}s of the different tissue subgroups. The blue coloured groups are the three most sensitive. **[C]** Cancer cell lines, within the tissue group Blood, are more responsive to IMP366 compared to the other cancers (p-value determined with the Mann-Whitney test). **[D]** Distribution of the EC_{50}s of the different haematological malignancies, comprising in the tissue group Blood.

As expected from the multilevel fixed effects model, the difference between maximal and minimum reported EC_{50}s was strongly reduced (see Figure 2-2 C). The previous analysis was conducted with the EC_{50}s values (based on the Bayesian sigmoid model), thus, the new data set was reanalysed and compared to the previous data set. The initial trends, derived from the 'Lim, 2016' data set still hold true (Lim, 2016): the median EC_{50}s from cancer cell lines within the tissue classes Soft Tissue and Thyroid are the lowest (1.67 µM and 3.32 µM respectively) (see Figure 2-3 A and B). However, the most sensitive cancer cell lines overall reside within the Blood tissue class, comprising lymphoma, leukaemia and multiple myeloma cancer cell lines (see Figure 2-3 C). Within these haematological malignancies, BL cell lines are particularly responsive (see Figure 2-3 D), confirming the initial results (Lim, 2016). Interestingly, the Sanger Institute could not find any CFEs correlating with sensitivity to IMP366 (the ANOVA results for all three inhibitors are in section 2.2.2).

2.2.2 Haematological malignancies are highly responsive to the NMT inhibitors IMP1031 and 1036

The Tate laboratory developed, through fragment derivation, a new ultra-potent class of NMT inhibitors, based on the aminomethylindazole scaffold (Bell et al., 2017; Mousnier et al., 2018). Two examples of this series of inhibitors were screened, in collaboration with the Sanger Institute, in 708 cancer cell lines in a second screen batch, that is at a different point of time, compared to the screen of IMP366. The structures and enzymatic potencies of IMP1031 and IMP1036 are shown in Figure 2-4 A (Bell et al., 2017). 96% of the cancer cell lines screened with these two inhibitors are shared with the screen of IMP366 (see Figure 2-4 B) and the overall representation of tissue classes is very similar between the two screen batches (see Figure 2-4 C). Some of the EC_{50}s, provided by the Sanger Institute, are outside of the actual experimental screening range (see Figure 2-4 D) and have been extrapolated, based on their methodology. Nevertheless, the reported EC_{50}s follow the trend of enzymatic potency, with IMP1031 being more potent. Additionally, there is an excellent correlation between the reported values between the two inhibitors (see Figure 2-4 E), with a slight shift in the Spearman coefficient towards IMP1031,

representing its increased cellular potency. The correlations between IMP1031/1036 and the previously screened IMP366 are less strong (see Figure 8-1).

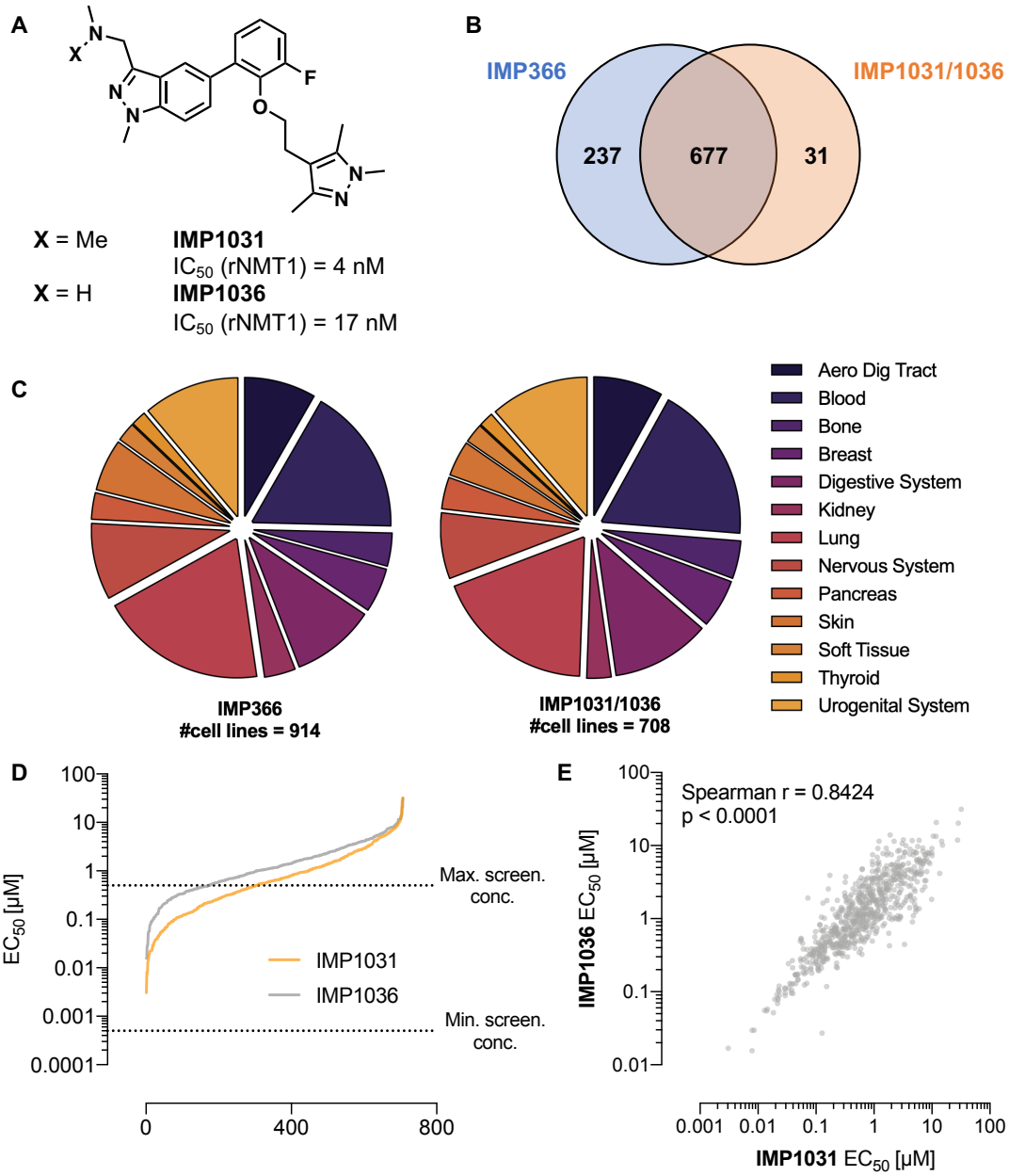

Figure 2-4: Structure of IMP1031 and 1036, tested cell lines, and correlation between the potencies.

[A] Structure of IMP1031 and IMP1036 and their respective potency against recombinant NMT1 (rNMT1). **[B]** Overlap and differences of the screened cell lines between the three screens. **[C]** Distribution of the cell lines, according to tissue subtype, between the screens (left: IMP366, right: IMP1031/1036). **[D]** Range of the EC_{50}s of IMP1031 and IMP1036 within the screened concentrations. **[E]** Correlation between the reported EC_{50}s of IMP1031 and IMP1036.

This is likely due to batch effects, more precisely the different years and conditions in which the compounds have been screened. Additionally, the reported maximum EC_{50} for IMP366 is 1570 µM, compared to slightly over 30 µM for the two other inhibitors (See Table 2-1).

Table 2-1: Median, maximum and minimum EC_{50}s of all the NMTi screened.

Compound	Median EC_{50}	Maximum EC_{50}	Minimum EC_{50}	Dynamic Range
IMP1031	638 nM	32 µM	3 nM	1.0×10^4
IMP1036	1.16 µM	31 µM	17 nM	1.8×10^3
IMP366	6.73 µM	1570 µM	19 nM	8.1×10^4

Potentially, this due to the different concentration ranges used in the screens (500 nM to 500 pM for IMP1031 and 1036, and 20 µM to 78 nM for IMP366), combined with the methodology to extrapolate potency, utilising the values of all other tested drugs. The extrapolated EC_{50}s should therefore not necessarily be interpreted as absolute values, but indicate trends in cancer cell line sensitivity to a given inhibitor.

Similar to IMP366 the tissue group Blood was enriched with the most sensitive cell lines (compared to IMP366 also by median EC_{50}) for IMP1031 (see Figure 2-5 A & B) and IMP1036 (see Figure 8-2). These haematological malignancies were significantly more sensitive, compared to all the others (see Figure 2-5 C), and in line with the data from IMP366, BL cancer cell lines were particularly responsive to IMP1031 (see Figure 2-5 D) and IMP1036 (see Figure 8-2). While haematological malignancies consist of some of the most sensitive cancer cells, several other tissue groups, such as the Bone, Soft Tissue, Nervous System, and Aero Digestive Tract tissue groups also contain cancer cells with high responsiveness to NMT inhibition. This demonstrates that sensitivity to NMT inhibition is not solely driven by cancer cell line origin from the haemopoietic system.

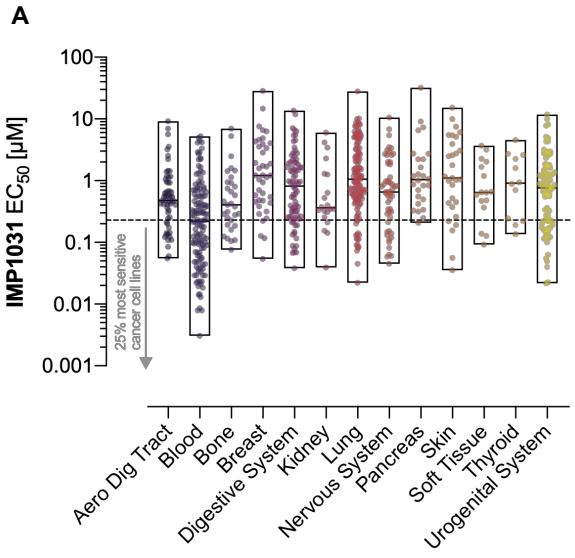

B

Tissue	Median EC50 [µM]	
	IMP1031	IMP1036
Aero Dig Tract	0.48	1.15
Blood	**0.22**	**0.56**
Bone	**0.40**	1.13
Breast	1.22	1.70
Digestive System	0.81	1.86
Kidney	**0.36**	**0.87**
Lung	1.05	1.40
Nervous System	0.65	**1.06**
Pancreas	1.04	1.81
Skin	1.11	1.68
Soft Tissue	0.64	1.24
Thyroid	0.91	2.02
Urogenital System	0.77	1.14

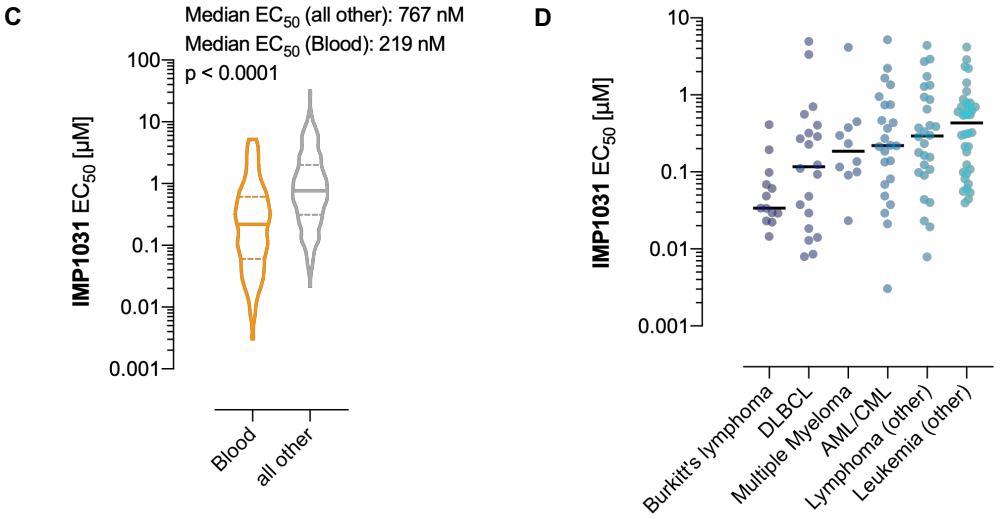

Figure 2-5 Cancer cell lines of the tissue subgroup Blood, in particular Burkitt's lymphoma, are enriched in the most responsive cell lines to IMP1031.

[A] Distribution of the reported EC_{50}s across the different tissue subgroups. **[B]** Median EC_{50}s of the different tissue subgroups. The blue coloured groups are the three most sensitive for the respective NMT inhibitor. **[C]** Cancer cell lines, within the tissue group Blood, are more responsive to IMP1031 compared to the other cancers. **[D]** Distribution of the EC_{50}s of the different haematological malignancies, comprising the tissue group Blood.

The Sanger Institute reported different CFEs correlating with sensitivity and resistance for IMP1031 and IMP1036 (and none for IMP366). However, after correcting for multiple hypothesis testing, none of those correlated significantly (FDR < 0.05) with sensitivity or resistance (see Table 2-2).

Table 2-2: Reported CFEs for the different NMTi:

Compound	Feature	ΔMean EC_{50}	ANOVA p-value	FDR [%]
IMP1031	Loss.cnaPANCAN381..ARFGAP3	**0.8**	$1.44e^{-04}$	11.22
	MAP3K1_mut	**-1.49**	$1.70e^{-04}$	12.17
IMP1036	BBRM1_mut	**-0.58**	$6.93e^{-04}$	23.2
IMP366	NA	NA	NA	NA

Red indicates resistance correlating with this feature. Green indicates sensitivity correlating with this feature. This data was provided by the Sanger institute.

It has been proposed in different patents that NMT2 deficient cancers are particularly responsive to NMT1/2 inhibitors (Berthiaume and Beauchamp, 2017; Berthiaume et al., 2014); however, neither NMT1 nor NMT2 mRNA expression correlated with sensitivity to IMP1031 (see Figure 2-6 A & B). The same is observed for IMP1036 and IMP366 (see Figure 8-3). Indeed, haematological malignancies have lower NMT2 expression and similar NMT1 expression, compared to other cancer cell lines (see Figure 2-6 C), but the lack of correlation of sensitivity to IMP1031 and NMT2 mRNA expression across different cancer cell lines indicates that NMT2 deficiency is not a predictor for responsiveness to NMT inhibition. Another potential parameter, which could affect the efficacy of a given drug is doubling time. These were obtained from the CCLE (Barretina et al., 2012), and indeed correlate with sensitivity to IMP1031. Importantly, not all cancer cell lines have their doubling times determined in the CCLE, so only a subset of the cancer cell lines could be used in this analysis: 249 out of 708 cancer cell lines (35%) for IMP1031/1036 and 318 out of 914 (35%) for IMP366. This also had an impact on the tissue distribution, compared to the original screens, potentially introducing sampling errors (see Figure 8-4 A). Additionally, there might be variation in culturing methods between the two institutes, hence, there might be additional variation in the reported doubling times of a given cancer cell line.

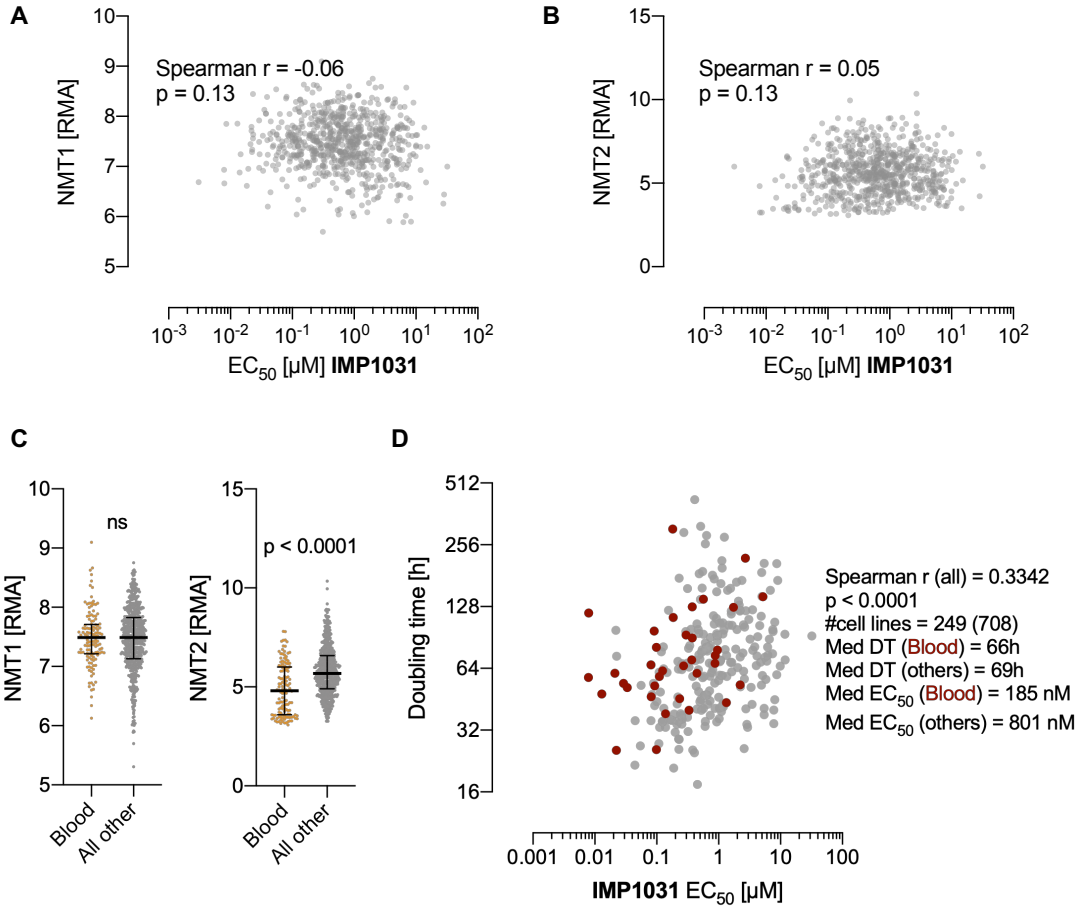

Figure 2-6: Sensitivity towards IMP1031 does not correlate with NMT1/2 expression, but correlates with doubling time.

[A] Correlation between sensitivity to IMP1031 and NMT1 expression in all cancer cell lines. **[B]** Correlation between sensitivity to IMP1031 and NMT2 expression in all cancer cell lines. **[C]** Cancer cell lines from the Blood tissue subgroup have similar NMT1 expression and lower NMT2 expression, compared to the other cancer cell lines (error bars: interquartile range; p-value obtained with Mann-Whitney test). **[D]** Correlation between sensitivity to IMP1031 and doubling time of the cell lines (249 out of 708 cancer cell lines had a corresponding doubling time). Red dotes comprise cancer cell lines of the tissue subgroup 'Blood'.

While a correlation between doubling time and sensitivity to IMP1031 is observed, this does not suffice to explain the increased sensitivity of haematological malignancies (which have a correlation of Spearman r = 0.3889; p-value = 0.0213, thus, very comparable to the overall trends). The median doubling time is only marginally lower (66 h), compared to other cancer cell lines (69 h), while a strong difference in median EC_{50} (3-fold) is observed between the cancer cells from the Blood group, compared to all others (see Figure 2-6 D). Similar to IMP1031, also for IMP366 and IMP1036 there is a correlation between doubling time and sensitivity;

however, again doubling time does not seem to account for the strongly increased sensitivity of the Blood tissue group for IMP1036 and IMP366 (see Figure 8-4 B & C).

As there have been controversies around the reproducibility of pharmacogenomic screens (Haibe-Kains et al., 2013), a dozen cancer cell lines were tested in-house with the CellTiter Blue assay (see CellTiter Blue assay) with IMP1031 and IMP1036 to assess reproducibility of the reported data. Haematological malignancies were emphasised in these experiments.

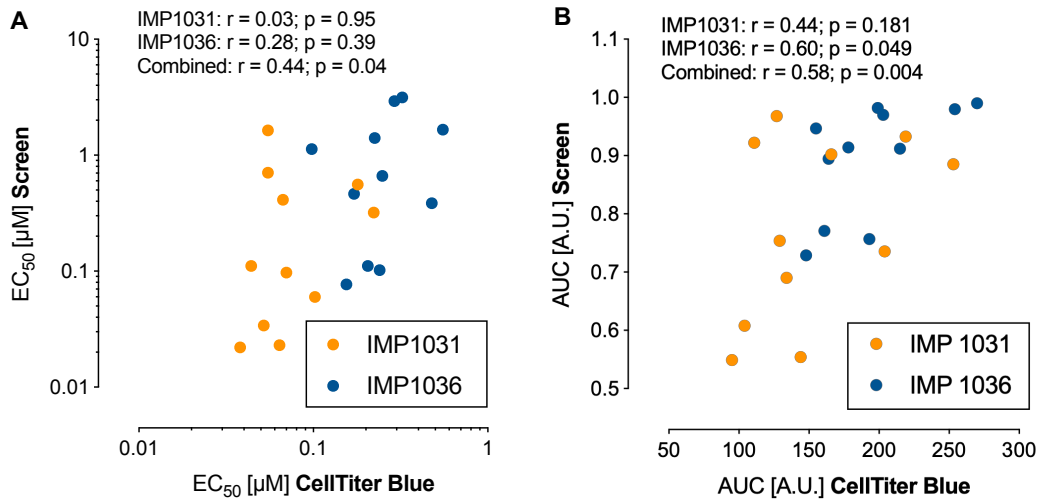

Figure 2-7: Good reproducibility in overall trends for the reported AUC; less so for the EC_{50}s.

[A] Correlation between all the EC_{50}s, provided by the Sanger institute, and all the EC_{50}s, assessed in-house with the CellTiter Blue assay. **[B]** Correlation between all the AUCs, provided by the Sanger institute, and all the AUCs, assessed in-house with the CellTiter Blue assay.

In the case of the EC_{50}s, there is a trend for correlation for IMP1036 (which does not reach significance), and no correlation for IMP1031. Only if both inhibitors are combined there is a significant correlation between the results of the screen and the in-house screening with the CellTiter Blue assay (see Figure 2-7 A). To note is that the Sanger reported EC_{50}s for both inhibitors of >1 µM, which were not reproduced by the in-house CellTiter Blue assay results. On the other hand, the area-under-curve (AUC) correlated better between the reported values by the Sanger Institute and the in-house results, that is with higher Spearman correlation coefficients and higher statistical significance (see Figure 2-7 B). These results likely stem from the

differential assessment of potency: whereas the Sanger Institute uses an algorithm to assess simultaneously the potency of 100 of compounds across 100s of cancer cell lines and infer some of the potencies, based on observations with other inhibitors (Vis et al., 2016), the in-house results were calculated individually fitted to a sigmoidal function (see Figure 8-5). A similar trend is observed for IMP366 and IMP1088: the EC_{50} range does not change much between the different cancer cell lines; however, the more resistant cell lines still show residual metabolic activity (shown in section 2.2.4). Overall, this indicates that the EC_{50}s reported by the Sanger Institute are likely a mixed read-out between EC_{50} and residual metabolic activity, compared to the CellTiter Blue assay-based assessment of potency.

To conclude, there is a clear trend across the three different NMT inhibitors, screened in two different batches in terms of years, for haematological malignancies to be the most responsive cancer types. Nevertheless, also cancer cell lines with different tissue origin also showed responsiveness to NMT inhibition, indicating that tissue origin *per se* does not suffice to explain this sensitivity. The proposed concept, within the patent sphere, of NMT2-deficiency rendering cells more susceptible to NMT inhibition was not confirmed for any of the three inhibitors; nor does NMT1 expression influence the potency of the three inhibitors. Variation in doubling times in the cancer cell lines does not satisfactorily explain the differential responsiveness to NMT inhibition between the Blood tissue group, compared to the others. Nor did any of CFEs, tested for by the Sanger Institute, correlate significantly with sensitivity or resistance. To conclude, likely a feature highly prevalent in the haematological malignancies exists (which is also present in some other cancer cell lines originating from different tissues) that confers these cancer cell lines with a strong susceptibility to NMT inhibition.

2.2.3 Mutations or expression of NMT substrates as markers for sensitivity or resistance

The effects of NMT inhibition are driven by modulation of the NMT substrates, through potential gain-of-function (GOF) or loss-of-function (LOF), hence one could argue that mutations and/or expression patterns of the NMT substrates might be responsible for differential effects of an NMT inhibitor across cancers. To address

this question, whole genome expression data in form of micro-array data and pre-processed sequencing data with called mutations across all the genes were obtained from the Sanger Institute (Iorio et al., 2016). These data were combined with CoTMyr NMT substrates identified in humans, for which strong proteomics or other biochemical validation was available (Broncel et al., 2015; Kallemeijn et al., 2019; Mousnier et al., 2018; Thinon et al., 2014; Utsumi et al., 2018).

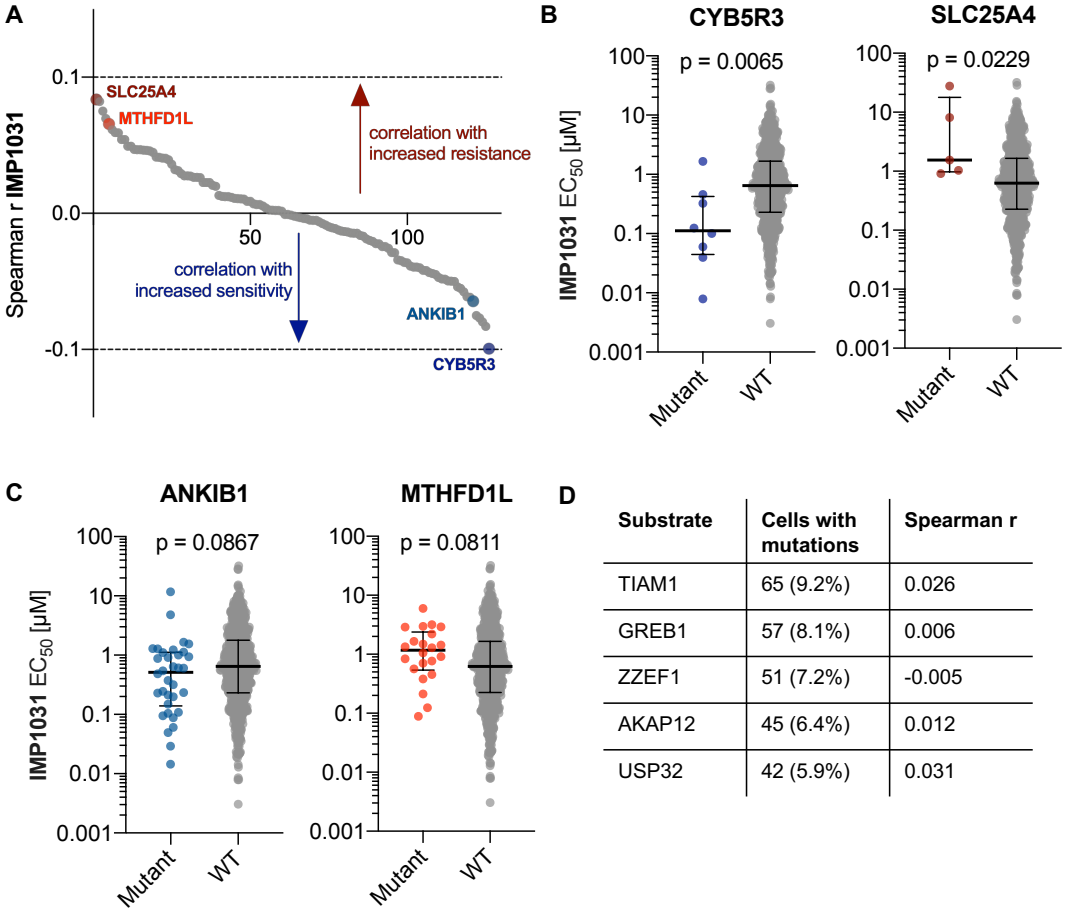

Substrate	Cells with mutations	Spearman r
TIAM1	65 (9.2%)	0.026
GREB1	57 (8.1%)	0.006
ZZEF1	51 (7.2%)	-0.005
AKAP12	45 (6.4%)	0.012
USP32	42 (5.9%)	0.031

Figure 2-8: (Rare) Mutations in some NMT substrates correlate weakly with sensitivity or resistance.

[A] Summary graph of all the Spearman coefficients for the correlation between mutations in a given NMT substrate and sensitivity to IMP1031. **[B]** Left: CYB5R3 mutations are significantly correlated with increased sensitivity; right: SLC25A4 mutations are significantly correlated with increased resistance. **[C]** Left: Cells with ANKIB1 mutations have a trend of increased sensitivity; right: Cells with MTHFD1L mutations have a trend of increased resistance. (p-values determined with the Mann-Whitney test, error bars = interquartile range) **[D]** Table of the top5 NMT substrates with the biggest prevalence of mutations and the corresponding Spearman coefficients.

CoTMyr substrates were emphasised, as post-translational myristoylation usually occurs only after activation of caspases, e.g. in the case of apoptosis (Martin et al., 2011). While it might be possible, that PTMyr could play a role in the apoptotic cascades, it does not seem to occur in non-dying cells (see section 5.2.1 for more details). The vast majority of called mutations in the NMT substrates were missense mutations (86.0%); 4.5% were nonsense mutations, which should cause complete loss of the NMT substrate in the respective cancer cell line. The remaining mutations were frame-shifts (6.3%) and exonic splicing silencer mutations (3.2%). To identify if mutations in a given NMT substrate correlate with sensitivity or resistance, a list of Spearman correlations was generated, correlating on the one hand, the potency IMP1031; on the other hand, a binary list that consisted of all the cancer cell lines that do, or do not have a mutation (that is missense, frameshift and exonic splicing silencer mutations) in a respective NMT substrate. This approach is similar to the approach used by the Broad Cancer Dependency Map (Tsherniak et al., 2017). The resulting Spearman coefficients are summarised in Figure 2-8 A. Overall, only very weak to no correlations ($0.1 > r > -0.1$) were observed (and after multiple hypothesis testing correction with Benjamini-Hochberg FDR none of the q-values were below 0.05), already indicating that mutations in NMT substrates do not predict for sensitivity to NMT inhibition. While the presence of mutations in NMT substrates such as CYB5R3 or SLC25A4 correlates with increased or decreased potency of IMP1031 (see Figure 2-8 B), these mutations are only present in 1.1% and 0.7% of the cancer cell lines. NMT substrates such as ANKIB1 or MTHFD1L, for which more than 20 (that is ~3%) of the tested cancer cell lines present mutations, trends can be observed; however, these did not reach significance (see Figure 2-8 C). In the case of NMT substrates, for which larger number of cancer cell lines present mutations in the respective gene, there is no correlation with potency of IMP1031 (see Figure 2-8 D).

Similar trends to IMP1031 are observed partially for IMP1036, but e.g. ANKIB1 mutations do not even show the trend of increased sensitivity to IMP1036 (see Figure 8-6 A). Within the top 10 NMT substrate, for which mutations correlate with sensitivity to IMP1031, only CYB5R3, GORASP1 and MARCKSL1 are overrepresented in the Blood group (see Table 8-1). Thus, occurrence of mutations in NMT substrates is, in general, a poor predictor for responsiveness across larger numbers of cancer cell

lines; and, additionally, cannot serve as a potential explanation for the increased responsiveness of haematological malignancies as one would expect potentially overrepresentation of defining mutations in this tissue group. Moreover, the called mutations in NMT substrates might just accumulate over time due to impaired DNA damage repair in the cancer cell lines, thus be just passenger mutations. In line with this argument, none of the NMT substrates have been identified as cancer driver genes in the TCGA (Bailey et al., 2018). This does not exclude the possibility that a mutation might predict sensitivity in a small subset of cancer cells (as shown before), but it does not suffice to explain broader trends.

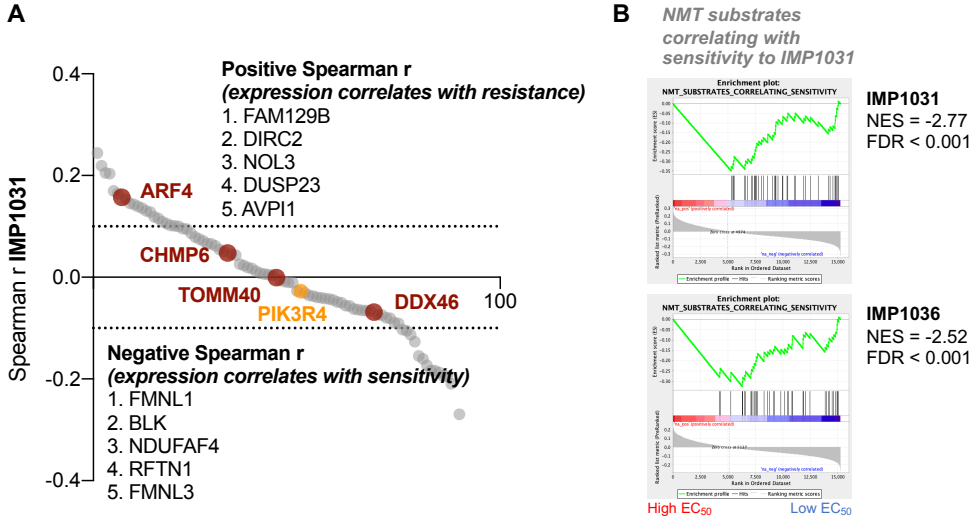

Figure 2-9: Expression pattern of NMT substrates correlates with sensitivity.

[A] Correlation between sensitivity to IMP1031 and expression of NMT substrates. Substrates in red are considered common essential genes (essential in >75% of the tested cell lines); substrates in orange are considered essential in at least 25% of the cancer cell lines. The top 5 NMT substrates with either positive or negative Spearman coefficients are shown. Dotted lines indicate spearman coefficients of 0.1 to -0.1 (N = 89). **[B]** NMT substrates correlating with increased responsiveness for IMP1031 were summarised in a gene set, and GSEA was utilised to test if expression of those NMT substrates correlates with lower EC_{50}s for IMP1031 (top) and IMP1036 (bottom)

The expression pattern of NMT substrates, on the other hand, correlates more clearly with the efficacy of the NMT inhibitors across different cancer cell lines. This is in line with the observations made by the Sanger Institute that tissue origin and gene expression are the best predictors of responsiveness to a given drug (Iorio et al., 2016) (as mentioned in subchapter 2.1). The correlation (calculated again as Spearman coefficients) of expression for a given NMT substrate and potency of IMP1031 is shown in Figure 2-9 A. NMT substrates for which >75% of the cell lines

depend on for optimal proliferation were considered as common essential in the CRISPR data from the Broad Institute (Meyers et al., 2017). Within this group, only ARF4 expression correlates with increased resistance ($r > 0.1$), potentially indicating that more resistant cells have high levels of ARF4 mRNA, which should correlate with protein levels, which take potentially longer to be degraded. This hypothesis assumes of course good correlation between mRNA level and protein level which might not be the case for all protein-coding genes (Schwanhausser et al., 2011). There is however the possibility of the confounding effect that the expression pattern of NMT substrates in the more sensitive cancer cell lines has no functional consequence, but only relates to tissue origin of the cell lines. The five NMT substrates, whose mRNA levels correlate with resistance, are expressed at low levels in cancer cell lines of the Blood tissue subgroup, which represent most of the sensitive cancer cell lines. The same observation applies *vice versa* for the five NMT substrates, whose mRNA levels correlate with sensitivity (see Figure 8-6 B). It is possible to show that NMT substrates that correlate with efficacy in IMP1031 are also enriched in the cell lines with high responsiveness to IMP1036 (see Figure 2-9 B) and IMP366 (see Figure 8-6 C). To conduct this analysis, the substrates with negative Spearman correlations were summarised in a new gene set (named 'NMT substrates correlating with sensitivity to IMP1031'). Gene Set Enrichment Analysis (GSEA) was used to compare the quartile of the most sensitive cell lines *versus* the quartile of the most resistant cancer cell lines for each inhibitor (Subramanian et al., 2005). It is possible to observe that mRNA expression of this subset of NMT substrates is higher in the sensitive cell lines. However, it is difficult to distinguish correlation and causality here, and experiments to potentially follow up such an angle are non-trivial. An analysis aiming to understand what distinguishes sensitive and resistant cancer cell lines on the level of biological functions is conducted in Chapter 4.2.1 and will be discussed there. Overall, the data presented indicate that identifying what drives the sensitivity to NMT inhibition of haematological malignancies might provide a good starting point to understand the differential effect of NMT inhibitors in cancer. This approach might subsequently provide insides for potential genetic markers that are valid across different cancer types.

2.2.4 Burkitt's lymphoma and DLBCL cell lines are being arrested in G2/M and start to die after 24 hours of NMT inhibition

As haematological malignancies, particularly Burkitt's lymphoma, are highly susceptible to NMT inhibition, two benchmark NMT inhibitors (IMP366 and IMP1088) (Frearson et al., 2010; Kallemeijn et al., 2019; Mousnier et al., 2018) were used against a panel of different B cell lymphomas, with emphasis on BL and DLBCL cell lines, originating from the GC reaction (Basso and Dalla-Favera, 2015) (see Figure 2-10 A). The structure and enzymatic data for IMP1088 are shown in Figure 1-10 (the corresponding growth-inhibition curves are shown for IMP1088 in Figure 8-7 and for IMP366 in Figure 8-8). The different lymphomas were further subdivided by sporadic (sBL) vs. endemic (eBL) in the case of Burkitt's lymphoma (Schmitz et al., 2014) and ABC (activated B cell like) vs. GCB (Germinal centre B cell like) for DLBCL (Alizadeh et al., 2000).

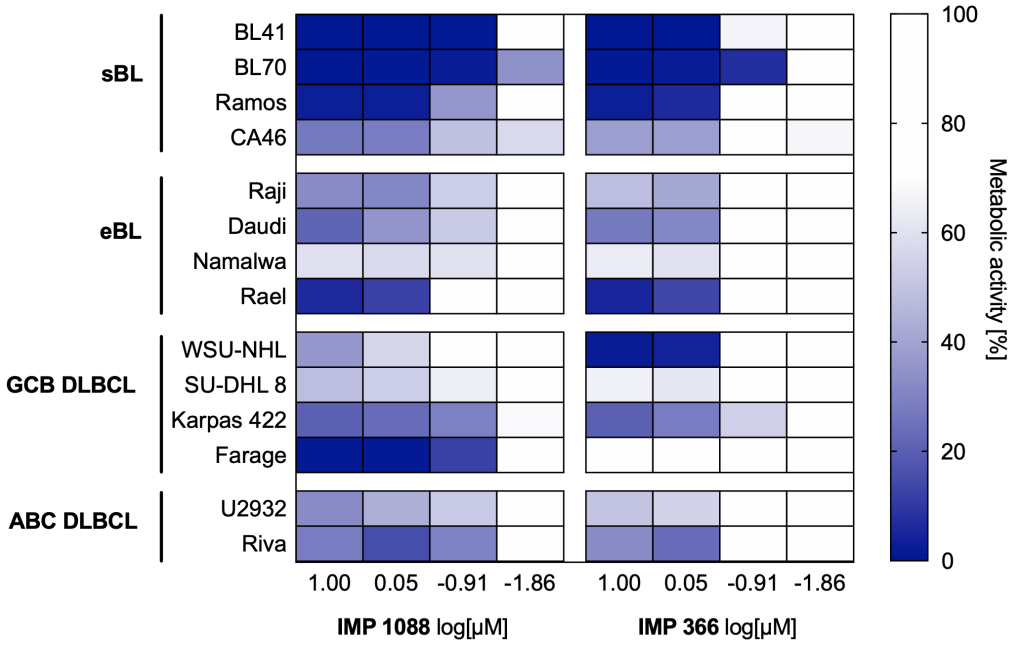

Figure 2-10: IMP1088 and IMP366 kill effectively a panel of B cell lymphomas.

Heatmap showing the effect on the metabolic activity, measured with CellTiter Blue, of the two NMT inhibitor IMP1088 and IMP366 against a panel of Burkitt's lymphoma and DLBCL cell lines.

For most of the tested cell lines a similar trend was observed, especially taking the differential in-cell potency between the two NMT inhibitors into account (Kallemeijn et al., 2019). One exception was the Farage cell line, that was resistant to IMP366;

however, as this cell line was responding to IMP1088 and IMP1031/1036 (see Figure 8-5), it could be that this was a unique phenomenon with the IMP366–potentially a particular ATP-binding cassette (ABC) transporter, CYP protein or permeability issue in context of this cell line.

The observation from the pharmacogenomic screens with NMT inhibitors that BL cancer cell lines are more responsive than DLBCL cell lines are reproduced in these data. There might be a trend that sBL cancer cell lines are more responsive than the eBL ones. This could potentially be explained by different mutational landscape between the two subtypes, with endemic eBL having fewer and different driver mutations (Grande et al., 2019; Love et al., 2012; Schmitz et al., 2012); but the numbers of tested cell lines are not sufficient to make a definitive statement. There is no clear observable difference between ABC DLBCL vs. GCB DLBCL.

One can assume that protein turnover of NMT substrates is critical for any cell toxicity an NMT inhibitor might exhibit, the time frame in which NMT inhibitors affect broad cellular function (such as cell cycle, apoptosis and number of viable cells) was identified via flow cytometry, using the highly sensitive sBL cell line BL41, as a first starting point. The experimental design is shown in Figure 2-11 A. Within these phenotypical markers, no change was observed within 6 hours of NMT inhibition. However, at 24 hours of NMT inhibition a slight increase in G2/M phase could be observed (see Figure 2-11 B), and a similar slight increase of apoptotic cells (see Figure 2-11 C).

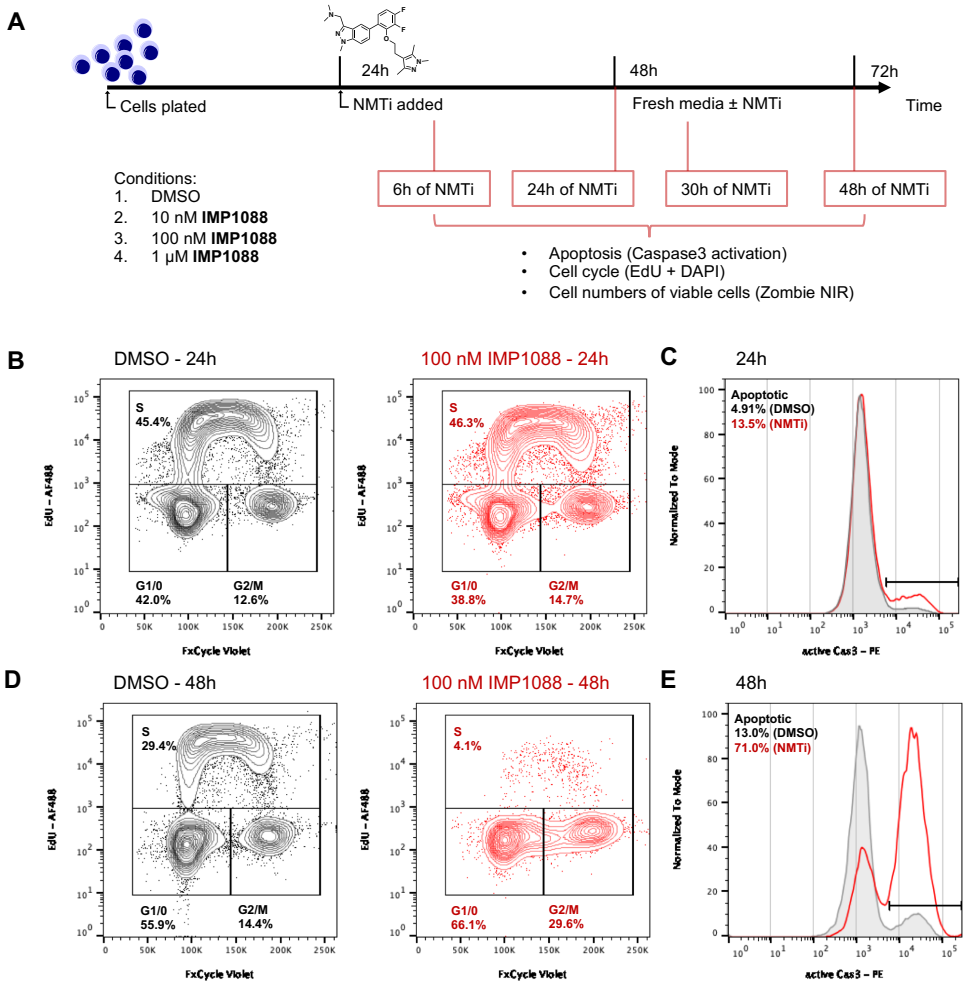

Figure 2-11: Experimental design and example fluorescence-activated cell sorting (FACS) plots to determine the temporal effects of IMP1088 on BL41.

[A] Experimental design to assess the temporal effects of IMP1088 on BL41. Cells are plated and left overnight to recover. IMP1088 (1 µM, 100 nM, 10 nM) or DMSO is added. Two hours prior to fixation, EdU is pulsed in the cells to monitor DNA synthesis. Subsequent use of different flow cytometry stainings allows to follow cell cycle, apoptosis induction and cell viability across conditions and time points (6, 24, 30 and 48 hours). **[B]** Representative flow cytometry analysis of the cell cycle; black DMSO at 24 hours; red 100 nM of IMP1088 at 24 hours. **[C]** Representative flow cytometry analysis of caspase3 activation; grey: DMSO at 24 hours; red: 100 nM of IMP1088 at 24 hours. **[D]** Representative flow cytometry analysis of the cell cycle; black DMSO at 48 hours; red 100 nM of IMP1088 at 48 hours. **[E]** Representative flow cytometry analysis of caspase3 activation; grey: DMSO at 48 hours; red: 100 nM of IMP1088 at 48 hours.

This effect strongly increases over the next 24 hours (see Figure 2-11 D and E) with quantifications shown in Figure 2-12 A to D, indicating a collapse of cellular viability and ongoing programmed cell death via caspase 3 activation in BL41 from 24 hours onwards.

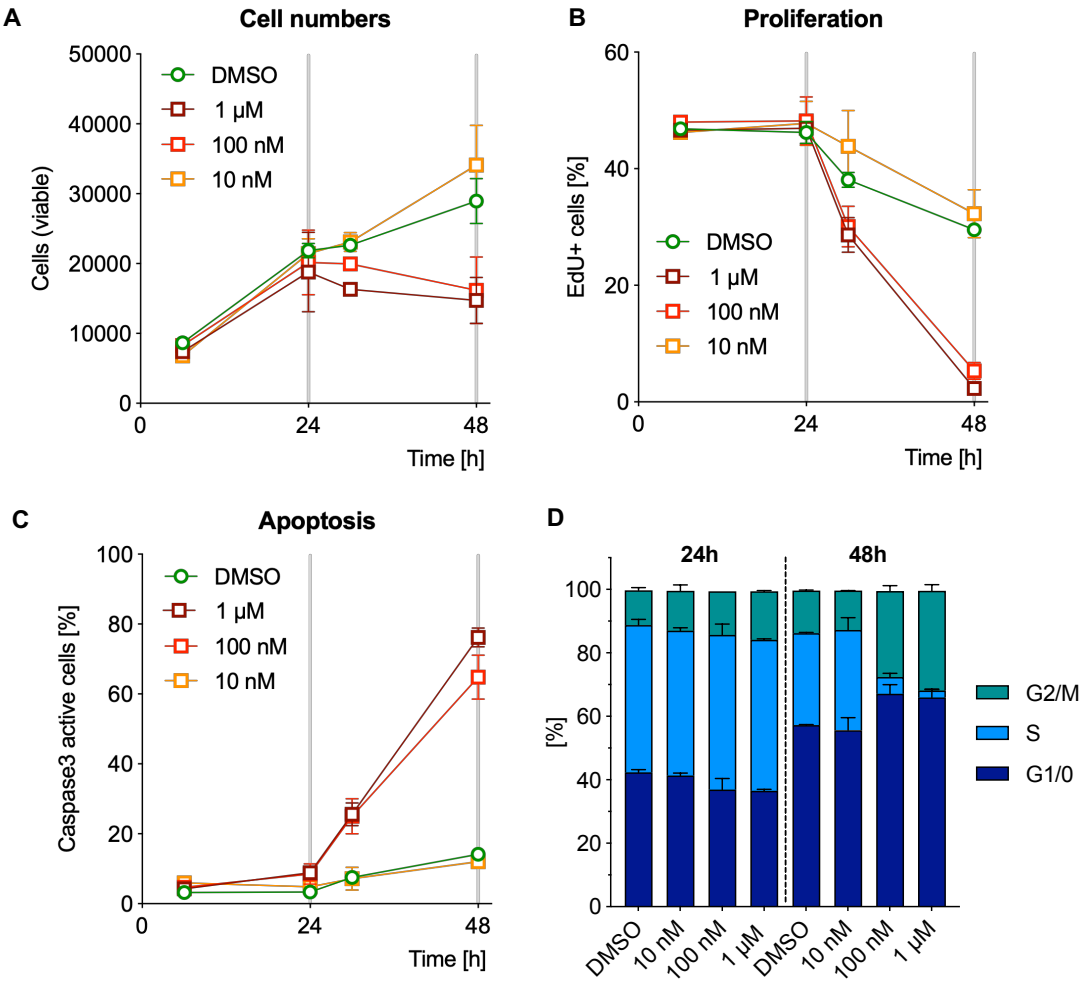

Figure 2-12: NMT inhibition, with IMP1088, causes G2/M accumulation and induction of apoptosis in the sBL cell line BL41 after 24 hours.

[A] Quantification of the viable (Zombie NIR negative) cells. **[B]** Quantification of the relative number of proliferating cells (EdU^+). **[C]** Quantification of the induction of apoptosis ($caspase3^+$). **[D]** Quantification of the cell cycle distribution at 24 hours and 48 hours. (For all graphs N = 2, error bars = SEM)

These results indicate that at around 24 hours a 'tipping point' is reached. Within this time frame either a certain amount of crucial for the cell viability myristoylated substrates have been degraded; and/or, a certain amount of non-myristoylated, therefore potentially toxic substrates (as described for SRC and LYN, see (Honda et al., 2016)), have been synthesised affecting larger proportions of the cells and killing those. The induction of apoptosis is independent of G1 or G2/M arrest in BL41 (see Figure 8-9). IMP366 acted similarly in BL41, taking the reduced cellular potency into account (see Figure 8-10), confirming a conserved effect across structurally different NMT inhibitors.

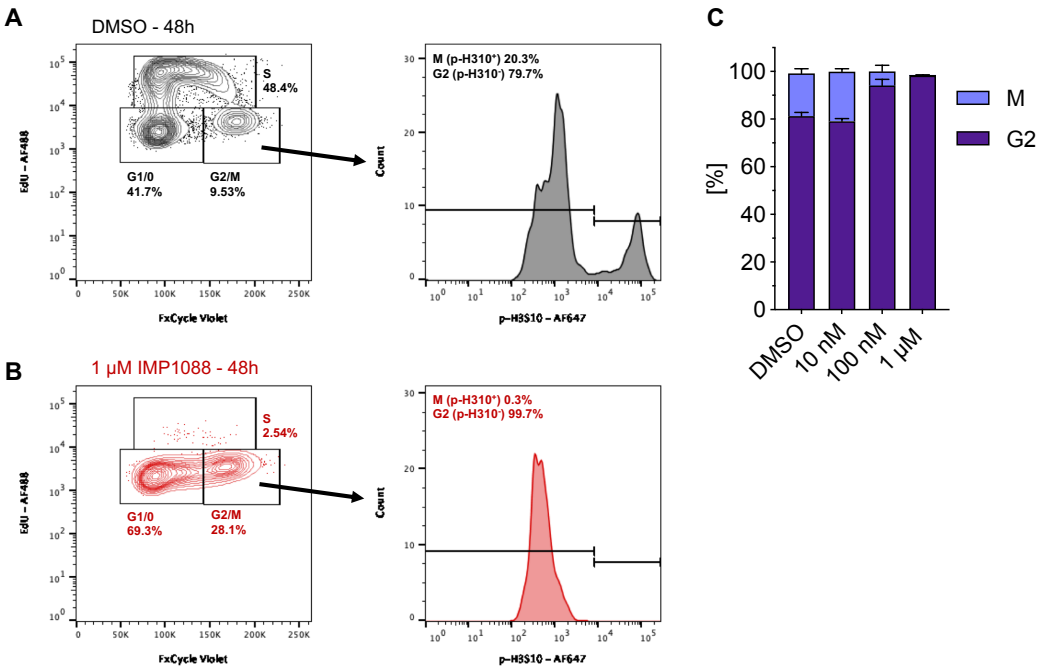

Figure 2-13: NMT inhibition causes specifically G2 arrest in BL41.

[A] Representative flow cytometry analysis of BL41, treated with DMSO for 48 hours, to distinguish G2 vs. M phase (left), utilising p-H3S10 as a marker for mitotic cells (right). **[B]** Representative flow cytometry analysis of BL41, treated with 1 µM IMP1088 for 48 hours, to distinguish G2 vs. M phase (left), utilising p-H3S10 as a marker for mitotic cells (right). **[C]** Quantification of the G2/M distribution at 48 hours with different concentrations of IMP1088 (N = 2, error bars = SEM).

To investigate the nature of the G2/M accumulation, phosphorylation of S10 of histone 3 (p-H3S10), a critical marker for entry into mitosis (Crosio et al., 2002), was utilised to distinguish G2 and M phase. In control conditions, within the cells that are in the G2/M phase, ~20% entered mitosis (see Figure 2-12 A). This population completely disappeared (in the relatively larger G2/M population) upon treatment with IMP1088 (see Figure 2-12 B), in a dose dependent manner (see Figure 2-12 C). These results show that entry into mitosis does not occur upon NMT inhibition. Interestingly, it was previously observed that cancer cell lines (cervical cancer, breast cancer and lung cancer) are arrested in G1/0 phase (Thinon et al., 2016). However, in the fluorescence-activated cell sorting (FACS) analysis in this publication, sub-G0 cells were not excluded, which could influence the relative quantifications for each cell cycle phase.

The accumulation in G2 and activation of apoptosis was also observed in the eBL cell line Raji (see Figure 8-11 A to D), with the already observed trend that Raji is

more resistant (see Figure 2-10). Utilising the same approach to distinguish G2 and M phase, Raji cells did not enter mitosis (see Figure 8-11 E), indicating a conserved effect of NMT inhibition across the BL cancer cell lines.

To ensure that the specific time frame until toxicity of NMT inhibition is apparent was not unique to Burkitt's lymphoma cell lines, additionally two ABC DLBCL cancer cell lines, U2932 and Riva, were tested with slight modifications to the experimental set-up. As DLBCL cell lines were overall less sensitive to IMP1088 and IMP366, the duration of the experiment was increased from 48 hours to 72 hours of NMT inhibition (see Figure 2-14 A). Interestingly, already at 24 hours of inhibition, DNA synthesis was already reduced in the Riva cancer cell line, whereas cell numbers and fraction of cells with caspase 3 activation was unaffected (see Figure 2-14 B to D). Similar to the two BL cancer cell lines, Riva accumulated in G2/M after 24 hours of NMT inhibition (see Figure 2-14 E). The same results were obtained for other cancer cell line U2932 (see Figure 8-12). Overall, across the two tested BL and the two DLBCL cancer cell lines, NMT inhibition did not affect cell cycle, cell numbers, or induction of apoptosis within the first 6 hours; however, by 24 hours the cells reach a 'tipping point', with subsequent cell cycle arrest and loss of viability. Dr. Monica Faronato, a postdoctoral fellow in the Tate laboratory, showed a similar effect for different adherent cancer cell lines comprising of breast, cervical and pancreatic cancer cell lines (data not shown).

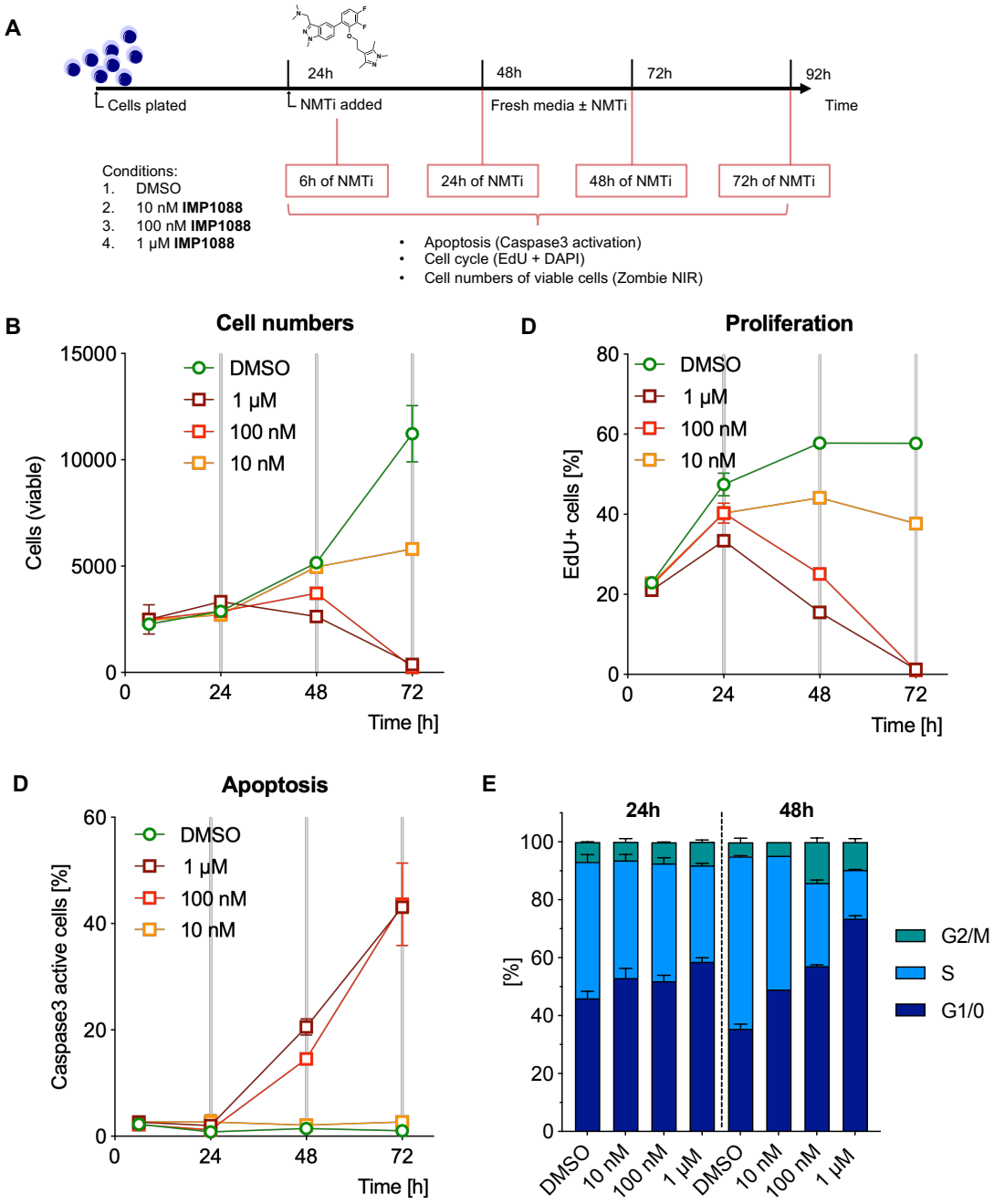

Figure 2-14: IMP1088 causes G2/M accumulation and apoptosis induction in the ABC DLBCL cell line Riva.

[A] Quantification of the viable (Zombie NIR-) cells. **[B]** Quantification of the relative number of proliferating cells (EdU^+). **[C]** Quantification of the induction of apoptosis ($caspase3^+$). **[D]** Quantification of the cell cycle distribution at 24 hours and 48 hours. (For all graphs N = 2, error bars = SEM)

2.3 Conclusions

In this chapter, pharmacogenomics screens, using three different NMT inhibitors, IMP366, IMP1031 and IMP1036, were analysed. Across the three screens, haematological malignancies (cells from the tissue subgroup Blood in the GDSC nomenclature) and particularly BL cancer cell lines were highly responsive to NMT inhibition. While doubling time of the cancer cell lines correlated with responsiveness, it failed to explain the increased responsiveness of haematological malignancies. There was no correlation observed between NMT1 (or NMT2) expression and the potency of the different NMT inhibitors. The presence of mutations in CoTMyr NMT substrates did not have a predictive value either, with the additional caveat that mutations in NMT substrates have so far not been identified as driver mutations, thus, could be only passenger mutations in a majority of the cancer cell lines (Bailey et al., 2018). Expression levels of a subset of NMT substrates correlate with sensitivity. However, to distinguish if this correlation is an actual functional causality or an artefact, dependent on expression from the originating tissue, is however not possible at this point. Overall, these data indicate that a different approach is needed to understand the differential effect of NMT inhibition on cancer cell lines to develop a genetic hypothesis.

The increased responsiveness of haematological malignancies was confirmed, using the inhibitors from the screens themselves, and additionally IMP1088, a picomolar potent inhibitor of NMT, which was recently reported (Mousnier et al., 2018). It became apparent from testing four different cell lines (BL41, Raji, U2932 and Riva) that NMT inhibition did not affect proliferation or apoptosis within the first 24 hours. In Riva however, a slight reduction of DNA synthesis was already observed after 24 hours of NMT inhibition, but no induction of apoptosis. This was followed by cell cycle arrest in G2 and G1/0 and breakdown of cell viability (evident in the induction of apoptosis and loss of cell numbers/viability). At this point, a two-fold strategy was applied to identify a potential molecular marker or phenotype for increased sensitivity/resistance towards an NMT inhibitor:

1. Identify mechanistically what is occurring on the level of the phosphoproteome and transcriptome within the first 24 hours in a BL cancer cell line upon NMT inhibition. It was assumed that the subsequent pathway

enrichment analysis might increase mechanistical understanding of what occurs upon NMT inhibition, which could yield in a genetic hypothesis (see Chapter 3).

2. Utilise the pharmacogenomics screen data and identify which pathways (e.g., increased/decreased cell cycle, translation, mitochondria, metabolic signatures, etc.) are enriched in the sensitive cell lines *versus* the resistant cell lines. Subsequently, extract key genes of those pathways, driving the sensitivity or resistance, and identify which transcription factors and/or oncogenic pathways are upstream. The identified upstream factors can then be validated further (see Chapter 4).

Chapter 3. Multi-omics study shows that NMT inhibition disrupts correct RNA processing in the Burkitt's lymphoma cell line BL41

3.1 Introduction

Previous studies into the mode of action of NMT inhibition utilised global proteomics to measure changes on the whole proteome level (Lim, 2016; Thinon et al., 2016) to infer from subsequent GO enrichment analysis biological pathways affected by NMT inhibition. However, significant changes in the global proteome were only observed at 2 or 3 days after NMT inhibition; within the first 24 hours no significant changes were observed (Thinon et al., 2014). To note is that those experiments are only able to measure a certain proportion of the proteome, e.g., in the case of (Thinon et al., 2014), 1069 proteins out of ca. 20,000 protein coding genes (Willyard, 2018). Therefore, changes on the global proteome might occur, but may have been missed due to the technicalities of mass spectrometry.

As presented and discussed in the previous chapter, the first 24 hours seem to be crucial for the effect of NMT inhibition across several cancer cell lines, as subsequently cells arrest and die, with varying kinetics of cell death. Dissecting which biological pathways and functions are affected within this time frame should help to further understand the mode of action of NMT inhibition. This approach might subsequently guide biomarker identification. Utilising gene expression changes after genetic or chemical perturbation is already widely used to characterise mode of actions of the respective chemical or genetic perturbation. This resulted in the generation of thousands of gene sets, summarised in the Molecular Signature Data Base (MSigDB), which can be used for GSEA. (Liberzon et al., 2015). Additionally, connectivity between different perturbations can be assessed, with e.g. the Connectivity Map by the Broad Institute (Lamb et al., 2006; Subramanian et al., 2017). This has been recently expanded also to changes on the chromatin and with phosphoproteomics (Litichevskiy et al., 2018). Other examples in the literature utilised RNAseq or phosphoproteomics to understand the mode of action of diverse inhibitors and differential effects of drugs (Ben-David et al., 2018; Manier et al., 2017; Pan et al., 2009; Wacker et al., 2012). The sBL cell line BL41 was chosen as an

example of a highly responsive cell line to NMT inhibition. mRNAseq and phosphoproteomics experiments (see subchapters 7.5 and 7.6 in the material and methods for details) were conducted. For both experiments 6 hours, 18 hours and 24 hours of NMT inhibition with 100 nM IMP1088 were compared to a matching control (0.004% DMSO, corresponding to the DMSO concentration in the treated samples) (see Figure 3-1).

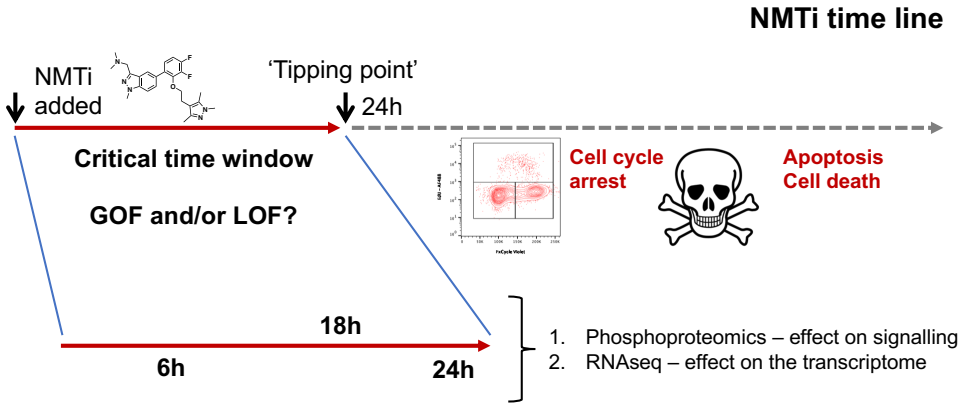

Figure 3-1: Effect of NMTi over time and design of the multi-omics study.

As shown in the previous chapter, haematological malignancies consistently do not show any (strong) phenotypical effects (that is reduction of proliferation or induction of cell death) within the first 24 hours of inhibition. After reaching a 'tipping point' they start to arrest in G2 and undergo programmed cell death. This indicates that the time window of the first 24 hours must be crucial–a time window in which the LOF and/or the GOF of NMT substrates slowly reaches a critical point at 24 hours. Hence, phosphoproteomics and mRNAseq experiments were conducted at 6, 18 and 24 hours comparing matched controls with samples treated with 100 nM IMP1088 to understand the impact of NMT inhibition on the transcriptome and signalling networks respectively in this critical 24 hours.

The timepoints of 18 and 24 hours were chosen due to their proximity to the 'tipping point'. It was assumed that breakdown of viability (e.g., through activation of executioner caspases, such as caspase 3 (Parrish et al., 2013)) in larger proportions of the cells would confound pathway analysis at later time points, due to activation of various cell death programs that are just secondary effects and not specific to NMT inhibition. The 6-hour timepoint served as an example to understand more immediate effects of NMT inhibition on the cell. To note is that across the cell lines tested in the previous chapter no difference in programmed cell death or proliferative capacity was observed within 6 hours of NMT inhibition. The controls were grown in parallel to

avoid confounding effects of comparing cells in a given point with growth. The results of those different omics data set will be subsequently presented and discussed.

3.2 Results

3.2.1 Phosphoproteomics reveals phosphorylation changes on proteins involved in splicing and RNA processing

The workflow for the phosphoproteomics experiment is shown in Figure 3-2. The enrichment workflow was done by Andrew Jones, senior research scientist of the Proteomics STP in the Francis Crick Institute. The prepared cell lysates, according to the experimental set-up shown in Figure 3-1, were reduced and alkylated, labelled with TMT for subsequent quantification and phospho-peptides were enriched on TiO_2 beads, for subsequent MS/MS analysis. The subsequent bioinformatics analysis was done with the MaxQuant and Perseus software package (Cox and Mann, 2008; Tyanova et al., 2016).

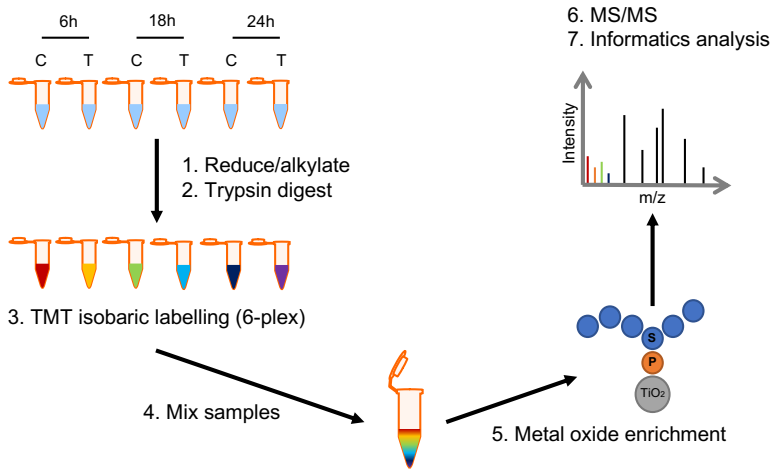

Figure 3-2: Experimental workflow of the phosphoproteomics experiment.

Cells were treated with 100 nM IMP1088 or a respective concentration of DMSO for 6, 18 or 24 hours respectively and then lysed. Lysates were reduced, alkylated and digested with trypsin. The samples were isobarically labelled with TMT, mixed and a TiO_2 based metal oxide enrichment was utilised to enrich for phosphorylated peptides. The samples were then run on mass spectrometer and analysed with the MaxQuant/Perseus software package with added Phospho-Site Plus annotations.

7098 phosphorylation sites were identified, 5864 with high fidelity (>75%) of correct localisation of the phospho-site on the given peptide. In some cases, several

potential phosphorylation sites exist on the peptide, and the Andromeda Search Engine of MaxQuant cannot assess which one is phosphorylated (Cox and Mann, 2008). For each biological condition the median TMT reporter intensity was subtracted from all corrected TMT reporter intensities to normalise the data (see subchapter 7.5 in the material and methods for details); for each time point the control sample was subtracted from the treated sample. Thus, positive log2 fold-change values indicate increased phosphorylation upon NMT inhibition with IMP1088, whereas negative log2 fold-changes indicate decreased phosphorylation. A cut-off of at least a 2-fold change was considered in a first instance to assess the number of changing phospho peptides (See Table 3-1). There is a strong trend for increased phosphorylation over decreased phosphorylation for all measured time points, which increasing numbers towards the 'tipping point'.

Table 3-1: Phosphorylation changes on peptides of at least twofold in BL41, treated with 100 nM IMP1088.

Time point	Increased phosphorylation	Decreased phosphorylation
6 hours	35	8
18 hours	112	20
24 hours	170	7

BCLAF1 was a prominent protein, showing increased phosphorylation on multiple sites across all three time points. BCLAF1 is involved in the control of apoptosis upon DNA damage (Lee et al., 2012). Another example with strongly increased phosphorylation at 6 hours of NMT inhibition was TRA2A, part of the pre-mRNA splicing machinery (Tacke et al., 1998) (see Figure 3-3 A). To understand more globally, the function of the proteins that undergo changes in phosphorylation, a 1D-enrichment was applied to the data (Cox and Mann, 2012); an approach used in previous phosphoproteomics studies, in this case investigating cell cycle (Sharma et al., 2014). To note is that the directionality (the score of the enrichment) only indicates increased (> 0) or decreased phosphorylation (< 0) in a given biological pathway. This does not necessarily correlate with activation or inhibition of the pathway.

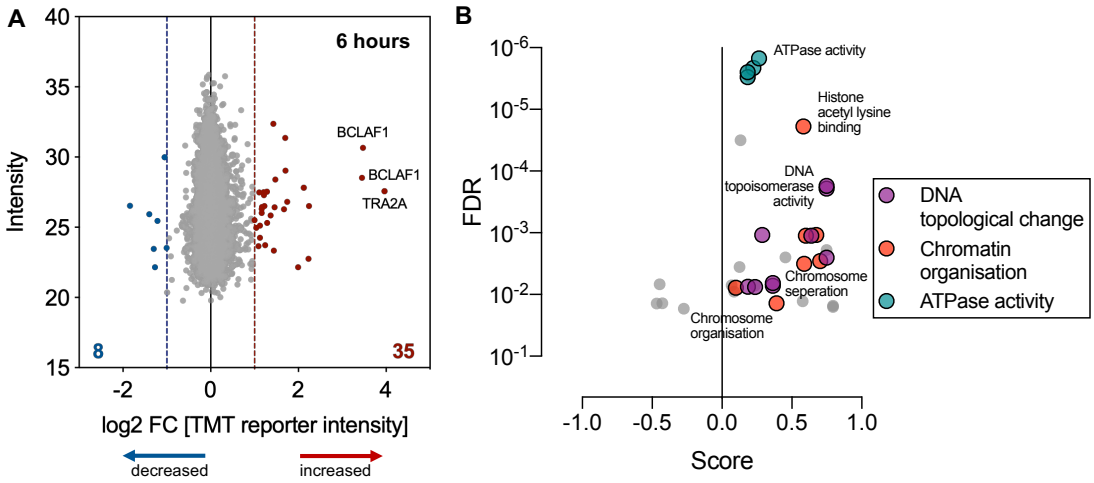

Figure 3-3: Phosphorylation changes at 6 hours with IMP1088 show increased phosphorylation on proteins involved in chromosome organisation.

[A] Scatter plan showing intensity of a given phospho-peptide the phosphorylation change compared to control. Red and blue lines (and dots) indicate changes of at least 2-fold. **[B]** 1D enrichment plot showing GOBP and GOMF enrichment of the phosphorylation changes.

Proteins involved in three biological functions, DNA topological changes, chromatin organisation and ATPase activity, based on GOBP and GOMF terms, showed increased phosphorylation at 6 hours of inhibition with IMP1088 (see Figure 3-3 B). DNA topological changes and chromatin organisation are quite closely related, likely due to overlapping roles of proteins involved in both. Interestingly, only the phosphorylation changes on proteins, involved in chromatin organisation, persist at the later time points (see results of the later time points). Concerning the third biological function, ATPase are usually thought to be involved ion transport across membranes (Kaplan, 2002); however, the phosphorylation changes on ATPases are not observed at later time points. Overall, with exception of TRA2A and BCLAF1, with the phosphorylation changes at 6 hours of NMT inhibition were not large in either number or amplitude, compared to the data of the later time points.

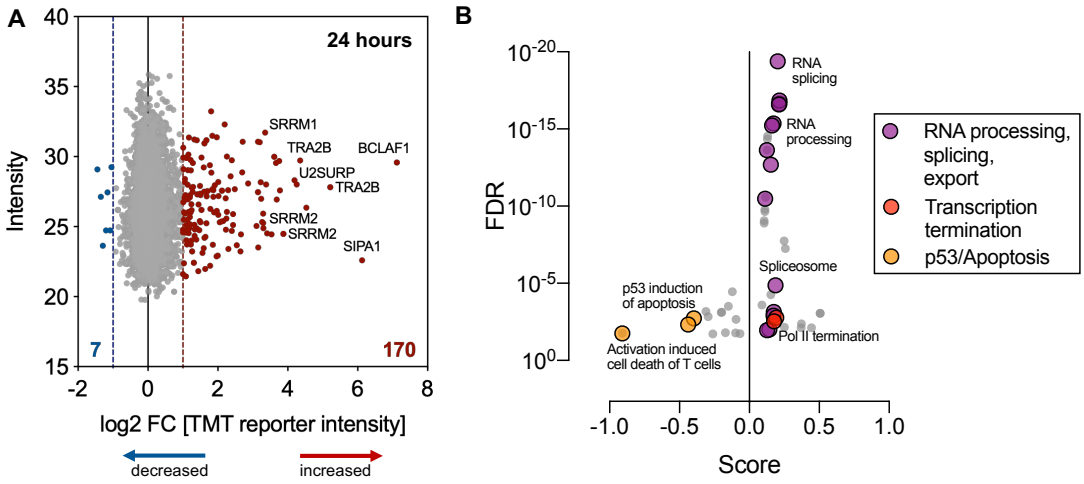

Figure 3-4: Phosphorylation changes at 24 hours with IMP1088 show increased phosphorylation on proteins involved in RNA processing and splicing.

[A] Scatter plan showing intensity of a given phospho-peptide the phosphorylation change compared to control. Red and blue lines (and dots) indicate changes of at least 2-fold. **[B]** 1D enrichment plot showing GOBP and GOMF enrichment of the phosphorylation changes.

Conversely to the 6-hour timepoint, in the two timepoints closer to the 'tipping point' an overall increase of phosphorylation is observed. SR-proteins, particularly SRRM1/2, show strong increased of phosphorylation on different serine sites. SRRM1/2 are involved in the pre-mRNA splicing machinery (Blencowe et al., 2000) and studies investigating DNA damage response (Bennetzen et al., 2010), HIV infection (Wojcechowskyj et al., 2013) or liver cancer (Zhu et al., 2017) show that phosphorylation changes affect splicing (see Figure 3-4 A for 24 hours and Figure 8-13 A for 18 hours). It seems that phosphorylation disproportionally increases on proteins involved in RNA processing. Indeed, the 1D enrichments for both 24 hours (see Figure 3-4 B) and 18 hours of NMT inhibition (see Figure 8-13 B) show highly significant enrichment for the GOBP and GOMF terms which relate to RNA processing, splicing and RNA export. Additionally, proteins involved Pol II termination show also increased phosphorylation across both time points. The differences between 18 and 24 hours of NMT inhibition lies within the pathways, for which proteins show decreased phosphorylation. For 18 hours, phosphorylation on proteins involved in the ER stress/UPR, chromatin organisation (e.g. HDAC regulation) and also immune signalling pathways is reduced (see Figure 8-13 B). At 24 hours, phosphorylation was decreased on proteins involved in cell death and p53-mediated

apoptosis. As shown in sections 2.2.4, at 24 hours, the proportion of BL41 that had activated caspase 3 started to increase (see Figure 2-12 C for IMP1088 and Figure 8-10 C for IMP366). Thus, maybe the phosphorylation changes related to apoptosis are driven by the start of programmed cell death in a subset of cells.

To confirm the increased phosphorylation on proteins involved in RNA processing and splicing upon NMT inhibition, a second biological replicate was prepared. In the second biological replicate, 4526 phospho-sites were identified with high confidence in localisation of the phosphorylated amino acid. 3628 phosphorylation sites were identified across both experiments (See Figure 8-14 A). At 24 hours of NMT inhibition an increase of phosphorylation on proteins, such SRRM1/2 or HNRNPH1, involved in RNA processing and splicing was observed also in the second biological replicate (see Figure 8-14 B). To assess reproducibility between the different biological replicates and conditions a hierarchical one-minus Pearson correlation was applied (see Figure 8-14 C). The two 24-hour timepoints cluster well together; however, the two 18-hour and 6-hour timepoints did not cluster together. This could be due to biological variability or due to a variety of factors, such as overall biological noise, sampling errors in the selection of peptides for subsequent MS2 runs in the mass spectrometer, or differences in enrichment, that can influence reproducibility in phosphoproteomics (Riley and Coon, 2016). Nevertheless, a 2D-enrichment in the overlapping phospho-sites between the two biological replicates at 24 hours, indicates phosphorylation changes on very similar pathways, namely related to (m)RNA processing and transcription (see Figure 8-14 D). As shown in the next subchapter, mRNA processing is indeed affected on a transcript level.

3.2.2 mRNAseq in BL41 reveals a global RNA processing defect upon NMT inhibition

The phosphoproteomics strongly implied the involvement of RNA processing and splicing; thus, mRNAseq (polyA enriched RNAseq) was conducted (Kukurba and Montgomery, 2015) in the same experimental conditions (that is time points and concentration of inhibitor) as the phosphoproteomics (see Figure 3-1 and see subchapter 7.6 in the material and methods for details). The principal informatician Probir Chakravarty, from the Bioinformatics and Biostatistics team in the Crick,

applied DESeq2 to the aligned sequencing reads, to identify significantly differentially expressed genes and generate ranked lists for GSEA (Love et al., 2014; Subramanian et al., 2005). These lists were analysed and interpreted by the author of this thesis.

A first observation was the reduction in the numbers of significantly differentially expressed genes over time. At 6 hours 6704 genes are differentially expressed, 17 of them more than 2-fold (see Figure 8-15 A). This number is reduced to 4953 (30 genes with differential gene expression of more than 2-fold) at 18 hours (see Figure 8-15 B), and to 2436 (28 genes with more than 2-fold change in expression) for 24 hours (see Figure 8-15 C). At 6 hours, there is a proportion of significantly differentially expressed genes, which are not significantly differentially expressed at later time points; however, there is an overlap in the genes affected over time of NMT inhibition (see Figure 8-15 D).

To understand which biological pathways within the cell were affected by the differential gene expression, GSEA was performed on the ranked lists (Subramanian et al., 2005). The analysis was run utilising the curated gene sets (without the chemical and genetic perturbations), including canonical pathways, KEGG, REACTOME and Biocarta from the MSigDB (Liberzon et al., 2015; Liberzon et al., 2011). GSEA crucially depends on the biological accuracy and interpretability of the input gene sets, thus, this study emphasised gene sets which are curated by various consortia, such as KEGG (Kanehisa et al., 2016), REACTOME (Fabregat et al., 2017) and Biocarta (Nishimura, 2001). Alternatively, one could use gene sets based on transcription factor and miRNA targets, such as motif and ChIPSeq-derived gene sets (Liberzon et al., 2011); however, a disadvantage here might be high context dependence of transcription factor binding and the multitude of biological functions a single transcription factor can be involved in, see the example of NF-κB which is involved in inflammation, immune responses cell growth, and cell survival in a context-dependent manner (Park and Hong, 2016). Thus, curated biological pathways were emphasised in the different GSEA analysis across this thesis.

The resulting GSEA results were summarised and visualised in networks with CytoScape (Shannon et al., 2003) and the EnrichmentMap (Merico et al., 2010) plug-in, following the recently published work-flow (Reimand et al., 2019). The resulting network for 6 hours of NMT inhibition is shown in Figure 3-5 A. On the one hand,

gene sets related to translation and the ribosome were upregulated (see Figure 3-5 B) and so are gene sets related to mitochondrial respiration, amino acid transport and glucose metabolism.

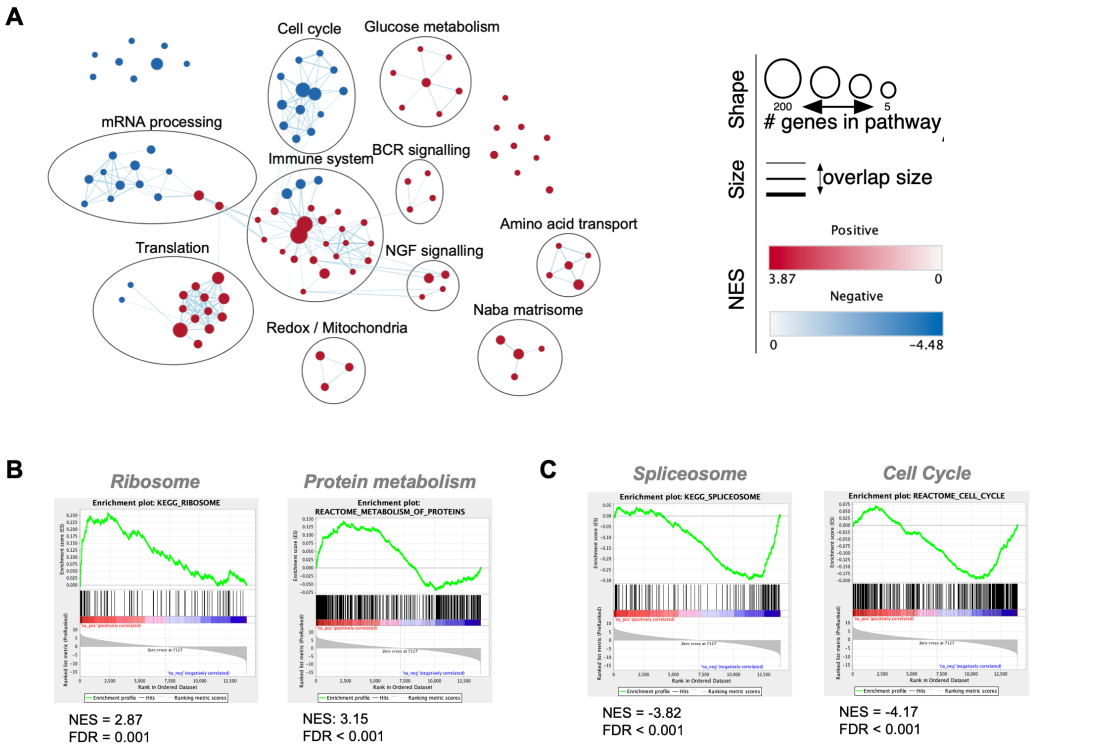

Figure 3-5: GSEA and subsequent EnrichmentMap analysis indicates downregulation of genes involved in mRNA processing and cell cycle progression with 6 hours of NMTi.

[A] Network, created with the EnrichmentMap plug-in into CytoScape summarising the GSEA (FDR < 0.01, Jaccard Overlap combined = 0.375, k constant = 0.5). **[B]** Example GSEA plots, consisting of genes that are upregulated, here shown KEGG_Ribosome and Reactome_Metabolism_of_Proteins. **[C]** Example GSEA plots, consisting of genes that are downregulated, here shown KEGG_Spliceosome and Reactome_Cell_Cycle.

Additionally, the same trends apply for gene sets related to the extra-cellular matrix (ECM) and gene sets related to the immune system and the B cell receptor signalling. On the other hand, already at 6 hours the downregulation of several gene sets related to mRNA processing, such as KEGG Spliceosome, was observed. Another major biological function affected are gene sets related to cell cycle (see Figure 3-5 B). Overall, this shows that already within 6 hours of NMT inhibition there is an impact on the expression of a large number of genes, implicated in a plethora of biological pathways, with cell cycle and mRNA processing related gene sets being downregulated. This is interesting in light of the cell cycle arrest observed after 24

hours of NMT inhibition, and the increased phosphorylation on proteins involved in mRNA processing and splicing before the cells reach the 'tipping point'. An interpretation of those results could be that the lack of transcribed cell cycle related proteins results subsequently in failure to engage correctly with cell cycling, and that the reduction of proteins involved in the RNA processing machinery causes subsequent increased phosphorylation due to either compensation or simply failure of the RNA processing machinery.

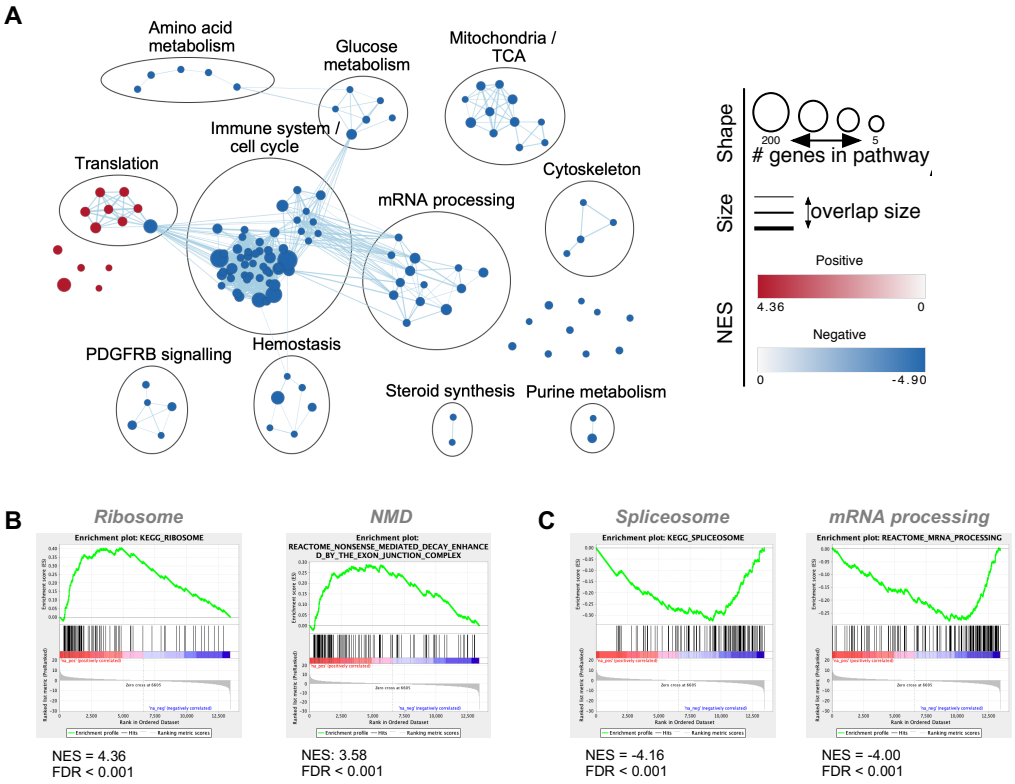

Figure 3-6: GSEA and subsequent EnrichmentMap analysis indicates downregulation of genes involved in every major biological pathway, but translation, with 24 hours of NMTi.

[A] Network, created with the EnrichmentMap plug-in into CytoScape, summarising the GSEA (FDR < 0.01, Jaccard Overlap combined = 0.375, k constant = 0.5). **[B]** Example GSEA plots, consisting of genes that are upregulated, here shown KEGG_Ribosome and Reactome_NMD_Enhanced_by_Exon_Junction_Complex. **[C]** Example GSEA plots, consisting of genes that are downregulated, here shown KEGG_Spliceosome and Reactome_mRNA_processing.

At 24 hours (see Figure 3-6 A) and already at 18 hours (see Figure 8-16 A) of NMT inhibition, every major biological pathway is being downregulated, with the exception of genes involved in translation and protein synthesis (e.g., ribosomal proteins and

translation initiators, see Figure 3-6 B and Figure 8-16 B). There are still some cell cycle related genes upregulated at 18 hours (see Figure 8-16 B), potentially a compensatory mechanism. Protein metabolism and tricarboxylic acid (TCA) cycle-related related gene sets, that were upregulated at 6 hours, are downregulated at 18 hours (see Figure 8-16 C). An increase of genes involved in the nonsense-mediated decay (NMD) is observed at 24 hours (see Figure 3-6 B), with decrease of genes involved in mRNA processing and splicing, similar to the previous time points (see Figure 3-6 C).

While the effect of NMT inhibitors is rather pleiotropic on the cells, there is a consistency across both the mRNAseq and phosphoproteomics data sets for the involvement (and potential failure) of the RNA splicing and processing machinery. There is strong increase of phosphorylation on several proteins, involved in the splicing and RNA processing machinery, towards the 'tipping point'; on the other hand, the mRNA expression of genes, involved in this machinery, is consistently downregulated from 6 hours of NMT inhibition onwards. This prompted the question if canonical splicing is affected in BL41 upon NMT inhibition.

Miriam Llorian Sopena, bioinformatics officer from the Bioinformatics and Biostatistics team in the Francis Crick Institute, used rMATS (Shen et al., 2014) to detect alternative canonical splicing (see subchapter 7.7 in the material and methods for detail).

The initial, filtered outputs indicated effects on canonical splicing driven by NMT inhibition. Particularly a large group of genes seemed to be affected by mutually exclusive exon changes (MXE), with 637 events identified at 6 hours of NMT inhibition, 87 events at 18 hours, further diminished to 22 events at 24 hours of NMT inhibition. (See Figure 3-7 A). Focussing on the largest group of events, MXE, it became apparent that those were wrongly annotated as classical MXE.

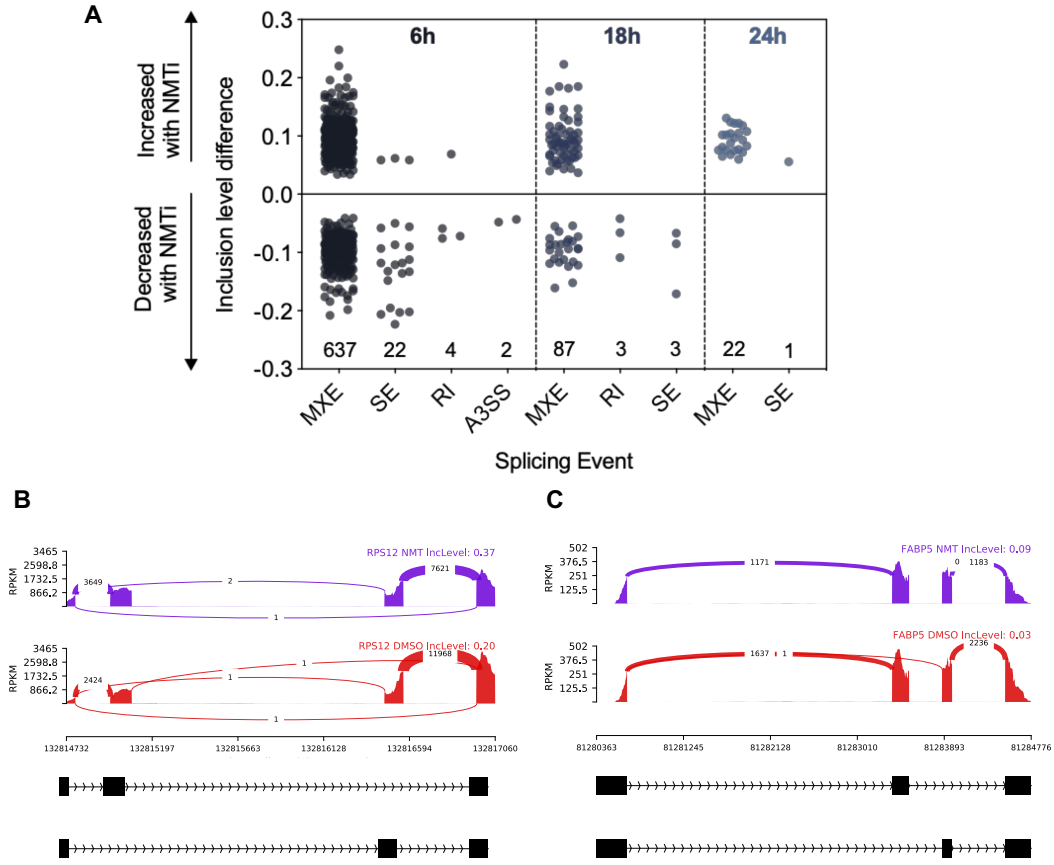

Figure 3-7: Initial analysis indicated alternative splicing events in the MXE class upon NMT inhibition; however, it is actually a shift in coverage towards the 5'.

[A] rMATs output for the different time points. (MXE: mutually exclusive exon; SE: skipped exon; RI: retained intron; A3SS: alternative 3' splice site) **[B]** Sashimi plot of *RPS12* at 6 hours of NMT inhibition. Violet: samples treated with 100 nM IMP1088; red: samples treated with DMSO. **[C]** Sashimi plot of *FABP5* at 6 hours of NMT inhibition. Violet: samples treated with 100 nM IMP1088; red: samples treated with DMSO.

As shown for the examples of *RPS12* (see Figure 3-7 B) and for *FABP5* (see Figure 3-7 C), two example genes with the lowest FDRs (determined by rMATs), the as MXE defined event is actually a shift of coverage towards the 5'-end. In both cases there is an increase of sequence coverage towards the 5'-end, away from the 3'-end. This is obvious in the change of ratio of junction reads: the ratio is increased if one divides the junction reads towards the 5'-end by the junction reads for the 3'-end, for the NMT inhibitor treated samples; for *RPS12*: DMSO = 0.2; NMTi = 0.48; for *FABP5*: DMSO = 0.73; NMTi = 0.99. In both cases the ratio increases, indicating more sequence coverage towards the 5'-end. To understand in greater detail the nature of those 'non-canonical' MXE events, DEXSeq was used to assess differential exon

expression (Anders et al., 2012). rMATs specifically looks for alternative splicing (such as such as skipped exons, alternative 5' splice site, alternative 3' splice site, mutually exclusive exons and retained introns), taking exon spanning and junction reads into account, whereas DEXSeq just identifies differentially expressed exons (Anders et al., 2012; Shen et al., 2014).

Over 45,000 exons were differentially expressed at 6 hours of NMT inhibition (see Figure 8-17 A). The number of differentially expressed exons is reduced over time with NMT inhibition to ~18,000 at 18 hours (see Figure 8-17 B), to over 7000 at 24 hours (see Figure 8-17 C). A similar subset of genes was affected by the differential exon expression, with ~7,500 genes affected by differential exon expression at 6 hours, reduced over time to ~2,700 affected genes at 24 hours (see Figure 8-17 D). These numbers indicate that the initial analysis of rMATs greatly underestimated the extent of the RNA processing phenotype in the transcriptome, likely due its algorithm looking for specifically for alternative splicing (Shen et al., 2014). To understand the effect of the differential exon expression in a given gene on the differential expression of the whole gene, the two lists were combined. This showed that at least for 6 hours and 24 hours of NMT inhibition, genes, affected by differential exon expression, are overall more downregulated then upregulated. At 18 hours a more even distribution is observed, in the sense that the genes affected by differential exon coverage are equally up and down regulated. Additionally, it is overall higher expressed genes (with higher baseMean) that are affected by differential exon expression (see Figure 8-18). DEXSeq2 shows for the genes *RPS12* (see Figure 3-8 A) and *FABP5* (see Figure 3-8 B) that exons towards the 5'-end of the gene are higher expressed upon NMT inhibition, and then expressed at lower levels towards the 3'-end. Following the trend for a reduction in the number of significantly differentially expressed exons (and reduction in the number of identified MXE events in rMATS), the effect was reduced at 24 hours of NMT inhibition (see Figure 8-19).

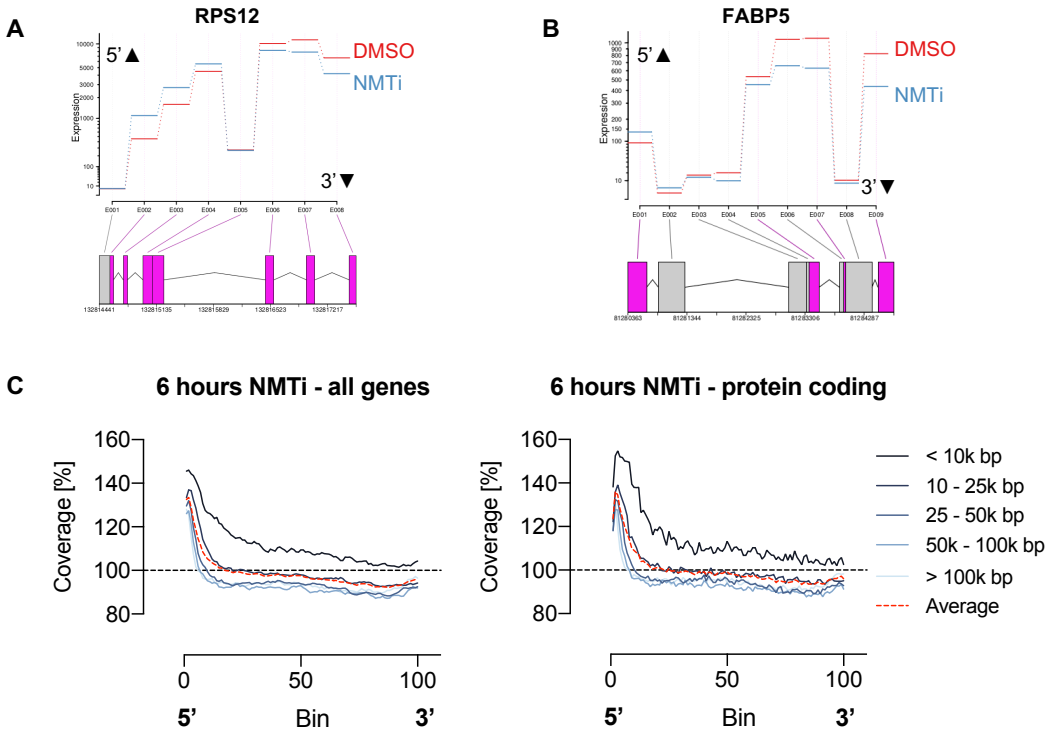

Figure 3-8: NMTi causes differential exon expression, with increased exon expression towards the 5'-end and loss towards the polyA tail.

[A] Differential exon expression shown for RPS12 at 6 hours (violet marks significantly differentially expressed exons). **[B]** Differential exon expression shown for FABP5 at 6 hours (violet marks significantly differentially expressed exons). **[C]** Gene coverage for all genes (left) and protein-coding genes (right) for 6 hours of NMT inhibition.

This was however not limited to those two genes. The 7500 genes, independently if protein-coding or not, were affected by increased coverage towards the 5'-end with diminishing coverage towards the 3'-end (see Figure 3-8 C). This bias in coverage towards the 5'-end of the genes was unexpected, particularly in a polyA enriched RNAseq data set. One would expect a 3'-bias, towards the 3'-UTR where polyadenylation typically occurs (Elkon et al., 2013). Interestingly the number of bins with positive coverage is reduced with increasing length of the transcript, indicating that all genes are affected after a certain number of transcribed base-pairs. The effect becomes less pronounced over time, towards the 'tipping point' (in line with the reduction of the supposed MXE events in rMATs): one could argue potentially that the system achieves compensation; however, the apparent recovery could just be an artefact of a loss of cell viability.

Overall, the differential coverage, with increased exon expression at the 5'-end, and loss towards the 3'-end, of the genes potentially indicates a change in mRNA length, possibly due to premature termination. Transcription and RNA processing (that is capping, splicing, and cleavage, followed by polyadenylation) occurs in a co-transcriptional fashion with a multitude of proteins and snRNAs involved in the process (Bentley, 2014). mRNA length can e.g. be controlled by the expression levels of the small nuclear RNA (snRNA) U1 (Berg et al., 2012; Kaida et al., 2010); DNA damage can impact U1 levels, thus mRNA length (Devany et al., 2016); additionally, elongation rates (influenced by e.g., DNA damage from UV irradiation) can impact the length of transcripts (Williamson et al., 2017); moreover, proteins, such as SCAF4 and SCAF8, have 'anti termination' properties and protect from premature termination and polyadenylation (Gregersen et al., 2019). Additionally, through 3'-end sequencing it was shown that particularly circulating immune cells utilise intronic polyadenylation (IpA) to diversify their transcriptomes (Singh et al., 2018). This has also consequences for malignancies derived from immune cells; in the case of CLL, the usage of differential IpAs, compared to healthy tissue, is a mechanism to inactivate tumour suppressors by truncating the proteins (Lee et al., 2018). Interestingly, it was observed that genes in circulating immune cells that are affected by IpA usage, have a modest downregulation of full-length mRNA transcripts, similar to what is observed in BL41 at 6 hours and 24 hours of NMT inhibition. As the observation of an apparent change in mRNA length was observed in a polyA enriched RNAseq data set, one could assume that BL41 suffers from premature termination and polyadenylation upon NMT inhibition.

To validate this, total RNAseq at 6 hours and 24 hours was conducted. If mRNA length is also affected here (measured as in Figure 3-8 through differential coverage upon NMT inhibition) this would indicate premature termination, that is followed in some cases by polyadenylation in others not. If, however this is not observed in a total RNAseq data (which comprises of a much larger amount of pre-mRNA than processed mRNA), this would indeed indicate the usage of (potentially intronic) polyadenylation sites (PAS) towards the 5'-end of the genes, resulting in shorter mRNAs.

3.2.3 NMT inhibition causes reduced U1 levels, subsequently induce shortening of mRNA length in BL41, and renders this cell line susceptible to transient NMT inhibition

Analog to the mRNAseq data set, Miriam Llorian Sopena, used DESeq2 (Love et al., 2014) to create lists of differentially expressed genes and DEXSeq (Anders et al., 2012) to create lists of differentially expressed exons (see subchapter 7.7 in the material and methods). These lists were subsequently analysed and interpreted by the author of this thesis. In comparison with the mRNAseq the number of significantly differentially expressed genes was reduced in the total RNAseq from 6704 to 1309 for 6 hours (see Figure 8-21 A) and from 2436 to 1893 at 24 hours (see Figure 8-21 B). Those differences could be due to sampling bias, in the case of mRNAseq towards polyadenylated RNA, whereas total RNAseq also takes all the pre-mRNA and all types of ncRNA into account (Kukurba and Montgomery, 2015). More importantly there were–especially compared to the ~45,000 differentially expressed exons in the mRNAseq at 6 hours–basically no differentially expressed exons in the total RNAseq for neither 6 hours of NMT inhibition (67 differentially expressed exons) or 24 hours (20 differentially expressed exons) (see Figure 8-21 C and D). Due to the lack of differentially expressed exons, it is clear that the differential coverage of the genes is only observed for polyadenylated RNA, indicating that what is observed in the mRNAseq data set is indeed a change in mRNA length upon NMT inhibition, due to differential PAS usage, towards the 5'-end of a given gene. As the differential exon expression is not observed on the total RNA level, this could potentially also impact the differences in numbers of significantly differentially expressed genes.
There was a high correlation between the overlapping significantly differentially expressed genes at 24 hours for the mRNAseq and total RNAseq (see Figure 8-22 A) and the STAT values for all genes (Figure 8-22 B). Unsurprisingly, the correlation between GOBP, GOMF, and GOCC terms, using a 2D enrichment (Cox and Mann, 2012) between the mRNAseq and total RNAseq is high, with most terms being on a straight line. An upregulation of gene sets related to the immune response, and downregulation of genes involved in the cell cycle, translation, and RNA processing is observed in both sequencing data sets. The results of the 2D enrichment interestingly differed to some extent from the network analysis, based on

GSEA, shown in Figure 3-6. Whereas e.g., immune system related gene sets are downregulated in the GSEA, they are positively enriched in the 2D enrichment. This is not due to the use of GO terms in the case of the 2D enrichment, and the use of the annotated gene sets in the case of the GSEA, as using the C5 gene sets (all GO terms) (Liberzon et al., 2015) yields in a similar network for the GSEA (data not shown). The discrepancy between the two enrichment methods relates likely in the different statistical tests and assumptions used in the respective methods. 1D enrichments are based on Wilcoxon-Mann-Whitney (and non-parametric MANOVA for 2D), testing if the numerical values of a given annotation (in this case e.g. a GOBP term) have a preference that is larger or smaller than the overall distribution of all numerical values in the given omics data set; multiple hypothesis testing is corrected by Benjamini-Hochberg FDR procedure (Cox and Mann, 2012). GSEA, on the other hand, utilises ranked lists (either generated *a priori* or through inputting the normalised whole genome expression data into the software), and calculates its enrichment scores based on Kolmogorov-Smirnov statistics, testing if the genes of a given gene set are enriched on either end of the ranked list (with FDR to control for multiple hypothesis testing). Independently of the divergence between GSEA and 2D enrichment for the mRNAseq at 24 hours, it is clear that a very high correlation is present between the pathways affected by expression changes between the mRNAseq data set and total RNAseq data set.

Conversely, this was not the case at 6 hours of NMT inhibition. The correlation between the overlapping, differentially expressed genes at 6 hours was worse than for 24 hours (see Figure 3-9 A). The lack of correlation was even stronger for the STAT values between the mRNAseq and total RNAseq data sets at 6 hours (see Figure 3-9 B). Furthermore, also within the 2D enrichment at 6 hours, there were clear differences between GO terms enriched in the mRNAseq *versus* GO terms enriched in the RNAseq (see Figure 3-9 C). GO terms, related to the immune system were strongly upregulated in the mRNAseq; however, most of them have scores around zero, indicating no change, for the total RNAseq, with some actually being downregulated. GO terms, related to RNA processing and translation were stronger affected in the total RNAseq than in the mRNAseq.

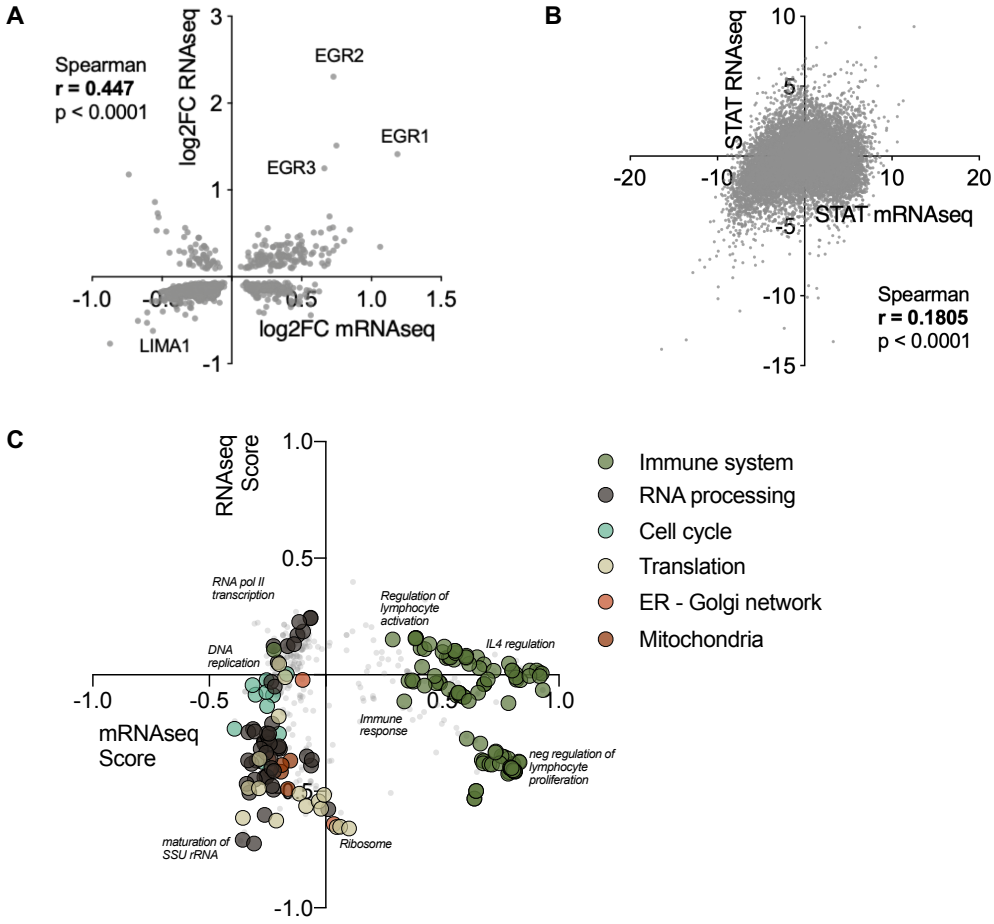

Figure 3-9: Total RNAseq and mRNAseq do not correlate at early time points of NMTi.

[A] Correlation between overlapping, differential expressed genes, comparing the FCs mRNAseq and total RNAseq. **[B]** Correlation between the STAT values of the two RNAseq data sets. **[C]** 2D-enrichment analysis comparing the two RNAseq data sets.

Interestingly, this disconnect between total RNAseq and mRNAseq occurs within the timeframe in which mRNA length is impacted the most with a bias towards shorter transcripts. Potentially, the shortening of mRNAs, caused by NMT inhibition, creates a situation in which pre-mRNA and mRNA do not correlate anymore, causing downstream loss of cell viability, once the proteome starts to be affected by this. It has been shown that incorrect mRNA length control can be lethal to cells (Gregersen et al., 2019), and it is easily imaginable that broad (uncontrolled) shortening of mRNAs across basically all biological functions will elicit downstream cytotoxity.

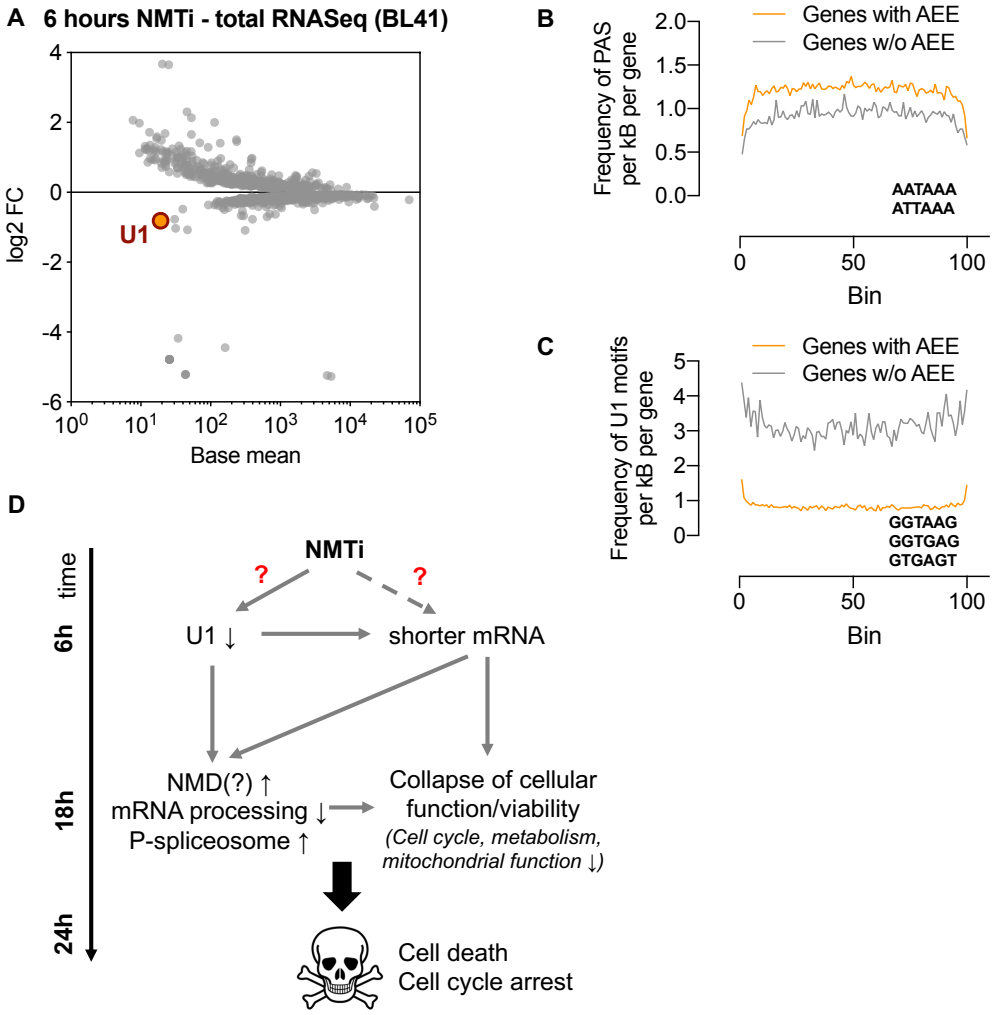

Figure 3-10: U1 expression is downregulated at early time points upon NMTi, resulting in a potential model for the observation on the transcriptome level.

[A] U1 expression is downregulated at 6 hours of NMT inhibition. **[B]** Comparison of the frequency of polyadenylation site frequency for the genes affected by alternative exon expression (AEE) and those that are not. **[C]** Comparison of the frequency of U1 binding motifs for the genes affected by alternative exon expression (AEE) and those that are not. **[D]** NMT inhibition causes (through an unknown mechanism) within the first 6 hours a downregulation of U1, that impacts the length of the mRNAs. It cannot be excluded that the mRNA length is also impacted by other means. This causes subsequent failure of the transcriptional machinery, with downregulation of genes involved in it and increased of phosphorylation. Additionally, NMD related genes are upregulated. This broadly impacts all types of essential cellular functions (cell cycle, metabolism, mitochondria) and the cells subsequently arrest and die.

As total RNAseq allows for the possibility to quantify also ncRNAs, it was observed that amongst those ncRNAs the snRNA U1 is downregulated at 6 hours of NMT

inhibition with IMP1088 (see Figure 3-10 A). Based on previous work, showing that U1 protects from premature termination and polyadenylation (Kaida et al., 2010) and is directly involved in the control of mRNA length in activated immune cells and neurons (Berg et al., 2012), it would be a possible explanation for the effect on mRNA length upon NMT inhibition (raising the question how NMT inhibition would cause a downregulation of U1). As recent research has shown that also other factors can impact mRNA length (such as DNA damage through U1 downregulation (Devany et al., 2016) and mRNA anti-terminator proteins (Gregersen et al., 2019)), it cannot be excluded that there are other driving mechanisms for the premature termination and polyadenylation, upon NMT inhibition in BL41. The frequency of polyadenylation sites was higher in the genes that were affected by differential exon expression ($p < 0.0001$, Mann-Whitney test), thus the putative shortening of the mRNA (see Figure 3-10 B). Additionally, the frequency of U1 motifs was decreased in this subset of genes ($p < 0.0001$, Mann-Whitney test) (see Figure 3-10 C), in line with a potential involvement of U1 protecting from premature termination and polyadenylation. It was shown that under normal circumstances, circulating immune cells that express genes with intronic polyadenylation sites have usually an increased frequency of polyadenylation sites and a decreased frequency of U1 binding motifs (Singh et al., 2018). Hence, the reduction of U1 levels could indeed cause disproportionally premature termination and polyadenylation in this subset of genes. An attempt to discover the potential PAS within the intronic regions was hampered by low numbers of reads across intronic regions in the mRNAseq experiment (5-10% across all genes). Increased sequencing depth to capture more intronic gene regions, or ideally 3'-end sequencing to uncover the actual PAS could definitely prove the usage of intronic PAS (Hoque et al., 2013), as observed for immune cells (Lee et al., 2018; Singh et al., 2018).

The combination of these observations gives a potential model (see Figure 3-10 D): NMT inhibition causes shortening of mRNAs in a subset of genes, which have intrinsically a higher frequency of polyadenylation sites and lower number of U1 binding sites, through reduction of U1 levels. This might be less a direct effect on the U1 snRNA itself but could be rather linked to early phosphorylation changes on the spliceosome upon NMT inhibition, that subsequently impact U1 levels. These early phosphorylation changes will be presented in Chapter 5. Nonetheless, this causes a

failure of correct mRNA length in a subset of genes, potentially increased NMD (from literature it is not clear if premature termination and polyadenylation would necessarily trigger NMD, see (Berg et al., 2012; Gregersen et al., 2019; Kaida et al., 2010; Lee et al., 2018; Singh et al., 2018)), and impacts subsequently major essential biological functions, resulting in cell death. The delay between the impact on mRNA length and cell death is likely due to protein turnover: once the synthesis of correct new proteins fails due to the lack of the correctly transcribed mRNAs (in the sense of length) and enough of the 'correct' proteome has been degraded, the cellular viability collapses. However, this is currently speculation and needs to be confirmed through analysing nascent protein synthesis upon NMT inhibition and additional 3'-end sequencing to identify the putative newly used polyadenylation sites (Hoque et al., 2013) (see Chapter 6 for an outlook and potential future experiments).

In collaboration with Dr. Monica Faronato, we conducted mRNAseq at 24 hours of NMT inhibition with 100 nM IMP1088 in the cancer cell line HeLa, as previously most of the data have been generated in this cancer cell line (Mousnier et al., 2018; Thinon et al., 2016; Thinon et al., 2014). The cells were plated, treated and lysed by Dr Faronato; the author of this thesis did the subsequent RNA extraction; the RNA was sequenced within the Advanced Sequencing Facilities at the Crick; Miriam Llorian Sopena did the alignment of the mRNAseq data, and used DESeq2 (Love et al., 2014) and DEXSeq (Anders et al., 2012) to generate the lists; those were subsequently analysed and interpreted by the author of this thesis. Compared to BL41 at 24 hours, there was a trend towards upregulation of genes in HeLa, with overall stronger fold changes (see Figure 8-23 A). However, there were no differentially expressed exons (36 in total, see Figure 8-23 B), indicating that the mRNA length phenotype occurred uniquely in BL41 upon NMT inhibition. This is interesting in the context of immune cells showing a larger proportion of intronic polyadenylation events compared to other tissues (Singh et al., 2018). Analog to BL41, GSEA was run on the ranked lists (Subramanian et al., 2005), utilising the curated gene sets (minus chemical and genetic perturbations) (Liberzon et al., 2015) and visualised/summarised with CytoScape and EnrichmentMap (Merico et al., 2010; Reimand et al., 2019; Shannon et al., 2003) (see Figure 8-23 C). Interestingly, gene sets related to mRNA processing were also overall downregulated in HeLa upon NMT inhibition, but the mRNA length shortening did not occur in HeLa.

Additionally, similar to BL41 most major biological functions (cell cycle, mitochondria, metabolism related gene sets) were downregulated. Contrary to BL41, gene sets involved in translation, were also downregulated in HeLa. Uniquely in HeLa, genes related to the UPR are upregulated, in alignment with previous observations on the global proteome level (Thinon et al., 2016). One cannot exclude that differences arise from different origin of tissue; however, it is clear that the strong mRNA processing phenotype seems to occur uniquely in BL41 compared to HeLa. While NMT inhibition did not cause alternative splicing *per se*, reports have shown that mutations of splicing components (which are particularly prevalent especially in leukaemia cell lines) render cells very sensitive to interference with the splicing machinery (Obeng et al., 2016; Seiler et al., 2018b; Zhou et al., 2015). The possibility was considered that this transcriptional defect by NMT inhibition could harm preferably cells with mutations in the splicing machinery. To test this hypothesis, the cells of the pharmacogenomics screens of IMP1031 and IMP1036 were divided in cells that have either hotspot mutations or LOF mutations on components of the splicing machinery according to the recent publication looking at mutations on splicing components and alternative splicing in the TCGA data set (Seiler et al., 2018a). Neither the presence of hotspot mutations nor LOF mutations correlated with increased sensitivity to IMP1031 or IMP1036 (see Figure 8-24). This shows that there must be another factor, likely related to RNA processing, that drives sensitivity of NMT inhibitors.

The observation that within 6 hours RNA processing was severely affected in BL41, raised the question if shorter pulses of NMT inhibition suffice to negatively affect the cells, even if the NMT inhibitor is washed out. It was observed that in HeLa 24 hours of inhibition with IMP1088, followed by stringent wash-outs did not affect cell viability afterwards (Mousnier et al., 2018). The experimental design, based on the results in (Mousnier et al., 2018), for the experiment in BL41 is shown in Figure 3-11 A: cells were incubated for 6, 24 or 48 hours with different concentrations of IMP1088 (ranging from 1 µM to 1 nM). For the 6 hours and 24 hours incubation, the cells were washed multiple times with PBS and then left to recover until the experimental endpoint of 48 hours. For 6 hours, incubation with 1 µM of IMP1088 caused an impact on total cell numbers, proliferative capacity (and cell cycle arrest) and slight induction of apoptosis (see Figure 3-11 B to E).

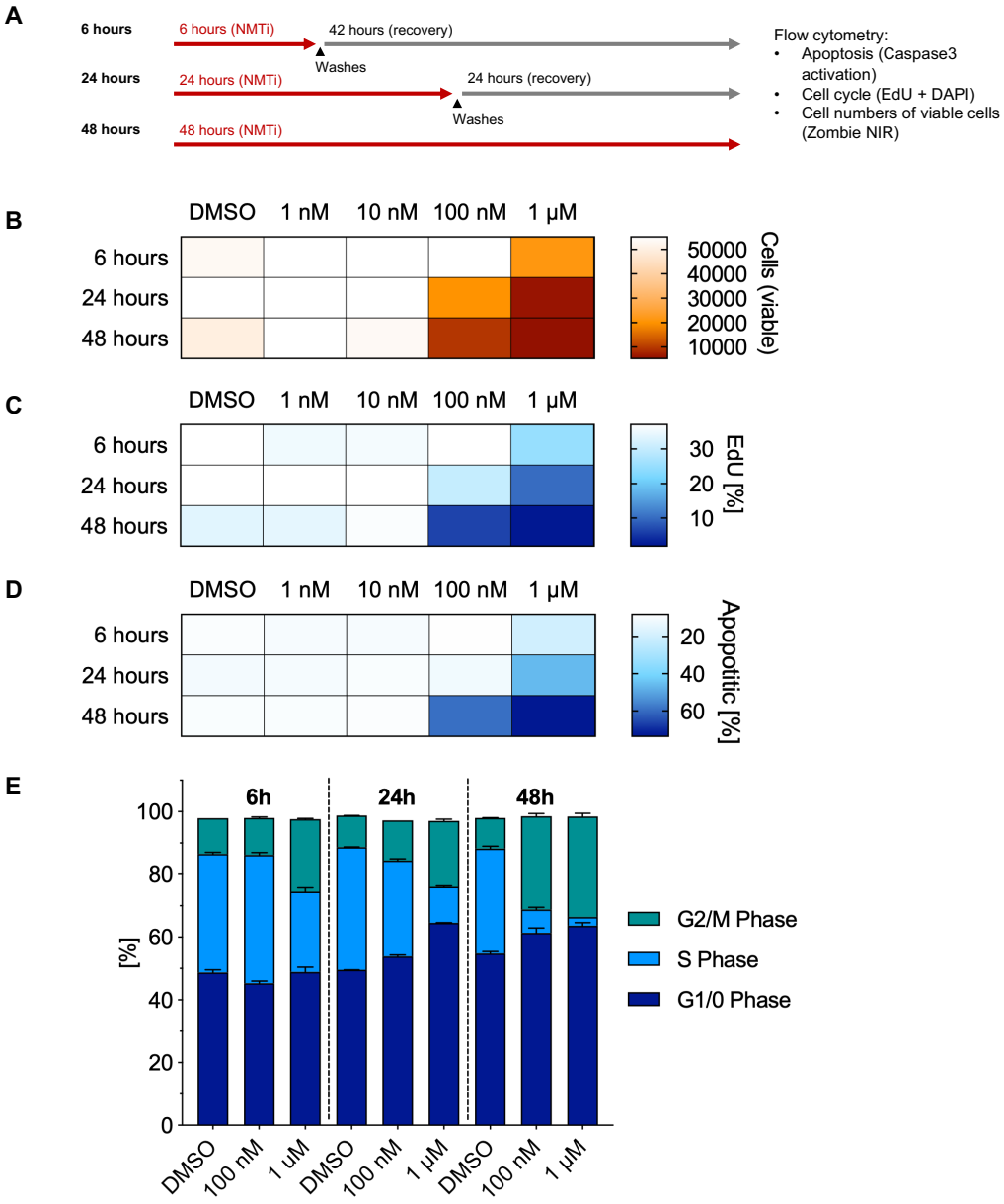

Figure 3-11: Short pulses of NMT inhibition suffice to negatively affect BL41.

[A] Experimental scheme, showing the three conditions. Cells were incubated for 6 hours, 24 hours or 48 hours with varying concentrations of IMP1088 (1 nM to 1 µM). In the case of the 6-hour incubation and 24-hours incubation, cells were washed multiple times, and left to recover in normal media for 42 and 24 hours respectively. At the endpoint of the experiment cell numbers, apoptosis induction and cell cycle profile were assessed via FACS. **[B]** Heatmap showing the effect on cell numbers. **[C]** Heatmap showing the effect on DNA synthesis. **[D]** Heatmap showing the effect caspase 3 activation. **[E]** Quantification of the cell cycle distribution at the end point, comparing the highest concentration for all experimental set ups.
(For all graphs N = 2, error bars = SEM)

1 µM IMP1088 is the equivalent of 30 times the EC_{50} (EC_{50} of IMP1088 in BL41 = 28 ± 11 nM), indicating that it is necessary to rapidly and strongly engage the target

completely to observe the subsequent loss in cell numbers with such a short transient inhibition of NMT. On the other hand, 100 nM of IMP1088 for 24 hours sufficed to negatively affect BL41 after further 24 hours of recovery, indicating a certain irreversibility of the damage done in the first 24 hours. Cell numbers were reduced (see Figure 3-11 B) and the proliferative capacity was impaired (see Figure 3-11 C). 100 nM did not suffice to still cause increased apoptosis (see Figure 3-11 D), but cell cycle effects with increased G2/M accumulation are observed (see Figure 3-11 E). This is in stark contrast to the HeLa cell line, which recovered after being treated for 24 hours with IMP1088 and was left to recover for 24 hours. (Mousnier et al., 2018) As the mRNA length phenotype was only observed in the case of BL41, but not in HeLa, one can argue that this might explain the potential difference in ability to recover from transient NMT inhibition.

3.3 Conclusions

In this chapter the effect of NMT inhibition on BL41 was characterised via a combination of phosphoproteomics, mRNAseq and total RNAseq at different timepoints of NMT inhibition with IMP1088, based on the observation that the cell viability collapses after 24 hours. The phosphoproteomics, particularly at the later time points, showed strong increased phosphorylation on proteins involved in RNA processing and splicing across two biological replicates. RNA processing and splicing is also implicated in the downstream pathway enrichment analysis of the mRNAseq: expression of genes involved in this RNA processing, splicing and transport were downregulated already within 6 hours of NMT inhibition. This prompted the question if NMT inhibition causes alternative splicing. An initial analysis was conducted, using the R program rMATs (Shen et al., 2014), to assess this question. rMATs identified a large number of MXE events upon NMT inhibition, especially after 6 hours of NMT inhibition. However, it became apparent that rMATs wrongly annotated a coverage shift towards the 5'-end as MXE. To understand the extent of this phenomenon, DEXSeq (Anders et al., 2012) was used to identify differential exon expression, independent of canonical splicing. This revealed a large number of differential expressed exons, confirming the shift of coverage towards the 5'-end of the genes, across a large number (>7500) genes. This shift in coverage

towards the 5'-end in a polyA enriched RNAseq data set indicates changes in mRNA length through premature termination and polyadenylation at PAS shortly after the first exons of a given gene.

To confirm that this mRNA shortening was only occurring within the polyadenylated RNA species, and not a result of massive premature termination, total RNAseq was conducted. The lack of differential exon coverage in the total RNAseq shows that the shortening of the mRNAs, is indeed likely due to usage of PAS early after the first exons and not just general premature termination. Additionally, there was a lack of correlation between differentially expressed genes and pathways between the mRNA and pre-mRNA at 6 hours of NMT inhibition, within the timeframe in which the mRNA length is impacted the starkest. U1 and its variants have been implicated in the control of mRNA length (Berg et al., 2012; Devany et al., 2016; Kaida et al., 2010; O'Reilly et al., 2013), thus, its observed downregulation at 6 hours of NMT inhibition is likely causing the changes in mRNA length. Curiously, this occurs within 6 hours of NMT inhibition, a time frame that fits the GOF (or change of function) of an NMT substrate, rather than LOF through degradation of the pre-existing pool of myristoylated substrates. Additionally, this mRNA length phenotype does not occur in the HeLa cell line, and indeed BL41 does not recover from transient NMT inhibition, whereas HeLa does (Mousnier et al., 2018). Literature shows that immune cells (normal and malignant) are using heavily IpA to diversify their transcriptome or shut down tumour suppressors (Lee et al., 2018; Singh et al., 2018), so it is possible that the mRNA shortening, observed in BL41, might be driven by differential tissue origin. As the whole genome transcriptomics and phosphoproteomics data sets heavily implied the spliceosome, the question arose if hotspot mutations or LOF mutations described for the splicing machinery (Seiler et al., 2018a) render cells more susceptible to NMT inhibition. This was not the case, indicating that a different factor, likely involved in transcription and RNA processing, might be driving the strong sensitivity of a subset of cancer cell lines, particularly the haematological malignancies. Other reports have described a particular strong dependence of MYC driven cancers on the splicing machinery (Hsu et al., 2015; Koh et al., 2015), and BL41 of course, due to its MYC translocation (Schmitz et al., 2014), would likely suffer more from interference in correct mRNA length transcription than other cell lines. As a first hint towards a potential implication of MYC, the tissue subgroup

'Blood' within the pharmacogenomics screens has significantly higher expression of MYC, compared to all the other tissues (Median robust multiarray average (RMA) (Blood) = 11.67; Median RMA (all others): 10.86; $p < 0.0001$ by Mann-Whitney). As shown in the next chapter, dividing the cells in a tissue and cancer-type agnostic way, just by sensitivity to a given NMT inhibitor and identify biological functions enriched in the sensitive cell lines, it became clear that transcription and RNA processing (and other biological functions) were strongly enriched in the sensitive cell lines. A key upstream transcription factor upstream of those functions is indeed MYC and led to the concept that MYC deregulation is synthetically lethal with NMT inhibition. In Chapter 5 the attempt to identify potential NMT substrates, driving the U1 downregulation, is shown and discussed.

Chapter 4. NMT inhibitors are synthetically lethal in cancer cell lines with high levels of MYC and/or structural alterations of MYC and MYCN

4.1 Introduction

In the previous chapter, the response of the BL cell line BL41 to NMT inhibition was measured via whole genome transcription changes and phosphoproteomics to elicit which biological pathways are disturbed by NMT inhibition. These timepoints were within the time frame before the cells arrest in cell cycle and undergo apoptosis. Phosphorylation on proteins involved in RNA processing and splicing was consistently increased towards the 'tipping point'; additionally, the mRNAseq revealed a putative defect in control of mRNA length upon NMT inhibition. This RNA processing phenotype was not observed in a different cancer cell line HeLa. There is evidence in the literature that cells, driven by MYC, have an increased demand on the spliceosome (Hsu et al., 2015; Koh et al., 2015). While NMT inhibition did not cause alternative splicing *per se* in BL41, but a shortening of mRNA length across a large number of genes, it was hypothesised that the MYC translocation in BL41 is the reason this cell line was so particularly responsive to NMT inhibition compared to other cell lines. A combinational effect of altered/deregulated RNA processing in a MYC high/deregulated background, making cancer cell lines with higher MYC levels more susceptible to NMT inhibition. This would also fit the observation that the Blood tissue group, comprising of all the haematological malignancies, has overall a higher median expression of MYC compared to all other cancers of the other tissue subgroups. Additionally, MYC translocations or ectopic expression is found very often in these haematological malignancies (Delgado and Leon, 2010).

In this chapter, an unbiased approach comparing sensitive and resistant cancer cell lines to the three different NMT inhibitors, IMP366, IMP1031 and IM1036, via GSEA was conducted (Subramanian et al., 2005). This analysis revealed that sensitive cell lines have high expression of genes involved in transcription, RNA processing, translation and nuclear transport. The key upstream transcription factor upstream of those genes was revealed to be indeed MYC.

4.2 Results

4.2.1 Sensitive cell lines to NMT inhibition are enriched in genes related to transcription, RNA processing & splicing, translation and nuclear transport

As shown in subchapter 2.2.2 and 2.2.3 none of the CFEs the Sanger Institute tested for, NMT1/2 expression, or mutations in NMT substrates correlated with sensitivity or resistance in the pharmacogenomics screens. An RNA processing defect, through shortening of the mRNAs, seems to be responsible for the high responsiveness of at least the Burkitt's lymphoma cell line BL41. As discussed in subchapter 3.2.3, known hotspot or LOF mutations in proteins involved in splicing (Seiler et al., 2018a) do not predict sensitivity in the pharmacogenomics data. While it is possible to show that the expression of a subset of NMT substrates correlates with sensitivity, it is unclear if this is just an artefact of differential expression across the tissues which are more sensitive (particularly the Blood Tissue group), or actual functional consequence of the substrate themselves. Thus, a tissue and cancer type-agnostic approach was applied, aiming to understand what differs on a biological level between the sensitive against the resistant cancer cell lines (that is e.g. increased cell cycle, AKT signalling, or translation). A similar approach has been used by the Broad Institute. They showed that differential drug responses in their MCF7 cell line strains is due to different expression patterns, resulting in activation and inhibition of various biological pathways. As an example, MCF7 strains highly enriched in cell cycle signatures were more sensitive to cell cycle inhibitors (Ben-David et al., 2018).

To apply a similar approach to the pharmacogenomics screens with the three different NMT inhibitors, IMP366, IMP1031 and IMP1036, the overlapping cell lines (677 cancer cell lines, see Figure 2-4 B) between the three screens were divided–by quartiles–in the most sensitive and resistant cell lines. The data of the most potent inhibitor used in the screens, IMP1031, was used to conduct the initial analysis (see Figure 4-1 A). The quartile of the most sensitive cell lines had a median EC_{50} of 115 nM; the most resistant ones had a median EC_{50} of 3.5 µM, a 30-fold difference between the two groups, indicating a strong differential response to NMT inhibition.

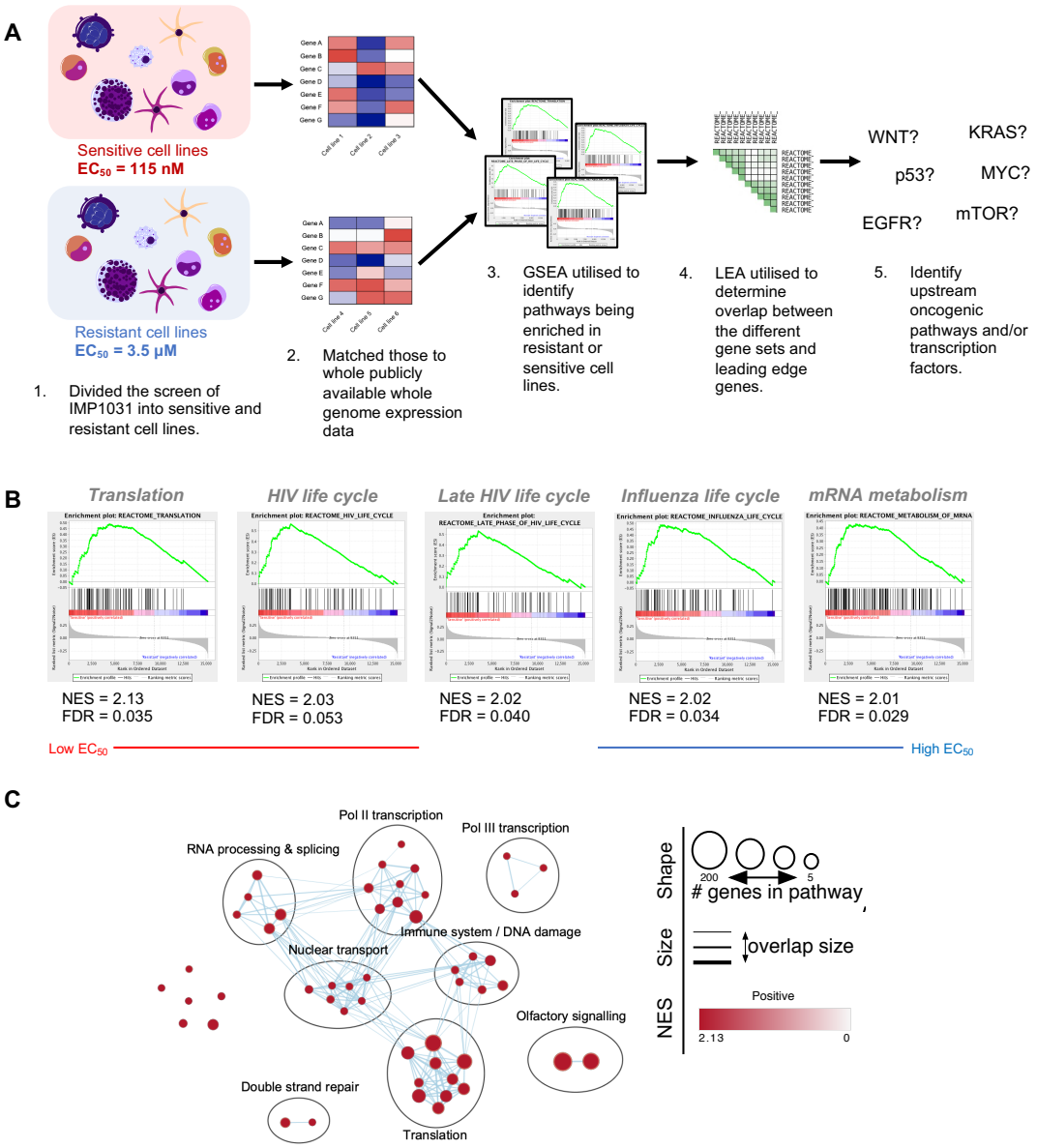

Figure 4-1: Cell lines with high expression of genes involved in RNA processing, ribosomal proteins, Pol II and III transcription are more sensitive to NMT inhibition.

[A] (1) Within the pharmacogenomics screen of IMP1031 the cell lines were divided by quartiles in the most resistant and most sensitive cell lines. **(2)** These were matched to the publicly available whole genome expression data from the COSMIC data base (Iorio et al., 2016). **(3)** GSEA was used to identify biological pathways enriched in the sensitive/resistant cell lines (Subramanian et al., 2005). **(4)** A leading-edge analysis was conducted on the Top10 gene sets to identify the leading-edge genes which were subsequently summarised into a new gene set 'Sensitive to NMTi'. (5) These 137 genes, summarised in the 'Sensitive to NMTi' gene set were put into the MSigDB to identify top upstream (oncogenic) pathways and transcription factors (Liberzon et al., 2015). **[B]** GSEA plots of the five strongest enriched gene sets in the sensitive cell lines by NES. **[C]** Network, created with the EnrichmentMap plug-in into CytoScape, showing gene sets enriched in the sensitive (to IMP1031) cancer cell lines (FDR < 0.1, Jaccard Overlap combined = 0.375, k constant = 0.5).

The cancer cell lines were matched to the publicly available expression data (Iorio et al., 2016). Similar to the analysis conducted in the Chapter 3, GSEA was run (Subramanian et al., 2005), comparing the sensitive and resistant cancer cell lines, using the annotated gene sets without the chemical and genetic perturbation (Liberzon et al., 2015). This yielded in the identification of several gene sets that are enriched in the sensitive cancer cell lines (see Figure 4-1 B). The viral gene sets are enriched for proteins involved in transcription, translation (initiation) and nuclear export and import, as different viruses usually hijack the cellular machinery for their own reproduction (Liberzon et al., 2015). In line with these results, gene sets related to mRNA metabolism and translation are also enriched within the sensitive cancer cell lines. As shown in Figure 4-1 C, taking all significantly enriched gene sets into account (with an FDR < 0.1), it is apparent that sensitive cell lines have high expression of genes involved in Pol II and Pol III transcription, RNA processing & splicing, translation and nuclear transport. Additionally, gene sets related to DNA damage, the immune system (this is likely due to the enrichment of haematological malignancies within the sensitive cancer cell lines) and olfactory signalling are enriched in the sensitive cancer cell lines. Interestingly, there were no gene sets significantly correlating with resistance (that is being downregulated in the sensitive cancer cell lines). This indicates that the upregulation of a given biological function does not confer resistance, but being in a state of high transcription and translation renders a given cell more susceptible to NMT inhibition. Gene sets related to cell cycle were not significantly enriched (data not shown), implying that cycling *per se* does not explain increased sensitivity. This would confirm the observation that haematological malignancies, which are much more susceptible to NMT inhibition, have comparable doubling times to the other more resistant cancer cell lines (see section 2.2.2).

As a large number of genes are part of the gene sets that correlate with sensitivity, the 10 most enriched gene sets by normalised enrichment score (NES) were used for subsequent leading-edge analysis (see Table 8-2). The aim of this analysis was to identify a subset of driver genes that could be used for validation with the two other NMT inhibitors, IMP1036 and IMP366, to test its predictive power. This subset of genes could then also be used to subsequently identify potential upstream (oncogenic) pathways and transcription factors. In doing so, 137 leading edge or

driver genes were identified from the 10 gene sets. These 137 genes were summarised in a new gene set or signature 'Sensitive to NMTi'. As expected, this new gene set is strongly enriched in the sensitive cell lines, treated with IMP1031. More importantly however, the 'Sensitive to NMTi' gene set is also strongly enriched in the sensitive cancer cell lines (compared to the resistant) for the NMT inhibitors IMP1036 and IMP366 (see Figure 4-2 A), serving as a first validation of the importance of those genes and the predictive capability for NMT inhibition.

To further validate the 'Sensitive to NMTi' gene set, the CRISPR gene essentiality data of the Broad Cancer Dependency Map (DepMap) was utilised (Meyers et al., 2017; Tsherniak et al., 2017). Firstly, to have a different method of interfering with myristoylation (genetic knockout of NMT1 vs. NMT inhibition); secondly, to use a different whole genome expression data set, generated in cancer cell lines, cultured in a different institute (Barretina et al., 2012). This was deemed important in light of potential genetic drift in the cell lines, yielding in different transcriptional program of the supposedly same cancer cell line (Ben-David et al., 2018; Liu et al., 2019). The cancer cell lines, screened by the Broad institute, were divided by their gene effect score for NMT1, as this is the essential paralog (see section 1.2.3), in the quartile of the cells that are the most dependent on NMT1 (which have the lowest gene effect scores) and cancer cell lines that are less dependent on NMT1 (which have the highest gene effect scores). The CCLE RNAseq data (Cancer Cell Line Encyclopedia and Genomics of Drug Sensitivity in Cancer, 2015) was matched to the respective cancer cell lines, and GSEA was applied (Subramanian et al., 2005) with the 'Sensitive to NMTi' gene set. The 'Sensitive to NMTi' gene set was enriched in the cells, more dependent on NMT1. This indicates that cells that have high expression of these subset of genes are more dependent on myristoylation, independent of the type of interference used.

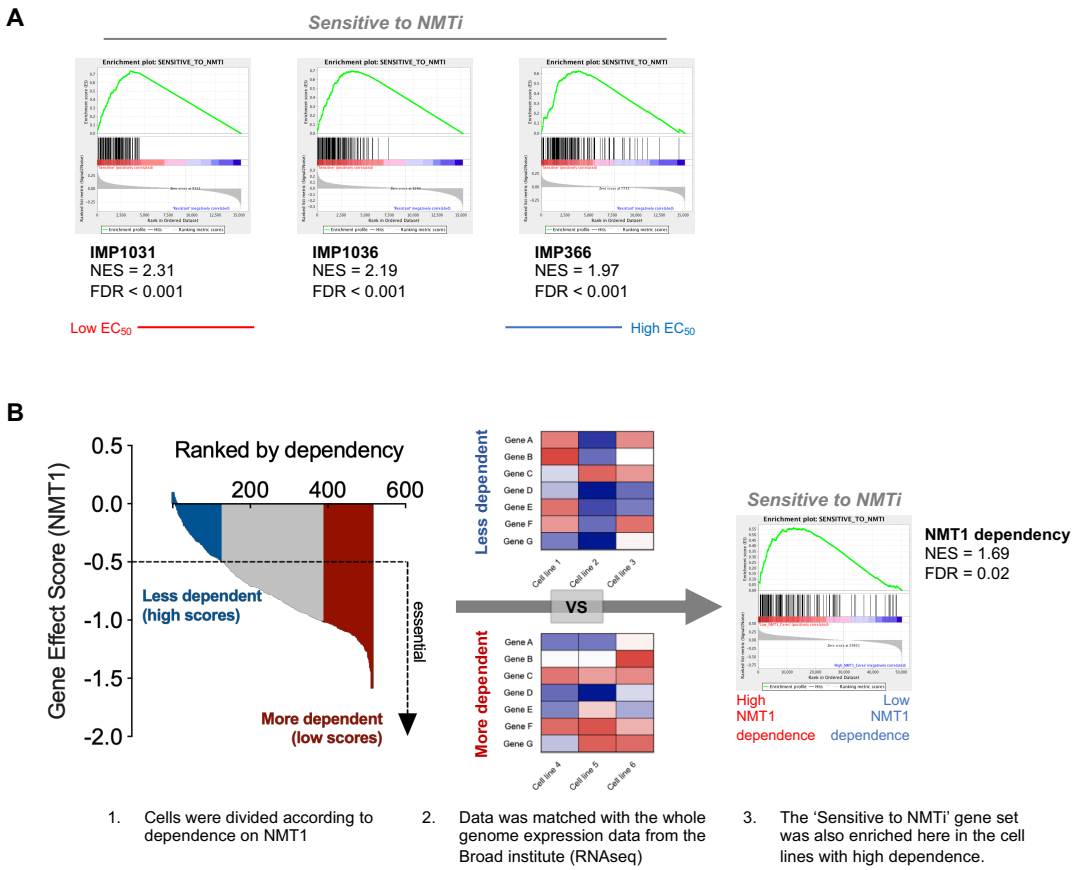

Figure 4-2: 'Sensitive to NMTi' gene set enriched in for all three NMT inhibitors in the sensitive cell lines and in the Broad institute DepMap in cells more dependent on NMT1.

[A] GSEA plots for IMP1031, IMP1036 and IMP366 showing that the 'Sensitive to NMTi' gene set is significantly enriched in all three cases in the sensitive cell lines. **[B] (1)** Cell lines from the Broad DepMap project were divided by quartiles into the cells less dependent on NMT1 (higher gene effect scores) and very dependent on NMT1 (lower effect scores). **(2)** Those cell lines were matched to the RNAseq data, publicly available in the CCLE by the Broad institute. **(3)** The 'Sensitive to NMTi' gene set is enriched in cell lines that are more dependent on NMT1.

To elucidate which oncogenic pathways or transcription factors are upstream of the 'Sensitive to NMTi' signature, the genes were used as an input into the MSigDB, assessing enrichment in the Hallmark gene sets as a starting point (Liberzon et al., 2015). The results are shown in Table 4-1. Of particular interest was the top hit, being the Hallmarks MYC targets V1. This was particularly interesting in light of the observations in the previous chapter that a MYC deregulated lymphoma cell line showed an RNA processing defect upon NMT inhibition, and the frequent observed deregulation of MYC in all types of haematological malignancies, ranging from BL

with its MYC translocations, DLBCL, multiple myeloma to leukaemia (Delgado and Leon, 2010). Across these malignancies, MYC is usually associated with worse patient outcomes (Schick et al., 2017).

Table 4-1: The 5 strongest enriched Hallmark gene sets, using the 'Sensitive to NMTi' signature.

Gene Set Name	Genes in overlap	FDR q-value
Hallmark MYC targets V1	15	$2.72e^{-15}$
Hallmark DNA Repair	13	$2.65e^{-14}$
Hallmark Unfolded Protein Response	10	$3.17e^{-11}$
Hallmark E2F targets	11	$3.33e^{-10}$
Hallmark Allograft Rejection	10	$5.52e^{-9}$

However, the implications of a synthetic lethality between high levels of MYC and NMT inhibition would go beyond haematological malignancies, due to MYCs crucial role in tumour initiation, and more important in tumour maintenance, across a large number of different malignancies across different tissues (Dang, 2012; Gabay et al., 2014). Additionally, it would explain why several other cancer cell lines of different tissue origin are responsive to NMT inhibition (see sections 2.2.1 and 2.2.2).

4.2.2 MYC expression and/or structural alterations of MYC/MYCN correlate with increased sensitivity to NMT inhibition or increased dependence on NMT1

As shown in the previous section, the observation that MYC was the most significantly enriched upstream node of the 'Sensitive to NMTi' signature, raised the question whether MYC expression on its own was able to distinguish sensitive and resistant cell lines within the pharmacogenomics screens. To test for this hypothesis, the cancer cell lines were divided by quartile into two groups by their *MYC* mRNA expression, obtained from the published whole genome expression data (Iorio et al., 2016). And indeed, *MYC* expression on its own was able to distinguish significantly sensitivity towards the NMT inhibitors IMP1031 (see Figure 4-3 A), IMP1036 (see Figure 4-3 B) and IMP366 (see Figure 8-25 A).

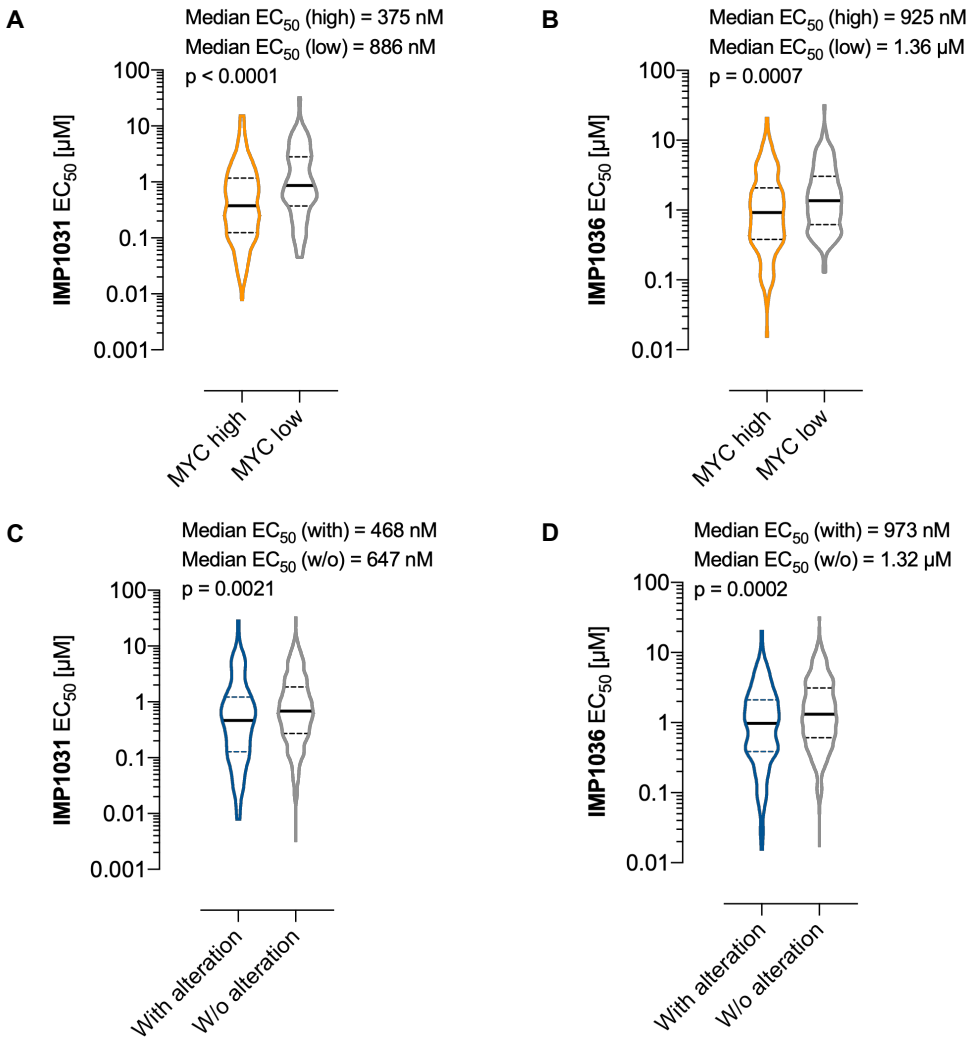

Figure 4-3: Cell lines with high MYC expression or alterations in the MYC/MYCN genomic loci are more responsive to the NMT inhibitors IMP1031 and IMP1036.

[A] Comparison of the EC_{50}s for IMP1031 of the quartiles with highest and lowest expression of *MYC*. (both groups: 177 cell lines) **[B]** Comparison of the EC_{50}s for IMP1036 of the quartiles with highest and lowest expression of *MYC*. **[C]** Comparison of the EC_{50}s for IMP1031 of cells with and without mutations and/or RACS and/or CN gains of >8 in the genomic loci of *MYC/MYCN*. (with: 124 cell lines; without: 552 cell lines) **[D]** Comparison of the EC_{50}s for IMP1036 of cells with and without mutations and/or RACS and/or CN gains of >8 in the genomic loci of *MYC/MYCN*.
(For all graphs: p-values determined with the Mann-Whitney test)

Mutations, CN gains and RACSs are reported by the Sanger in their pre-processed omics data sets (Iorio et al., 2016), and the presence of those in *MYC* or *MYCN* loci increases their respective mRNA expression (see Figure 8-26 A). Additionally, the presence of those structural alterations correlates with increased activation of different MYC hallmark gene sets (see Figure 8-26 B) (Liberzon et al., 2015), thus,

their predictive capacity for responsiveness to NMT inhibition was investigated. The pharmacogenomics screen data sets were divided by cancer cell lines with alterations (that is CN gains of >8 and/or presence of mutations and/or presence of RACSs for *MYC* and/or *MYCN*) and without. For IMP1031 and IM1036 (see Figure 4-3 C and D respectively) cancer cell lines that have these alterations in the genetic loci are significantly more sensitive to NMT inhibition than the ones without. While a clear trend is observed for IMP366, it did not reach significance (p-value = 0.107) (see Figure 8-26 B). To understand in greater detail the effect of the individual type of structural alteration, the analysis was conducted in cancer cell lines with or without CN gains, mutations or RACSs respectively (See Figure 8-27 A).

The strongest effect was observed for mutations for both IMP1031 and IMP1036, with the biggest differences in median EC_{50}s. The presence of RACS had no significant effect on the median EC_{50}s between the two groups. As shown in Figure 8-27 B different cell lines are affected by the respective structural alteration, with cancer cell lines of the Blood tissue particularly strong enriched in the group with mutations, likely driving the strong effect seen there (see Figure 8-27 C). The enrichment of the Blood tissue group within the group of cancer cells with mutations in *MYC*/*MYCN* is likely due the fact that e.g. Burkitt's lymphoma is known to have large proportion of mutations on *MYC* (>70% present mutations) (Love et al., 2012; Schmitz et al., 2012). Overall, the presence of structural alterations was less predictive than *MYC* mRNA expression on its own. This is likely due to the fact that *MYC* expression can be upregulated through other means, such as deregulated Wnt signalling through loss of APC (Dang, 2012). The inclusion of these cancer cell lines in the group without alterations might explain the weaker predictive capacity of the presence of structural alteration on *MYC*/*MYCN*. Nonetheless, the 'Sensitive to NMTi' signature is enriched in the cancer cell lines with structural alterations (see Figure 4-4 A).

Additionally, several negative regulators of the MYC oncogenic program have been shown to be subject to shallow deletions in the TCGA data, potentially increasing the complexity even further (Schaub et al., 2018). To test for the possibility that heterozygous loss of a single copy of negative regulators (that is MGA, MNT, MXD4, MXD3 and MXI1 (Schaub et al., 2018)) has an impact on the efficacy of NMT inhibition, cell lines with such a shallow loss were compared to the remaining cell

lines (11% of these cell lines had MYC amplifications). No consistent trend of increased sensitivity or resistance was observed for IMP1031 and IMP1036–in case of the former, the cancer cell lines with shallow loss of a member of the MDX family were more resistant to IMP1031 (see Figure 8-28 A and B).

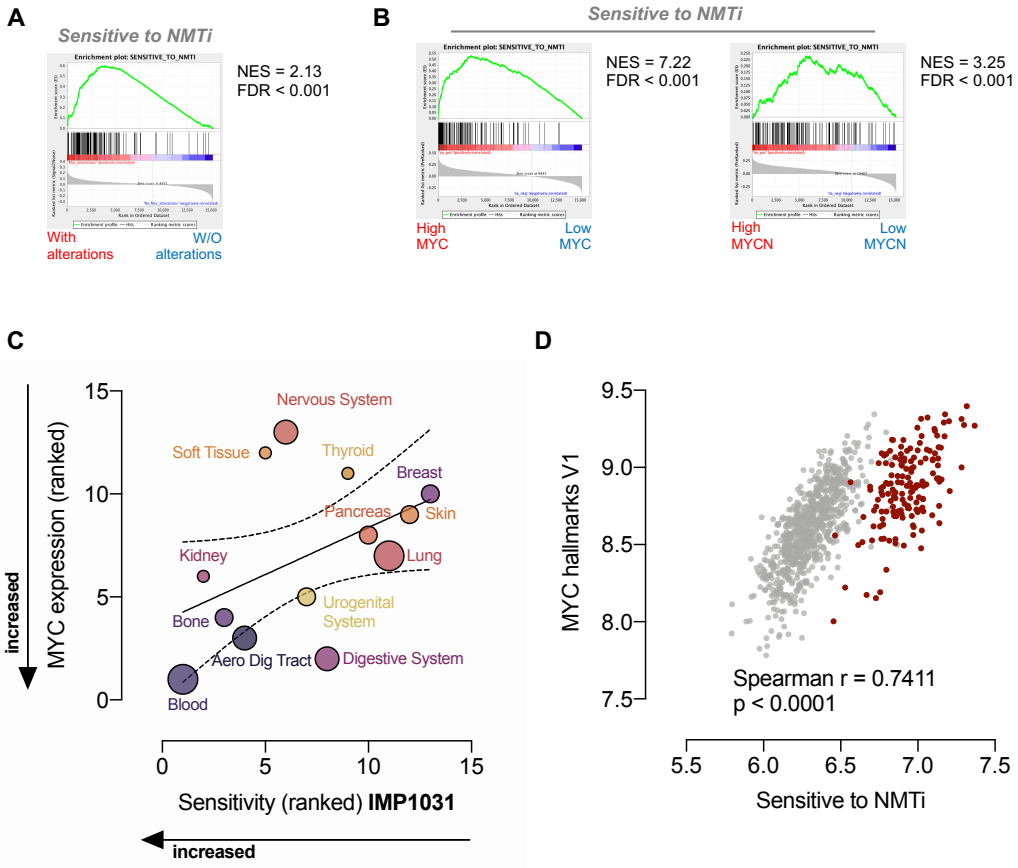

Figure 4-4: The 'Sensitive to NMTi' gene set is in cells with high MYC or MYCN expression or structural alterations, and MYC expression in the tissues predicts sensitivity.

[A] GSEA plot showing that cells with structural alterations in MYC/MYCN are enriched in the 'Sensitive to NMTi' gene set. **[B]** GSEA plots showing that MYC (left) and MYCN (right) expression correlates positively with the 'Sensitive to NMTi' gene set. **[C]** Sensitivity to IMP1031 (EC_{50}s were used as measure) and median expression of MYC of each tissue subtype were plotted. The size of the circle indicates number of cell lines in each tissue subclass. The dotted lines are the 90% CI of the linear regression function plotted. **[D]** Correlation for the activation of the MYC hallmarks V1 gene set and the Sensitive to NMTi gene set. The red dots are cells from the tissue subgroup 'Blood'.

To understand the link between *MYC* (or *MYCN*) upregulation and the 'Sensitive to NMTi' gene set, the expression of *MYC* (or *MYCN*) was correlated, via Spearman, to all other genes in the COSMIC microarray data (Iorio et al., 2016), resulting in a

large list of Spearman coefficients. This list of coefficients was used as a ranked list for GSEA as a surrogate of gene activation by MYC or MYCN respectively (Subramanian et al., 2005). This approach is similar to the analysis of other research groups that assessed downstream activation of biological functions of MYC and MYCN (Schaub et al., 2018; Subramanian et al., 2005). Both *MYC* and *MYCN* expression (see Figure 4-4 B) correlate with activation of the 'Sensitive to NMTi' gene set. Ranking the different tissues of the pharmacogenomic screen of IMP1031 by median *MYC* expression and median EC_{50} shows a relationship between the two. Cancer cell lines from tissues with higher median MYC expression have a lower median EC_{50} for IMP1031, the most potent inhibitor used in the pharmacogenomic screens (see Figure 4-4 C). However, the tissue groups Nervous System, Soft Tissue and Digestive System did not follow this trend. The tissue group Nervous System contains several NB cancer cell lines with the highest MYCN expression overall (data not shown). The sensitivity for this group might not be driven by MYC, but by MYCN. For the two other tissue groups it remains unknown why they are more sensitive or resistant, than anticipated by their respective *MYC* expression. As shown in Figure 4-4 D the activation of the MYC hallmarks V1 gene set, strongly correlates with the activation of the 'Sensitive to NMTi' signature. For this analysis, the geometric mean of all the RMA values, from the Sanger microarray data (Iorio et al., 2016), of the respective gene set was calculated for each cancer cell line and correlated. The cancer cell lines from the tissue group Blood have a higher activation of the 'Sensitive to NMTi' gene set. This is due to the presence of certain immune system related genes, such as CD247, CXCR4, CD28, in the 'Sensitive to NMTi' signature as it was derived from an unbiased approach, without further filtering by biological functionality or similar and the strong enrichment of haematological malignancies in the sensitive cancer cell lines.

To test the validity of the NMT-MYC relationship in an additional different context, the data from the recent CRISPR gene essentiality screen by the Sanger Institute was analysed (Behan et al., 2019). After combining the CRISPR data with the COSMIC expression data (Iorio et al., 2016) 87 cell lines (27%) were identified as dependent on NMT1 (see Figure 4-5 A). To note is that the relative number of cell lines, dependent on NMT1, differ quite drastically from the CRISPR gene essentiality data from the Broad Institute (Meyers et al., 2017), in which >75% of the cell lines

were classified as dependent on NMT1. The Broad Institute utilises a set of core-essential as benchmark for their gene effect score (Hart et al., 2014; Meyers et al., 2017), whereas the Sanger institute uses their 'adaptive daisy model' to distinguish core-fitness and context-specific genes (Behan et al., 2019). The differences are still striking, despite different methodology, and not limited to NMT1. Also, the methionine aminopeptidases MetAP1 and MetAP2, both defined as common essential in the Broad DepMap (with 69% and 88% of the cell lines being dependent), are only considered as essential for cell fitness in 46% and 30% respectively in the data from the Sanger DepMap (Behan et al., 2019; Meyers et al., 2017). The different assessment of gene essentiality could be in the end a question of cut-off, as the Sanger institute aimed to discover the smallest subset of core-essential genes.

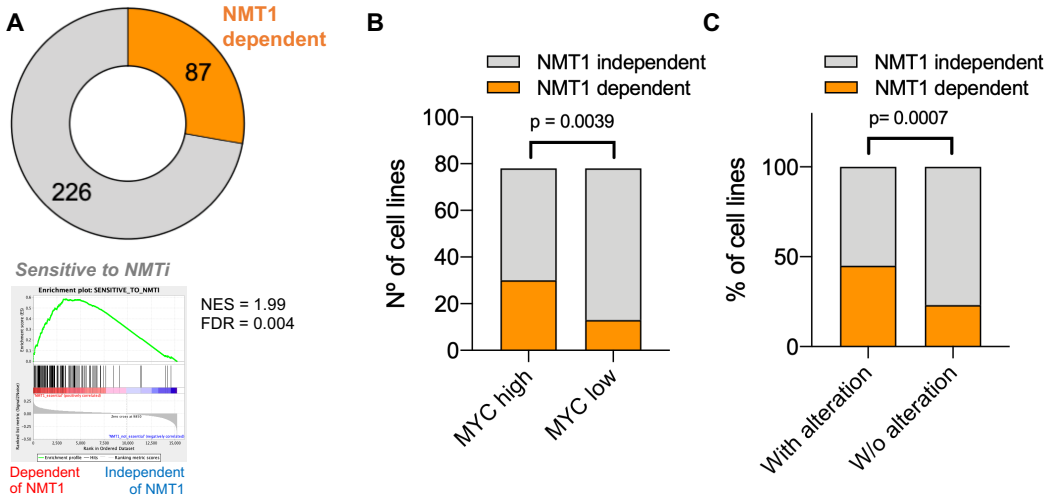

Figure 4-5: Cells dependent on NMT1 are overrepresented in the MYC high cells and/or cells with alterations in the MYC/MYCN loci in the Sanger DepMap.

[A] The 87 cell lines, dependent on NMT1, are enriched in the 'Sensitive to NMTi' gene set, compared to the cells that are not dependent (see GSEA plot). **[B]** Cells that are dependent on NMT1 are overrepresented in the cells with highest *MYC* mRNA expression, compared to cells with lowest *MYC* mRNA expression. **[C]** Cells that are dependent on NMT1 are overrepresented in cell lines with alterations (that is mutations and/or CN gains and/or RACS in the *MYC/MYCN* loci).
(For all graphs: p-values determined with the Fisher's exact test)

Nonetheless, the cells dependent on NMT1 within the Sanger DepMap were enriched for the 'Sensitive to NMTi' gene set (see Figure 4-5 A). This again validates that high expression of these genes correlates with increased dependence on myristoylation. The cells were divided by quartiles into the cancer cell lines with the highest expression and the lowest expression of *MYC*, similar to the previous

approaches. The quartile with the cells with the highest expression of *MYC* is overrepresented in cells dependent on NMT1, compared to the quartile with the lowest expression (NMT1 dependent cancer cell lines in the MYC high quartile: 30 – 38.5%; NMT1 dependent cancer cell lines in the MYC low quartile: 13 – 16.7%) (see Figure 4-5 B). The effect of the presence of structural alterations (that is: CN gains of >8 and/or mutations present and/or RACS) in the *MYC*/*MYCN* loci on the dependence on NMT1 was also analysed in this data set. Similar to the results obtained from the pharmacogenomics screens, cancer cell lines that presented structural alterations in the *MYC*/*MYCN* loci present are overrepresented with cell lines that are dependent on NMT1 (NMT1 dependent cancer cell lines with alterations: 31 out of 69 (45%); NMT1 dependent cancer cell lines without alterations: 58 out of 250 (23%)) (see Figure 4-5 C) The observation that MYC high cells were more dependent on NMT1 in CRISPR gene essentiality screens was also made within the data from the Broad Institute dependency map (see Figure 4-5 A and B) (Meyers et al., 2017; Tsherniak et al., 2017). Cancer cell lines with high *MYC* mRNA expression, compared to the ones with low *MYC* mRNA expression, had significantly lower median gene scores for NMT1, indicating increased dependence (see Figure 8-29 A). Dividing the cancer cell lines, screened by the Broad institute, by cells that have 4 copies of MYC (log2 ploidy > 1) and/or mutations in *MYC*, and those without, yields in a similar trend, however, it did not reach significance with a p-value of 0.06 (see Figure 8-29 B). Overall, these data demonstrate that cells with high levels of *MYC* mRNA (or structural alterations in *MYC* and in parts *MYCN*) correlate with increased dependency on myristoylation compared to other cells, independently if myristoylation is blocked by a dual NMT1/2 inhibitor as used in the pharmacogenomics screens, or by genetic knockout of the essential paralog NMT1.

4.2.3 Enforced expression of MYC or MYCN in isogenic models increases lethality of NMT inhibition; and PDX with MYC translocation are highly responsive to NMTi *in vitro*

To test the observations from the previous subchapter that *MYC* mRNA expression increases the responsiveness to NMT inhibition, the P-493-6 cell line was used: an immortalised B cell line that allows for the control of MYC levels depending

on culture conditions (Pajic et al., 2000). Upon treatment with doxycycline a 'MYC low' state is induced; upon combined treatment of doxycycline and β-estradiol the 'MYC medium' state is induced; the 'MYC high' state is the default under normal cell culture conditions.

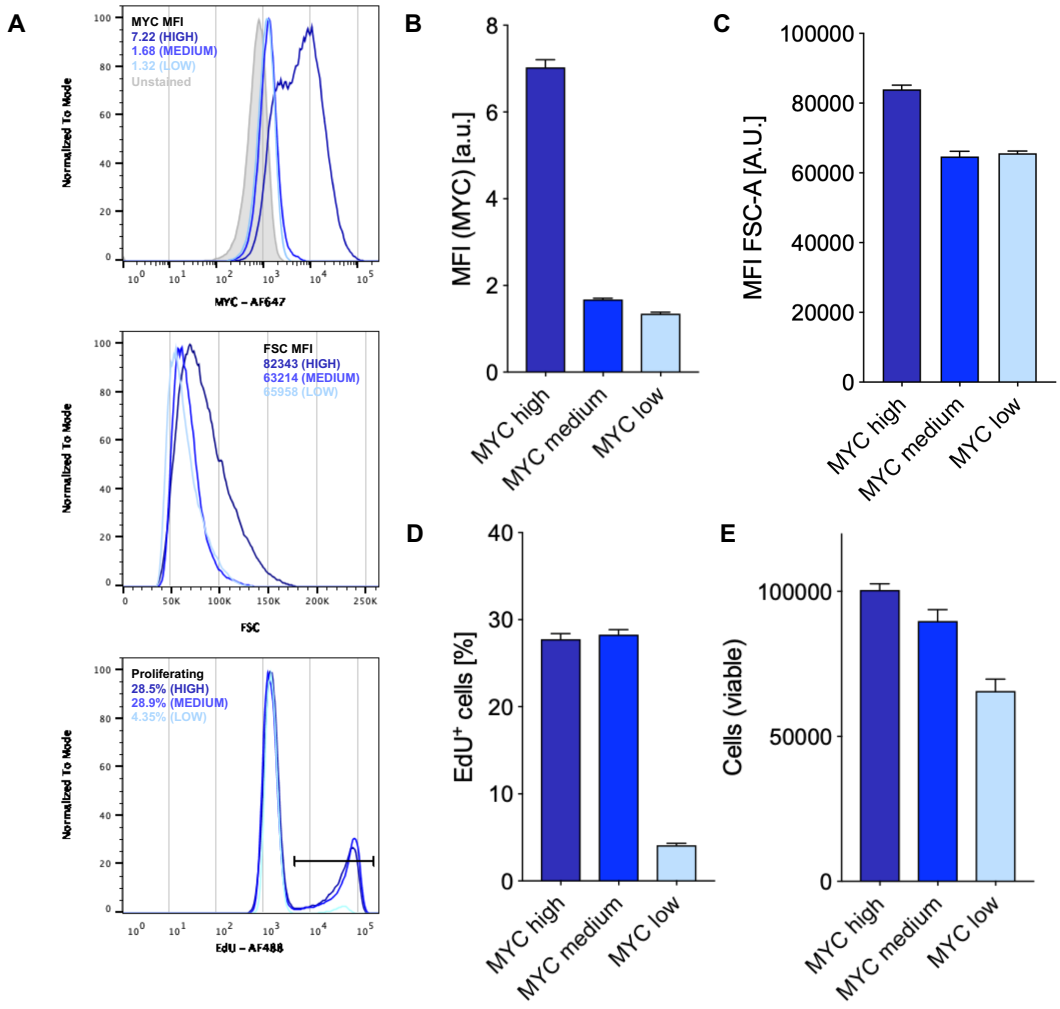

Figure 4-6: Validation of the P-493-6 cell line and the effect of MYC expression on cell size, DNA synthesis and cell numbers.

[A] Top: Representative flow cytometry analysis of the MYC protein levels upon no treatment (dark blue; MYC high), adding 100 ng/mL doxycycline and 1 µM β-estradiol for 48 hours (blue; MYC medium), and 100 ng/mL doxycycline for 48 hours (light blue; MYC low). Middle: Representative flow cytometry analysis of the cell size by forward scatter upon induction of the different MYC states. Bottom: Representative flow cytometry analysis of the EdU incorporation upon induction of the different MYC states. **[B]** Quantification of the MYC MFI. **[C]** Quantification of the FSC MFI. **[D]** Quantification of the EdU incorporation. **[E]** Quantification of the cell numbers after 48 hours of induction of the different MYC states.

To validate that the different culture conditions were indeed causing different MYC states, flow cytometry was employed. The cells were left for 48 hours in the respective condition and were subsequently analysed. The different conditions caused different protein levels of MYC, with profound effects on cell size and DNA synthesis, as shown by the FACS analysis with representative examples shown in Figure 4-6 A. MYC levels were strongly increased in the MYC high condition with higher median fluorescence intensities (MFI) (see Figure 4-6 B), impacting cell size, measured by forward scatter (see Figure 4-6 C). The relative number of cells engaging in DNA synthesis (measured as EdU incorporation) was similar between MYC medium and high (see Figure 4-6 D); however, the cell numbers were higher in the MYC high condition, indicating potentially faster cycling (see Figure 4-6 E).

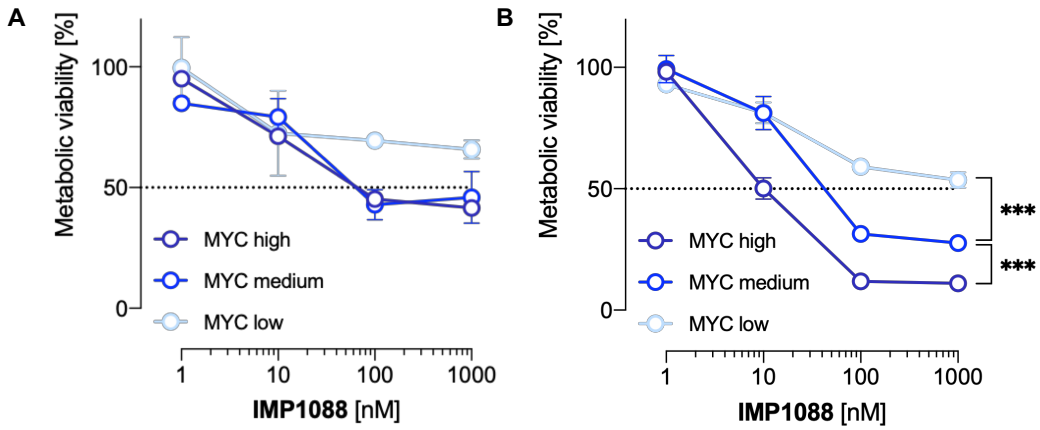

Figure 4-7: IMP1088 preferentially reduces viability in MYC high cells.

[A] Metabolic viability, assessed by CellTiter Blue, of the different MYC states after 48 hours of treatment with IMP1088. **[B]** Metabolic viability, assessed by CellTiter Blue, of the different MYC states after 72 hours of treatment with IMP1088.
(For all graphs: N = 4, error bars = SEM, ANOVA)

As the genetic system of the P-493-6 induced different MYC levels, the effect of IMP1088 for 48 hours and 72 hours of inhibition was tested dependent on these levels. The cells were cultured for 24 hours in the respective media conditions to induce the different expression levels of MYC. Additional media and compound was added after this initial incubation period, and the experiment was ended after two days or three days of NMT inhibition. After two days of inhibition, the MYC high and medium cells were less metabolically active, indicating increased cell death, than the MYC low cells (see Figure 4-7 A).

At 72 hours the MYC high cells were showing a stronger decline in metabolic viability than the two other MYC conditions, clearly showing increased toxicity of NMT inhibitors upon higher levels of MYC expression, confirming the trends observed in the previous subchapter (see Figure 4-7 B). The same results were obtained with IMP366 considering the overall reduced cellular potency of this compound, compared to IMP1088 (Kallemeijn et al., 2019) (see Figure 8-30).

To orthogonally validate the synthetic lethality, the effect of IMP1088 over time on several parameters with different MYC levels was measured via flow cytometry. The cells were preincubated for 24 hours in the respective media condition to induce the different MYC levels. After this incubation period, the NMT inhibitor (concentrations ranging from 1 µM to 10 nM) in fresh media was added, and the cells were harvested (with prior EdU pulse) and fixed for subsequent analysis via flow cytometry (see Figure 4-8 A). In line with the results obtained with the CellTiter Blue assay, 100 nM of IMP1088 had a small to no effect on the cell numbers of MYC low. However, it caused a reduction of viable cells in the MYC medium cells, and a large reduction of viable cells in the MYC high cells at the later time points (see Figure 4-8 B). Notably, the MYC low cells were actually completely unaffected in terms of cell numbers, but still showed decreased metabolic activity, implying that NMT inhibition does not affect cell viability *per se*, but might cause reduced mitochondrial activity if MYC levels are low. The reduction in cell numbers was driven by increased cell death, as evident in the relative drop of cells with intact membranes (measured by incorporation of Zombie NIR), compared to the control (see Figure 4-8 C). Cell cycle analysis revealed that at 72 hours of NMT inhibition the few remaining cells in the MYC high state still engage in DNA synthesis upon NMT inhibition, whereas the MYC medium cells arrest completely in G1/0. On the other hand, the MYC high cells show an increase in G2/M upon NMT inhibition, likely due to their continued engagement of cycling, in accordance with the role of MYC in G1 to S transition (Santoni-Rugiu et al., 2000) and DNA replication (Dominguez-Sola et al., 2007).

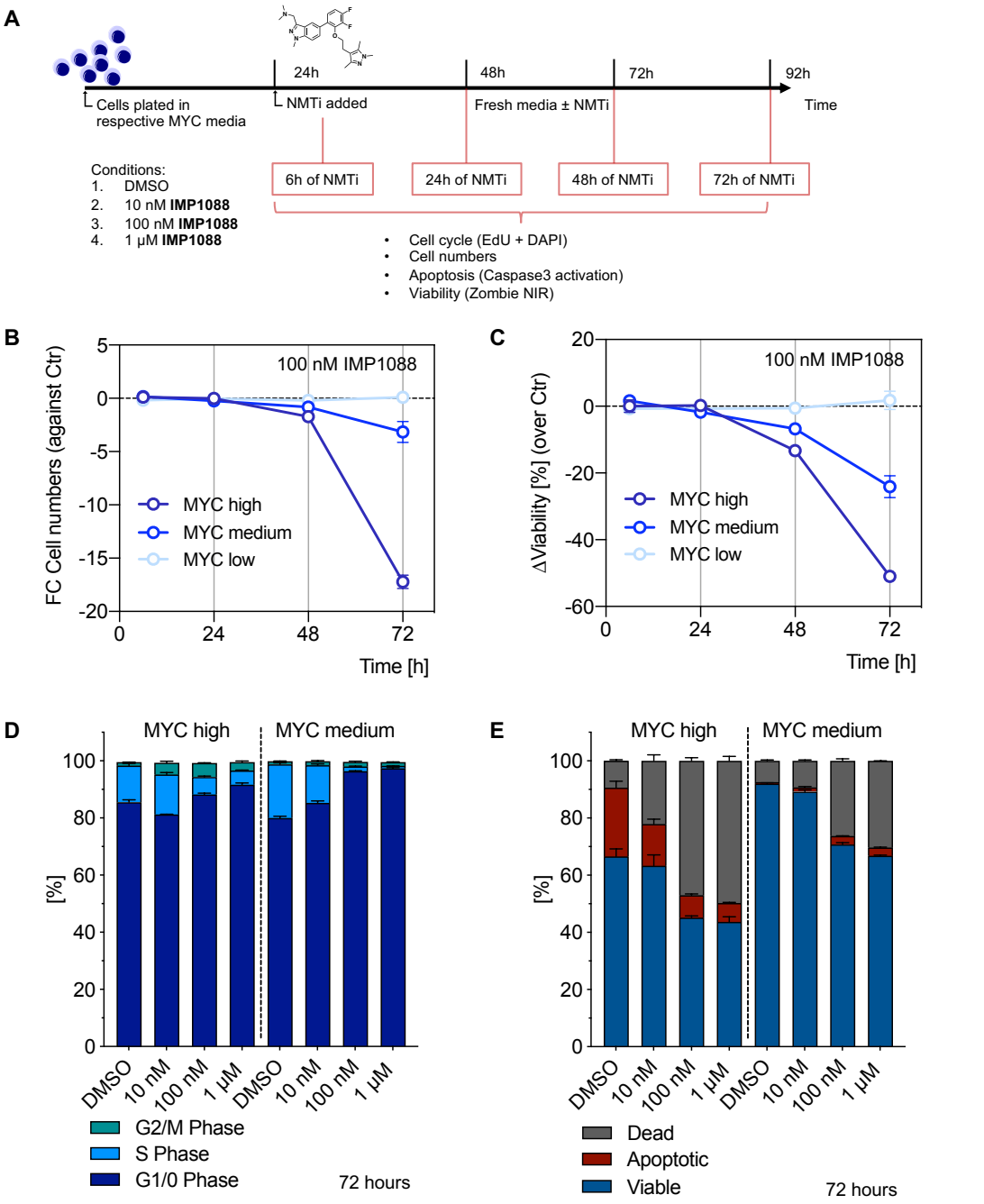

Figure 4-8: NMT inhibition kills rapidly MYC high cells and causes G2/M accumulation.

[A] Experimental design to assess the temporal effects of IMP1088 on the P-493-6 cell line with induction of the different MYC states. Cells were plated in the different conditions to induce MYC, and left for 24 hours. IMP1088 (1 µM, 100 nM, 10 nM) or DMSO was added. *(Legend continued on the next page)*
Two hours prior to fixation, EdU was pulsed to assess DNA synthesis. Subsequent use of different FACS stainings allows to follow cell cycle, apoptosis induction and cell viability across conditions and time points (6, 24, 48 and 72 hours). **[B]** FC in cell depletion compared to the DMSO for all the MYC states, showing the effect of 100 nM

IMP1088, compared to control for each time point. **[C]** Change in viability (as measured by Zombie NIR negative) showing the effect of 100 nM IMP1088, compared to DMSO for each time point. **[D]** Quantification of the cell cycle distribution at 72 hours. **[E]** Quantification of the relative numbers of viable, apoptotic cells (with intact membranes and activated caspase 3), and dead cells (w/o intact membranes) after 72 hours of NMT inhibition.
(For all graphs N = 2, error bars = SEM)

Additionally, the MYC high cells also suffered from more cell death and apoptosis, compared to the MYC medium cells (see Figure 4-8 E). The data showed that cells with MYC levels below the threshold necessarily to engage actively in cycling are barely affected by NMT inhibition, whereas cells with strongly enforced levels of MYC are rendered highly susceptible to NMT inhibition to a point where even lower concentration of 10 nM IMP1088 affect cells negatively (see Figure 8-31 and Figure 8-32). The effects on DNA synthesis across all the time points and concentrations are shown in Figure 8-33.

As synthetic lethality was observed with MYC, the question arose if this synthetic lethality would also work in a different cellular context (suspension *versus* adherent) and with MYCN (N-Myc). Thus, the Shep-ER-MYCN cell was obtained from collaborators, an NB cancer cell line that upon treatment with tamoxifen expresses high levels of MYCN to mimic the highly aggressive MYCN amplified form of NB (Rickman et al., 2018; Valentjin et al., 2005). As shown in Figure 4-9 A, treatment with 100 nM of Tamoxifen for 24 hours caused increased MYCN protein levels. The increased MYCN levels affected global protein synthesis (see Figure 4-9 B), measured by O-propargyl-puromycin incorporation (OPP) (Liu et al., 2012); additionally, there was increased DNA synthesis and cell cycling upon induction of MYCN (see Figure 4-9 C), in line with known biology of MYCN (Bell et al., 2007).

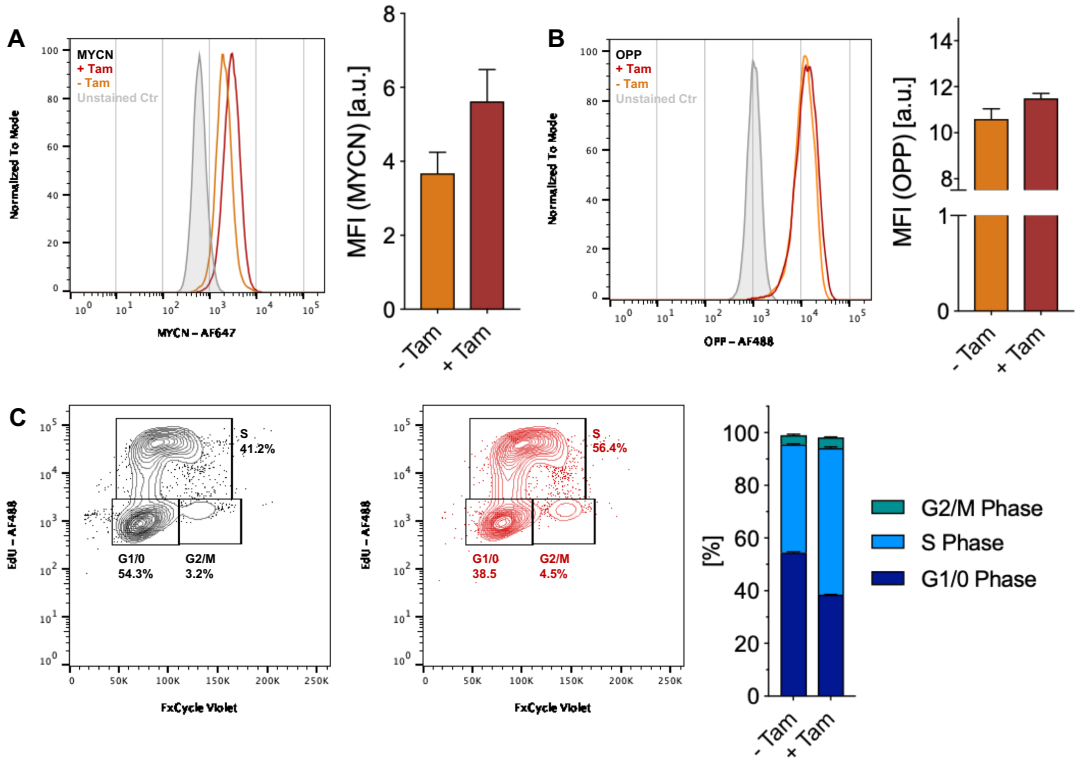

Figure 4-9: Validation of the MYCN-ER-Shep cell line and the effect of MYCN amplification on protein synthesis and cell cycle.

[A] Left: Representative flow cytometry analysis of the MYCN induction upon treatment with 100 ng/mL Tamoxifen for 24 hours. Right: Quantification of the MYCN MFI. **[B]** Left: Representative flow cytometry analysis of the OPP incorporation upon treatment with 100 ng/mL Tamoxifen for 24 hours. Right: Quantification of the OPP MFI. **[C]** Left: Representative flow cytometry analysis of the cell cycle distribution. (Black: Control; Red: with tamoxifen). Right: quantification of the cell cycle analysis.
(For all graphs N = 3, error bars = SEM)

Similar to enforced MYC expression, enforced MYCN expression also increased the toxicity of the two NMT inhibitors IMP1088 (see Figure 4-10 A) and IMP366 (see Figure 4-10 B) at 72 hours of incubation. These results show that the synthetic lethality is independent of tissue context, and applies to at least two of the paralogs of the MYC family.

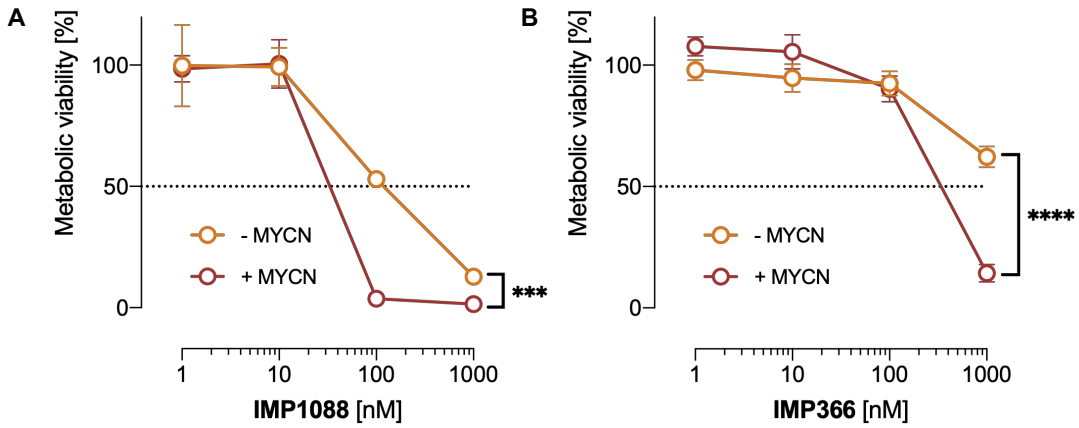

Figure 4-10: Induction of MYCN increases toxicity of NMT inhibition.

[A] Metabolic viability, measured with CellTiter blue, ± induction of MYCN after 72 hours of treatment with IMP1088. **[B]** Metabolic viability, measured with CellTiter blue, ± induction of MYCN after 72 hours of treatment with IMP366.
(For all graphs: N = 4, error bars = SEM, Student t-test)

To orthogonally confirm the synthetic lethality with enforced MYCN expression and to assess differences in cell death kinetics, flow cytometry was applied, similar to the previously tested P-493-6 cell line. The cells were plated and left overnight to allow for attachment. Tamoxifen (100 nM) was given for 24 hours to induce MYCN, or EtOH in control conditions. The media was removed and fresh media with(out) IMP1088 (in various concentrations) or Tamoxifen was added. For the later time points (48 hours and 72 hours) fresh media was added to the cells with respective concentrations of Tamoxifen and IMP1088 (see Figure 4-11 A). Prior to fixing the cells were pulsed with EdU. Very comparable to the P-493-6 cell line, the induction of MYCN caused a rapid loss of viable cells (see Figure 4-11 B), in parallel with a stark loss of membrane integrity indicating increased cell death (Figure 4-11 C).

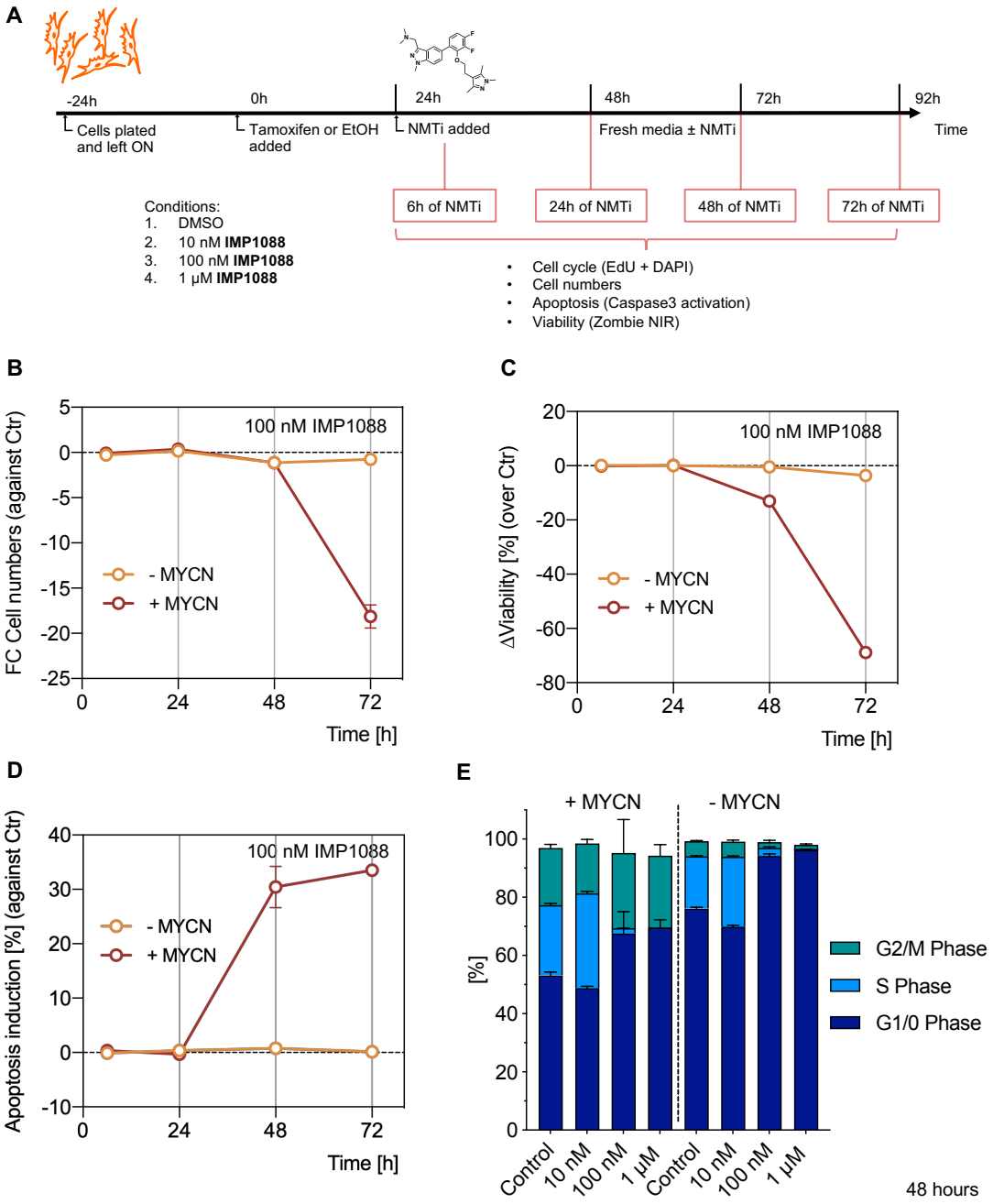

Figure 4-11: NMT inhibition kills rapidly cells upon MYCN induction and causes G2/M accumulation.

[A] Experimental design to assess the temporal effects of IMP1088 on the MYCN-ER-Shep cell line with induction of MYCN. Cells were plated and left overnight to recover. After 24 hours Tamoxifen or EtOH was added to induce MYCN. After 24 hours of induction of MYCN, IMP1088 (1 µM, 100 nM, 10 nM) or DMSO was added. *(Legend continued on the next page)*
Two hours prior fixing, EdU is pulsed in the cells to monitor DNA synthesis. Subsequent use of different flow cytometry stainings allows to follow cell cycle, apoptosis induction and cell viability/numbers across conditions and time points (6, 24, 48 and 72 hours).
[B] FC in cell depletion compared to the control for all the MYC states, showing the effect

of 100 nM IMP1088, compared to control for each time point. **[C]** Change in viability (as measured by Zombie NIR^+) showing the effect of 100 nM IMP1088, compared to control for each time point. **[D]** Activation of caspase 3 showing the effect of 100 nM IMP1088, over the control for each time point. **[E]** Quantification of the cell cycle distribution at 48 hours.
(For all graphs N = 2, error bars = SEM)

Increased activation upon treatment with 100 nM IMP1088 of caspase 3 (over the control) was observed from 24 hours onward in the MYCN induced condition, but not in the control condition. Similar to the observations in the P-493-6 cell line, enforced MYCN expression caused increased G2/M accumulation in the Shep-ER-MYCN cell line (see Figure 4-11 E). Dr. Faronato obtained similar results in the CellTiter Blue assay and FACS experiment in a different model of MYCN amplification, the SKNAS-ER-MYCN cell line (Ushmorov et al., 2008) (data not shown). In conclusion, several isogenic systems with inducible MYC or MYCN show that the toxicity of NMT inhibition increases with increasing levels of MYC or respectively MYCN, causing rapid loss of viability and cell numbers.
Additionally, we kindly obtained from Martin Janz, a collaborator, several patient derived xenografts (PDX) lymphoma cell lines, all with MYC translocations. These could be grown *in vitro* and *in vivo*, and the effect of NMT inhibitors on those cell lines was assessed. Details about the type of lymphoma, markers, and translocation are shown in Table 4-2 and were provided (unpublished data).

Table 4-2: Tested lymphoma PDX and details.

Cell line	Diagnosis	Nanostring	FISH
LY11212	DLBCL	GCB	BCL2 break, BCL6 break, MYC break, 8;14 fusion positive
LY12318	DLBCL	ABC	MYC break, BCL2 break, 8;14 fusion positive
LY12657	Plasmablastic lymphoma	N/A	MYC break, 8;14 fusion positive

To note are the BCL2 and MYC translocations for the two DLBCL cell lines, LY11212 and LY12318. defining so called ‘double hit DLBCL’. These ‘double hit’ DLBCL are associated with worse clinical outcome in the clinic (Riedell and Smith, 2018).

Plasmablastic lymphoma is also prone to relapse and acquire resistance to chemotherapy, thus also has poor clinical outcomes (Castillo et al., 2015).

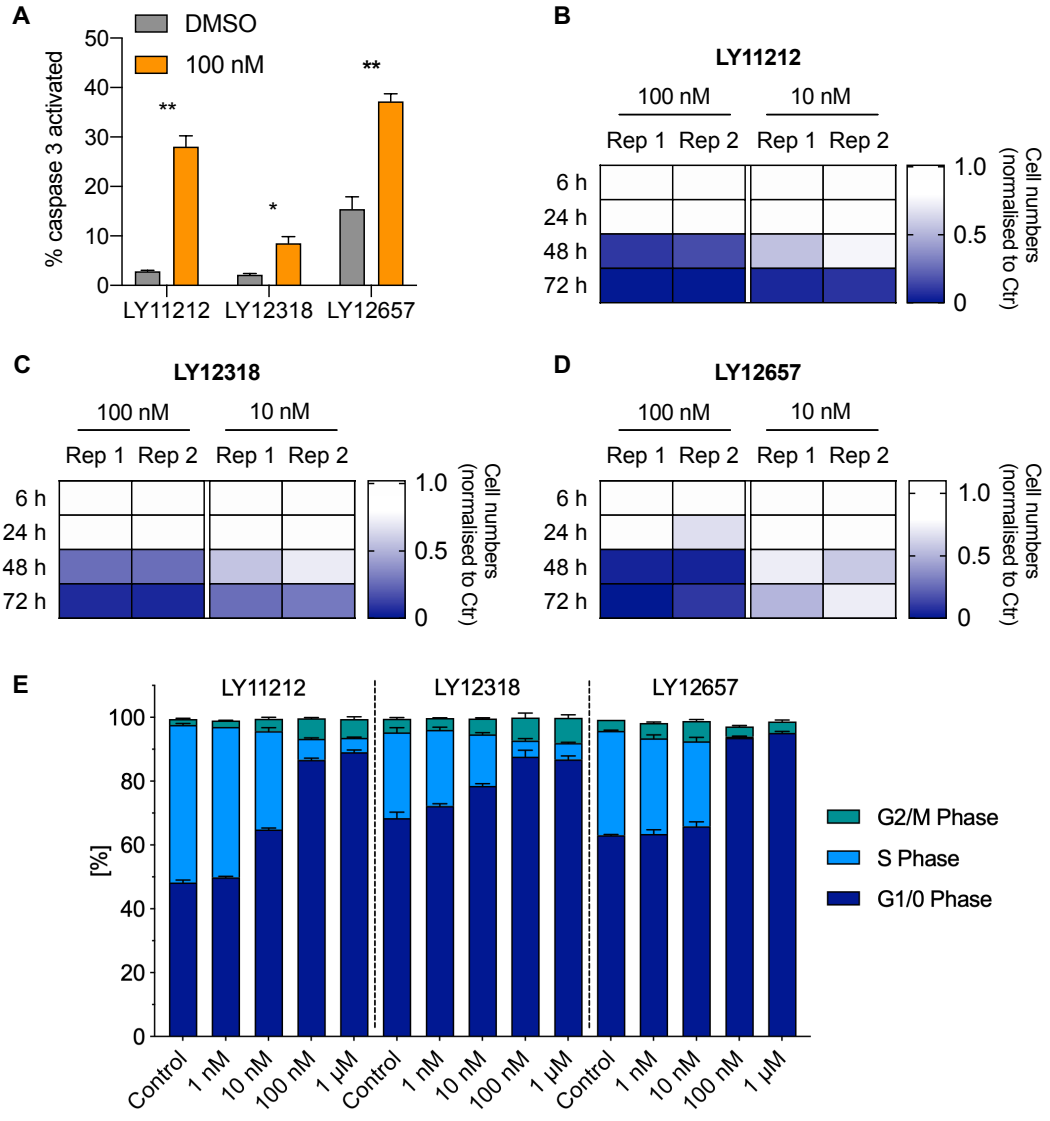

Figure 4-12: Lymphoma PDX (DLBCL and plasmablastic lymphoma), with MYC translocation, are highly responsive to NMT inhibition.

[A] Induction of caspase3 at 24 hours of NMT inhibition. **[B]** FC in cell numbers for LY11212, normalised to the control for all the time points, showing the effect of 100 and 10 nM IMP1088. **[C]** FC in cell numbers for LY12318, normalised to the control for all the time points, showing the effect of 100 and 10 nM IMP1088. **[D]** FC in cell numbers for LY12657, normalised to the control for all the time points, showing the effect of 100 and 10 nM IMP1088. **[D]** Quantification of the cell cycle distribution at 48 hours.
(For all graphs N = 2, error bars = SEM)

The same experimental setup as shown in Figure 2-14 was applied to measure the effect of IMP1088 over time on the three different PDX. Surprisingly, induction of

apoptosis was already observed within 24 hours of NMT inhibition (see Figure 4-12 A). This was followed by a rapid reduction in cell numbers, across the three PDX (see Figure 4-12 B to D). Particularly in LY11212 and LY12657 <5% viable cells were detected at 48 hours of treatment with NMT inhibition. Additionally, 10 nM of IMP1088 sufficed to negatively affect LY11212 and LY12318, with some delay in effect (towards 72 hours, instead of 48 hours for 100 nM). G2/M accumulation was observed for LY11212 and LY12318; interestingly, LY12657 was arrested in G1/0 (see Figure 4-12 E). The detailed cell number, proliferation and apoptosis data for the all the concentrations and time points of LY11212 are shown in Figure 8-35; the data for LY12318 are shown in Figure 8-36; and the data for LY12657 are shown in Figure 8-37. While no PDX, without a MYC translocation was tested, the lymphoma PDXs with MYC translocations are exceptionally susceptible to NMTi. Notably, the kinetics in induction of cell death are faster compared to the tested immortalised cancer cell lines. Already at 24 hours of inhibition with IMP1088 at least a 2-fold increase of caspase 3 activation, compared to control, was observed for each of the PDX.

These data, and the data obtained in two isogenic models with inducible MYC or MYCN levels, demonstrate synthetic lethality between NMT inhibition and levels of either MYC paralog, confirming the trends observed in the pharmacogenomics and CRISPR gene essentiality screens, shown in section 4.2.2.

4.2.4 High levels of MYC accelerate the breakdown of most biological functions and the MYC program itself upon NMTi

To elucidate the differential toxicity of NMT inhibition, dependent on the MYC level, total RNAseq was conducted to compare the effect of NMT inhibition, dependent on MYC levels. The P-493-6 cell line was cultured for 24 hours in the respective media condition to induce medium MYC levels or high MYC levels, and 100 nM IMP1088 were added for 24 hours (or a respective control). The aim of this experiment was to primarily identify differential behaviour upon NMT inhibition, dependent on the different MYC levels. As anticipated under control conditions, the MYC high cells expressed many more RNA copies of *MYC* than the MYC medium cells (see Figure 4-13 A). Thus, also as expected, the MYC high, in control

conditions, have higher activation of the MYC transcriptional program–the Hallmark MYC V1 gene set served as a surrogate for this transcriptional program (Liberzon et al., 2015). Additionally, the gene set 'Sensitive to NMTi' was also enriched in the MYC high cells (see Figure 4-13 B).

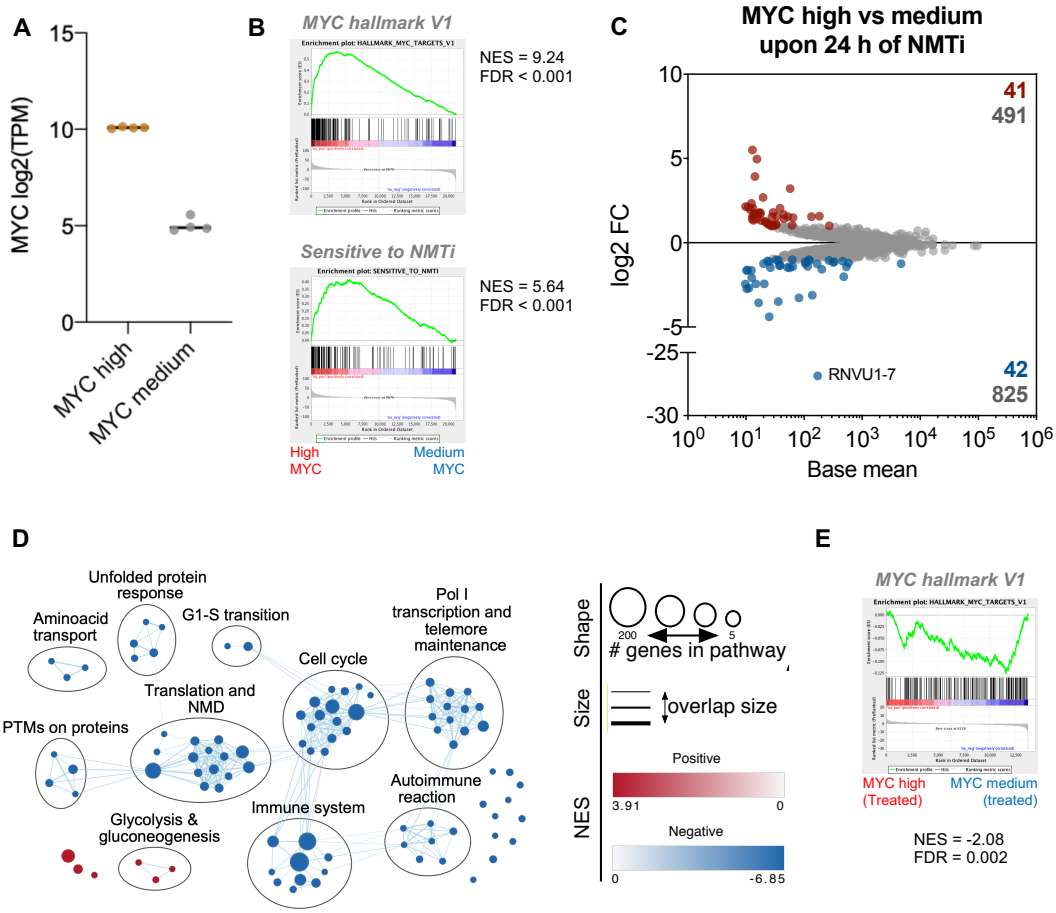

Figure 4-13: High levels of MYC, combined with NMT inhibition, cause a rapid breakdown of the MYC transcriptional program.

[A] MYC expression levels after 48 hours, comparing MYC high and MYC medium under control conditions are shown. **[B]** Effect of higher MYC expression on the activation of the Hallmark MYC V1 and the Sensitive to NMTi gene set. **[C]** Scatter plot showing the log2FC and baseMean of all significantly changing genes upon, comparing MYC high and MYC medium (both treated for 24 h with 100 nM IMP1088). **[D]** Network, created with the EnrichmentMap plug-in into CytoScape, summarising the GSEA, comparing MYC high (treated) and MYC medium (treated). (FDR < 0.01, Jaccard Overlap combined = 0.375, k constant = 0.5) **[E]** Effect of 100 nM IMP1088 after 24 hours on the MYC hallmark V1 gene set, comparing MYC high and MYC medium.

This further confirms the correlation between MYC activation and the 'Sensitive to NMTi' gene set observed across the COSMIC cancer cell lines, discussed in section 4.2.2.

To assess the differential effect of NMT inhibition, dependent on MYC levels, the MYC high were compared to the MYC medium cells (the comparison was done on 'treated over control' MYC high vs. 'treated over control' MYC medium). A first observation was that one of the strongest significantly, differentially expressed genes was RNVU1-7, a U1 variant. This snRNA was strongly induced in the treated MYC medium cells, upon treatment with NMT inhibitor, but not in the MYC high cells, resulting in a massive log2FC difference between the two conditions. Few publications are available about variants of U1 and their function. One of the publications implied that subsets of U1 variants are expressed in HeLa and human ESCs, and similar to the parental U1 can cause shortening of mRNA in a subset of genes and are involved in gene expression control (O'Reilly et al., 2013). To note is that the snRNA U1 and its variants have very high sequence similarity, in times only a single base-pair is different. The initial work describing the role of the snRNA U1 in protecting from premature termination and polyadenylation, would target all U1 variants with its antisense morpholino oligonucleotide (Kaida et al., 2010). Nonetheless, the downregulation of RNVU1-7 is interesting, particularly in light of the mRNA shortening phenotype in BL41 (see Chapter 3). To fully understand the effect of NMT inhibition on mRNA length control, potentially dependent on MYC levels, 3'-end sequencing, comparing all the different conditions, would be needed (Hoque et al., 2013) (see Chapter 6).

To identify which pathways were differentially affected by the NMT inhibition in the different MYC states, GSEA was performed on data set, shown in Figure 4-13 C (Subramanian et al., 2005). The analysis was run utilising the curated gene sets as in previous analysis across this thesis (Liberzon et al., 2015). The resulting GSEA results were also summarised and visualised in networks with CytoScape and the EnrichmentMap plug-in, following the recently published work-flow, as in the previous analysis in the sections 3.2.2, 3.2.3 and 4.2.1 (Merico et al., 2010; Reimand et al., 2019; Shannon et al., 2003). As shown in Figure 4-13 D upon NMT inhibition, several key biological function, ranging from cell cycle, translation, Pol I transcription and telomere maintenance were down regulated in the MYC high condition compared to

the MYC medium condition. This could indicate a collapse of all of these functions. Compared to BL41, Pol II RNA processing and splicing was not among the major pathways, differentially affected by NMT inhibition in the two MYC levels. *MYC* mRNA levels themselves were not significantly differentially affected by the NMT inhibition between MYC high and MYC medium, that is no downregulation was observed in either case (data not shown); however, it seems that the MYC driven transcriptional program is disproportionally more negatively affected in the MYC high cells, treated with NMTi (see Figure 4-13 E).

While a mechanistical reason for this synthetic lethality remains unknown to date (see section 6.1.4 for a possible mechanism), it is clear that such a lethal synergy could have wide clinical implications. Firstly, two 'double-hit' DLBCL PDX, LY11212 and LY12318, usually associated with worse clinical outcome (Riedell and Smith, 2018), were shown *in vitro* to be highly susceptible to NMT inhibition. Also, a plasmablastic lymphoma, LY12657, again a disease known for its poor patient outcome, was shown to be quickly decimated by NMT inhibition (Castillo et al., 2015).

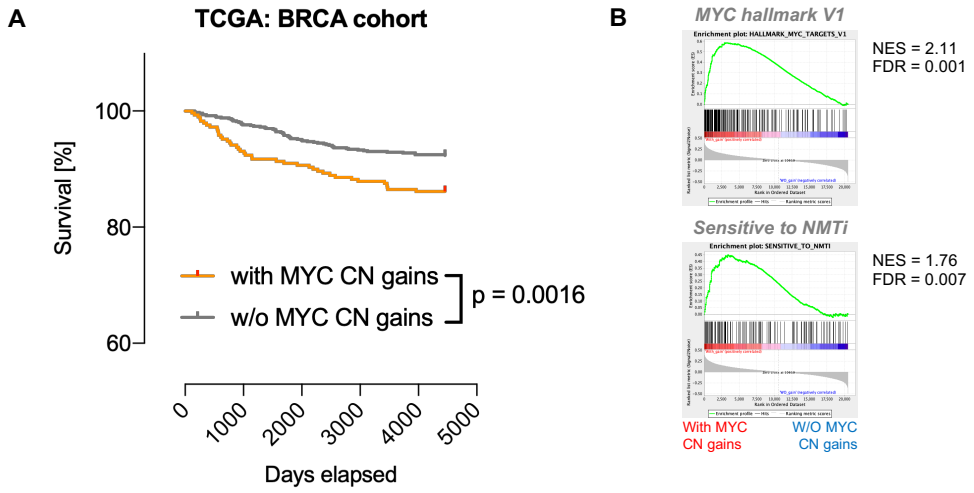

Figure 4-14: CN gains in MYC correlate with worse clinical outcome in the TCGA BRCA cohort and increased activation of the MYC signatures and the 'NMTi sensitivity' signature.

[A] Kaplan-Meyer plot showing that patients in the TCGA BRCA cohort with MYC CN gains (CN > 2) have a worse clinical outcome. **[B]** Those patients are enriched for the MYC Hallmark V1 gene set and the 'Sensitive to NMTi' gene set.

Another example would be breast cancer, the most common cancer in the USA (30% for females, and 15% of all new cancer cases independent of sex). It is responsible for 14.6% of all cancer related deaths in women (Siegel et al., 2019). MYC

amplifications are common in the basal type breast cancer which is usually more aggressive, hence, associated with worse prognosis (Xu et al., 2010). Indeed, within the TCGA BRCA (Breast invasive carcinoma), CN gains in MYC (Schaub et al., 2018) correlate with worse clinical outcome (see Figure 4-14 A), and increased activation of the MYC hallmark V1 genes. Importantly, the patients that have CN gains present in their cancers, are also enriched in the 'Sensitive to NMTi' signature (see Figure 4-14 B). This could indicate that the patients that would do worse in a clinical setting might benefit the most from NMT inhibition. Unpublished data from the laboratory showed higher sensitivity of the triple negative breast cancer (TNBC) cell line MDA-MD-231, compared to ER positive cell lines, such as MCF7 and T47D (data not shown).

4.3 Conclusions

In this chapter an unbiased, tissue and cancer agnostic approach, comparing sensitive and resistant cancer cell lines to IMP1031 using GSEA was applied. This analysis revealed that sensitive cancer cell lines have higher expression of genes involved in transcription, RNA processing and splicing, nuclear transport, translation and DNA damage, compared to the resistant ones. Leading-edge analysis on this initial GSEA results yielded in a 'Sensitive to NMTi' gene set, which was subsequently validated by testing it with the data sets of IMP1036 and IMP366 (Iorio et al., 2016) and two different CRISPR gene essentiality screens, conducted by the Broad and the Sanger Institute (Behan et al., 2019; Meyers et al., 2017). A key upstream node of this 'Sensitive to NMTi' signature is MYC and there is an excellent correlation between the activation of the 'MYC hallmarks V1' gene set and the 'Sensitive to NMTi' signature across all the cancer cell lines in the COSMIC data base (Iorio et al., 2016). In addition, it was shown that cancer cell lines with high levels of *MYC* mRNA or structural alterations in the *MYC* gene (or *MYCN* for the pharmacogenomics screens) are more dependent on myristoylation. This outcome is independent of myristoylation being blocked by dual NMT1/2 inhibitors or by knockout of the essential paralog NMT1.

To validate if there is indeed a synthetic lethality between (enforced) MYC expression and NMT inhibition, several isogenic cellular models were obtained, which allow for

inducible levels of MYC or MYCN. The P-493-6 cell line, a B-cell line (Pajic et al., 2000), shows a clear trend of increased toxicity with the two benchmark NMT inhibitors IMP1088 and IMP366 with increased expression of MYC (Kallemeijn et al., 2019). Cell numbers are depleted to a much larger extent in the MYC high conditions and a rapid breakdown of cellular viability is observed. Furthermore, the same results were obtained with the Shep-ER-MYCN cell line (Valentjin et al., 2005). Enforced expression of MYCN combined with inhibition of NMT with IMP1088 or IMP366 causes a rapid loss of cellular viability, compared to the condition without ectopic expression of MYCN. While not shown in this thesis, the same results were obtained from a colleague in the laboratory with a third isogenic cell line, that also has an inducible MYCN expression system (Ushmorov et al., 2008). A Collaborator provided three lymphoma PDXs that can be passaged *in vivo* and in *vitro*. All of these PDXs carry a MYC translocation and they were all highly susceptible to NMT inhibition, with an even more rapid onset of programmed cell death than observed in the other immortalised cell line models. Importantly and potentially clinically relevant, two of these PDX were 'double hit' DLBCL and one plasmablastic lymphoma–both of these diseases are associated with poor patient outcome (Castillo et al., 2015; Riedell and Smith, 2018).

Total RNAseq on the P-493-6 cell line in the MYC high and medium conditions, treated with IMP1088, reveals a stronger breakdown (measured as downregulation of genes) of several key biological functions (ranging from cell cycle, translation to Pol I transcription) in the MYC high context compared to MYC medium. Despite showing a strong increase of the MYC transcriptional program (the 'Hallmark MYC V1' gene set is used as a surrogate (Liberzon et al., 2015)) in untreated conditions, this program is affected to a much larger extent in the MYC high cells, treated with NMT inhibitor, compared to MYC medium cells, treated with NMTi.

The synthetic lethality between NMT inhibition and high levels or rather enforced expression of MYC has strong clinical implications, ranging from MYCN amplified neuroblastoma (Rickman et al., 2018), to double hit lymphoma (Riedell and Smith, 2018), to lymphoblastic lymphoma (Castillo et al., 2015), and to potentially some cancers affecting very large proportion of the population, as MYC amplifications are amongst the most observed across several different cancer types (Ciriello et al., 2013; Kalkat et al., 2017; Schaub et al., 2018). As an example, in the TCGA BRCA

(breast invasive carcinoma) cohort amplifications of MYC are associated with worse clinical outcome, as expected from other studies (Schaub et al., 2018; Xu et al., 2010). Importantly, patients suffering from MYC amplified breast cancer show higher expression of genes that mark cancer cell lines as more sensitive to NMT inhibition. This could indicate that across several cancer types, patients that usually would have a worse clinical outcome because of MYC deregulation, might benefit the most from NMT inhibition, with major translational implications based on these findings.

Chapter 5. Signalling is affected within minutes to hours of NMT inhibition in BL41, indicating a potential GOF

5.1 Introduction

Due to the applied dual strategy, described in Chapter 3 and Chapter 4, a synthetic lethality between deregulated MYC expression and NMT inhibition was identified. Genetic or chemical interference is disproportionally more toxic to cancer cell lines with ectopic MYC or MYCN expression, validated in two isogenic cell line systems and confirmed in five large-scale cancer cell line screens, using chemical and genetic perturbation of myristoylation. However, an unanswered question is which NMT substrate(s) are driving this increased sensitivity of MYC high cells. The Tate laboratory developed a plethora of chemical biology tools to identify NMT substrates through the combination of metabolic tagging (through an alkyne analogue of myristic acid) in mammalian cells with either NMT inhibition (Thinon et al., 2014), or with specifically designed capture reagents to identify modified peptides (Broncel et al., 2015). Recently, members of the group additionally developed an approach which does not need any metabolic labelling, and utilises SrtA mediated tagging to identify myristoylated proteins, or rather show inhibition of myristoylation on those (Goya Grocin et al., 2019). The approach of combining metabolic tagging through a myristate analogue with NMT inhibition was applied in this study to identify NMT substrates that show a strong response within the first six hours of NMT inhibition in BL41. The aim was to identify NMT substrate candidate(s) that might drive the mRNA shortening phenotype, described in Chapter 3.

5.2 Results

5.2.1 Identification of NMT substrates affected within six hours of NMT inhibition in BL41

To identify a subset of NMT substrates that could be involved in the initial U1 downregulation (see section 3.2.3), or in general for the premature termination and

polyadenylation, the time for the pulse of YnMyr was reduced from a typical overnight pulse with(out) NMT inhibitor for mammalian cells (Broncel et al., 2015; Kallemeijn et al., 2019; Thinon et al., 2014) to 6 hours. The experimental set up is shown in Figure 5-1 (for more details please see section 1.1.3).

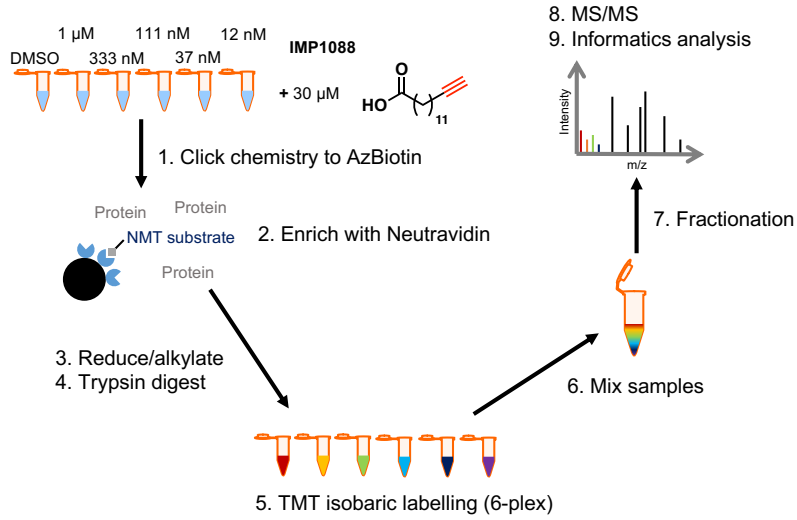

Figure 5-1: Chemical proteomics workflow for the identification of NMT substrates.

Cells were preincubated with a concentration gradient of IMP1088 (ranging from 1 µM to 12 nM) for 30 minutes, then 30 µM of YnMyr (an alkyne version of myristic acid) was added for 6 hours. The cells were lysed, and then clicked to AzBiotin for subsequent Neutravidin enrichment. The next steps included reduction and alkylation, tryptic digest, isobaric labelling with a TMT 6-plex, mixing of the samples, and a 6x fractionation. Lastly, the samples were run on a mass spectrometer and analysed with bioinformatics tools.

The cells were treated with a gradient of IMP1088, ranging from 1 µM to 12 nM (one in three dilution), in biological triplicate; the cells were preincubated for 30 minutes with either the NMT inhibitor or DMSO control, and subsequently pulsed for 6 hours with 30 µM YnMyr, a concentration based on previous work (Lim, 2016; Thinon et al., 2014). The cells were lysed, “clicked” to a biotin handle with an azide, enriched on Neutravidin beads, reduced, alkylated, and digested. The following part of the workflow was done by Aaron Borg, former senior research scientist of the Proteomics STP in the Francis Crick Institute. The peptides were labelled with a TMT 6-plex, mixed, fractionated and then run on a Fusion Lumos mass spectrometer. Subsequent analysis was conducted with the software package MaxQuant and Perseus by the author of this thesis (Cox and Mann, 2008; Tyanova et al., 2016). In a summarised MaxQuant search, pooling all biological triplicates together, 948 protein groups were identified in total: 193 of those protein groups had an N-terminal

glycine–the prerequisite for myristoylation, and 45 of these 193 were identified as known CoTMyr NMT substrates (Broncel et al., 2015; Kallemeijn et al., 2019; Mousnier et al., 2018; Thinon et al., 2014; Utsumi et al., 2018).

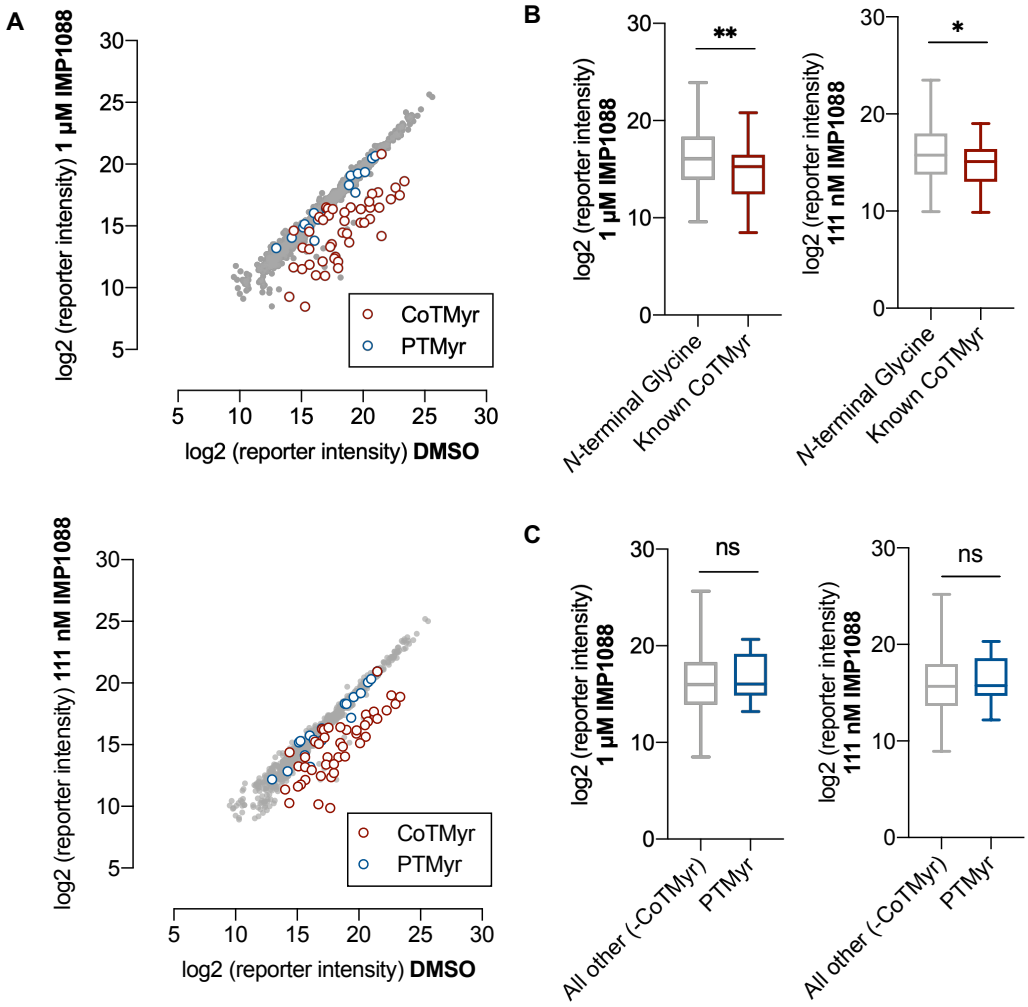

Figure 5-2: Co-translationally myristoylated proteins are affected by NMT inhibition, whereas post-translational myristoylated substrates are not.

[A] Top: 2D plot, comparing DMSO vs. the samples treated with 1 µM of IMP1088. Bottom: 2D plot, comparing DMSO vs. the samples treated with 111 nM of IMP1088. **[B]** Left: Comparison of the effect of 1 µM IMP1088 on all previously identified CoTMyr substrates (N = 45) and proteins that have an *N*-terminal glycine. Right: Comparison of the effect of 111 nM IMP1088 on all previously identified CoTMyr substrates (N = 45) and proteins that have an *N*-terminal glycine. **[C]** Left: Comparison of the effect of 1 µM IMP1088 on all previously identified PTMyr substrates against all other identified proteins. Right: Comparison of the effect of 111 nM IMP1088 on all previously identified PTMyr substrates against all other identified proteins.
(P-values were determined with Mann-Whitney test, error bars = minimum to maximum values).

An additional 18 PTMyr substrates were identified in the overall search (Martin et al., 2011; Thinon et al., 2014). As shown in Figure 5-2 A, the known CoTMyr substrates were strongly enriched in the control samples, compared to either the samples treated with 1 µM of IMP1088 or the ones treated with 111 nM of IMP1088. On the other hand, the PTMyr substrates were not enriched, indicating that these were not actually myristoylated, but just enriched on the beads via protein-protein interactions or unspecific binding. Indeed, while the log2 reporter intensities of the CoTMyr NMT substrates are significantly lower compared to the proteins with *N*-terminal glycine (see Figure 5-2 B), the PTMyr substrates have a similar median log2 reporter intensities, compared to the identified protein groups (excluding the known CoTMyr substrates; see Figure 5-2 C). The enrichment of CoTMyr substrates in the control occurs, as expected, in a concentration dependent manner and with 12 nM of IMP1088 no enrichment in the control is observed anymore (see Figure 8-38). Taken together, this indicates that PTMyr NMT substrates are unlikely to be involved in the initial effects of NMT inhibition, as post-translational myristoylation needs activation of peptidases to expose internal glycines, such as in the case of apoptosis induced cleavage after caspases are activated (Martin et al., 2011; Thinon et al., 2014). One can however not exclude that PTMyr might impact the kinetics of cell death, and might play a major role in protecting certain proteins from degradation after initial caspase cleavage (Timms et al., 2019).

Interestingly, utilising multiple hypothesis testing corrected t-tests, to compare DMSO against the treated samples within the proteins that have an N-terminal glycine, two new protein groups (GCSAM and CDCA3) were enriched across nearly all samples, that is concentrations tested (see Figure 5-3 A and B and Figure 8-39 A to C). GCSAM (also known as HGAL) is described as a GC specific gene for which high expression correlates with better survival in DLBCL patients (Lossos et al., 2003), through potentially reduced motility, hence dissemination, of the lymphoma cells (Jiang et al., 2010). The human GCSAM was overexpressed in the HSC compartment of the mice, causing lymphoid hyperplasia and amyloidosis via increased BCR activation (Romero-Camarero et al., 2013).

CDCA3, part of the SCF ubiquitin ligase, is involved in mitotic entry (Uchida et al., 2012), and its overexpression has been implicated in various cancers (Adams et al., 2017; Zhang et al., 2018). A number of cancer cell lines (31%) is dependent on

CDCA3 in CRISPR essentiality screens (Meyers et al., 2017), and the interference with myristoylation on it, could potentially be responsible for the observed G2 arrest the tested cancer cell lines in this thesis.

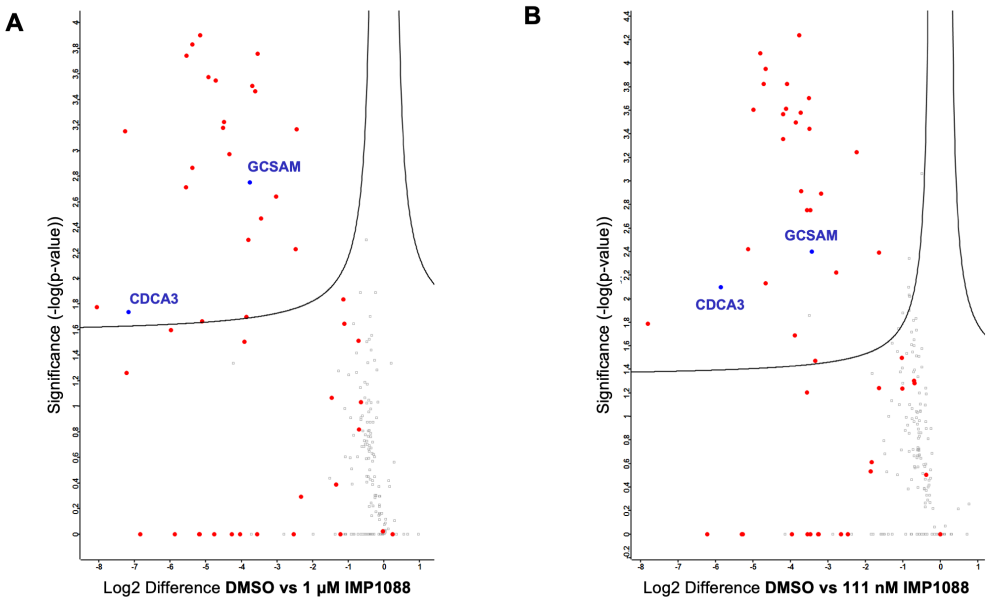

Figure 5-3: GCSAM and CDCA3 were identified as novel NMT substrates.

[A] Volcano plot showing the enrichment of known NMT substrates in the DMSO control vs 1 µM IMP1088. Two novel NMT substrates (GCSAM and CDCA3; blue) were also enriched in the DMSO treated sample. **[B]** Volcano plot showing the enrichment of known NMT substrates in the DMSO control vs 111 nM IMP1088. Two novel NMT substrates (GCSAM and CDCA3; blue) were also enriched in the DMSO treated sample (FDR<0.02, s0-value = 0.5).

The identification rate of CoTMyr substrates was slightly lower (<50 CoTMyr) than in previous studies that usually identified 50+ CoTMyr substrates through combining metabolic labelling with either NMT inhibitors or capture reagents to identify modified peptides (Broncel et al., 2015; Kallemeijn et al., 2019; Thinon et al., 2014). This is likely due to the shorter pulse of YnMyr.

To define a subset of substrates that could be responsible for the downregulation of U1, or in general for the premature termination and polyadenylation, the substrates with a strong response within 6 hours of NMT inhibition were emphasised. It was assumed that the substrates that have strong reduction of reporter intensity, compared to control conditions, are the ones with sufficiently high protein turnover, to explain the effects within 6 hours of NMT inhibition. The strongest effect observed was on BLK, a kinase belonging to the SFK family (Drebin et al., 1995), with a loss of intensity compared to control of over 50% at the highest concentration of NMT

inhibitor. A problem of the TMT-based quantification, compared to e.g. the previously used SILAC (Thinon et al., 2014), is that one cannot asses complete inhibition of myristoylation on a given NMT substrate–there will always be a value of TMT reporter intensity given, and if it corresponds to partial inhibition or complete inhibition is not clear. Other NMT substrates, such as BSN, PRMT1, or DDX46 had nearly no change in reporter intensity, compared to control (see Figure 5-4 A). This is not due to potential ratio compression, observed for TMT labelling for which only MS2 is used, as the experiment was run using MS3, eliminating ratio compression (Ting et al., 2011). Thus, the most likely reason is a combination of low protein turnover for those substrates, combined with potentially incomplete inhibition, allowing for some incorporation of YnMyr that does not differ much between control and the samples treated with NMT inhibition. A cut-off of at least a 20% reduction in reporter intensity (N = 28 out of 47), compared to control was chosen to assess which substrates have a sufficiently fast turnover within 6 hours to cause the very early effects in BL41. The lowest of those reporter intensities within this subset of NMT substrate was assumed to represent maximum inhibition at that time point, hence equalled to 0%, and sigmoidal curves were generated to assess the TC_{50}s for each individual substrate (see Figure 5-4 B). The median TC_{50} was 69 nM, with a range from 36 to 275 nM. These numbers are very much in range of the observed EC_{50} in BL41, which is 28 ± 11 nM.

More interestingly, after conducting gene ontology enrichment with g:Profiler (Reimand et al., 2007), it is apparent that those 28 CoTMyr substrates where disproportionally enriched for proteins that are involved in signalling, including BCR signalling (Rickert, 2013), likely due to the presence of several SFK members. The 28 CoTMyr substrates were mostly considered membrane bound, GTP binding, and they are involved in signalling through phosphatase activity and tyrosine kinase activity (see Figure 5-4 C). This led to the hypothesis that aberrant signalling, upon NMT inhibition, is the most likely cause for the mRNA shortening phenotype, observed in BL41. The observation that proteins disproportionally involved in signalling are affected by high protein turnover, thus also of the myristate, fits the general observation that signalling proteins are generally unstable (Schwanhausser et al., 2011).

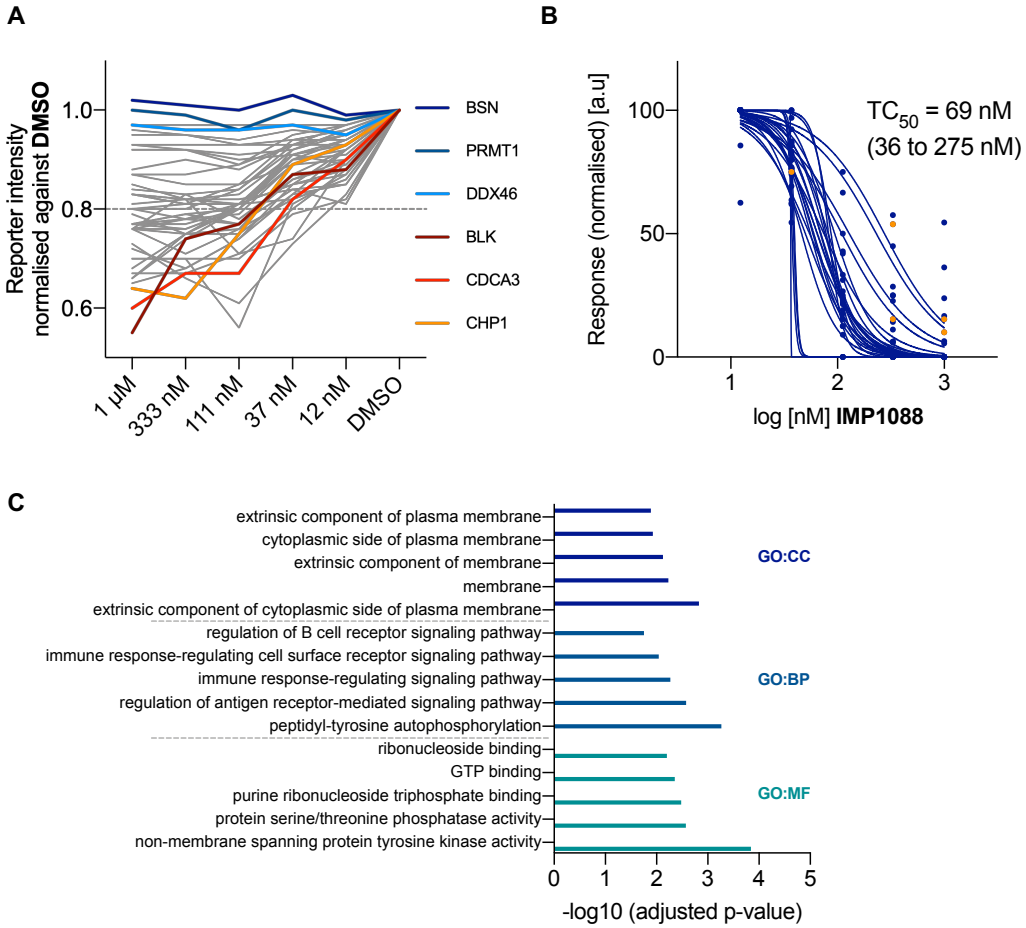

Figure 5-4: NMT substrates that were affected strongest by NMT inhibition within 6 hours are enriched for proteins involved in GTP binding and signalling.

[A] Concentration dependent effect on the reporter intensities, normalised to DMSO, for the previously 45 identified CoTMyr NMT substrates, plus GCSAM and CDCA3. **[B]** TC_{50} curves, for the CoTMyr NMT substrates that had at least a 20% reduction of reporter intensity, compared to DMSO treated cells (N = 28). **[C]** Gene ontology enrichment analysis of the substrates that had at least a 20% reduction of reporter intensity, compared to DMSO treated cells.

5.2.2 Deregulated signalling upon NMT inhibition within minutes to hours of NMT inhibition affects proteins involved in RNA processing

To test the hypothesis whether signalling is affected by NMT inhibition within minutes to hours of NMT inhibition, phosphoproteomics at five time points (5, 10, 15, 30 and 90 minutes) with 100 nM of IMP1088 was conducted in BL41. As the time points are very close to each other, matching DMSO controls were not prepared in this case, and only a control of BL41, treated for 90 minutes with equally matching

0.004% of DMSO was used to normalise the phosphorylation changes upon NMT inhibition. The workflow for the experiment was equivalent to what is described in Chapter 3.2.1, with the same division in labour. For each time point the control sample was subtracted, so that negative fold changes indicate loss of phosphorylation on a given peptide, whereas positive fold changes indicate increase of phosphorylation on a given peptide. 5478 phospho-sites were identified with a localisation score of >0.75.

A pronounced “spike” of differential phosphorylation was observed at 10 minutes with a trend towards loss-of-phosphorylation (see Figure 5-5 A), that stabilises at 15 minutes again. Additionally, the 10-minute time point had the poorest overall correlation, compared to all other time points (see Figure 5-5 B). Moreover, the phospho-peptides affected the strongest at 10 minutes, normalised again at 15 minutes; however, towards 90 minutes of NMT inhibition they follow the observed trend of the 10-minute time point, indicating that a long-term compensation is not achieved (see Figure 5-5 C). An interpretation of this could be that one or several NMT substrates involved in signalling are being synthesised at the ribosome, and due to the lack of the myristate do not recognise properly their substrates anymore and (de)phosphorylate substrates that should not be (de)phosphorylated. This initial ‘spike’ in aberrant signalling is followed by a recovery within the cell signalling by feedback mechanisms in the given signal pathway; however, over time, due to continued synthesis of the non-myristoylated substrates, the directional effect is visible at the later time points, even after the apparent recovery at 15 minutes of NMT inhibition. There is indeed evidence in the literature that myristoylation is necessary for kinase activity of SRC (Patwardhan and Resh, 2010), and that overexpression of a G2A mutant of SRC or LYN causes aberrant signalling leading to chromosome missegregation (Honda et al., 2016). Additionally, the myristate is necessary for correct substrate recognition in the case of the phosphatases PPM1A and PPM1B (Chida et al., 2013). Moreover, the myristoylated phosphatase PPM1G is implicated in RNA processing and splicing (Allemand et al., 2007; Petri et al., 2007); however, nothing is known about the importance or role of myristoylation on PPM1G. Alternatively, the ‘spike’ at 10 minutes is due to a technical artefact (however, this is unlikely as all samples were processed at the same time in the same manner), or an effect of e.g. media exchange. This would be expected rather at 5 minutes, not at 10

minutes, thus, indicating that this 'spike' is a real biological signal, caused by NMT inhibition.

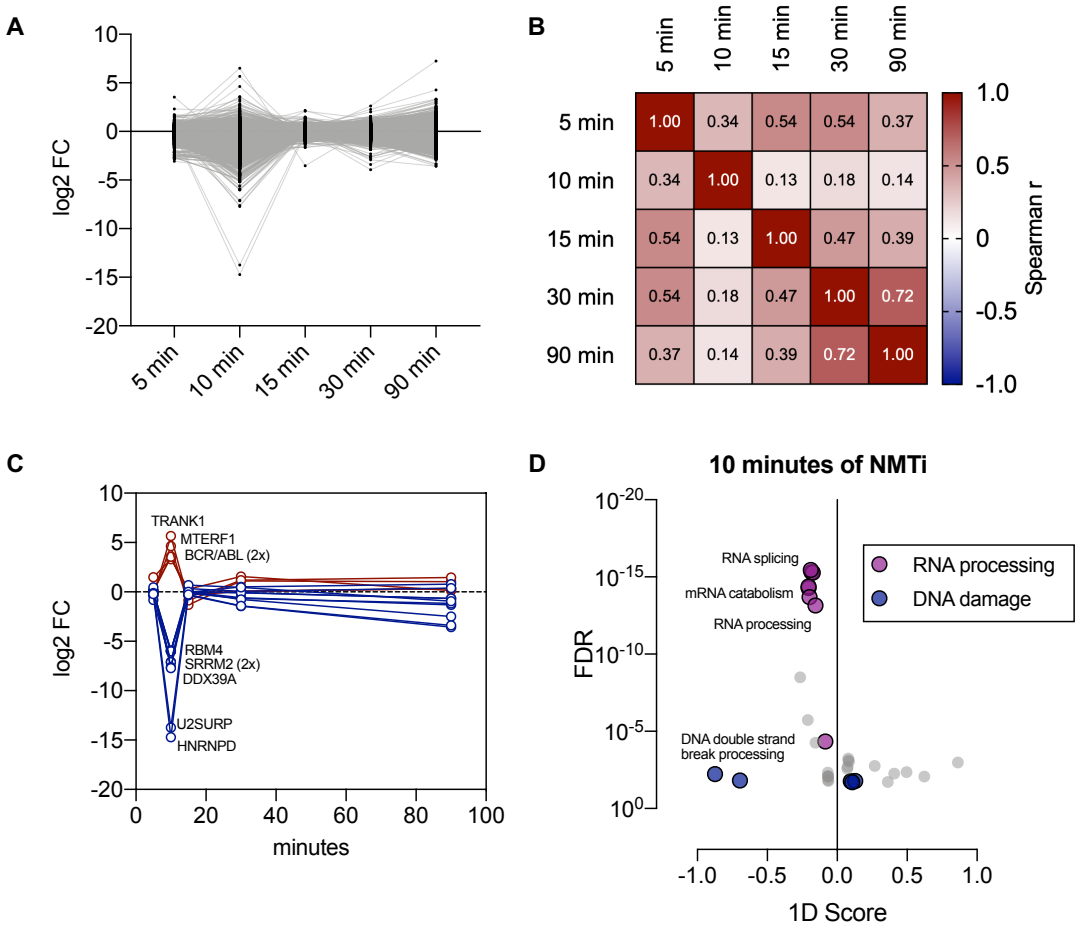

Figure 5-5: Phosphoproteomics at early time points reveals a potential "spike" in signalling upon 10 minutes of NMT inhibition.

[A] Scatter plot showing the phosphorylation changes, normalised against the control, over the course of NMT inhibition. **[B]** Correlation matrix between the different time points with Spearman correlation. **[C]** Scatter plot showing the trends of the strongest phosphorylation changes at 10 minutes of NMT inhibition. **[D]** 1D enrichment plot showing GOBP and GOMF enrichment of the phosphorylation changes at 10 minutes of NMT inhibition.

To define the biological pathways that are particularly affected by the phosphorylation changes, a 1D enrichment (Cox and Mann, 2012) for each of the early timepoints was conducted, similar to previous analysis in section 3.2.1. This analysis reveals that phosphorylation changes occur particularly on proteins involved in RNA processing and splicing (for 10 minutes, see Figure 5-5 D; for 5 and 15 minutes, see Figure 8-40 A and B). Other pathways, such as DNA double strand

break processing at 10 minutes, or ion transport at 15 minutes are found to be affected, but are not consistent across the different time points, which are only separated by minutes, and have overall larger FDRs, indicating less significant enrichment.

At the later time points (30 and 90 minutes) the involvement of RNA processing and splicing persists (see Figure 5-6 A and B), with addition of phosphorylation changes on other parts of the transcriptional machinery, particularly related to RNA pol II termination.

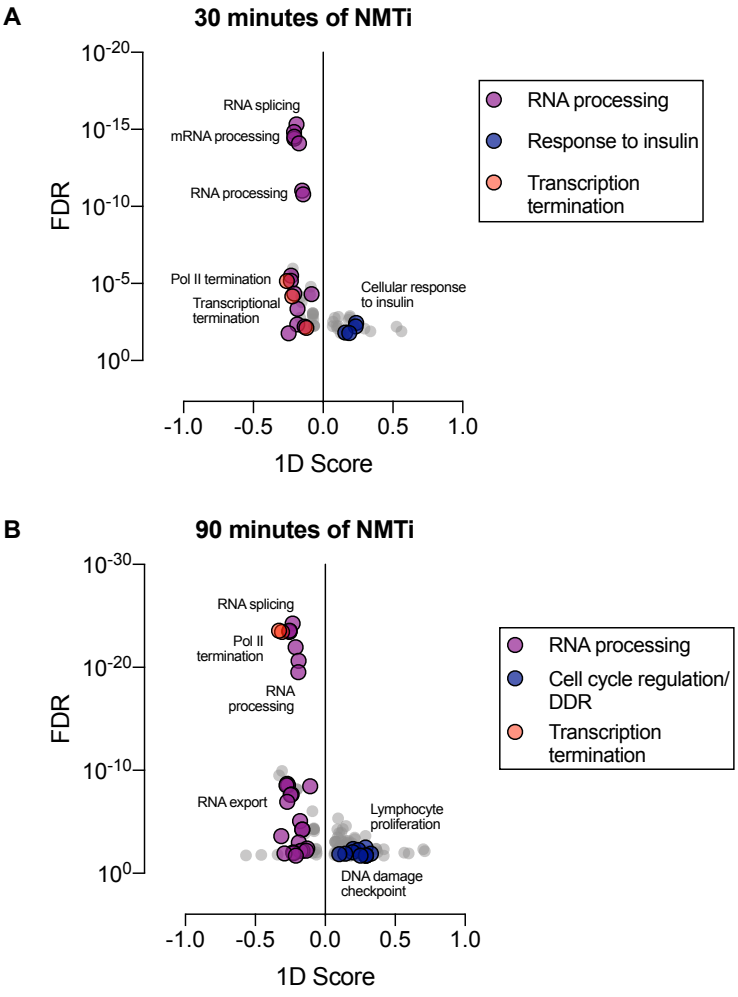

Figure 5-6: Phosphorylation is persistently reduced on proteins involved in RNA processing upon NMT inhibition.

[A] 1D enrichment plot showing GOBP and GOMF enrichment of the phosphorylation changes at 30 minutes of NMT inhibition. **[B]** 1D enrichment plot showing GOBP and GOMF enrichment of the phosphorylation changes at 90 minutes of NMT inhibition.

While further validation is needed, a hypothesis could be that in the moment that the NMT inhibitors block myristoylation, non-myristoylated substrates are being synthesised, which are disproportionally involved in signalling. These non-myristoylated kinases (e.g. SFK members) or phosphatases (e.g., PPM1A, PPM1B, PPM1G and the myristoylated calcineurin subunits PPP3R1 and PPP3R2) then cause aberrant (de)phosphorylation. These phosphorylation changes seem to particularly affect (and importantly persistently) proteins involved in RNA processing and splicing, and might be the primary cause of the premature termination and polyadenylation in a subset of genes, through consequential U1 downregulation, as described in Chapter 3. The challenge will remain to identify the potential kinases and phosphatases that are involved in this process, and to clearly define their substrate scope and what in each individual case happens, if the myristate is lacking on the *N*-terminus. Another observation from this early time points phosphoproteomics was that phosphorylation particularly on CDK motifs (particularly CDK1 and 2) was disturbed by NMT inhibition at those early time points (see Figure 8-40 C). This raised the question if NMT inhibition, particularly at early time points, could potentiate the effects of (clinical) CDK inhibitors, through what could be a change of function on several myristoylated proteins involved in signalling.

5.2.3 Pan CDK inhibition synergises with NMT inhibition

CDKs are key kinases and regulators of cell cycle and transcription (Malumbres, 2014), and additionally involved in many more biological functions such as WNT signalling, DNA damage and epigenetic regulation (Lim and Kaldis, 2013). Due to their role in cell cycle and transcription, they are considered an interesting target in cancer. Inhibitors have been developed to target several CDKs at once (pan-CDK inhibitors), specific CDK7 or 9 inhibitors disrupting transcription, or CDK4/6 inhibitors in RB wildtype cancers to cause G1 arrest and senescence (Asghar et al., 2015; Whittaker et al., 2017). In the case of the latter, three drugs (Palbociclib, Ribociclib and Abemaciclib) have been approved in hormone receptor positive breast cancer (Choo and Lee, 2018). As changes of phosphorylation on CDK motifs, particularly CDK1 and 2, were observed at 90 minutes of NMT inhibition (see previous section 5.2.2), the idea arose that NMT inhibitors could maybe potentiate

the effect of CDK inhibitors. An initial experiment was conducted with the chemical probe 'CDK1/2 inhibitor III' (see Figure 5-7 A), which was initially reported as highly specific for CDK 1 and 2 (Lin et al., 2005). However, subsequent research revealed that CDK1/2 inhibitor III acts as a pan-CDK inhibitor (Jorda et al., 2018). Nevertheless, BL41 were treated in varying concentrations of CDK1/2 inhibitor III with(out) 50 nM of IMP1088 for 24 hours. As IMP1088 is not yet very toxic in the cells in this time frame, it is easier to assess potential synergies. The concentration of 50 nM was chosen due to its proximity to the EC_{50} of IMP1088 in BL41 (28 ± 11 nM). The concentrations for the CDK1/2 inhibitor III were chosen, based on its assessed potency in BL41 (treated for 72 hours with the inhibitor, see Figure 8-41).

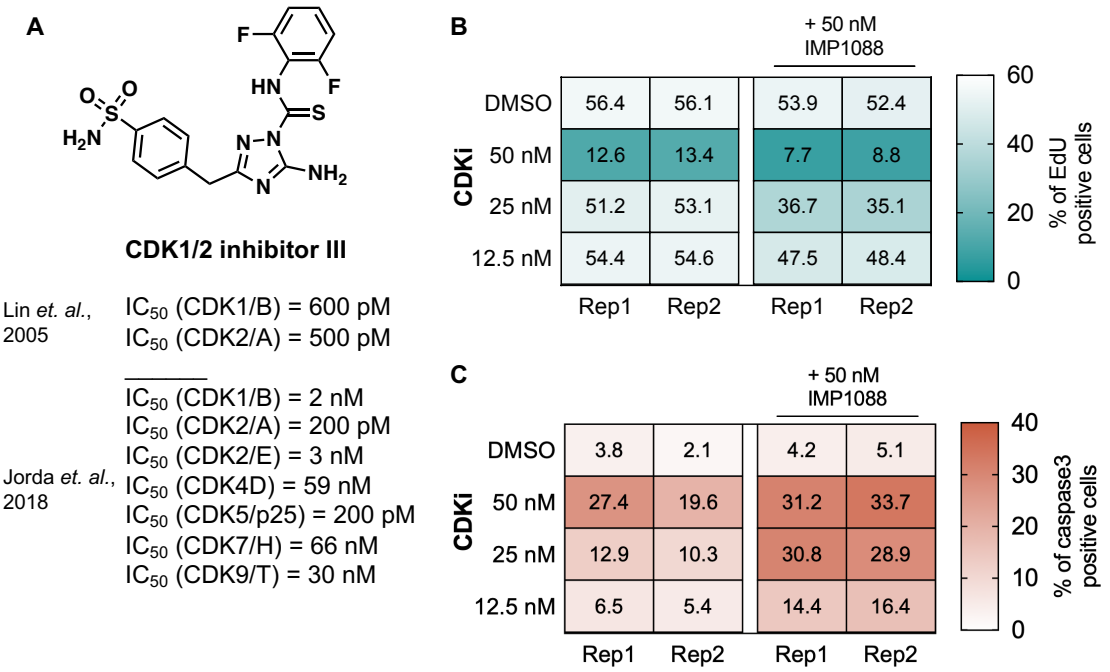

Figure 5-7: Synergy of pan-CDK inhibition, through CDK1/2 inhibitor III, and NMT inhibition.

[A] Structure of CDK1/2 inhibitor III with the initially reported enzymatic potencies (Lin et al., 2005), and the recently published enzymatic potencies across several CDKs (Jorda et al., 2018). **[B]** Effect of adding 50 nM of IMP1088 for 24 hours to CDK1/2 inhibitor III on DNA synthesis, measured by EdU incorporation. **[C]** Effect of adding 50 nM of IMP1088 for 24 hours to CDK1/2 inhibitor III on apoptosis, measured by caspase 3 induction.

Flow cytometry was utilised to distinguish the numbers of viable cells, effects on proliferation and apoptosis through caspase3 activation. Cell numbers were

unaffected by the addition of IMP1088 within 24 hours of combined treatment (see Figure 8-42) but an effect on the proliferative capacity was observed, that is DNA synthesis (see Figure 5-7 B). While IMP1088 on its own had a very small effect on the proliferative capacity within 24 hours, in line with previous results shown in section 2.2.4, it amplified strongly the effects of the CDK1/2 inhibitor III. To quantify the synergistic effect a combination index (CI) was calculated for each combination of concentrations, using the Response Additivity approach (Slinker, 1998), see Equation 1 **(1)**. A different calculation method for the CI is the Bliss Independence (Bliss, 1939), see Equation 1 **(2)**, which assumes differential non-overlapping mode of action in the respective drugs (Foucquier and Guedj, 2015). This might not befit the situation of CDK inhibition combined with NMT inhibition, as the latter seems to disturb phosphorylation on CDK motifs.

$$(1)\ CI = \frac{E_A + E_B}{E_{AB}} \qquad (2)\ CI = \frac{E_A + E_B - E_A \times E_B}{E_{AB}}$$

Equation 1: Formulas to calculate the combination index with Response additivity (1) or Bliss Independence (2).

CI = combination index, E_A = Effect of drug A, E_B = Effect of Drug B, E_{AB} = Effect of combination

The more conservative assessment would be the assessment of synergy by the CIs, calculated with the Response additivity assumption. However, the actual difference in calculated CIs is only marginal. Independently of the used calculation method, synergy (that is CI < 1) in reduction of proliferation is observed for each concentration of CDK1/2 inhibitor III tested (see Table 5-1).

Table 5-1: Combination indices for the effects on apoptosis and proliferation with CDK1/2 inhibitor III.

Concentration of CDK1/2 inhibitor III	Apoptosis		Proliferation	
	Response Additivity	Bliss Independence	Response Additivity	Bliss Independence
50 nM + IMP1088	0.76	0.74	0.94	0.92
25 nM + IMP1088	0.39	0.38	0.29	0.28
12.5 nM + IMP1088	0.38	0.38	0.42	0.42

The same synergistic effects were observed for the induction of apoptosis (see Figure 5-7 C and Table 5-1 for the combination indices). To conclude NMT inhibition, in a time frame, where it does not yet exhibit toxicity on its own, amplifies the toxicity of CDK1/2 inhibitor III. The cell numbers were not yet affected by this, but a stronger collapse of overall cell viability is apparent. This is the first evidence that NMT inhibition, through potential deregulated signalling can cause unexpected synergistic effects.

This observation raised the question if the same would be observed with clinically relevant pan-CDK inhibitors. Three different clinical inhibitors, targeting several CDKs at once, were chosen to test this. Firstly, AT7519 (see Figure 5-8 A), a pan-CDK inhibitor developed by Astex and initially designed against MM (Santo et al., 2010). It was tested in a Phase I trial against Non-Hodgkin's lymphoma (ClinicalTrials.gov Identifier: NCT00390117), and has proceeded in three Phase II trials against various haematological malignancies, such as CCL (ClinicalTrials.gov Identifier: NCT01627054), mantle cell lymphoma (ClinicalTrials.gov Identifier: NCT01652144) and MM (ClinicalTrials.gov Identifier: NCT01183949). Currently, a Phase II trial is recruiting patients to test AT7519 to treat solid tumours (ClinicalTrials.gov Identifier: NCT02503709). AT7519 was also shown to be synthetically lethal with MYCN overexpression (Dolman et al., 2015). In a more general sense, CDK1 interference has been described as synthetically lethal with MYC overexpression (Kang et al., 2014), and CDK9 inhibition was described to interfere disproportionally with the expression of MYC through disrupting super enhancer elements (Chapuy et al., 2013; Garcia-Cuellar et al., 2014; Loven et al., 2013). Thus, the expectation would be that MYC-deregulated cancers, or in general cancers with high levels of MYC would be more susceptible to pan-CDK inhibition, at least driven by to CDK1 and CDK9 inhibition. This was indeed already described for triple negative breast cancer and pan-CDK inhibition, with Dinaciclib (Horiuchi et al., 2012) (see sections 1.5.2 and 1.5.3 in the introduction for more details and context about current drug discovery approaches to target MYC). The second inhibitor tested is Dinaciclib, a highly potent CDK1/2/5/9 inhibitor with broad anti-tumour activity, initially developed by Merck (see Figure 5-8 B) (Parry et al., 2010). Currently, there are three Phase I clinical trials ongoing (ClinicalTrials.gov Identifiers: NCT01434316, NCT02684617, NCT0384520) against solid tumours and

haematological malignancies. 15 other clinical studies have been already conducted, amongst them one Phase III trial in patients with refractory CLL which was terminated early, but not attributed to safety. In this study, Dinaciclib showed potential as an anti-tumour drug (Ghia et al., 2015).

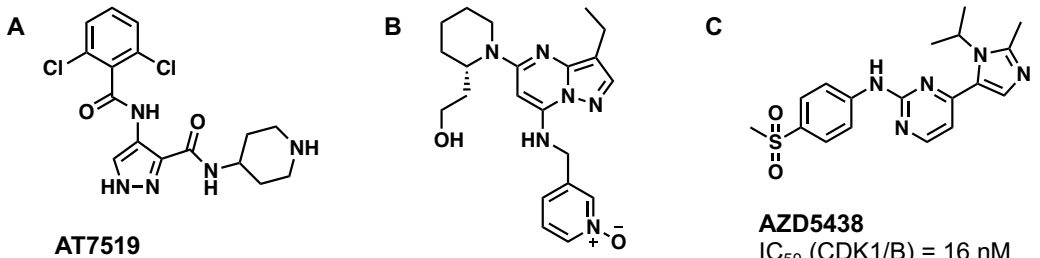

AT7519
IC_{50} (CDK1/B) = 210 nM
IC_{50} (CDK2/A) = 47 nM
IC_{50} (CDK4/D1) = 100 nM
IC_{50} (CDK5/p35) = 13 nM
IC_{50} (CDK6/D3) = 170 nM
IC_{50} (CDK9/T) < 10 nM
IC_{50} (GSK-3β) = 89 nM

Dinaciclib
IC_{50} (CDK1) = 3 nM
IC_{50} (CDK2) = 2 nM
IC_{50} (CDK5) = 1 nM
IC_{50} (CDK9) = 4 nM

AZD5438
IC_{50} (CDK1/B) = 16 nM
IC_{50} (CDK2/A) = 45 nM
IC_{50} (CDK2/E) = 6 nM
IC_{50} (CDK5/p25) = 14 nM
IC_{50} (CDK6/D3) = 21 nM
IC_{50} (CDK9/T) = 20 nM
IC_{50} (GSK-3β) = 17 nM

Figure 5-8: Structures of the three clinical CDK inhibitors AT7519, Dinaciclib and AZD5438.

[A] Structure and enzymatic potencies of AT7519. **[B]** Structure and enzymatic potencies of Dinaciclib. **[C]** Structure and enzymatic potencies of AZD5438.

Lastly, AZD5438 was tested, a CDK inhibitor developed by Astra Zeneca (Byth et al., 2009) (see Figure 5-8 C). The development of AZD5438 was stopped after disappointing Phase I clinical data (ClinicalTrials.gov Identifier: NCT00088790), as it was not tolerated in continuous dosing schedules. To note is that it was dosed four times a day with 40 mg in the trial arm with the highest dosage regime, causing a large number of adverse effects (Boss et al., 2010). Thus, this inhibitor was included, to test if addition of IMP1088, or any NMT inhibitor for that matter, could potentially improve the profile and allow less frequent dosage regimes for AZD5438. The same experimental set-up as for CDK1/2 inhibitor III was used to assess synergy. The concentrations range for the CDK inhibitors were chosen due to preliminary experiments testing them in BL41 for 72 hours (see Figure 8-41).

In the case of AT7519 and Dinaciclib, synergistic effects were observed in the induction of apoptosis, when combined with 50 nM of IMP1088 (see Figure 5-9 A and B). Dinaciclib was exceptionally potent, and at 2 nM and 1 nM it killed most of the cells on its own.

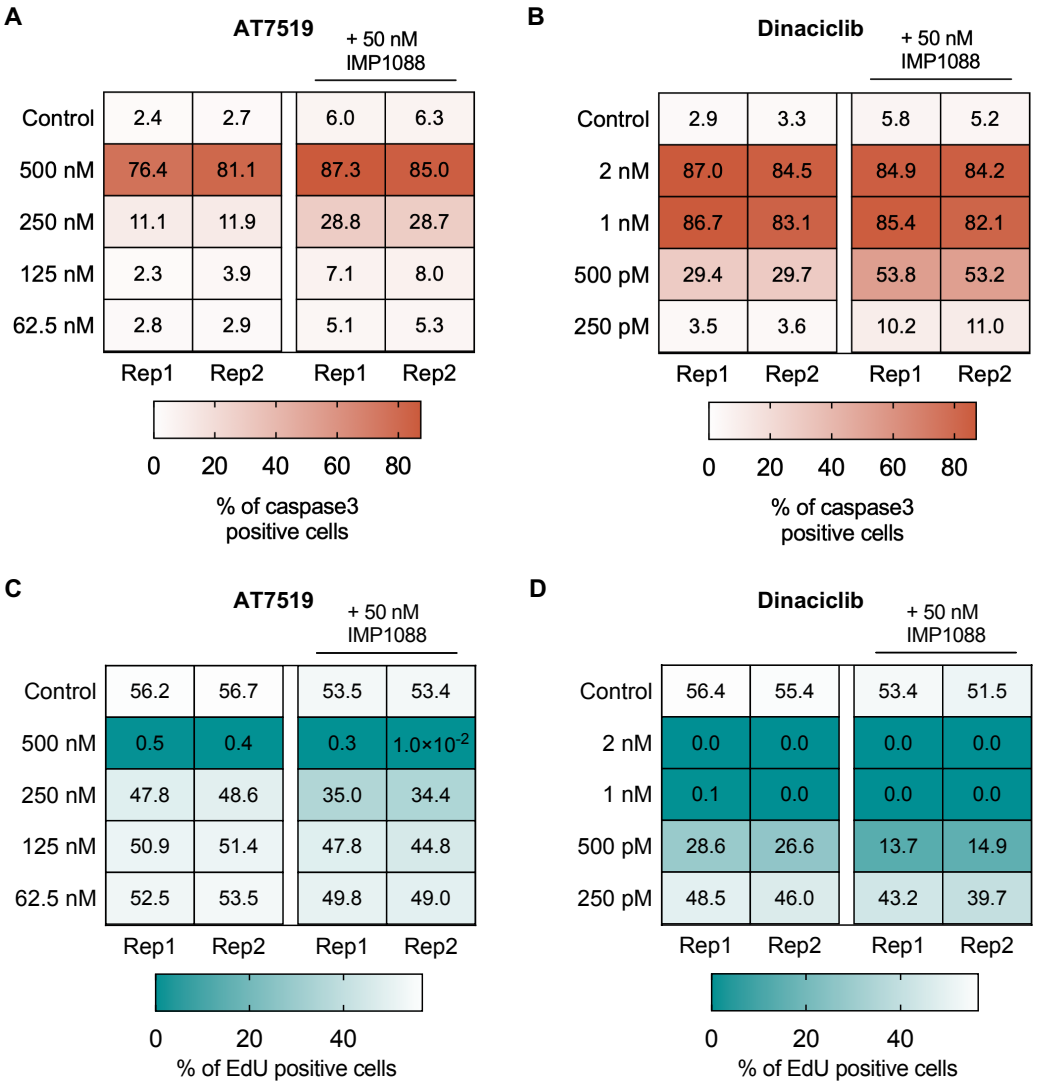

Figure 5-9: NMT inhibition synergises with clinical pan-CDK inhibitors.

[A] Effect of adding 50 nM of IMP1088 for 24 hours to AT7519 on DNA synthesis, measured by EdU incorporation. **[B]** Effect of adding 50 nM of IMP1088 for 24 hours to Dinaciclib on DNA synthesis, measured by EdU incorporation. **[C]** Effect of adding 50 nM of IMP1088 for 24 hours to AT7519 on apoptosis, measured by caspase 3 induction. **[D]** Effect of adding 50 nM of IMP1088 for 24 hours to Dinaciclib on apoptosis, measured by caspase 3 induction.

For both inhibitors, the synergistic effects are observed particularly at concentrations were the toxicity of the pan-CDK inhibitor does not dominate. This is also evident in the CIs for both inhibitors (see Table 5-2 for AT7519 and Table 5-3 for Dinaciclib). Similar to the increases in apoptosis, the cells also synergistically lost their proliferative capacity when treated in combination (see Figure 5-9 C and D). Similar to the apoptosis induction, this effect was particularly evident in the concentrations in which the respective CDK inhibitor did not dominate with its toxicity.

Table 5-2: Combination indices for the effects on apoptosis and proliferation with AT7519.

Concentration of AT7519	Apoptosis		Proliferation	
	Response Additivity	Bliss Independence	Response Additivity	Bliss Independence
500 nM + IMP1088	0.95	0.92	1.06	1.02
250 nM + IMP1088	0.48	0.47	0.55	0.53
125 nM + IMP1088	0.84	0.83	0.88	0.86
62.5 nM + IMP1088	1.48	1.48	1.00	0.99

Table 5-3: Combination indices for the effects on apoptosis and proliferation with Dinaciclib.

Concentration of Dinaciclib	Apoptosis		Proliferation	
	Response Additivity	Bliss Independence	Response Additivity	Bliss Independence
2 nM + IMP1088	1.04	1.02	1.04	1.02
1 nM + IMP1088	1.04	1.02	1.04	1.02
500 pM + IMP1088	0.57	0.56	0.74	0.72
250 pM + IMP1088	0.39	0.37	0.77	0.75

The effect of adding IMP1088 to AZD5438 was quite remarkable. On its own AZD5438 had a limited effect in BL41 on apoptosis and reduction of proliferation, especially compared to Dinaciclib and AT7519, and maybe expected from its growth inhibition curve. Those minor effects were however strongly amplified by IMP1088, across all concentrations tested, with strong synergy observed, as judged by the CIs (see Figure 8-43 and Table 8-3). E.g., apoptosis induction rose from in average 4% over control with 500 nM AZD5438 on its own, to 27% over control in combination with IMP1088 (IMP1088 on its own at 24 hours caused an increase of only 3.5% in the apoptotic cells). For none of the inhibitors a reduction of cell numbers was observed at this point of the combination treatment (see Figure 8-44). However, as proliferative capacity and overall viability of the remaining cells were starkly reduced, the overall cell viability should collapse faster if treatment is done longer. To conclude, IMP1088 showed synergistic effects with three clinical pan-CDK inhibitors, of which two are still being evaluated in clinical trials. Very interestingly, this occurred within a time frame, in which IMP1088 on its own does not yet show much toxicity. The

synergistic effects were particularly evident at concentrations at which the respective CDK inhibitor on its own did not dominate the cell toxicity.

5.3 Conclusion

In this chapter, a chemical proteomics workflow was used to identify potential candidates within the CoTMyr NMT substrates that could drive the premature termination and polyadenylation observed in BL41 within hours of NMT inhibition (see Chapter 3). To that aim, the pulse time of the myristic acid analogue was reduced compared to previous studies (Broncel et al., 2015; Kallemeijn et al., 2019; Mousnier et al., 2018; Thinon et al., 2014). Through this approach, it became evident that post-translational myristoylation is unlikely to be involved in the toxicity of NMT inhibition and two new (previously not annotated) NMT substrates were identified: CDCA3, involved in cell cycle (Adams et al., 2017; Uchida et al., 2012; Zhang et al., 2018); and GCSAM, a GC reaction specific gene (Jiang et al., 2010; Lossos et al., 2003; Romero-Camarero et al., 2013). Furthermore, the subset of NMT substrates that was strongly affected within those 6 hours was particularly enriched for proteins involved in signalling, in line with previous observations that those proteins tend to have low protein stability (Schwanhausser et al., 2011).

Based on these data, it was assumed that deregulated signalling upon NMT inhibition might be the initial trigger for the subsequent mRNA processing phenotype. Phosphoproteomics within minutes to hours shows indeed very early on changes in signalling, with pronounced ‘spike’ of phosphorylation changes at 10 minutes of NMT inhibition. Across all the tested time points, phosphorylation on proteins involved in RNA processing and later at 30 and 90 minutes also on proteins involved transcriptional termination was affected by NMT inhibition. While this needs further mechanistical validation, it could give a first explanation what is occurring in the cells within the first minutes/hours of NMT inhibition: the synthesis of NMT substrates continues, despite the lack of the myristate. This causes NMT substrates, involved in signalling such as kinases and phosphatases, to (de)phosphorylate proteins that usually would not be (de)phosphorylated, due to the lack of the myristate. To note is that at least some NMT substrates can indeed evade the N-terminal glycine degron pathway, upon NMT inhibition making a GOF situation indeed a possibility (Timms

et al., 2019). However, no systematic study into the degradation of all NMT substrates upon NMT inhibition has been conducted so far.

Moreover, phosphorylation on CDK motifs, particularly CDK1/2, was affected by NMT inhibition, leading to the idea that NMT inhibition might amplify the toxicity of CDK inhibitors within a time frame in which the NMT inhibitor on its own is not yet toxic. Indeed, one chemical probe, initially thought to be a CDK1/2 specific inhibitor (Jorda et al., 2018; Lin et al., 2005), but shown to be a pan-CDK inhibitor, and three clinical pan-CDK inhibitors, Dinaciclib (Parry et al., 2010), AT7519 (Santo et al., 2010) and AZD5438 (Byth et al., 2009), show strong synergistic effects when combined with an NMT inhibitor. This is particularly interesting in light of the common practice to use several agents in combination in cancer (Humphrey et al., 2011). On the other hand, synergistic drug combination, at least in the case of cancer, might play less of a role for the beneficial effects of combination therapy. The key benefit is to overcome patient and cancer heterogeneity through using drugs with different mode of action (Palmer and Sorger, 2017).

In this work, pan-CDK inhibitors have been tested, however the synergies observed with these inhibitors raise the question if similar synergies would be observed with e.g. the clinically approved CDK4/6 inhibitors (Choo and Lee, 2018), or with the recent wave of published and described CDK7 and CDK9 inhibitors and degraders (Kwiatkowski et al., 2014; Olson et al., 2018; Patel et al., 2018a). It also raises the question if synergy would be observed potentially with other kinase inhibitors. The focus in this thesis came from the initial observation of CDK1/2 motif phosphorylation disturbance; however, it is likely that non-myristoylated kinases and phosphatases might disturb many more signalling pathways.

Chapter 6. Discussion and outlook

The research presented in this thesis illustrates the potential applications of NMT inhibitors in cancer, and gives a potential inside in combination therapies that one could use in a clinical setting, as monotherapies are rarely used for cancer treatment (Humphrey et al., 2011). The surprising finding that MYC deregulation renders cells more susceptible to NMT inhibition explains the initial observations that particularly BL (Iorio et al., 2016; Lim, 2016), a malignancy defined by MYC translocation (Dalla-Favera et al., 1982; Schmitz et al., 2014), is amongst the most responsive cancer types. This last chapter will summarise and discuss the presented data, speculate on implications and give an outlook for NMT inhibition as a cancer treatment.

6.1.1 Haematological malignancies are particularly responsive to NMT inhibitors

The first part of this work analysed the data of three different pharmacogenomics screens, utilising three different NMT inhibitors, IMP366, IMP1031 and IMP1036 from two distinct chemical series. Across all the screens it was apparent that haematological malignancies, in particular the GC-derived B cell malignancy BL (Schmitz et al., 2014), were amongst the most responsive cancer subtypes. However, none of the CFEs (Iorio et al., 2016) the Sanger tested for correlated with increased sensitivity (or resistance). The claimed concept that NMT2 deficiency renders cells more susceptible to NMT inhibition (Berthiaume and Beauchamp, 2017; Berthiaume et al., 2014) could not be confirmed for any of the three NMT inhibitors; nor did NMT1 expression have an impact on responsiveness. The presence of mutations in CoTMyr NMT substrates did not have an alter the responsiveness of the cancer cells to NMT inhibition either; however, the expression of certain NMT substrates was enriched in the more sensitive cancer cell lines. If this is a real biological consequence or just an artefact of cell-of-origin remains unknown. Faster doubling time correlated with increased effect of the NMT inhibitor; however, this trend itself did not suffice to explain the increased sensitivity of the haematological malignancies. Additionally, this case might be observed for most anti-cancer drugs in general.

The observation that haematological malignancies, particularly BL cell lines, were highly susceptible to NMT inhibition could be confirmed through several validation experiments. To investigate the temporal dynamics of NMT inhibition, flow cytometry at different points of NMT inhibition was applied to define an 'NMT inhibition time line', taking several parameters into account, such as proliferation, apoptosis, cell numbers and cell cycle arrest. Across four different tested cell lines, two BL (BL41, Raji) and two DLBCL cell lines (Riva and U2931), NMT inhibition took about 24 hours to negatively affect the viability of the cells. From this point onward, a loss of proliferative capacity, cell cycle arrest and induction of programmed cell death is observed, with varying kinetics. It is apparent that events, more precisely the degradation of the pool of myristoylated substrates and/or the synthesis of non-myristoylated, toxic GOF NMT substrates, in these first 24 hours lay the foundation of the subsequent breakdown of cellular viability. Hence, phosphoproteomics, mRNAseq and in the end also total RNAseq were conducted within those 24 hours in a representative cell line BL41 of the very sensitive Burkitt's lymphoma.

6.1.2 NMT inhibition causes mRNA shortening in an unexpected short time frame and synergises with CDK inhibition

The results and analyses of the phosphoproteomics strongly implied RNA processing and splicing, as one of the major pathways affected in the first 24 hours of NMT inhibition in BL41. Increased phosphorylation was observed across several members, known to be involved in the spliceosome, such as SRRM1/2 (Blencowe et al., 2000), TRA2A/B (Tacke et al., 1998) or U2SURP (Will et al., 2002a). Thus, mRNAseq was conducted to, firstly, to identify via GSEA which biological functions were affected by differential gene expression (Subramanian et al., 2005); secondly, to identify potential alternative splicing upon NMT inhibition. The GSEA showed early downregulation in expression of spliceosome components, which was consistent over the three tested timepoints. This result implied again RNA processing and splicing as a major pathway affected by NMT inhibition. Hence, the mRNAseq data sets were used to assess alternative splicing upon NMT inhibition. The initial results from rMATs (Shen et al., 2014) indicated indeed alternative splicing, particularly MXE events affecting hundreds of genes within six hours of NMT inhibition. However, after

further analysis using the program DEXSeq to search for differential exon expression (Anders et al., 2012), these MXE events were revealed to be a sequence coverage shift towards the 5'-end of the gene. This sequence coverage shift affected 7500 out of 18000 expressed genes, and it was a surprising finding in a polyA enriched RNAseq data set. The shortening of mRNA length fits a phenotype of premature termination and polyadenylation, to be the cause of an increased sequence coverage. 3'-end sequencing (Hoque et al., 2013) would be needed to confirm the usage of PAS after the first exons. However, the combination of observed U1 downregulation and what is known about the effects thereof (Berg et al., 2012; Kaida et al., 2010), and the fact that the genes affected by putative mRNA shortening have an increased frequency of PAS signals and decreased frequency of U1 binding sites (Singh et al., 2018) makes it very plausible that NMT inhibition disrupts correct mRNA length processing through U1 downregulation. This U1 downregulation is likely a consequence of early phosphorylation changes on the spliceosome, as discussed in Chapter 5.

There are several things to note at this point: firstly, this occurred at a surprisingly short time frame of NMT inhibition (within 6 hours), implicating a gain or change-of-function of an NMT substrate rather than a LOF of an NMT substrates via degradation. Secondly, IpA has been particularly observed in immune cells and malignancies of these cells (Lee et al., 2018; Singh et al., 2018), raising the question if this mRNA shortening is due to the tissue origin of BL41 and how NMT inhibition would impact this. Myristoylation has previously been implicated in T cell proliferation and differentiation (Rampoldi et al., 2015) and in T cell mediated auto-immunity (Wen et al., 2019), even if the later has some issues in the quantification of actual myristoylation (see section 1.1.4 for more details). Some of the observed effects might be due to similar mechanisms. While DNA damage (Devany et al., 2016; Williamson et al., 2017), 'anti terminator' proteins (Gregersen et al., 2019) and U1 downregulation (Berg et al., 2012; Kaida et al., 2010) in general have been implicated in the expression of shorter mRNAs, regulatory mechanism are not known to date. DNA damage as a cause for the mRNA shortening in BL41 seems unlikely, as the G2 arrest is observed at much later time points, long after the mRNA shortening occurs.

The time frame of 6 hours would indicate that NMT substrates involved in signalling are likely driving this phenotype, as these tend to have shorter half-lives

(Schwanhausser et al., 2011). This potential involvement of NMT substrates that are directly involved in signalling, such as kinases and phosphatases, was confirmed via chemical proteomics with a short pulse of 6 hours of YnMyr. Subsequently, phosphoproteomics at early time points of NMT inhibition was conducted to test if there is an early effect on signalling in the cells upon NMT inhibition. Changes on proteins involved in RNA processing and Pol II termination were found. More work will be needed to identify the NMT substrates responsible for those phosphorylation changes. Two other interesting observations were made: firstly, BL41 do not recover from transient NMT inhibition, whereas HeLa do (Mousnier et al., 2018), perhaps due to this mRNA shortening in BL41 early on after NMT inhibition; secondly, the deregulation of signalling within minutes to hours of NMT inhibition has a surprisingly strong synergistic effect with pan-CDK inhibitors, such as the chemical probe CDK1/2 III (Lin et al., 2005) and clinical pan-CDK inhibitors, such as Dinaciclib (Parry et al., 2010), AT7519 (Santo et al., 2010) and AZD5438 (Byth et al., 2009). If the synergy is only due to the initially observed signalling deregulation on CDK motifs, or a combinational effect with the mRNA shortening is difficult to distinguish at this point. However, it raises the question, whether synergies would be also observed with the clinically approved CDK4/6 inhibitors (Choo and Lee, 2018) or CDK7 inhibitors currently being evaluated in the clinic (Hu et al., 2019; Patel et al., 2018b). The observations that transcription was affected in the context of a MYC-deregulated cancer, and that these cancers have increased demand in correct RNA processing and splicing (Hsu et al., 2015; Koh et al., 2015) was a first hint towards MYC as a potential genetic marker correlating with sensitivity to NMT inhibition.

6.1.3 NMT inhibition against MYC deregulated cancers?

Through a tissue and cancer subtype-agnostic bioinformatics approach, utilising published whole genome transcription data (Iorio et al., 2016) and GSEA (Liberzon et al., 2015; Subramanian et al., 2005), biological functions, enriched in the sensitive cell lines compared to the resistant cell lines, were identified. Genes involved in RNA splicing (e.g., HNRNPD, SNRPD1, U2AF1), transcription (e.g., CDK9, POLR2A, POLR2D), ribosomal proteins and translation initiators (e.g., EIF3E, EIF4E, RPL15, RPS16), proteasome subunits (PSMA8, PSMB8, PSMB9), and

various nuclear pore related genes (NUP107, NUP153, NUP210) were enriched in the sensitive cell lines, compared to the resistant cell lines. The here mentioned genes and others, identified by leading-edge analysis, were summarised in a new gene set 'Sensitive to NMTi'. This gene set was validated in the pharmacogenomics data of the NMT inhibitor IMP366 (Frearson et al., 2010), and the NMT inhibitors IMP1031 and IMP1036 (Bell et al., 2017; Mousnier et al., 2018). Furthermore, the same gene set was enriched in cancer cell lines with higher dependence on NMT1, assessed by CRISPR-based gene essentiality knockout, for both the Broad Institute (Cancer Cell Line Encyclopedia and Genomics of Drug Sensitivity in Cancer, 2015; Meyers et al., 2017) and the Sanger Institute (Behan et al., 2019). In conclusion, this gene set is highly validated across different data sets of different institutes, using different means to interfere with myristoylation.

The key upstream node of the 'Sensitive to NMTi' gene set was indeed MYC, maybe unsurprising due to its known role in transcription (Sabo et al., 2014; Walz et al., 2014) and ribosomal biogenesis (Cole and Cowling, 2008; Dai and Lu, 2008). Expression levels of *MYC* mRNA on their own were able to distinguish in the three pharmacogenomics screens (Iorio et al., 2016) and the two CRISPR gene essentiality screens (Behan et al., 2019; Meyers et al., 2017) sensitive or NMT1-dependent cell lines from resistant or less dependent cell lines. Sensitivity is defined as responsiveness to a given NMT inhibition and dependence is defined as sgRNA depletion of NMT1, assessed by the respective methodology of the Institute. Structural alterations in the genomic loci, such as mutations, CN gains and RACSs in *MYC* (and/or *MYCN*) also served as predictive markers of sensitive/dependent cancer cell lines; however, to a lesser extent than mRNA expression on its own. This could be due to confounding inclusion of cell lines that e.g. present RAS mutations or loss of APC both known to increase MYC levels (Dang, 2012), in the group without the structural alterations. There was an excellent correlation between the activation of the MYC Hallmark signature from the MSigDB (Liberzon et al., 2015) and the newly defined 'Sensitive to NMTi' gene set. In conclusion, these data clearly indicated that cells with high MYC expression would show increased responsiveness to NMT inhibition.

However, the 'Sensitive to NMTi' signature and the analysis in this thesis does not answer the question if some cancer cell lines might suffer from a lineage-dependent effects of MYC expression, beyond the 'canonical' MYC program (i.e., chromatin

remodelling, transcription, translation, and proliferation) (Schaub et al., 2018). Also, potential combinational effects on the response to NMT inhibition dependent on lineage, presence of mutations and CN alterations, and transcriptional programs in combination are not determined. Such an analysis, incorporating the simultaneous assessment of several omic-modalities (e.g., expression data, mutations/CN alterations in oncogenes/tumour suppressors, DNA methylation patterns, lineage, and of course the sensitivity to various NMT inhibitors and gene effect scores to NMT1) could be potentially achieved with recently published algorithms, such as multi-omics factor analysis (MOFA) (Argelaguet et al., 2018) or the updated version MOFA+ (Argelaguet et al., 2019).

Nonetheless, the hypothesis that increased MYC (or MYCN) expression increases the sensitivity to NMT inhibition was confirmed in two isogenic cell lines: one, derived from immortalised B cells, with inducible MYC (Pajic et al., 2000); the other, derived from NB, with inducible MYCN (Valentjin et al., 2005). In both cases, enforced expression of the respective paralog greatly increased the toxicity of the tested NMT inhibitors, accelerating the depletion of the cells and causing a more rapid onset of programmed cell death. These results served as the validation of the synthetic lethality between NMT inhibition with enforced expression of MYC and MYCN. In addition, three different PDXs of haematological malignancies, all with MYC translocations, were highly sensitive to NMT inhibition *in vitro*. The induction of apoptosis was already observed within 24 hours, compared to immortalised cell lines. Two of those were so-called ‘double hit’ DLBCL with additional BCL2 translocation, usually associated with worse clinical outcome (Riedell and Smith, 2018), and the other was a plasmablastic lymphoma, also with poor clinical prognosis (Castillo et al., 2015).

Total RNAseq, using one of the isogenic cell lines with inducible MYC, comparing the MYC high state, treated with NMT inhibitor, vs. the MYC medium state, treated with NMT inhibitor, revealed what seems to be a collapse of most major biological functions. Additionally, the MYC driven transcriptional program was strongly affected in the MYC high cells, compared to the MYC medium cells. Interestingly, one variant of U1, RNVU1-7, was upregulated in the MYC medium treated case, whereas it was not induced at all in the case of the MYC high cells, treated with NMT inhibitor. Not much is known about the U1 variants and their regulation (O'Reilly et al., 2013), and the initial publications identifying U1’s role in protecting from premature termination

and polyadenylation knocked down all of the U1 variants (Berg et al., 2012; Kaida et al., 2010). It remains to be determined if different MYC levels, combined with NMT inhibition, have a differential effect and potential mRNA shortening, or not. 3'-end sequencing could be used to elucidate in greater detail the effects of NMT inhibition, potentially dependent on MYC levels, on mRNA length through potentially premature termination and polyadenylation (Hoque et al., 2013).

Independently of these results, the described synthetic lethality between MYC deregulation and synthetic lethality with NMT inhibition has strong implications in the TCGA data set, thus for potential patients. The breast cancer (BRCA) cohort was used as an example, with breast cancer being responsible of 15% of all new cancer cases and 7% of all cancer related deaths in the US, independent of sex (Siegel et al., 2019). Within the BRCA cohort, patients with MYC CN gains (Schaub et al., 2018), are doing worse and are at the same time enriched for the 'Sensitive to NMTi' gene set. This could potentially indicate that NMT inhibitors might work particularly well in the patient with the more aggressive subtypes of breast cancer (Xu et al., 2010).

6.1.4 Why is there an increased demand for myristoylation in MYC deregulated cancers?

The synthetic lethality between disrupting myristoylation and enforced MYC expression has been validated; however, the question why increased MYC expression correlated with an increased need for myristoylation remains unanswered. This subchapter will propose a mechanistical reason for this, present some preliminary data on this mechanism, and discuss potential implications for other drugs and differentiation in cells.

The toxic effects of an NMT inhibitor will be likely crucially dependent on the protein turnover of the substrates, independently if the cell viability collapses through degradation of the myristoylated pool of substrates, or through toxic GOF of non-myristoylated substrates that are still being synthesised. MYC is known to bind Pol I (Grandori et al., 2005) and Pol III (Gomez-Roman et al., 2003) and increase translation in a general sense through increased ribosomal biogenesis (Cole and Cowling, 2008; Dai and Lu, 2008). Additionally, it is known that, at least

pathologically, increased MYC levels cause increased PERK activation and autophagy (Hart et al., 2012) and targeting the PERK/ATF4 pathway (Tameire et al., 2019) or IRE1/XBP1 pathway (Xie et al., 2018; Zhao et al., 2018) can be a potential mean to target MYC deregulated cancers. The implication of this combined effect on the two sides of the proteome, synthesis and degradation, might indicate a role for MYC in global acceleration of the protein turnover, a type of 'proteome remodeller' (see Figure 6-1 A).

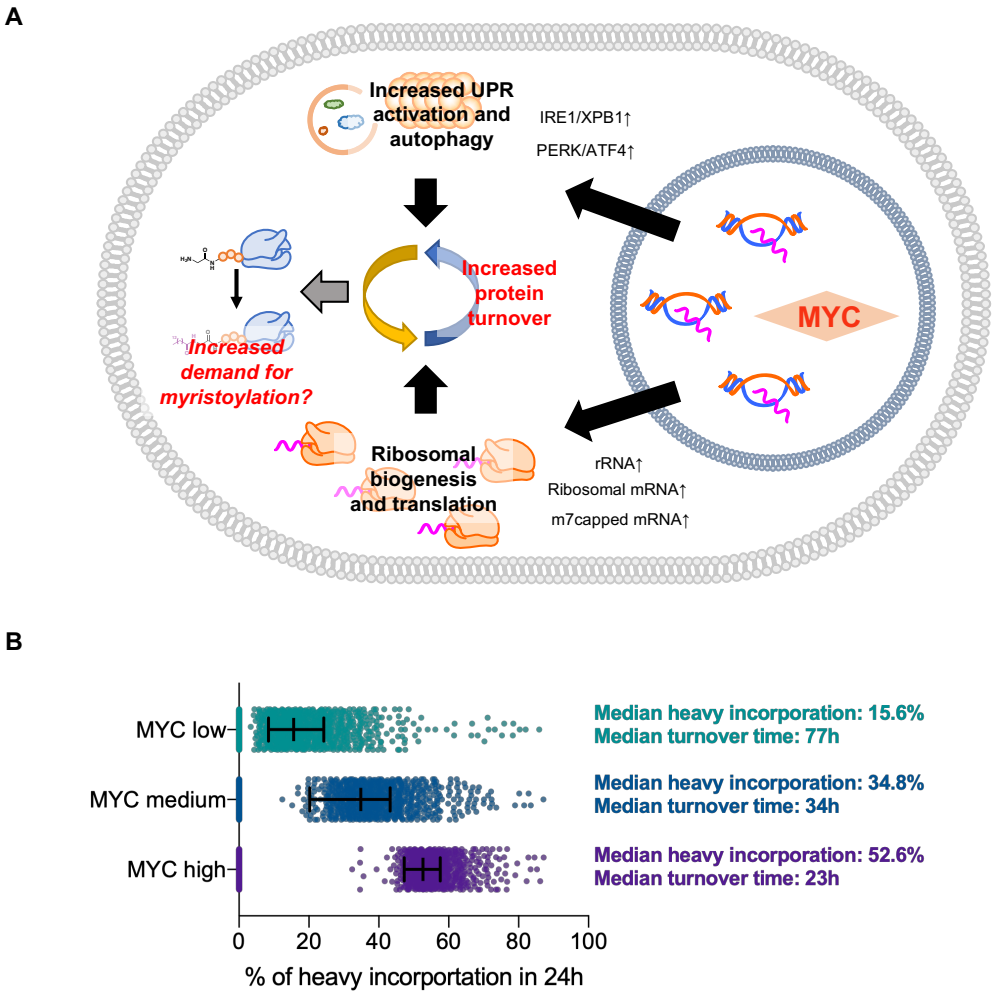

Figure 6-1: MYC, as a 'proteome remodeller'?

[A] The effects of MYC expression in the increase transcription of rRNA and ribosomal mRNA are already appreciated and well-known (Cole and Cowling, 2008; Dai and Lu, 2008; Gomez-Roman et al., 2003; Grandori et al., 2005). Recent research has shown that MYC also critically activates the UPR, namely the PERK/ATF4 (Tameire et al., 2019) arm and the IRE1/XBP1 arm (Xie et al., 2018; Zhao et al., 2018), and causes induction of autophagy (Hart et al., 2012). **[B]** A preliminary experiment using the P-493-6 cell line shows strong differences in protein turnover within the identified protein groups, measured as incorporation of heavy lysine or arginine, correlating with MYC levels.

In a preliminary experiment, Dr. Monica Faronato pulsed the P-493-6 cell line (Pajic et al., 2000) for 24 hours (after 24 hours of induction of the respective MYC level, see Material and Methods for the P-493-6 cell line) with heavy SILAC to observe global changes in the protein turnover (Mathieson et al., 2018). The data were jointly analysed, and within this single experiment to test the system, it became clear that MYC levels greatly increase the incorporation of heavy lysine and arginine in the proteome (see Figure 6-1 B). The observed average half-lives (assuming zero order kinetics for the turnover) of the proteins decrease with increased MYC levels.

This has a strong implication for the irreversible co-translational lipidation myristoylation. If on the one hand, protein synthesis is increased, the likelihood of synthesising toxic GOF substrates without the myristate is increased, which was already described for SRC and LYN (Honda et al., 2016); on the other hand, if protein degradation through e.g. MYC induced autophagy (Hart et al., 2012) is also increased, then the pool of myristoylated NMT substrates is depleted in a quicker manner, increasing also the toxicity on this side of the balance.

This has two potential implications for MYC biology:

Firstly, the role of MYC in controlling e.g. the differentiation process of haemopoietic stem cells (HSCs) is already known. MYC levels have to rise to cause the initial differentiation, followed by the expansion of the progenitor cells, and subsequent MYC downregulation once a mature state is reached (Wilson et al., 2004). This initial burst of MYC will cause various changes in transcription across the progenitors, and indeed these changes can be identified via single-cell RNAseq (scRNAseq) (Paul et al., 2015). However, the functional consequences for a cell do not occur on the transcriptional level, but largely on the proteome level; thus, there is a need to not only remodel the transcriptome, but also the proteome, which is indeed observed in the differentiation process (Cabezas-Wallscheid et al., 2014). Potentially, the capacity of MYC to drive translation on the one hand, and on the other to potentially induce autophagy (Hart et al., 2012) (or increased protein degradation?) is needed for this proteome remodelling.

Another example of differentiation with a need of MYC expression is the transition from GC B cells into plasma cells during the GC reaction. MYC is crucial for initiation and maintenance of the GC reaction, and MYC expression defines the positively selected GC B cells (Calado et al., 2012; Dominguez-Sola et al., 2012). Those positively selected cells within the GC reaction contain the precursors of the plasma

cells (Ise et al., 2018), thus, maybe also here MYC is needed to act as a 'gas pedal' in the differentiation process to a plasma cell, once the fate decision is taken through e.g., upregulation of BLIMP1, the master transcription factor of plasma cells (De Silva and Klein, 2015; Victora and Nussenzweig, 2012). It will firstly change the transcriptional program of the cells (Shi et al., 2015), and then be involved in remodelling the proteome throughout this differentiation process.

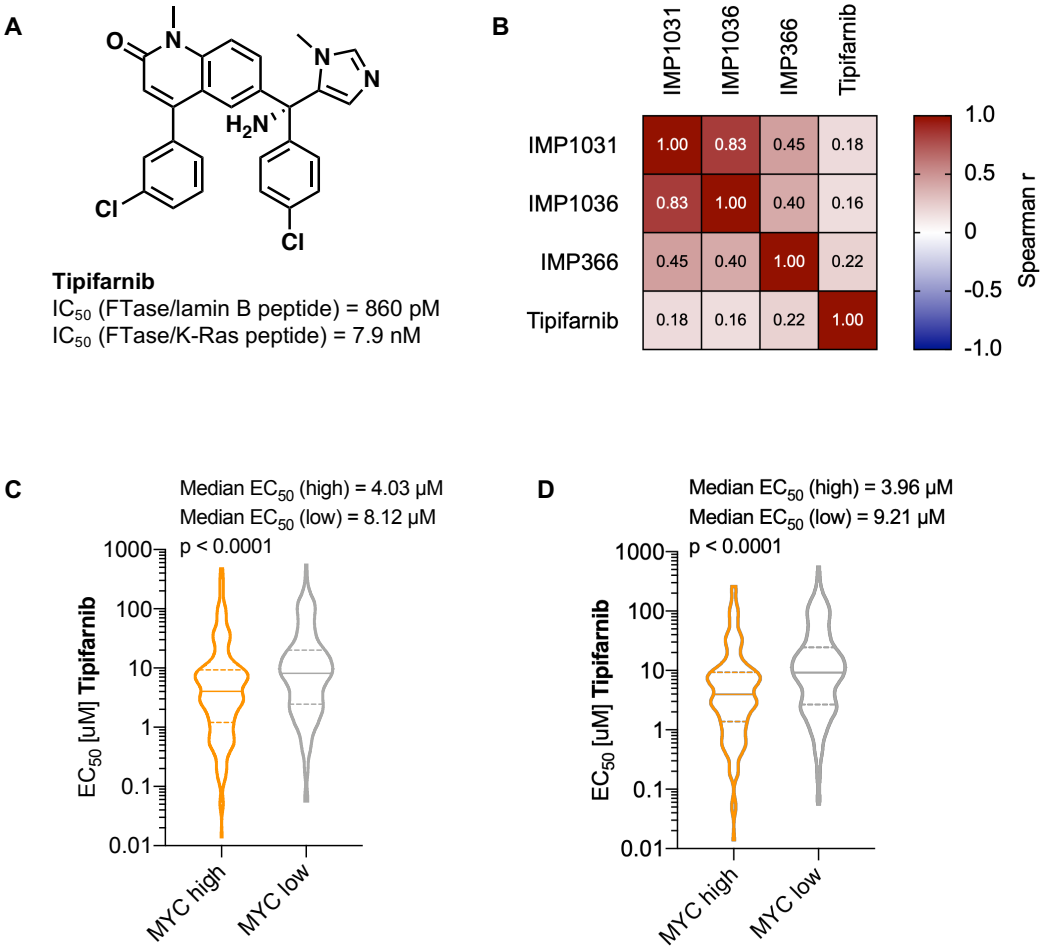

Figure 6-2: A link between MYC expression and FTase inhibition sensitivity?

[A] Structure and enzymatic potency of Tipifarnib (End et al., 2001). **[B]** Correlation of potency of Tipifarnib with the three NMT inhibitors IMP366, IMP1031, IMP1036. (N = 620 cancer cell lines) **[C]** Comparison of the EC_{50}s for Tipifarnib of the quartiles with highest and lowest expression of MYC, agnostic to RAS mutational status (both groups: 217 cancer cell lines). **[D]** Comparison of the EC_{50}s for Tipifarnib of the quartiles with highest and lowest expression of MYC, excluding cancer cell lines with mutated KRAS, HRAS or NRAS (both groups: 170 cancer cell lines). (For all graphs: p-values determined with the Mann-Whitney test)

Secondly, MYC levels seems to increase the toxicity of the irreversible co-translational myristoylation, as shown in this thesis. Other lipidations such as

prenylation would be yet another example lipidation that is irreversible, similar to myristoylation. It is involved in diverse biological functions, but, contrary to myristoylation occurring post-translationally (Palsuledesai and Distefano, 2015; Wang and Casey, 2016). As mentioned in subchapter 1.1.1, initial drug programs against farnesylation (one form of prenylation), were aiming at targeting RAS-dependent cancers, which little clinical success, and if, often independent of RAS mutational status (Berndt et al., 2011; Tsimberidou et al., 2010).

If MYC acts as a 'proteome remodeller', one could also expect increased toxicity for FTase inhibitors, such as Tipifarnib, dependent on MYC levels (End et al., 2001) (chemical structure shown in Figure 6-2 A). Tipifarnib has been tested by the Sanger Institute as part of the GDSC project (Iorio et al., 2016; Yang et al., 2013), so the trends in potency were compared to the those of the three NMT inhibitors. Overall low correlation was observed between the different NMT inhibitors and Tipifarnib, indicating that different cancer cell lines are sensitive to the respective inhibitors (see Figure 6-2 B). A second FTase inhibitor, FTI-277 (Lerner et al., 1995), was also tested, but basically all reported EC_{50} values were outside the screening range, thus, this inhibitor was excluded from further analysis. Combination of the Tipifarnib data with whole genome expression data revealed that cells with the highest MYC expression were doing worse than the cells with the lowest MYC expression (by quartiles) (see Figure 6-2 C). However, the group with the highest MYC expression were overrepresented with cell lines that have mutations in KRAS, HRAS or NRAS (28.31% in the MYC high group vs. 14.22% in the MYC low group; p-value = 0.0004 by Fisher's exact test). In order to avoid confounding results, all the cell lines with mutations in either of the RAS paralogs were excluded, interestingly yielding again in the result that the MYC high cancer cells are doing worse than the MYC low cancer cells (see Figure 6-2 D).

Currently, work in the laboratory is aiming at establishing through the application of triplex SILAC the proteome dynamics in the P-493-6 cell line upon induction of different levels of MYC, looking at protein synthesis, protein degradation and protein turnover (Boisvert et al., 2012). These data set will be used to look at the dynamics of NMT substrates. The dynamics in the turnover of NMT substrates might also hint at which substrates might be key drivers of the toxicity. This approach could be expanded to substrate of FTase. Additionally, such an endeavour could be

conducted in an MYCN system, such as the Shep-ER-MYCN cell line (Valentjin et al., 2005) or SKNAS-ER-MYCN cell lines (Ushmorov et al., 2008).

6.1.5 Outlook

Drug discovery suffers from an exceptionally high attrition in the clinical stage, with a more or less constant probability of a given drug to succeed, going from phase I trials to launch, of 7% in the last decade (9% for drugs in the area of oncology) (Dowden and Munro, 2019). At this stage, it is impossible to predict the probability of NMT inhibition to succeed as a drug against MYC-deregulated cancer; however, the *in vitro* data, presented in this thesis, is very promising. Moreover, a recent investigation in the protein turnover in primary cells showed that most NMT substrates identified in the study have a median half-life of three days, indicating a potentially good therapeutic window (Mathieson et al., 2018). This is also observable in the near absence of toxic effects on the MYC low condition in the P-493-6 cell line, with a median turnover of 77 hours over the whole proteome however. A key question for success will likely be the side effects of NMT inhibition on cells that dependent on MYC, such as the germinal centre reaction (Calado et al., 2012; Dominguez-Sola et al., 2012). Maybe the side effects are comparable to what is observed with Omomyc induction in the body (Soucek et al., 2008). Further investigation using mice and other appropriate *in vivo* systems will be needed. Key questions will be to understand more the dynamics in which NMT inhibition seems to be disproportionally toxic to MYC high cells: is it just a general acceleration of protein turnover, thus all NMT substrates? Do oncogenic MYC levels potentially drive only increased turnover on a subset of NMT substrates (or in general proteins)? Is it just a question of increased protein turnover, and if, why are genes related to transcription and nuclear export enriched in the sensitive cancer cell lines? Nonetheless this work might add a new concept of targeting MYC in oncology, next to the previous reported ones (Chen et al., 2018):

MYC high cells are highly dependent on myristoylation and thus NMT inhibition is synthetically lethal with MYC deregulation.

However, NMT inhibition as a concept to target cancer will only have its baptism by fire, once it reaches the clinical evaluation. A spin-out company, Myricx, has been formed based on different chemical inhibitor series for NMT, a decade worth of research on NMT by a great number of scientists, and also in parts on this work: the identified synthetic lethality between MYC deregulation and NMT inhibition has been patented in a 'new use' patent, filed on the 19th of December 2018, GB P029833. Myricx aims to test NMT inhibitors in the clinic as an antiviral, based on previous findings (Mousnier et al., 2018), and as an anticancer drug, based on the findings, presented in this thesis.

Chapter 7. Material and methods

7.1 Key resources

Key resources used in this work are summarised in

Table 7-1. Tissue culture specific reagents and the cell lines are summarised in the next section.

Table 7-1: Key Resources.

Inhibitors, reagents and chemicals		
Name	**Source**	**Identifier/Catalogue number**
IMP366	(Frearson et al., 2010; Thinon et al., 2014)	NA
IMP1031	(Bell et al., 2017; Mousnier et al., 2018)	NA
IMP1036	(Bell et al., 2017; Mousnier et al., 2018)	NA
IMP1088	(Bell et al., 2017; Mousnier et al., 2018)	NA
CDK1/2 III	Merck	217714
AT7519	Selleck Chemicals	S1524
AZD5438	Selleck Chemicals	S2621
Dinaciclib	Selleck Chemicals	S2768
YnMyr	(Heal et al., 2011)	NA
AzRB	(Broncel et al., 2015)	NA
Puromycin	Merck	P7255
Staurosporine	Merck	S4400
Doxycycline	Merck	D9891
β-Estradiol	Merck	E8775
Tamoxifen	Merck	H7904
Cytofix/Cytoperm Buffer	BD Bioscience	554714
Perm/Wash Buffer	BD Bioscience	554723
Perm Buffer III (PhosFlow)	BD Bioscience	558050
Protease inhibitor cocktail	Roche	11873480001
TCEP	Sigma-Aldrich	C4706
TBTA	Sigma-Aldrich	C678937

NeutrAvidin agarose beads	Pierce	29201
Sequencing-grade modified trypsin	Promega	V5111
Phosphatase inhibitor cocktail	Merck	4906845001
CellTiter Blue Assay	Promega	G8081
FxCycle Violet	ThermoFisher Scientific	F10347
Zombie NIR	Biolegend	423105
Antibodies		
α-Active Caspase3 (C92-605, PE)	BD Biosciences	550821
c-Myc (Y69, AF647)	Abcam	ab190560
N-Myc	Abcam	ab16898
p-Histone 3 (Ser10) (D2C9, AF647)	Cell Signalling	#3458
Kits		
Click-iT EdU Alexa Fluor 488 Flow Cytometry	ThermoFisher Scientific	C10420
DC protein assay kit	Bio-rad	5000111
TMT 6-plex kit	ThermoFisher Scientific	90061
High pH reversed-phase peptide fractionation kit	ThermoFisher Scientific	84868
Sep Pak C_{18} Plus Light Cartridge	Waters	WAT200685
High-Select TiO2 Phosphopeptide Enrichment Kit	ThermoFisher Scientific	A32993
High-Select Fe-NTA Phosphopeptide Enrichment Kit	ThermoFisher Scientific	A32992
miRNAeasy kit	Qiagen	217004
KAPA mRNA HyperPrep Kit	Roche	08098123702
KAPA RNA HyperPrep Kit	Roche	08098107702

7.2 Cell culture

Cells were either grown in DMEM high glucose with 10% FBS, with added non-essential amino acids (NEAA, 1 : 100), sodium pyruvate (NaPyr, 1 : 100), HEPES (1 : 000), penicillin/streptomycin (Pen/Strep, 1 : 100) and 2 µL β-mercaptoethanol per 500 mL of media; or in RPMI 1640 with 10% FBS added, and additional NaPyr (1 : 100), HEPES (1 : 100), Pen/Strep (1 : 100) and 2 µL β-mercaptoethanol per 500 mL of media.

All cell lines were grown at 5% CO_2 and 37ºC. Table 7-2 lists the tissue culture specific reagents, and the cell lines, their growth type and the source. Every cell line with known short-tandem repeat (STR) profile were validated by the Crick Cell Service facility. The cells were passaged every two to three days, and cells used in experiments were passaged for at least five times after thawing to guarantee proper recovery. Cell culture plastics were provided by the internal Crick Stores and Lab Logistics teams and were usually bought from Corning or ThermoFisher Scientific.

Table 7-2: Tissue culture specific reagents and cell lines.

Tissue culture specific reagents.			
Name	**Source**	**Identifier/Catalogue number**	
DMEM high glucose	ThermoFisher Scientific	61965059	
RPMI 1640	ThermoFisher Scientific	61870044	
NEAA	ThermoFisher Scientific	11140035	
NaPyr	ThermoFisher Scientific	11360039	
HEPES	ThermoFisher Scientific	15630056	
Pen/Strep	ThermoFisher Scientific	15140122	
β-mercaptoethanol	Merck	M3149-25mL	
Trypsin	ThermoFisher Scientific	25200056	
Cell lines			
Name	**Obtained from**	**Growth media**	**Growth type**
BL41	Crick Cell Services	RPMI 1640	Suspension
BL70	Crick Cell Services	DMEM	Suspension
Ramos	Crick Cell Services	RPMI 1640	Suspension
CA46	Crick Cell Services	RPMI 1640	Suspension
Raji	Crick Cell Services	RPMI 1640	Suspension

Daudi	Crick Cell Services	RPMI 1640	Suspension
Namalwa	Crick Cell Services	DMEM	Suspension
Rael	Georg Klein	DMEM	Suspension
WSU-NHL	Crick Cell Services	DMEM	Suspension
SU-DHL 8	Crick Cell Services	RPMI 1640	Suspension
Karpas 422	Crick Cell Services	DMEM	Suspension
Farage	Crick Cell Services	DMEM	Suspension
U2932	Crick Cell Services	DMEM	Suspension
Riva	Crick Cell Services	RPMI 1640	Suspension
Jurkat	Crick Cell Services	RPMI 1640	Suspension
HeLa	Crick Cell Services	DMEM	Adherent
MDA-MB-231	Crick Cell Services	DMEM	Adherent
P-493-6	Chi Van Dang	DMEM	Suspension
Shep-ER-MYCN	Linda Valentjin	DMEM	Adherent
LY11212	Martin Janz	DMEM	Suspension
LY12318	Martin Janz	DMEM	Suspension
LY12657	Martin Janz	DMEM	Suspension

7.3 CellTiter Blue assay

General procedure:

At the respective endpoints of the experiments (usually 48 or 72 hours of incubation with a given inhibitor) 20 µL/well (for a 96-well plate) of the CellTiter Blue Assay were added. The cells were left to incubate at 37 ºC for another two to four hours with the CellTiter Blue reagent, depending on the cell line and its metabolic activity. As an example, MDA-MB-231 needed four hours of incubation for a good signal-to-noise ratio; Raji only needed two hours of incubation to achieve this ratio. Subsequently, the fluorescence was measured at 570 nM using an EnVision plate reader.
As a negative control for cell death, the highest DMSO concentration was added to the cells (usually 0.4% DMSO); as a positive control for cell death, the cells were treated with 10 µg/mL Puromycin and 1 µM Staurosporine. The data was then normalised, using the software Prism 8 for macOS, GraphPad Software, La Jolla California USA, www.graphpad.com. To generate the growth inhibition curves, the

'log(inhibitor) vs. response – Variable slope (four parameters)' function of Prism 8 was used.

Suspension cell lines (except P-493-6):

Experiments for the suspension cell lines were performed in 96-well flat bottom plates and in technical quadruplicate. 50 µL/well of media with twice the respective drug concentration or positive/negative control for cell death (see general procedures) were prepared and warmed up to 37ºC in the incubator. 50 µL/well of a cell suspension in fresh media at a concentration of 1,000,000 cells/mL were added to the wells. This resulted in 100 µL of cell suspension in the desired condition at an initial density of 500,000 cells/mL at the beginning of the experiment (50,000 cells per well). Once the endpoint of the experiment was reached, the steps described in the general procedure section were applied.

P-493-6 cell line:

The experiment was performed in a 96-well flat bottom plate and in technical quadruplicate. On day zero, 50 µL/well of cell suspension at a concentration of 500,000 cells/mL were seeded in the respective media to induce the respective MYC level. MYC high: DMEM; MYC medium: DMEM with 0.1 µg/mL of Doxycycline and 1 µM of β-Estradiol; MYC low: DMEM with 0.1 µg/mL of Doxycycline. On day one, 50 µL of media (with the respective addition of Doxycycline and β-Estradiol), with twice the concentration for the respective inhibitor/control condition, was added to the wells with the cells. Once the endpoint of the experiment was reached, the steps described in the general procedure section were applied.

Adherent cell lines (except Shep-ER-MYCN):

The experiment was performed in a 96-well flat bottom plate and in technical quadruplicate. On day zero, in the case of HeLa, 1,600 cells were plated in each well in 50 µL of media; in the case of MDA-MB-231, 3,000 cells were plated in each well in 50 µL of media. The plates were left overnight in the incubator and on the following day 50 µL of media per well with twice the concentration of the respective

inhibitor/control condition were added. Once the endpoint of the experiment was reached, the steps described in the general procedure section were applied.

Shep-ER-MYCN:

The experiment was performed in a 96-well flat bottom plate and in technical quadruplicate. On day zero, 1,000 cells/well were plated in 50 µL of media. The plate was left overnight in the incubator and on the following day 50 µL of media ± 200 nM of Tamoxifen or ethanol was added to induce MYCN. On day two, 100 µL of fresh media (± tamoxifen) per well with the twice the desired concentration for the respective inhibitor/control condition were added. Once the endpoint of the experiment was reached, the steps described in the general procedure section were applied.

7.4 Flow cytometry

General:

Single-cell suspensions were stained with the following monoclonal antibody: α-Active Caspase3 (PE, 1 : 5), c-Myc (AF647, 1 : 100), p-H3S10 (AF647, 1 : 100) and N-Myc (1 : 100). To analyse DNA content, the cells were stained with FxCycle Violet (0.5 µL per 200 µL of cell suspension). To assess DNA synthesis, the Click-iT EdU Alexa Fluor 488 Flow Cytometry Assay Kit was used according to manufacturer's instructions (EdU final concentration used: 10 µM; incubation time: 2 h). Zombie NIR (0.5 µL per 100 µL of cell suspension) was used to exclude dead cells. The cells were fixed in a 4% solution of paraformaldehyde (PFA), 15 minutes at room temperature (RT), subsequently permeabilised with Cytofix/Cytoperm (20 minutes at RT) and Perm/Wash Buffer was used for the washes. Samples were acquired on a MACSQuant VYB (Miltenyi Biotec) and analysed using the FlowJo software (v10.4, Tree star).

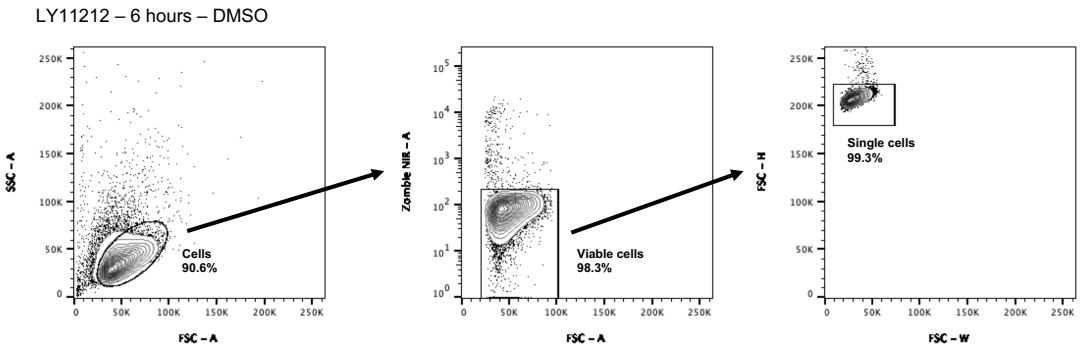

Figure 7-1: Example standard gating strategy.

Cells were selected, based on their size. Subsequently Zombie NIR positive cells and doublets were excluded. The here shown FACS plots were generated for the experiment in the PDX LY11212, shown in section 4.2.3.

An example of the standard gating strategy is shown in Figure 7-1; for the assessment of cell cycle or apoptosis, please refer to the flow cytometry gating examples shown in Figure 2-12. To note is that the labelling of the EdU was the first staining conducted after permeabilization to avoid interference of the copper, used in the 'Click chemistry', with the PE-based fluorophores.

An alternative protocol was applied for the staining of phosphorylated proteins, more specifically for the staining of phospho H3S10. The cells were fixed with ice-cold MeOH at -20ºC for 10 minutes. To permeabilise the cells the Perm Buffer III (BD Phosflow) was applied. The buffer was chilled to -20ºC before usage, and the cells were incubated for 20 minutes over ice with it.

Suspension cell lines (except P-493-6):

The experiments were conducted in 96-well U bottom plates and in technical duplicate or triplicate. On day zero, 50 µL of cell suspension (with a density of 500,000 cells/mL) are plated and left overnight in the incubator at 37ºC. On day one, 50 µL of media with twice the respective concentration of inhibitor or control were added. If the experiment was conducted for more than 48 hours of incubation, another 100 µL of fresh media with inhibitor or control were added on day two of the experiment. Two hours prior to fixation, EdU was pulsed according to the general methods.

P-493-6 cell line:

The experiments were conducted in 96-well U bottom plates and in technical duplicate or triplicate. On day zero, 50 µL of cell suspension (with a density of 500,000 cells/mL) were seeded in the wells in the media to induce the respective MYC level. were seeded in the media to induce the respective MYC level (see subchapter 7.3 for details). On day one, 50 µL of media (adjusted for the respective MYC condition) with twice the concentration of inhibitor or control were added. If the experiment was conducted for more than 48 hours of incubation, another 100 µL of fresh media (for the respective MYC condition) with inhibitor or control were added on day two of the experiment. Two hours prior to fixation, EdU was pulsed according to the general methods.

Shep-ER-MYCN cell line:

The experiments were conducted in a 24-well flat bottom well plate and in technical duplicate or triplicate. On day 0, 7,800 cells/well were plated in 500 µL of media. On day one 200 nM Tamoxifen or EtOH were added. On day two, the old media was carefully aspirated to not detach any cells, and 500 µL of media with the respective concentrations of inhibitor or controls were added. If the experiment was conducted for more than 48 hours of incubation, another 500 µL of fresh media with the respective concentration of inhibitor or control and MYCN condition were added on day three. Two hours prior to fixation, EdU was pulsed according to the general methods. To harvest the cells all the media was collected, to not loose floating apoptotic cells; trypsin was used to detach the remaining cells. The combined cells were spun down and then transferred to 96-well V bottom plates for subsequent fixation and staining.

7.5 Proteomics

7.5.1 Chemical proteomics

For the chemical proteomics experiment, in section 5.2.1, the previously established experimental conditions for mammalian cell culture were utilised

(Broncel et al., 2015; Kallemeijn et al., 2019; Mousnier et al., 2018; Thinon et al., 2014).

The cells, BL41 namely, were plated in 100 mm tissue culture dishes, at a density of 500,000 cells/mL in 6 mL of media, and left overnight in the incubator for recovery. The following morning, the cells were preincubated with varying concentrations (1 µM to 12 nM) of IMP1088 for 30 minutes. YnMyr at a final concentration of 30 µM was given for 6 hours. The cells were collected in falcon tubes, and washed twice with PBS, and subsequently lysed for 20 minutes in a PBS buffer containing 0.1% sodium dodecyl sulphate (SDS), 1% Triton X-100 and a protease inhibitor cocktail on ice. Insoluble material was removed via centrifugation.

After protein concentrations were determined DC protein assay kit and adjusted, the lysates were subject to CuAAC ligation to the AzRB capture reagent with 1 mM of $CuSO_4$, 1 mM of tris(2-carboxyethyl)phosphine (TCEP) and 100 µM of tris(benzyltriazolylmethyl)amine (TBTA) for 1 hour at RT under vortexing. The proteins were precipitated in MeOH : $CHCl_3$: H_2O (4 : 1 : 2), and resuspended in PBS with 1% SDS. The enrichment of the AzRB labelled proteins was carried on NeutrAvidin Agarose beads. Three washes with PBS and 1% of SDS, followed by two washes with 4M urea and 50 mM ammonium bicarbonate (AMBIC), followed by another three washes with 50 mM AMBIC were applied to wash-out unspecific binding proteins and enrich for the AzRB labelled proteins. Dithiothreitol (DTT) and iodoacetamide (IAA) were used to reduce and alkylate cysteine-cysteine bonds; sequencing grade modified trypsin was used for the subsequent on-bead digest overnight at 37ºC. The supernatant was collected from the vials, and the remaining beads were washed with 70 µL of 50 mM tetraethylammonium bromide (TEAB) and with 70 µL 1.5% trifluoroacetic acid (TFA) in water. Both washing solutions were combined with the supernatant, containing the peptide mixture. The samples were stage tipped and dried over vacuum.

The following steps were done by Aaron Borg, former senior research scientist in the Proteomics STP at the Crick:

A TMT 6-plex kit was used according to manufacturer's instructions, with the distribution of the samples in the different TMT channels shown in Table 7-3. After TMT labelling and mixing, the samples were additionally fractionated with a high pH

reversed-phase peptide fractionation kit and desalted using Sep Pak C_{18} Plus Light Cartridge, 130 mg bed volume. The samples were run on a one-hour gradient elution, DDA, with CID as activation selected, using the TMT MS3 SPS method. An Orbitrap Fusion Lumos Tribrid mass spectrometer was used for data acquisition.

Table 7-3: TMT channels and the corresponding samples for the chemical proteomics experiment.

TMT6-126	TMT6-127	TMT6-128	TMT6-129	TMT6-130	TMT6-131
DMSO	1000 nM IMP1088	333 nM IMP1088	111 nM IMP1088	37 nM IMP1088	12 nM IMP1088

7.5.2 Phosphoproteomics

The cells, BL41, were plated in T25 tissue culture flasks, at a density of 500,000 cells/mL in 15 mL of media, and left overnight for recovery in the incubator. The next day the cells were treated for the experiment in section 3.2.1 for 6, 18 and 24 hours with 100 nM IMP1088 or a corresponding concentration of DMSO (0.004%); for the experiment in section 5.2.2 the cells were treated for 5, 10, 15, 30 and 90 minutes with IMP1088. A control was prepared, which was treated for 90 minutes with the respective DMSO concentration (0.004%). At the end of the respective incubation period, the cells were collected in falcon tubes, and washed twice with PBS and lysed in an 8 M urea solution (adjusted to pH 7.5), with a protease inhibitor and phosphatase inhibitor cocktail. To disrupt the cell membranes five cycles of freeze-thawing over dry ice were applied.

The following steps were done by Andrew Jones, senior research scientist in the Proteomics STP at the Crick:

DTT and IAA were used to reduce and alkylate cysteine-cysteine bonds. The solution was diluted with a 50 mM solution of TEAB, until the urea concentration was below 2 M. The samples were digested using sequencing grade modified trypsin overnight at 37ºC. The peptides were subsequently desalted using a Sep Pak C_{18} Plus Light Cartridge, 130 mg bed volume, under vacuum. The samples were resuspended in 50 mM HEPES, adjusted to a pH of 8.5 and 30% (v/v) acetonitrile at a concentration

of 1 mg/mL. A TMT 6-plex kit was used according to manufacturer's instructions, with the distribution of the samples in the different TMT channels for the respective experiments shown in Table 7-4.

The labelled samples were combined and desalted again with a Sep Pak C_{18} Plus Light Cartridge and dried over vacuum. The samples were resuspended for the subsequent phospho-peptide enrichment. In the case of the phosphoproteomics experiment in section 3.2.1 only a TiO_2 enrichment was used; for the phosphoproteomics experiment in section 5.2.2 a TiO_2 enrichment and an additional Fe-NTA enrichment were applied.

Table 7-4: TMT channels and the corresponding samples for the phosphoproteomics experiment shown in sections 3.2.1 and 5.2.2.

Phosphoproteomics experiment shown in section 3.2.1					
TMT6-126	**TMT6-127**	**TMT6-128**	**TMT6-129**	**TMT6-130**	**TMT6-131**
DMSO 6h	Treated 6h	DMSO 18h	Treated 18h	DMSO 24h	Treated 24h
Phosphoproteomics experiment shown in section 5.2.2					
TMT6-126	**TMT6-127**	**TMT6-128**	**TMT6-129**	**TMT6-130**	**TMT6-131**
Control	5 min of NMTi	10 min of NMTi	15 min of NMTi	30 min of NMTi	90 min of NMTi

For the TiO_2-based enrichment and the Fe-NTA kit the manufacturer's instructions were followed. The Fe-NTA kit is applied on the flow-through that remained from the TiO_2-enrichment. The resulting peptide mixture was desalted with a Sep Pak C18 Plus Light Cartridge and dried over vacuum. The samples were run on a four-hour gradient elution, DDA, with CID as activation selected, using the TMT MS2 method. An Orbitrap Fusion Lumos Tribrid mass spectrometer was used for data acquisition.

7.5.3 Bioinformatical analysis of the proteomics

General:

The data were processed using MaxQuant (version 1.5.6.5), using the inbuilt Andromeda search engine (Cox and Mann, 2008). The MS/MS spectra were matched against the human reference proteome with isoforms (UniProt, accessed

July 2016) (Consortium, 2019). For the chemical proteomics experiment cysteine carbamidomethylation was used as a fixed modification, and methionine oxidation and N-terminal acylation were set as variable modifications. For the phosphoproteomics cysteine carbamidomethylation was used as a fixed modification, and N-terminal acylation, phosphorylation and methionine oxidation were set as variable modifications. As digestion mode 'Trypsin/P' was chosen, and a maximum of two missed cleavages allowed. Both the options 'match between runs' and 'unique and razor peptides' for protein quantifications were selected. The processed data was then further analysed with Perseus (version 1.5.6.0) (Tyanova et al., 2016). For all experiments the protein groups that are only identified by one side, that are potential contaminants, or that matched to the reverse database were excluded from further analysis. The following sections describe how the respective data sets were analysed.

Chemical proteomics:

The reporter intensities of the respective TMT channels were log2-transformed, and any protein group without any TMT quantification was excluded from the further analysis. Information about previously identified CoTMyr and PTMyr NMT substrates and proteins with N-terminal glycines were obtained from previous publications and data bases, such as UniProt (Broncel et al., 2015; Consortium, 2019; Kallemeijn et al., 2019; Martin et al., 2011; Mousnier et al., 2018; Thinon et al., 2014; Utsumi et al., 2018) and input as annotations into Perseus. The 2D plots, showing the relative enrichment in control vs. a given treated sample, were generated using GraphPad Prism 8.0 for MacOS X. To identify new potential NMT substrates, the biological replicates were normalised for each protein group by the median overall log2 TMT reporter intensity (normalising against potential technical variability between MS runs), and the treated samples were compared to the control with a Student t-test, adjusted for multiple hypothesis testing, with an FDR cut-off of <0.02 and a s_0-value of 0.5.

Phosphoproteomics:

The reporter intensities of the respective TMT channels were log2-transformed, and any protein group without any TMT quantification was excluded. Phosphopeptides with a localisation score of <0.75 were excluded. Information about the different (known) phosphorylation sites were obtained from PhosphoSitePlus (Hornbeck et al., 2015). To assess differential phosphorylation, the conditions of interest were subtracted from each other (in this case, treated minus control) and the resulting log2-changes were normalised by subtracting the median of each column. The 1D annotation enrichments (or 2D annotation enrichments) (Cox and Mann, 2012) were done with Perseus. The results of the different analysis were visualised with GraphPad Prism 8.0 for MacOS X.

7.6 Gene expression analysis

7.6.1 Sample preparation

BL41:

The experiment was conducted in T25 tissue culture flasks, at a density of 500,000 cells/mL in 10 mL of media, and left overnight for recovery in the incubator. The next morning 100 nM or a corresponding DMSO (0.004%) control was added to the wells. After 6 hours, 18 hours and 24 hours, the cells were collected in tubes, and after centrifugation the media was removed. The cells were lysed in QIAzol lysis reagent and stored at -80ºC until further processing.

P-493-6:

The P-493-6 were incubated, in biological quadruplicate, for 24 hours in the respective media conditions, to induce the respective levels of MYC (see subchapter 7.3 for details), at a density of 500,000 cells/mL in T25 tissue culture flasks in 10 mL of media. After 24 hours of induction of the respective MYC levels, the cells were treated for 24 hours with IMP1088 or a corresponding DMSO control (0.004%). At the endpoint of the experiment, the cells were collected in tubes, and after

centrifugation the media was removed. The cells were lysed in QIAzol lysis reagent and stored at -80ºC until further processing.

Purification of the RNA:

The RNA was purified from the prepared cell lysates with the miRNAeasy kit according to manufacturer's instructions.

7.6.2 RNAseq

Sequencing:

The RNAseq was performed by the Advanced Sequencing Unit, The Francis Crick Institute. The sequencing was performed on an Illumina HighSeq system, the read length was paired-end 100 bp, and the sequencing depth was 25 to 30 million reads per sample. For the mRNAseq library preparation the KAPA mRNA HyperPrep Kit was used; for the total RNAseq library preparation the KAPA RNA HyperPrep Kit was used.

Alignment and differential gene expression analysis:

The gene expression raw data were analysed by Probir Chakravarty, principal informatician, and Miriam Llorian Sopena, bioinformatics officer, at the Bioinformatics and Biostatistics unit, The Francis Crick Institute. Quality control of the reads and read trimming was performed with Trimmomatic (version 0.36) (Bolger et al., 2014). Alignment of the reads was carried out with STAR (version 2.5.2a) against the human transcriptome Ensembl GRch38 (release 86) (Dobin et al., 2013); counts per gene and sample were obtained using RSEM (version 1.2.31) (Li and Dewey, 2011). Gene level differential expression analysis was done using the program DESeq2 (version 1.18.1) (Love et al., 2014); genes with an adjusted p-value of <0.05 were considered statistically significant.

7.6.3 Gene set enrichment analysis

Gene set enrichment analysis was performed using the GSEA software (version 3.0) (Subramanian et al., 2005). For the analysis of the pharmacogenomics screens and CRISPR essentiality screens the data were obtained from the respective portals (Behan et al., 2019; Iorio et al., 2016; Meyers et al., 2017) (for the Broad institute data: release 18Q4). The published whole genome expression data was obtained from either the Sanger Institute in form of pre-processed and normalised micro-array data (Iorio et al., 2016), or from the Broad Institute in form of pre-processed and normalised RNAseq data (release 18Q4) (Cancer Cell Line Encyclopedia and Genomics of Drug Sensitivity in Cancer, 2015). The pre-processed data with SNPs, RACSs and CN alterations were obtained from the Sanger institute (Iorio et al., 2016). The data of MYC expression and mutations were extracted from the Broad Institute DepMap project (Tsherniak et al., 2017). The clinical and whole genome expression data (data version 2016_01_28) from the TCGA BRCA cohort was obtained from the Firebrowse project, conducted by the Broad institute (http://firebrowse.org). The CN alterations in the TCGA BRCA cohort were obtained from the TCGA Pan-Cancer Atlas (Schaub et al., 2018).

The whole genome expression data were matched to the respective patients or cancer cell lines of interest using R (version 3.5.1) (Team, 2014). The so-created data frames were subsequently used to generate the .gct files for subsequent GSEA with Microsoft Excel for Mac (version 16.16.10). The corresponding .cls files were also created with Microsoft Excel for Mac. Gene sets of interest were extracted from the MSigDB (Liberzon et al., 2015). The parameters in GSEA were kept as following: enrichment statistic: weighted; max size: 5000; min size: 5

For the mRNAseq (section 3.2.2) or total RNAseq analysis (sections 3.2.3 and 4.2.4), ranked lists based on the STAT value from DESeq2 were generated (Love et al., 2014). In this case pre-ranked GSEA was run with the same parameters as the GSEA, with one very important exception: enrichment statistic: classic.

To generate a surrogate for the differential transcriptional activation of MYC or MYCN the Spearman correlations between MYC (or MYCN) and every other gene of the COSMIC microarray transcription data were calculated (Iorio et al., 2016), using R (Team, 2014), similar to an approach used by a research team behind the Pan-Cancer Atlas (Schaub et al., 2018). One could combine the respective Spearman r

coefficients with the obtained p-value (or q-value after multiple hypothesis testing correction), in a formula such as shown in Equation 2; however, this had no impact on the subsequent GSEA, comparing the two created ranked lists (data not shown).

$$Rank = Spearman\ r\ \times\ -\log(p - value\ or\ q - value)$$

Equation 2: Generating rank-values in combining the Spearman r coefficient with the p- or q-value.

The same GSEA settings were applied for the so generated ranked lists, as for the previously mentioned ranked lists based on STAT values from DESeq2 (Love et al., 2014).

7.6.4 CytoScape and EnrichmentMap

To visualise the GSEA the recently published protocol was used (Reimand et al., 2019). CytoScape (V 3.7.1) (Shannon et al., 2003) and EnrichmentMap Pipeline Collection (V 1.0.0) (Merico et al., 2010) were used for this protocol. The FDR cut-off for the GSEA was varied, depending on the data set. Preferably a cut-off of <0.01 was chosen, but if only a few gene sets reached that threshold, a cut-off of <0.1 was chosen (see the figure legends for more information). The genes were filtered by expression, and the connectivity (edge cut-off based on Jaccard overlap combination index with a k constant of 0.5) was kept at 0.375 in the network. The annotation sets were created using the MCL Cluster algorithm, using the to 'similarity_overlap' option to create the clusters. Usually 4 words per label were allowed to define the clusters better. The resulting network was manually ordered so that gene sets that were downregulated were on one side and *vice versa* for the upregulated gene sets.

7.7 Alternative splicing and exon expression analysis

7.7.1 Differential splicing event analysis

The analysis of differential splicing was carried out with rMATs (version 3.2.5). The results were filtered by removing events with samples with less than 10 counts per event and/or less than 10% coverage per event and per sample to remove events

with low prevalence. Only alternative splicing events with an FDR of <0.05 were considered significant.

7.7.2 Differential exon expression analysis

The bin and exon level counts were obtained with HTSeq (version 0.6.1p1) (Anders et al., 2015) and the differential exon expression analysis was carried out with DEXseq (version 1.22.0) (Anders et al., 2012). Significant events were considered to be those with a p-value of <0.05. The transcript coverage plots were obtained using the R package 'bamsignals' (version 1.4.3) (Mammana A, 2019). The longest transcript with good prediction confidence per gene was selected and then binned 100 times. The trimmed mean for each bin across the transcript was plotted. The approach was done for transcripts of different length and for the 'protein coding genes' or 'all ensemble genes'.

7.8 Statistical analysis

GraphPad Prism 8.0 for MacOS X, R (v 3.5.1) (Team, 2014), and Perseus 1.5.6.0 (Tyanova et al., 2016) were used for statistical analysis. Each figure legend contains information on the applied statistical tests for the presented data and numerical p-values are shown in the respective figures. Overall, to test for correlations between to variables, Spearman correlations were applied; to compare two groups unpaired Mann-Whitney tests were applied. Several of the data sets (e.g., the lists of EC_{50}s, provided by the Sanger Institute, for the NMT inhibitors IMP366, IMP1031 and IMP1036, shown in section 2.2.1 and 2.2.2) were revealed to be not normally distributed, thus, nonparametric tests were applied across this work. To determine overrepresentation a Fisher's exact test was applied. Where other statistical tests were applied this is clearly stated in the respective legend of the figure.

Chapter 8. Appendix

8.1 Appendix Chapter 2: Pharmacogenomics screens identify haematological malignancies as highly responsive to NMT inhibition.

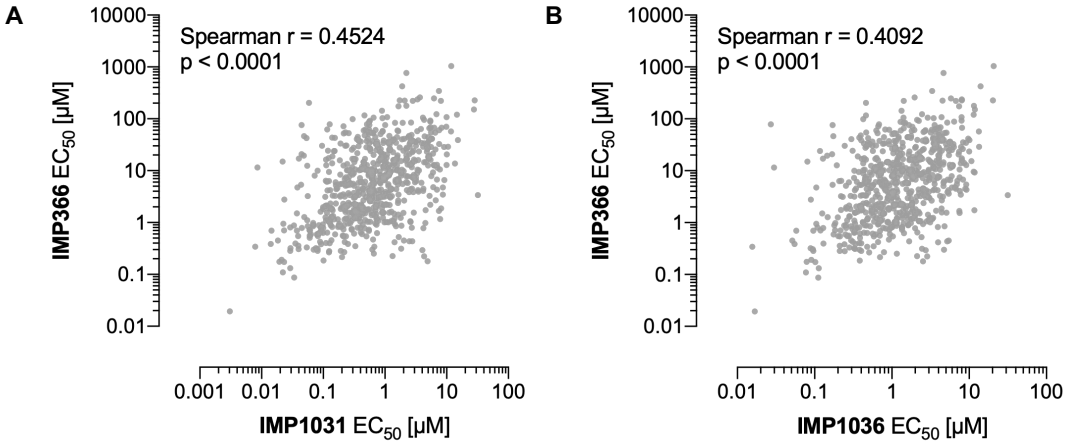

Figure 8-1: IMP366 correlates with IMP1031 and IMP1036 respectively.

[A] Correlation between the reported EC_{50}s of IMP366 and IMP1031. **[B]** Correlation between the reported EC_{50}s of IMP366 and IMP1036.

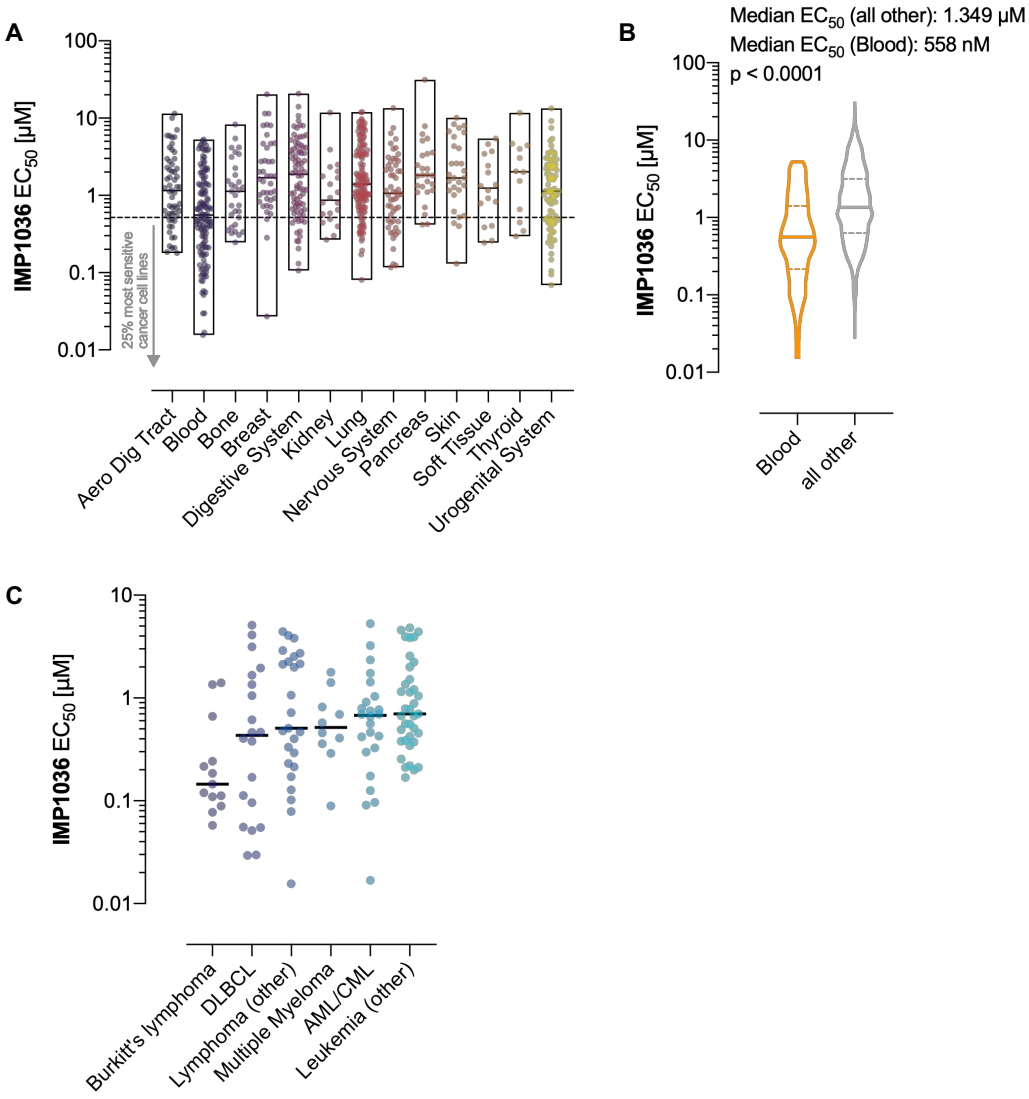

Figure 8-2: Cancer cell lines of the tissue subgroup Blood, in particular Burkitt's lymphoma, are enriched for the most responsive cell lines to IMP1036.

[A] Distribution of the reported EC_{50}s across the different tissue subgroups. **[B]** Cancer cell lines, within the tissue group Blood, are more responsive to IMP1036 compared to the other cancers. **[C]** Distribution of the EC_{50}s of the different haematological malignancies, comprising the tissue group Blood.

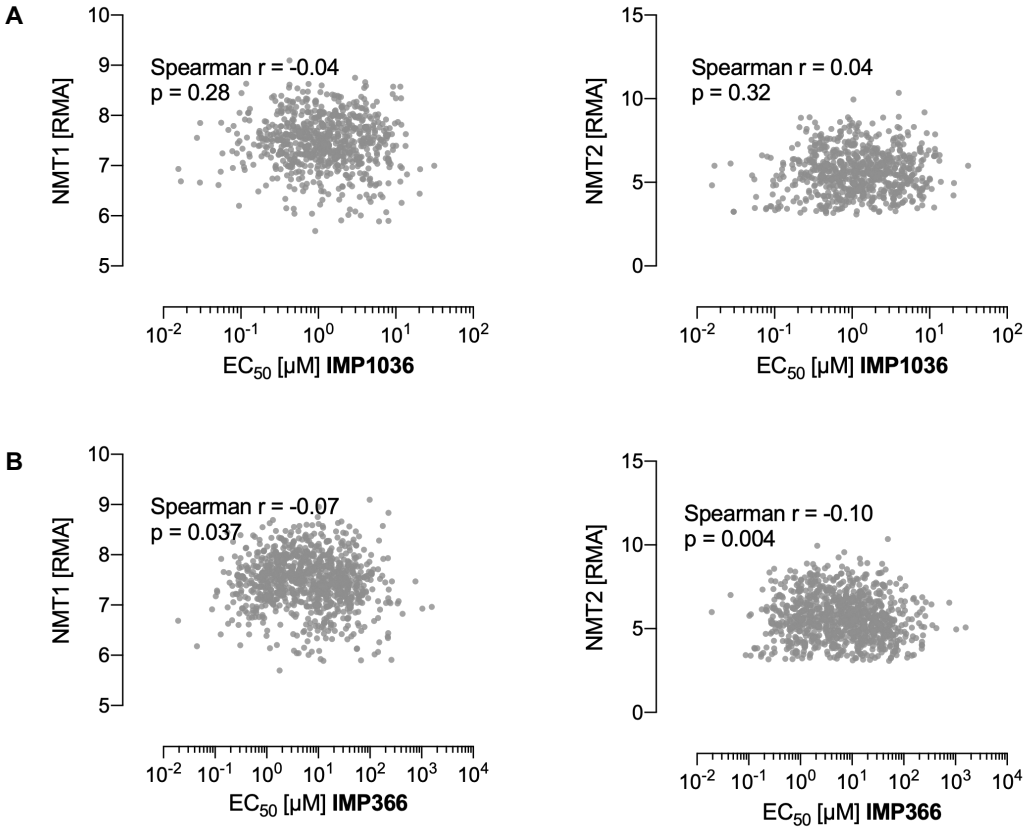

Figure 8-3: For neither IMP1036 nor IMP366 NMT1 or NMT2 expression are a predictor of sensitivity.

[A] Left: correlation between sensitivity to IMP1036 and NMT1 expression. Right: correlation between sensitivity to IMP1036 and NMT2 expression. **[B]** Left: correlation between sensitivity to IMP366 and NMT1 expression. Right: correlation between sensitivity to IMP366 and NMT2 expression.

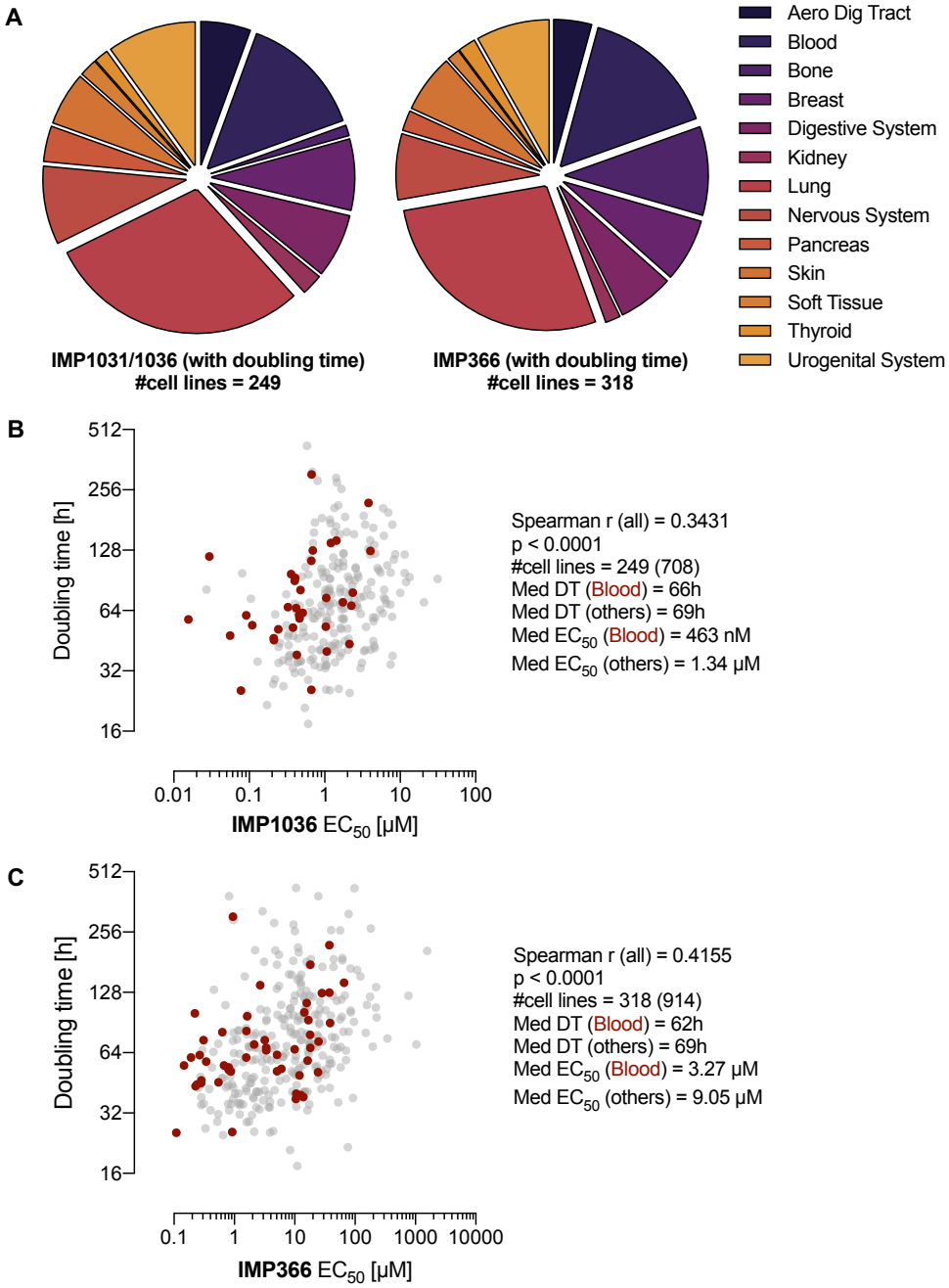

Figure 8-4: Doubling time of the cancer cell lines correlates with responsiveness to IMP1036 and IMP366.

[A] Distribution of the cell lines, according to tissue group for the cancer cell lines with doubling time. **[B]** Correlation between sensitivity to IMP1036 and doubling time of the cell lines. Red dotes comprise cells of the tissue subgroup 'Blood'. (249 out of 708 cancer cell lines had a corresponding doubling time) **[C]** Correlation between sensitivity to IMP1036 and doubling time of the cell lines. Red dotes comprise cells of the tissue subgroup 'Blood'. (318 out of 914 cancer cell lines had a corresponding doubling time).

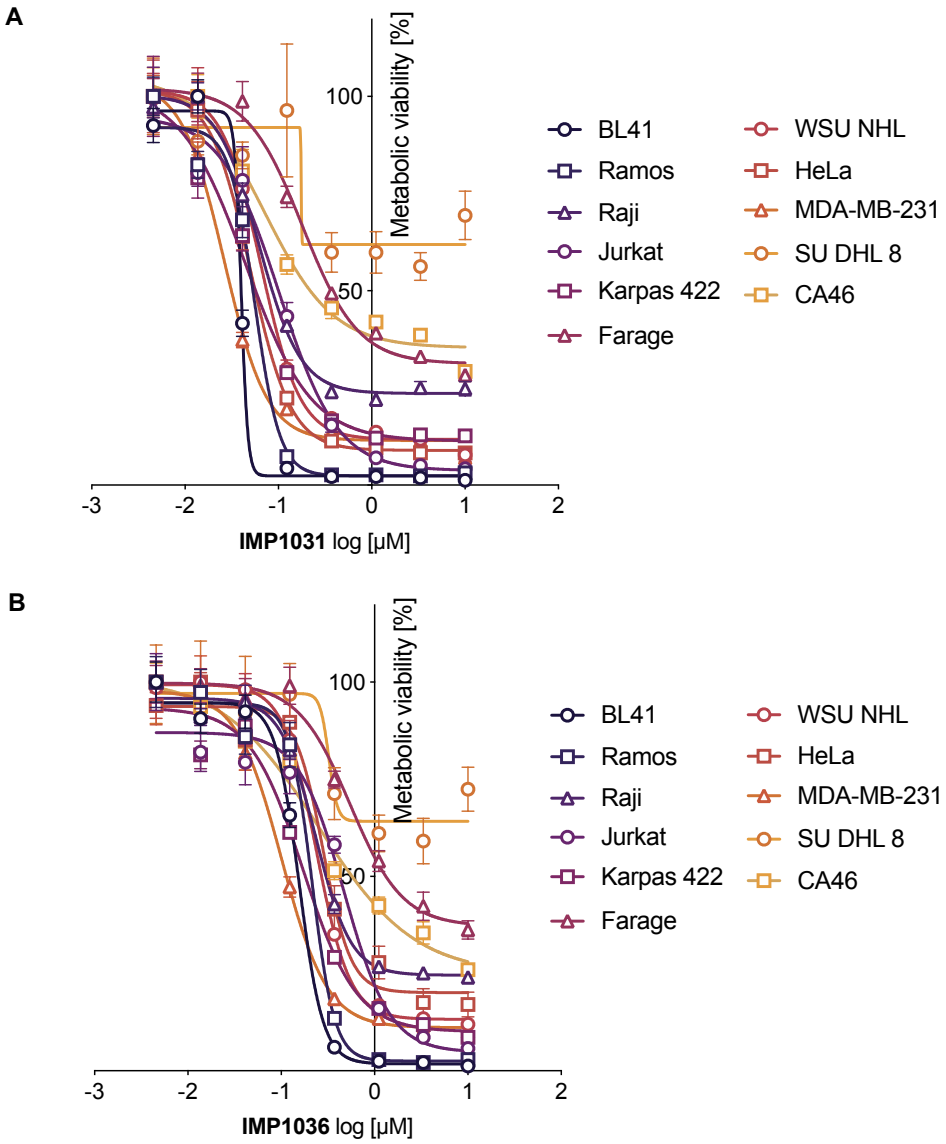

Figure 8-5: Growth inhibition curves for IMP1031 and IMP1036.

[A] Growth inhibition curves in cell lines, used in the cell line screen for IMP1031. **[B]** Growth inhibition curves in cell lines, used in the cell line screen for IMP1036. (For all graphs: N = 4, error bars = SEM)

Table 8-1: Occurrence of mutations in NMT substrates, correlating with increased responsiveness to IMP1031, in the Blood subgroup.

	Blood		Others		
NMT substrate	Nº of cell lines	Nº of cell lines	Nº of cell lines	Nº of cell lines	Overrepresented? ($p < 0.05$)
CYB5R3	4 (3.1%)	125	4 (0.7%)	574	Yes
GORASP2	3 (2.3%)	126	9 (1.6%)	569	No
LYPLA1	3 (2.3%)	126	4 (0.7%)	574	No
EEPD1	4 (3.1%)	125	8 (1.4%)	570	No
GORASP1	5 (3.9%)	124	6 (1.0%)	572	Yes
ANKIB1	8 (6.2%)	121	26 (4.5%)	552	No
CCNYL1	2 (1.6%)	127	3 (0.5%)	575	No
ARL2	1 (0.8%)	128	3 (0.5%)	575	No
FAM84B	2 (1.6%)	127	4 (0.7%)	574	No
MARCKSL1	6 (4.6%)	123	5 (0.9%)	573	Yes

A Fisher's exact test was used to test for overrepresentation of mutations in the two groups

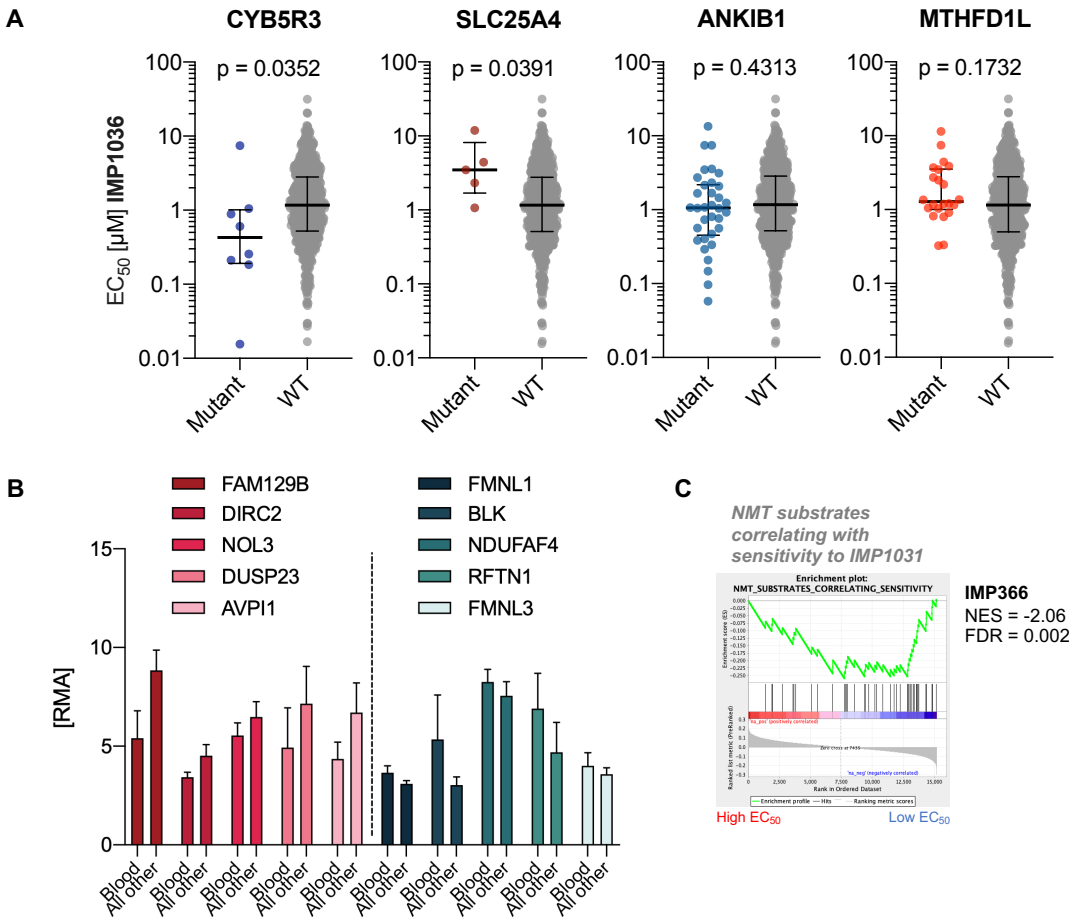

Figure 8-6: Mutations in NMT substrates as predictors of sensitivity for IMP1036, differential expression of NMT substrates in different cancer cell lines, and expression pattern as predictor for IMP366 potency.

[A] Effect of the presence of mutations in the NMT substrates CYB5R3, SLC25A4, ANKIB1 and MTHFD1 on the sensitivity to the NMT inhibitor IMP1036. (Error bars: interquartile range; p-values determined with the Mann-Whitney test) **[B]** Expression of the NMT substrates strongly correlating with sensitivity to the NMT inhibitor IMP1031, comparing the Blood group against all others. For all substrates the difference between Blood against all other was statistically significant, that is $p < 0.05$, tested with Mann-Whitney. **[C]** The gene set 'NMT substrates correlating with sensitivity to IMP1031' is enriched in the sensitive cancer cell lines to the NMT inhibitor IMP366.

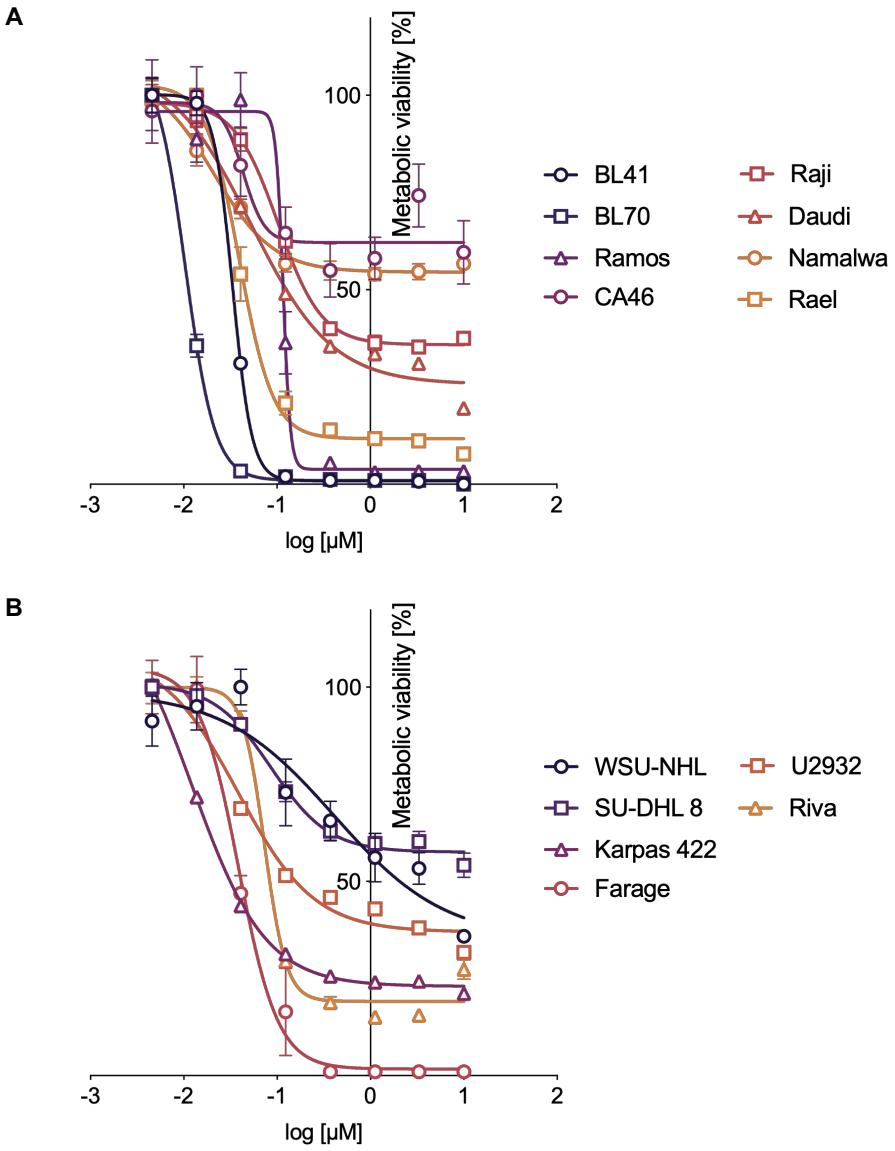

Figure 8-7: Growth inhibition curves for IMP1088.

[A] Growth inhibition curves in Burkitt's cell lines. **[B]** Growth inhibition curves in DLBCL cell lines.
(For all graphs: N = 4, error bars = SEM)

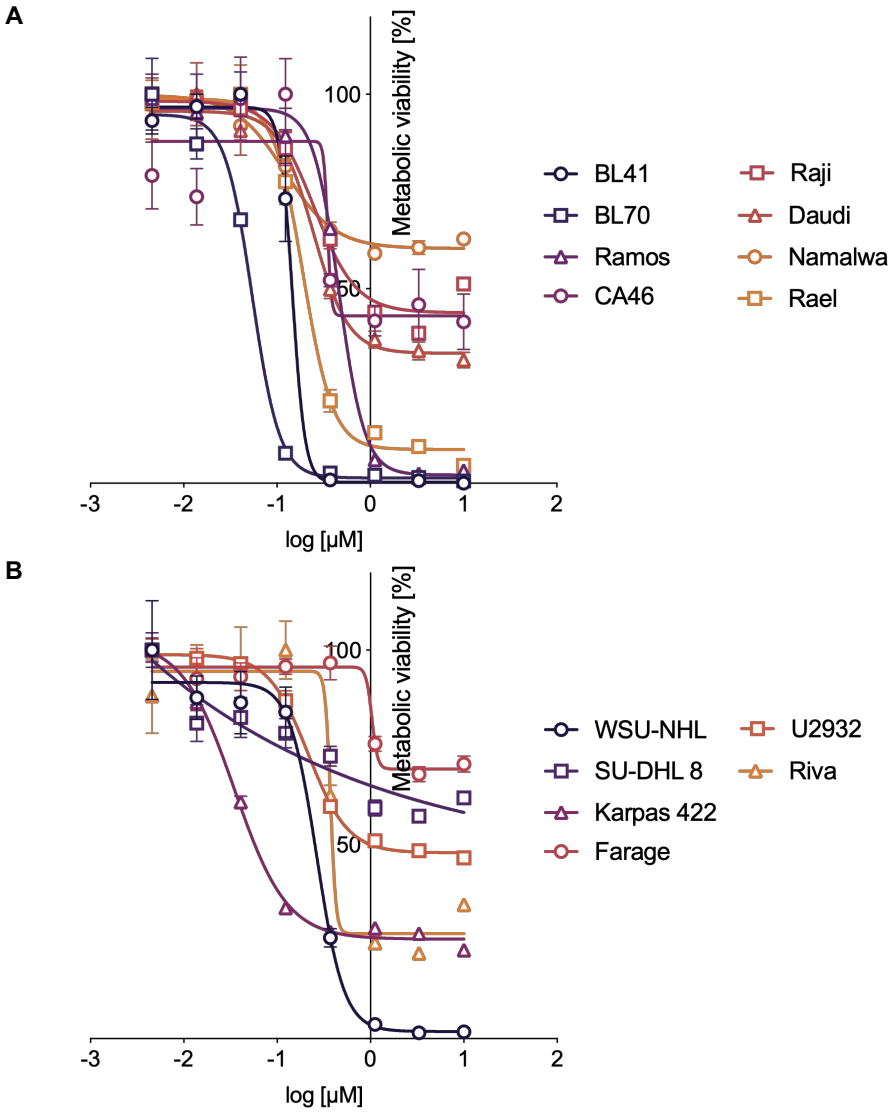

Figure 8-8: Growth inhibition curves for IMP366.

[A] Growth inhibition curves in Burkitt's cell lines. **[B]** Growth inhibition curves in DLBCL cell lines.
(For all graphs: N = 4, error bars = SEM)

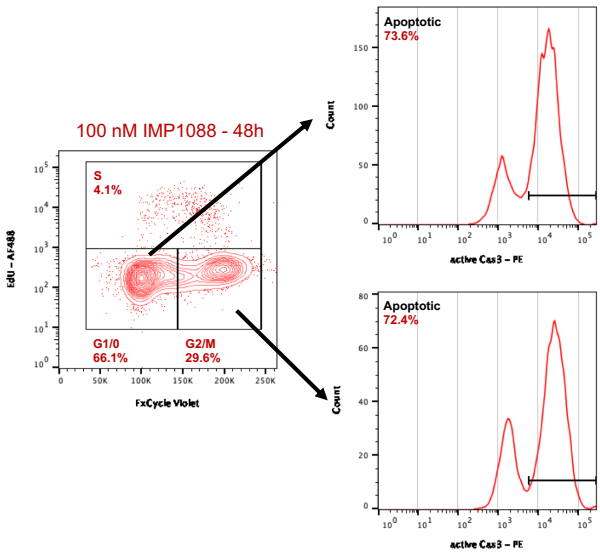

Figure 8-9: Apoptosis induction is independent of cell cycle arrest in BL41.

Representative flow cytometry analysis of the cell cycle (100 nM of IMP1088 at 48 hours) and apoptosis induction in cells in G1/0 and G2/M.

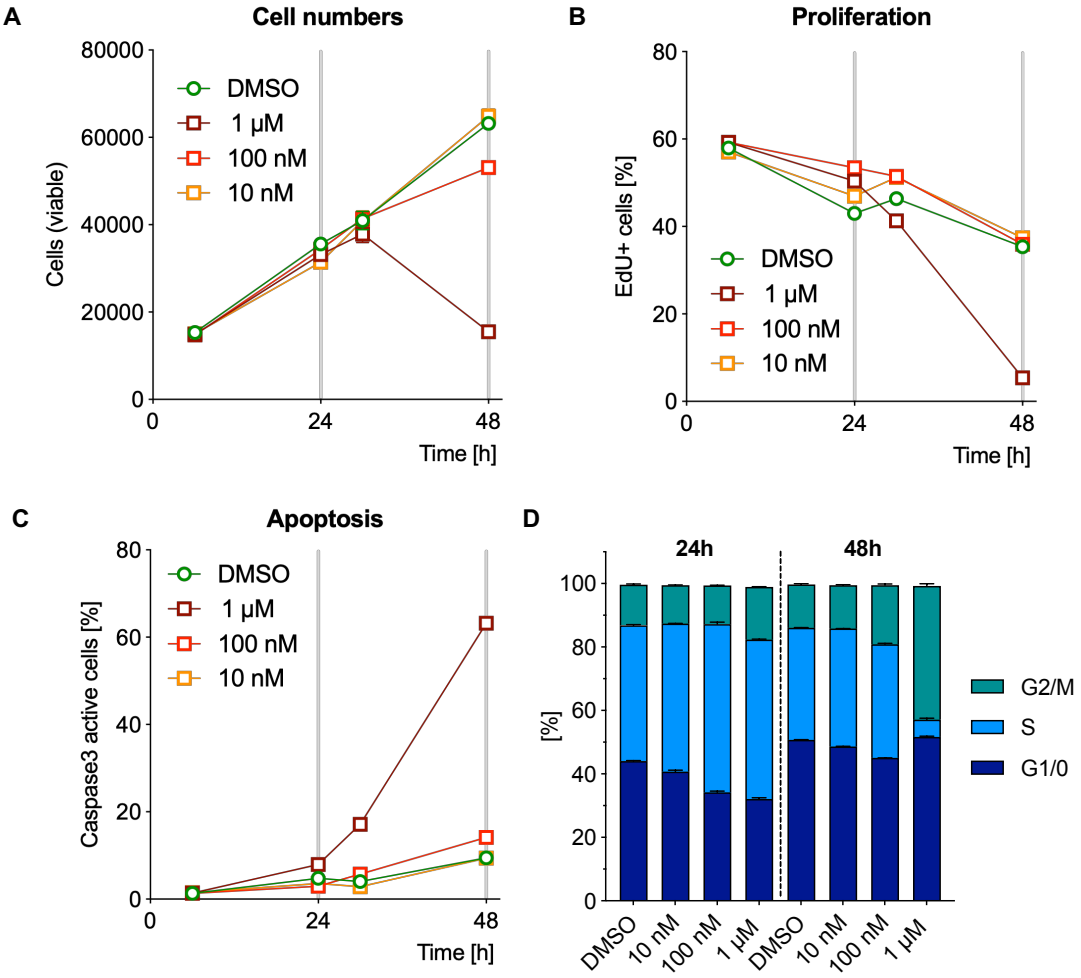

Figure 8-10: NMT inhibition, with IMP366, causes G2/M accumulation and induction of apoptosis in the sBL cell line BL41 after 24 hours.

[A] Quantification of the viable (Zombie NIR-) cells. **[B]** Quantification of the relative number of proliferating cells (EdU^+). **[C]** Quantification of the induction of apoptosis ($caspase3^+$). **[D]** Quantification of the cell cycle distribution at 24 hours and 48 hours. (For all graphs N = 2, error bars = SEM)

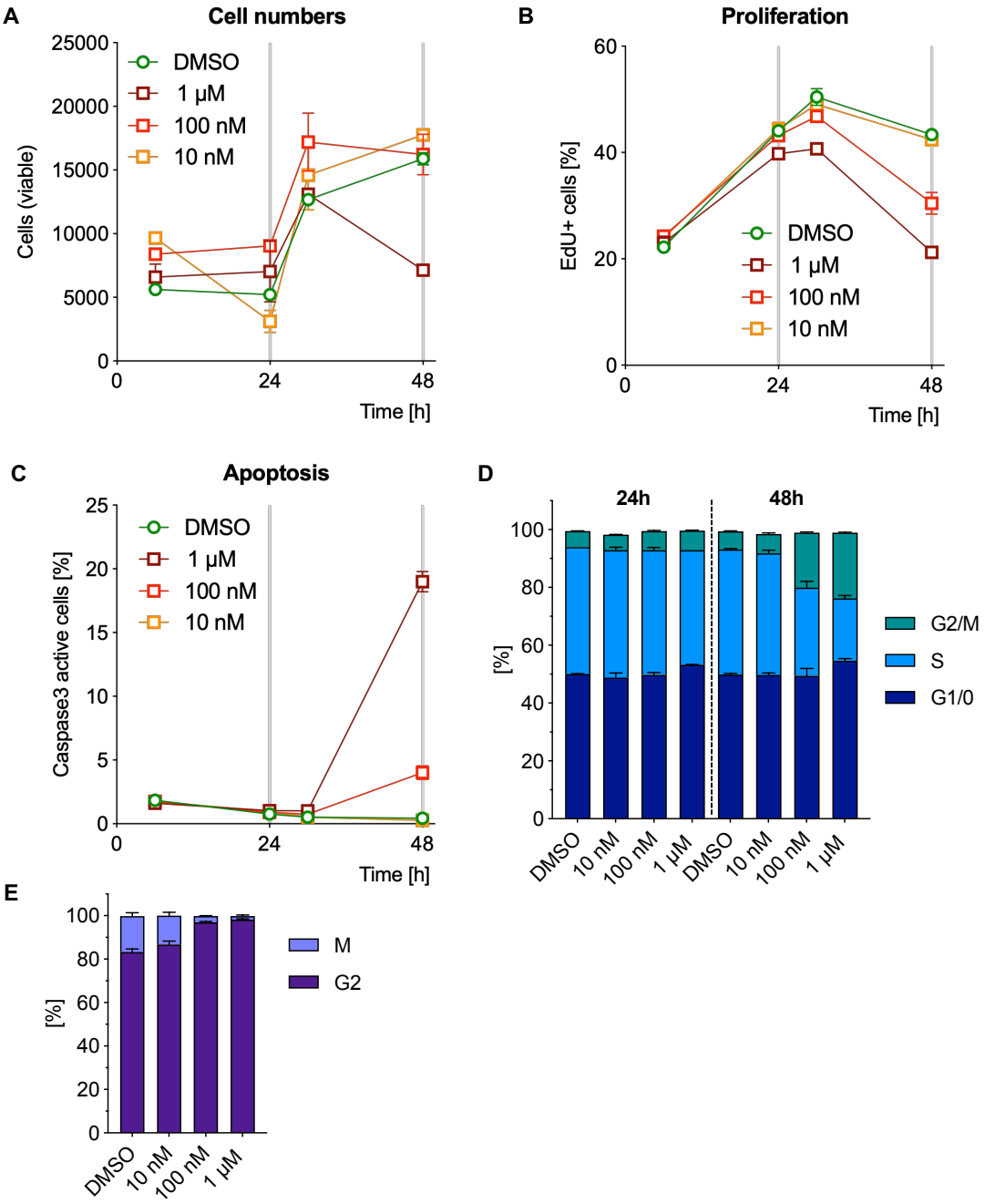

Figure 8-11: NMT inhibition, with IMP1088, causes G2/M accumulation and induction of apoptosis in the eBL cell line Raji after 24 hours.

[A] Quantification of the viable (Zombie NIR-) cells. **[B]** Quantification of the relative number of proliferating cells (EdU^+). **[C]** Quantification of the induction of apoptosis ($caspase3^+$). **[D]** Quantification of the cell cycle distribution at 24 hours and 48 hours. **[E]** Quantification of the G2/M distribution at 48 hours with different concentrations of IMP1088.
(For all graphs N = 2, error bars = SEM)

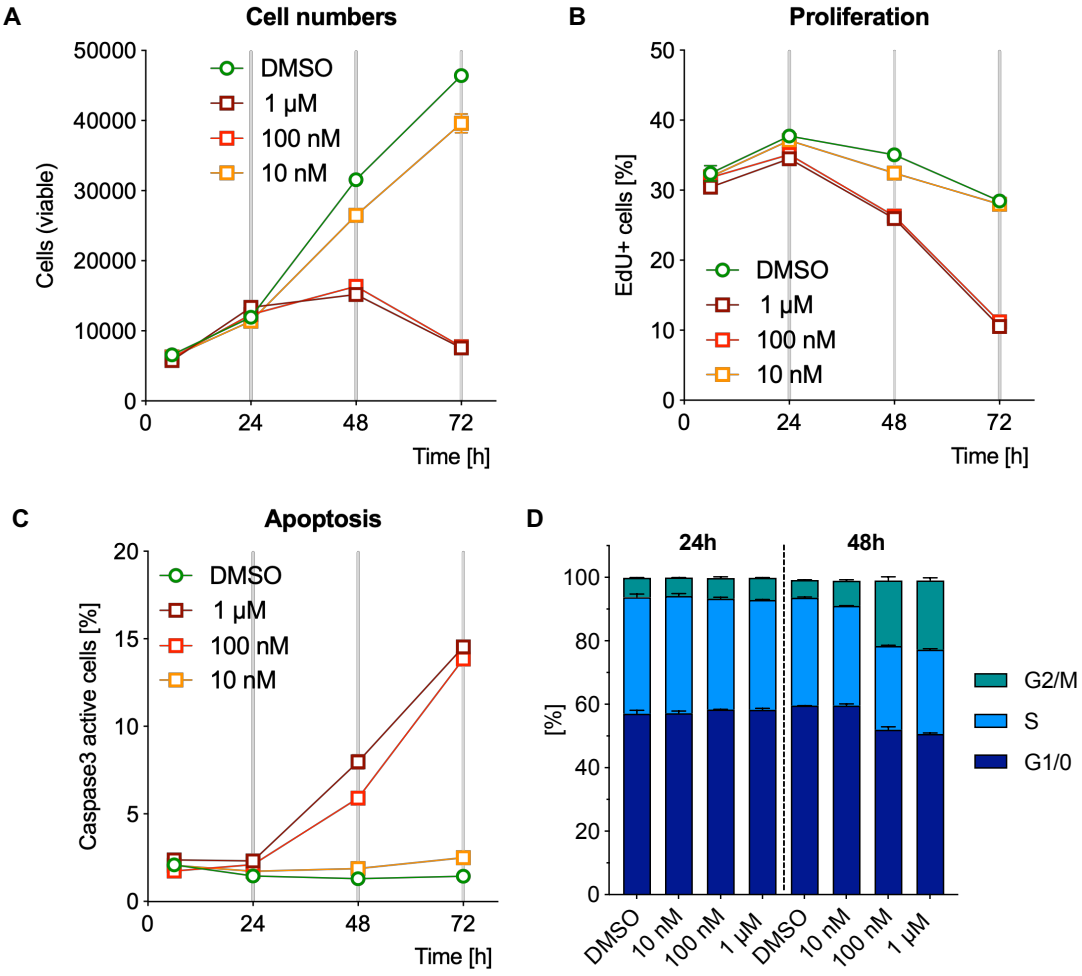

Figure 8-12: IMP1088 causes G2/M accumulation and apoptosis induction in the ABC DLBCL cell line U2932.

[A] Quantification of the viable (Zombie NIR-) cells. **[B]** Quantification of the relative number of proliferating cells (EdU^+). **[C]** Quantification of the induction of apoptosis ($caspase3^+$). **[D]** Quantification of the cell cycle distribution at 24 hours and 48 hours. (For all graphs N = 2, error bars = SEM)

8.2 Appendix Chapter 3: Multi-omics study shows that NMT inhibition disrupts correct RNA processing in the Burkitt's lymphoma cell line BL41.

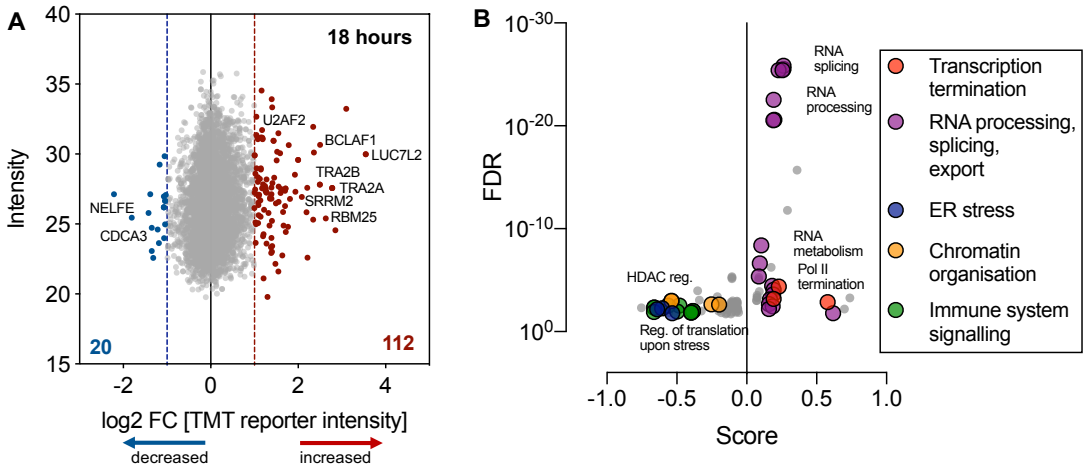

Figure 8-13: Phosphorylation changes at 18 hours with IMP1088 show increased phosphorylation on proteins involved in RNA processing and splicing.

[A] Scatter plan showing intensity of a given phospho-peptide the phosphorylation change compared to control. Red and blue lines (and dots) indicate changes of at least 2-fold. **[B]** 1D enrichment plot showing GOBP and GOMF enrichment of the phosphorylation changes.

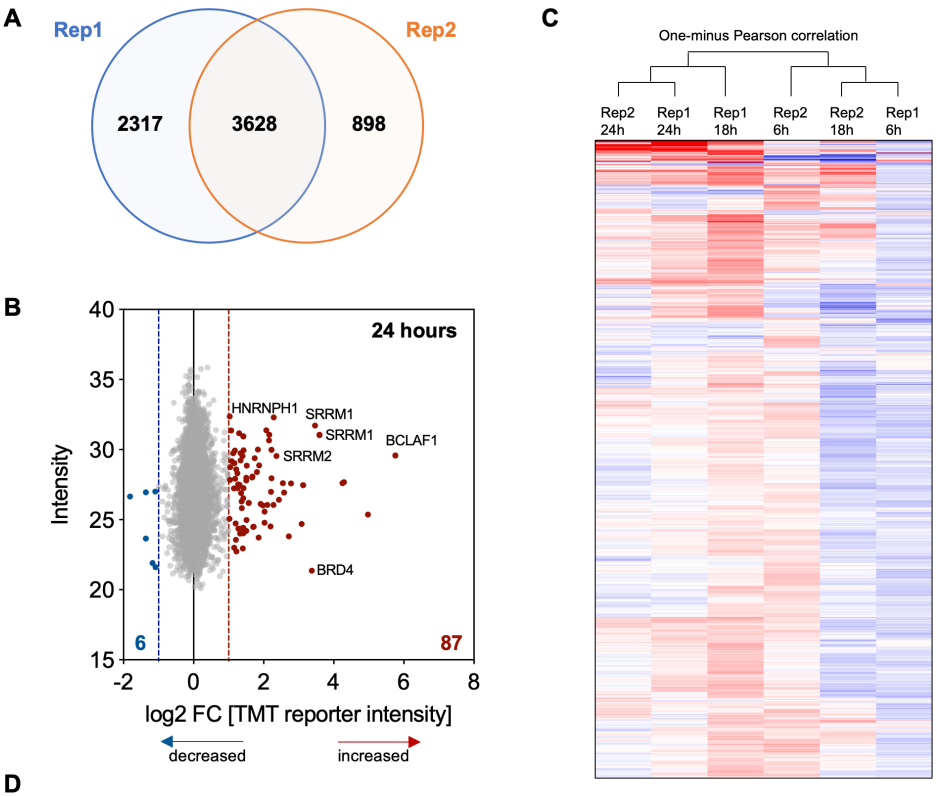

D

Name	Rep1 Score	Rep2 Score	FDR
RNA splicing	-0.19	-0.10	$3.34e^{-8}$
mRNA processing	-0.17	-0.08	$6.47e^{-7}$
RNA processing	-0.14	-0.08	$5.90e^{-6}$
Positive regulation of transcription initiation	-0.53	-0.64	$2.07e^{-5}$

Figure 8-14: Reproducibility assessed in a second phosphoproteomics experiment.

[A] Venn-diagram showing the phospho-peptides identified in both experiments and in each one uniquely. **[B]** Scatter plan showing intensity of a given phospho-peptide and the foldchange compared to control after 24 hours of NMT inhibition. Red and blue lines (and dots) indicate changes of at least 2-fold. **[C]** Hierarchical one-minus Pearson correlation clustering across the experiments and different time points. **[D]** Table showing the results of a 2D enrichment, comparing the 24-hour time points between the two biological experiments within the overlapping phosphopeptides.

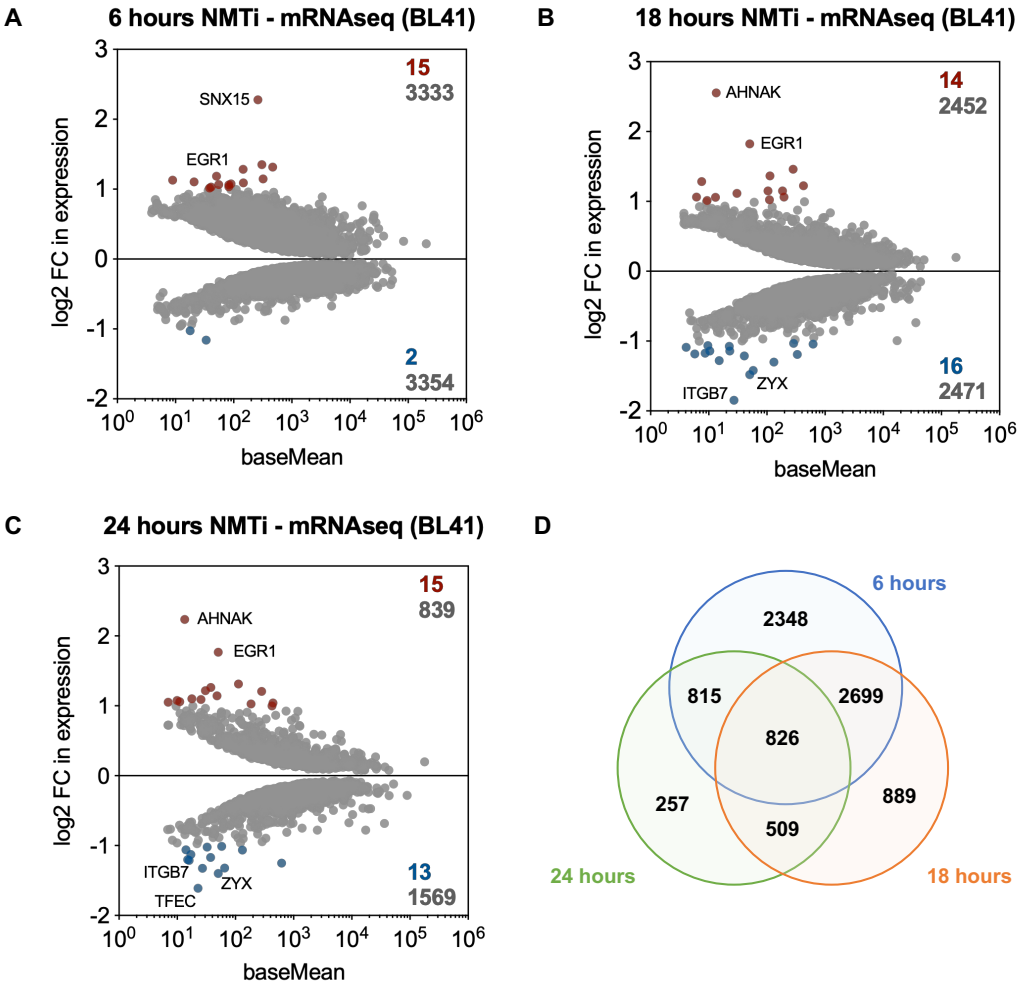

Figure 8-15: Significantly differentially expressed genes in the mRNAseq across all time points upon NMT inhibition.

[A] Scatter plot showing the log2FC and baseMean of all significantly changing genes upon 6 hours of treatment with IMP1088. Coloured dots indicate a FC of at least 2-fold (red: up; blue: down). **[B]** Scatter plot showing the log2FC and baseMean of all significantly changing genes upon 18 hours of treatment with IMP1088. **[C]** Scatter plot showing the log2FC and baseMean of all significantly changing genes upon 24 hours of treatment with IMP1088. **[D]** Venn-diagram showing the overlap of significantly differentially expressed genes across all time points.

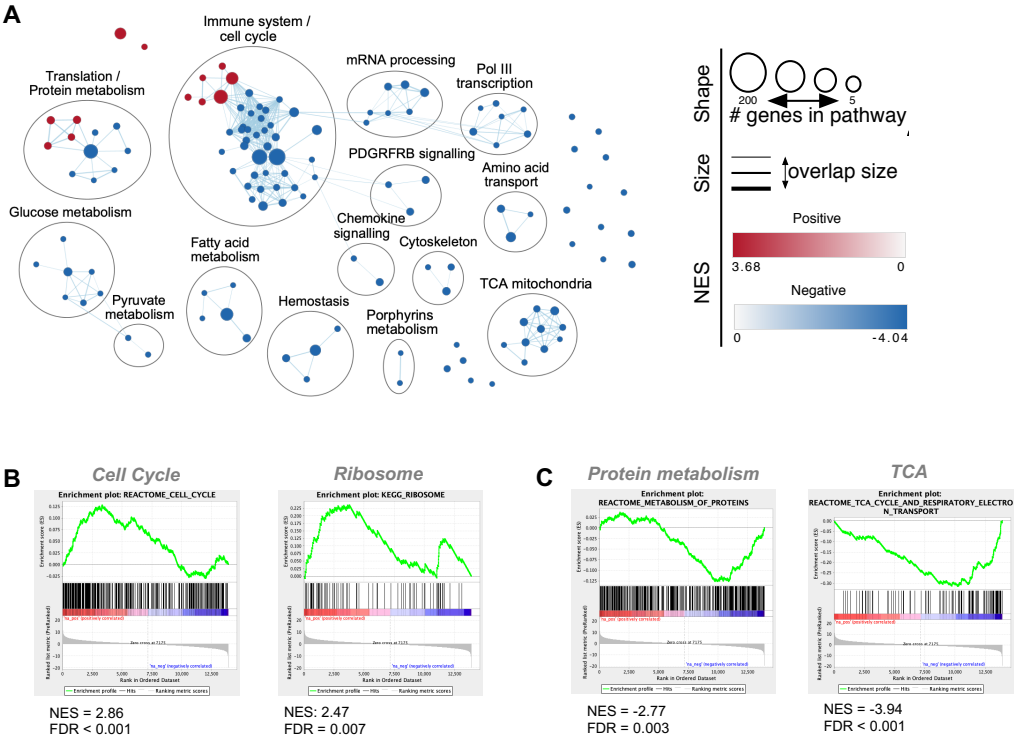

Figure 8-16: GSEA and subsequent EnrichmentMap analysis indicates downregulation of genes involved in mRNA processing with 18 hours of NMTi.

[A] Network, created with the EnrichmentMap plug-in into CytoScape, summarising the GSEA. (FDR < 0.01, Jaccard Overlap combined = 0.375, k constant = 0.5) **[B]** Example GSEA plots, consisting of genes that are upregulated, here shown KEGG_Ribosome and Reactome_Metabolism_of_Proteins. **[C]** Example GSEA plots, consisting of genes that are downregulated, here shown KEGG_Spliceosome and Reactome_Cell_Cycle.

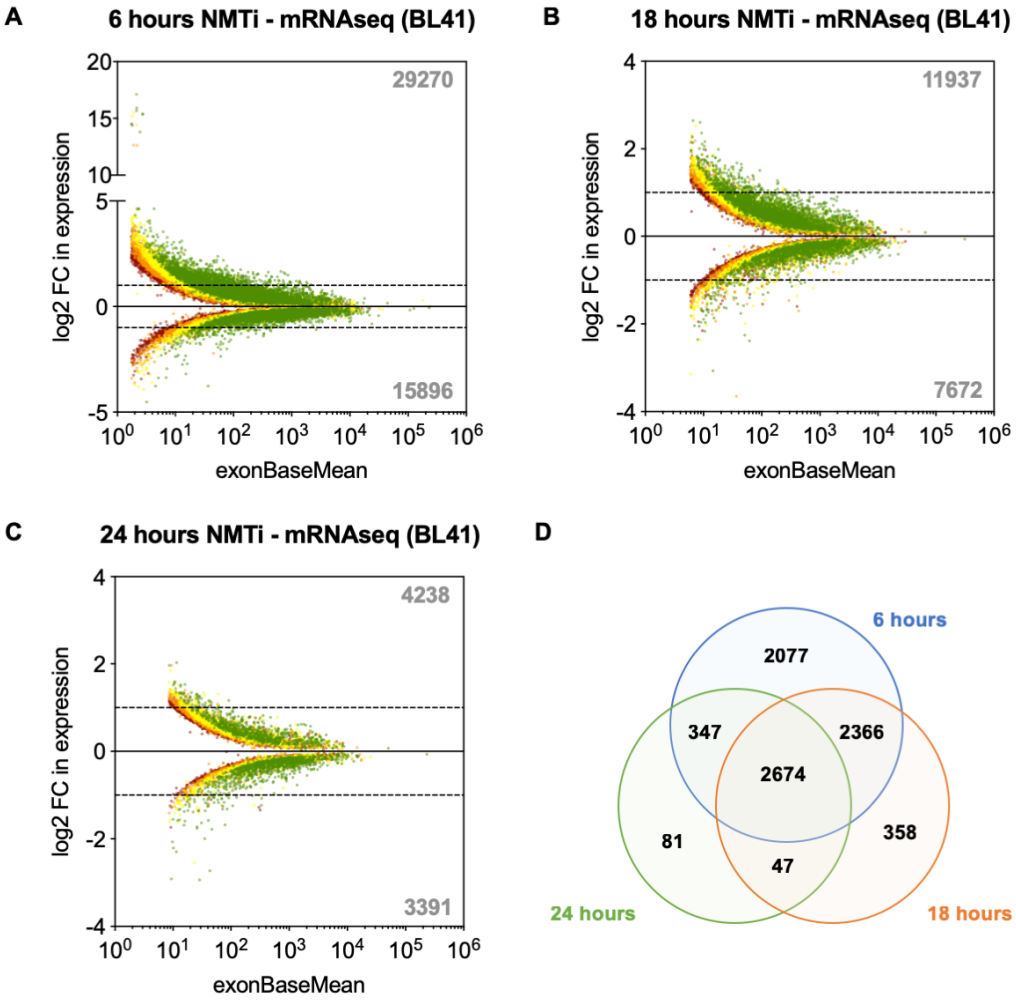

Figure 8-17: Differentially expressed exons and affected genes.

[A] Scatter plot showing the log2FC and exonBaseMean of all significantly changing exons upon 6 hours of treatment with IMP1088. Colour scheme indicates increased significance from red (lowest) to green (highest). **[B]** Scatter plot showing the log2FC and exonBaseMean of all significantly changing exons upon 18 hours of treatment with IMP1088. **[C]** Scatter plot showing the log2FC and exonBaseMean of all significantly changing exons upon 24 hours of treatment with IMP1088. **[D]** Venn-diagram showing the overlap of genes affected by differential exon expression.

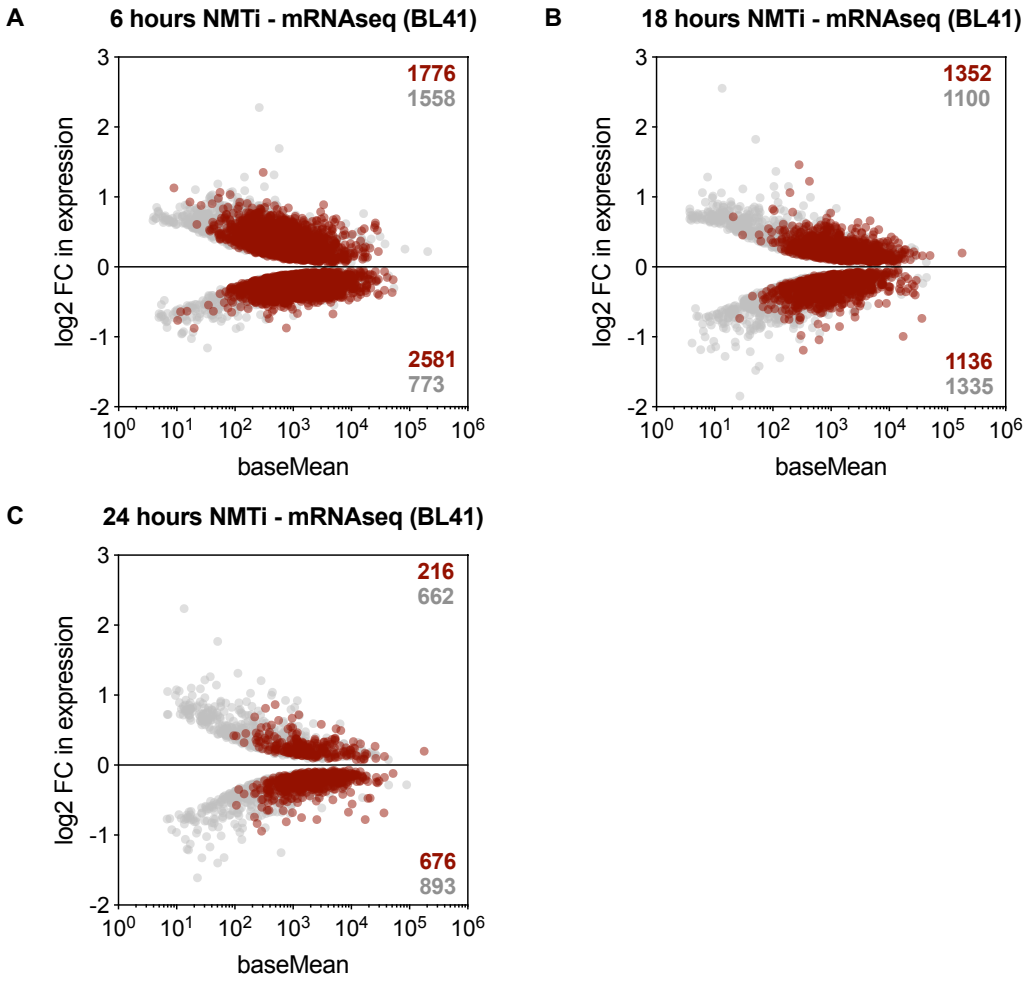

Figure 8-18: Effect of differential exon expression on differential gene expression.

[A] Scatter plot showing the log2FC and baseMean of all significantly changing genes upon 6 hours of treatment with IMP1088. Red dots are genes affected by differential exon expression. **[B]** Scatter plot showing the log2FC and baseMean of all significantly changing genes upon 18 hours of treatment with IMP1088. **[C]** Scatter plot showing the log2FC and baseMean of all significantly changing genes upon 24 hours of treatment with IMP1088.

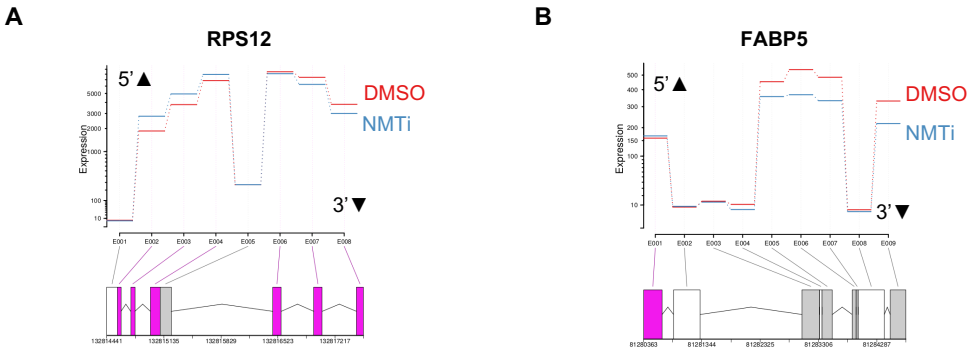

Figure 8-19: DEXSeq plots for 24 hours of NMT inhibition.

[A] Differential exon expression shown for RPS12 at 24 hours (violet marks significantly differentially expressed exons). **[B]** Differential exon expression shown for FABP5 at 24 hours (violet marks significantly differentially expressed exons).

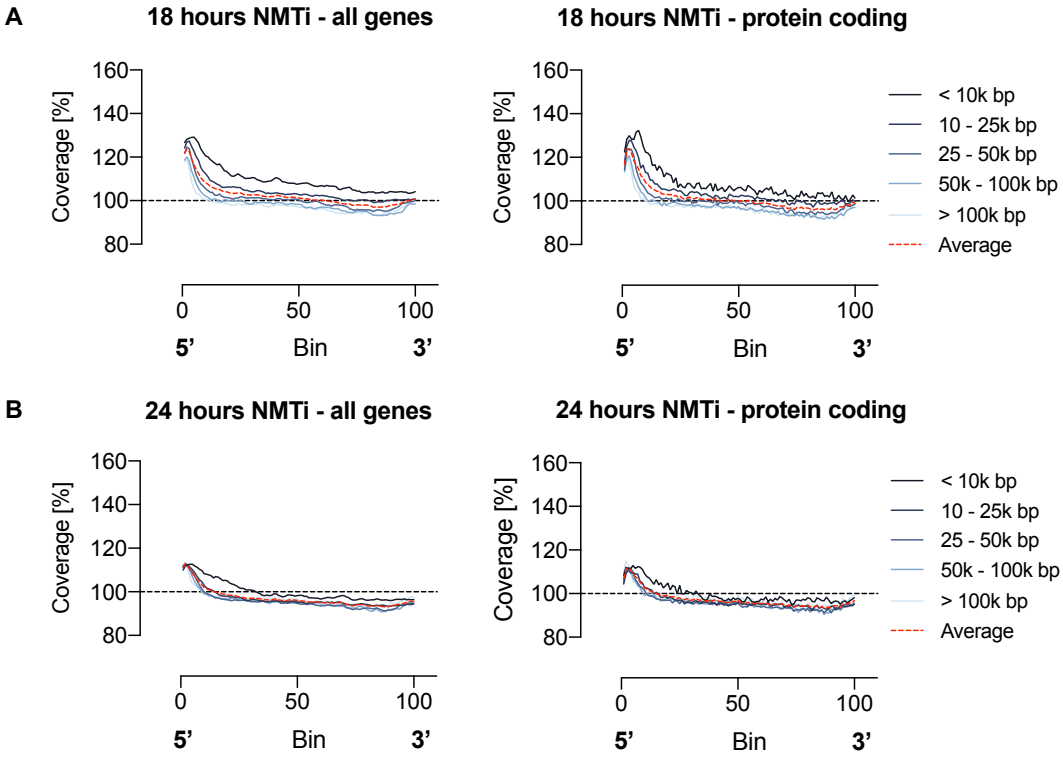

Figure 8-20: Gene coverage for 18 hours and 24 hours of NMT inhibition.

[A] Gene coverage for all genes (left) and protein-coding genes (right) for 18 hours of NMT inhibition. **[B]** Gene coverage for all genes (left) and protein-coding genes (right) for 24 hours of NMT inhibition.

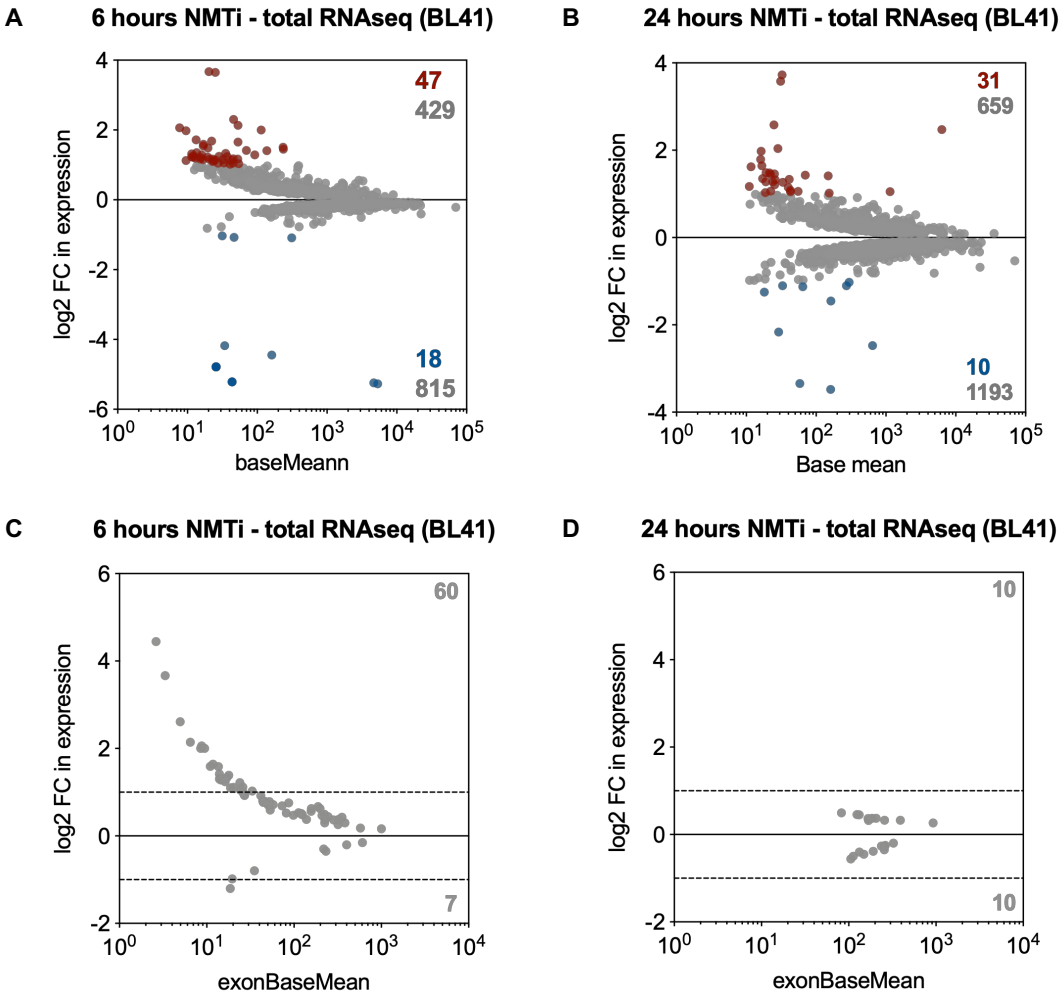

Figure 8-21: Differential gene and exon expression in the total RNAseq.

[A] Scatter plot showing the log2FC and baseMean of all significantly changing genes upon 6 hours of treatment with IMP1088. Coloured dots indicate a FC of at least 2-fold (red: up; blue: down). **[B]** Scatter plot showing the log2FC and baseMean of all significantly changing genes upon 24 hours of treatment with IMP1088. **[C]** Scatter plot showing the log2FC and exonBaseMean of all significantly changing exons upon 6 hours of treatment with IMP1088. **[D]** Scatter plot showing the log2FC and exonBaseMean of all significantly changing exons upon 24 hours of treatment with IMP1088.

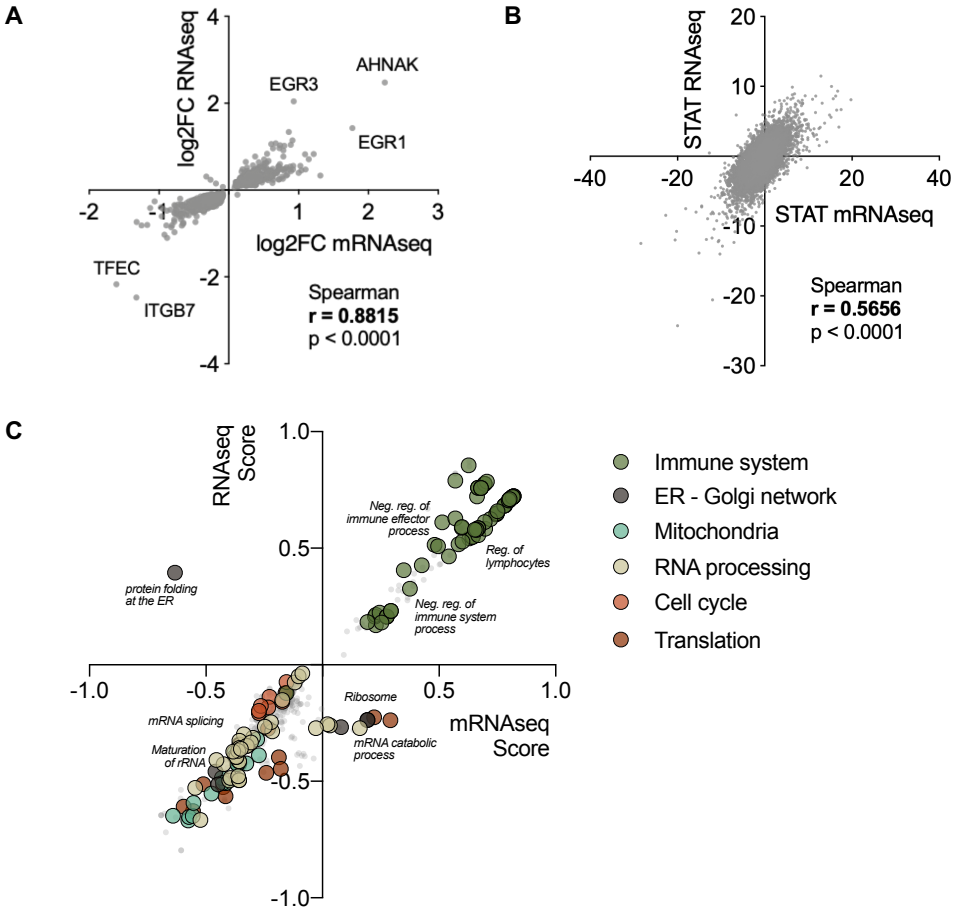

Figure 8-22: Total RNAseq and mRNAseq correlation for 24 hours of NMTi.

[A] Correlation between overlapping, differential expressed genes, comparing mRNAseq and total RNAseq. **[B]** Correlation between the STAT values between mRNAseq and total RNAseq. **[C]** 2D-enrichment analysis comparing the two RNAseq data sets.

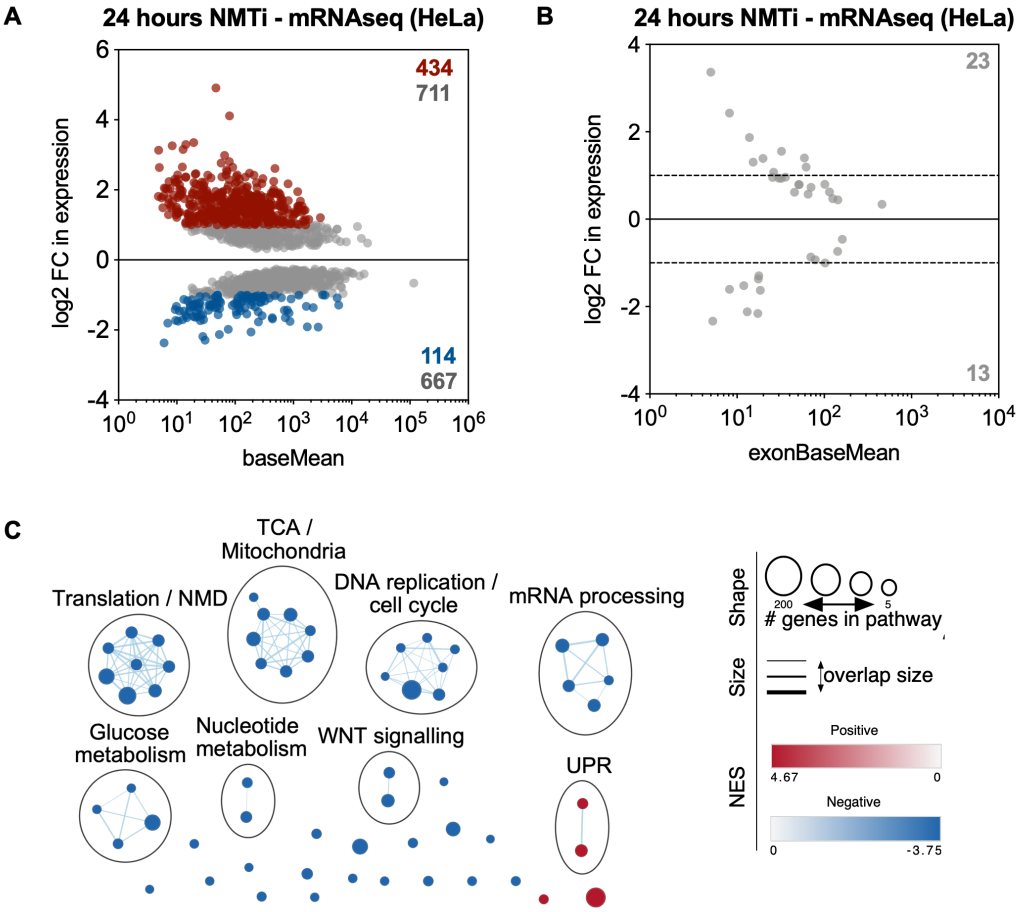

Figure 8-23: Differential gene and exon expression and pathway network in HeLa.

[A] Scatter plot showing the log2FC and baseMean of all significantly changing genes upon 24 hours of treatment with IMP1088. Coloured dots indicate a FC of at least 2-fold (red: up; blue: down). **[B]** Scatter plot showing the log2FC and exonBaseMean of all significantly changing exons upon 24 hours of treatment with IMP1088. **[C]** Network, created with the EnrichmentMap plug-in into CytoScape, summarising the GSEA. (FDR < 0.01, Jaccard Overlap combined = 0.375, k constant = 0.5)

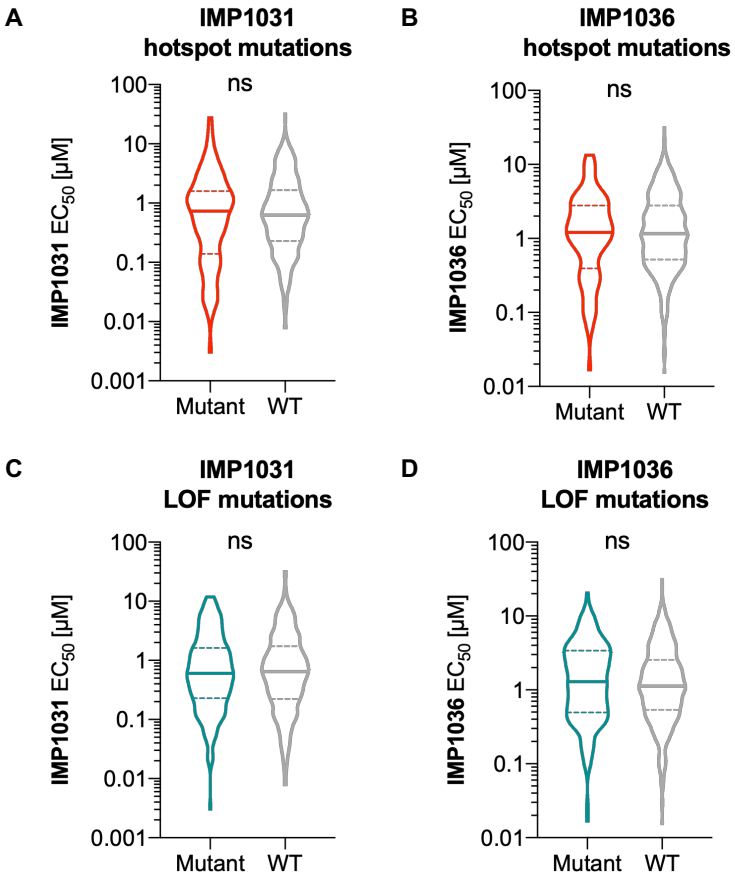

Figure 8-24: Effect of hotspot or LOF mutations on the sensitivity to the NMT inhibitors IMP1031 and IMP1036.

[A] Hotspot mutations in splicing components are not correlated with increased sensitivity to IMP1031. **[B]** Hotspot mutations in splicing components are not correlated with increased sensitivity to IMP1036. **[C]** LOF mutations in splicing components are not correlated with increased sensitivity to IMP1031. **[D]** LOF mutations in splicing components are not correlated with increased sensitivity to IMP1036.
(For all graphs: p-values determined with the Mann-Whitney test)

8.3 Appendix Chapter 4: NMT inhibitors are synthetically lethal in cancer cell lines with high levels of MYC and/or structural alterations of MYC and MYCN.

Table 8-2: The 10 strongest enriched gene sets in the sensitive cancer cell lines to the inhibitor IMP1031.

Gene set name	NES	FDR
REACTOME_TRANSLATION	2.13	0.03
REACTOME_HIV_LIFE_CYCLE	2.03	0.05
REACTOME_LATE_PHASE_OF_HIV_LIFE_CYCLE	2.02	0.04
REACTOME_INFLUENZA_LIFE_CYCLE	2.02	0.03
REACTOME_METABOLISM_OF_RNA	2.01	0.03
REACTOME_INFLUENZA_VIRAL_RNA_TRANSCRIPTION_AND_REPLICATION	1.99	0.03
REACTOME_SRP_DEPENDENT_COTRANSLATIONAL_PROTEIN_TARGETING_TO_MEMBRANE	1.99	0.03
REACTOME_RNA_POL_II_TRANSCRIPTION	1.97	0.03
REACTOME_RNA_POL_II_PRE_TRANSCRIPTION_EVENTS	1.97	0.03
REACTOME_HIV_INFECTION	1.95	0.03

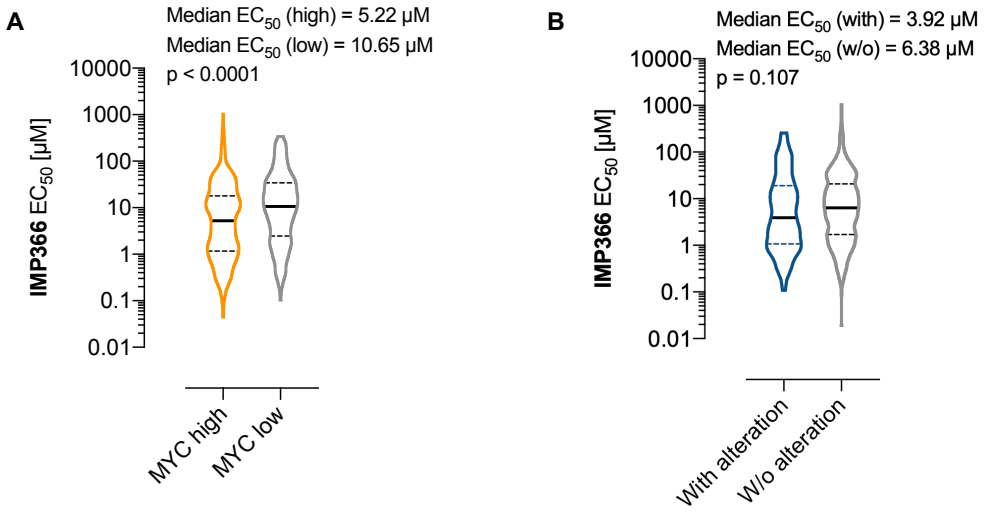

Figure 8-25: Cell lines with high MYC expression or alterations in the MYC/MYCN genomic loci are more responsive to the NMT inhibitor IMP366.

[A] Comparison of the EC_{50}s for IMP366 of the quartiles with highest and lowest expression of MYC (both groups: 228 cell lines). **[B]** Comparison of the EC_{50}s for IMP366 of cells with and without mutations and/or RACS and/or CN gains of >8 in the genomic loci of MYC/MYCN (with: 124 cell lines; without: 552 cell lines).
(For all graphs: p-values determined with the Mann-Whitney test)

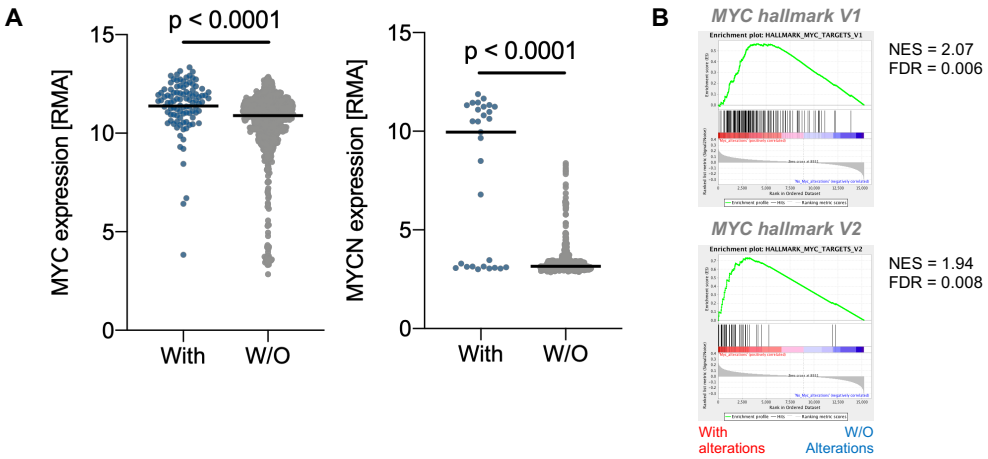

Figure 8-26: Cell lines with structural alterations in the MYC/MYCN loci have increased MYC and MYCN expression respectively and increased **activation of MYC gene sets.**

[A] Cells with structural alterations in the MYC locus (that is mutations and/or RACS and/or CN gains of >8 in the genomic loci of MYC) have higher MYC expression (With = 99; without = 577). **[B]** Cells with structural alterations in the MYCN locus have higher MYCN expression (With = 29; without = 647). **[C]** Cells with structural alterations in either MYC and/or MYCN show enrichment for MYC activation gene sets.
(For all graphs: p-values determined with the Mann-Whitney test)

A

	IMP1031			IMP1036		
	with	without	p-value	with	without	p-value
CN gains	512 nM	653 nM	0.21	1.07 µM	1.24 µM	0.059
Mutations	320 nM	662 nM	0.0002	670 nM	1.24 µM	0.0025
RACS	659 nM	646 nM	0.89	973 nM	1.22 µM	0.56

B

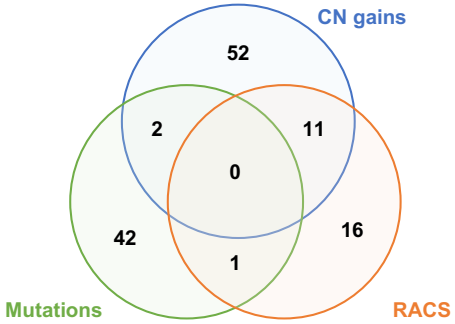

C

	Blood	All other
CN gains	4 (6%)	61 (94%)
Mutations	27 (49%)	28 (51%)
RACS	0 (0%)	28 (100%)

Figure 8-27: Mutations in MYC/MYCN are the strongest driver for increased sensitivity.

[A] Table showing for IMP1031 and IMP1036 the median EC_{50}s and p-values (Mann-Whitney) if the cells are divided by having CN gains (>8), having mutations or having RACS involving MYC/MYCN. **[B]** Venn-Diagram depicting the overlap of the cell lines in the table. **[C]** Distribution of the Blood tissue group within the different structural alterations.

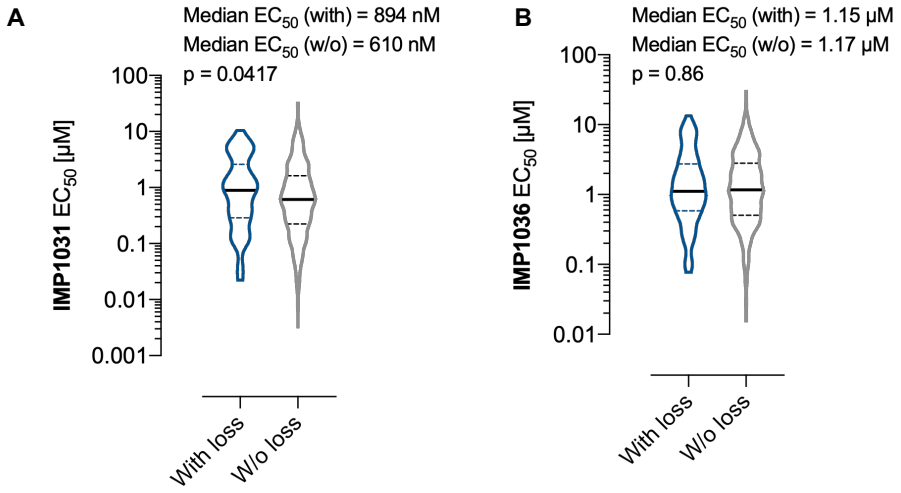

Figure 8-28: Heterozygous loss of an E-Box transcription inhibitor does not predict sensitivity to NMT inhibition.

[A] Comparison of the EC50s for IMP1031 of cancer cell lines with loss of an E-Box transcription inhibitor vs. the ones without. **[B]** Comparison of the EC50s for IMP1036 of cancer cell lines with loss of an E-Box transcription inhibitor vs. the ones without. (For both inhibitors: with loss = 111; without = 596.)
(For all graphs: p-values determined with the Mann-Whitney test)

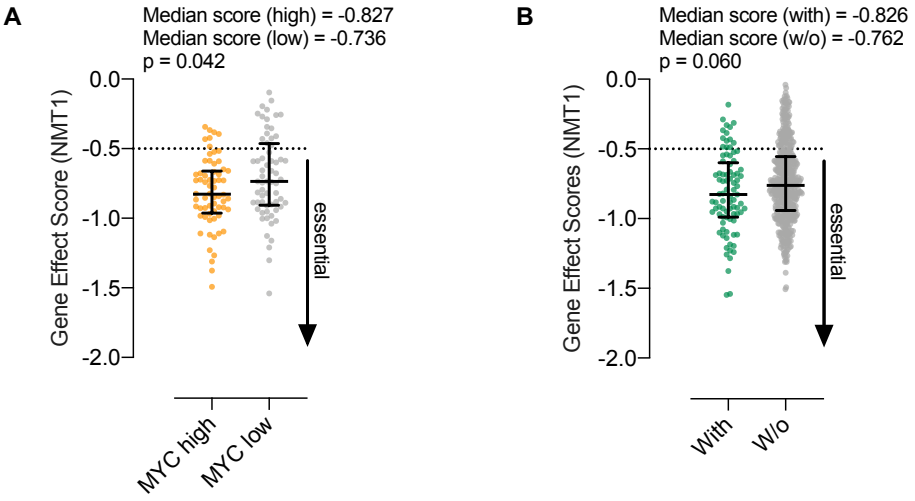

Figure 8-29: Cell lines with high MYC expression or CN gains of MYC are more dependent on NMT1.

[A] Comparison of the Ceres scores for NMT1 of cell lines between the quartiles with highest and lowest expression of MYC. (both groups: 64 cell lines) **[B]** Comparison of the Ceres scores for NMT1 of cell lines with ploidy of MYC > 4 or a mutation in MYC (with) and the other cell lines (w/o) (With: 85 cell lines; Without: 472 cell lines).
(For all graphs: p-values determined with the Mann-Whitney test; error bars = interquartile range)

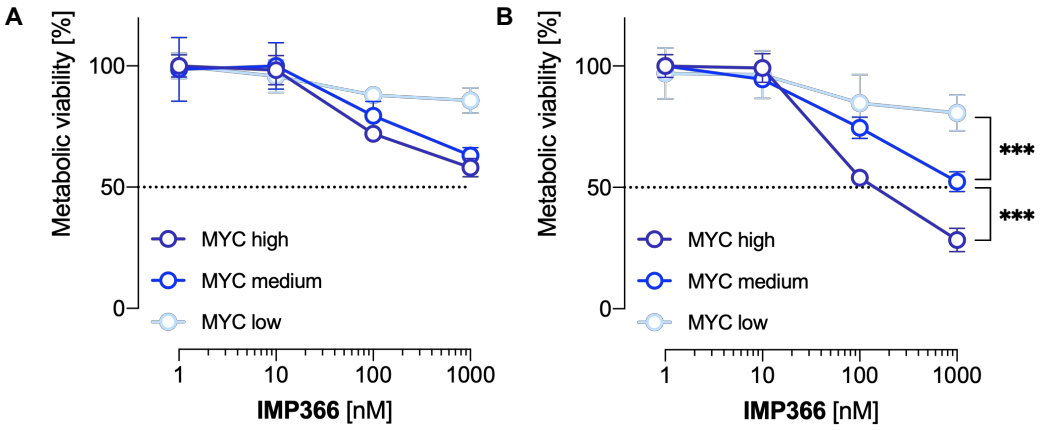

Figure 8-30: IMP366 reduces metabolic viability in MYC high cells stronger than with the other MYC levels.

[A] Metabolic viability of the different MYC states after 48 hours of treatment with IMP366. **[B]** Metabolic viability of the different MYC states after 72 hours of treatment with IMP366.
(For all graphs: N = 4, error bars = SEM, ANOVA)

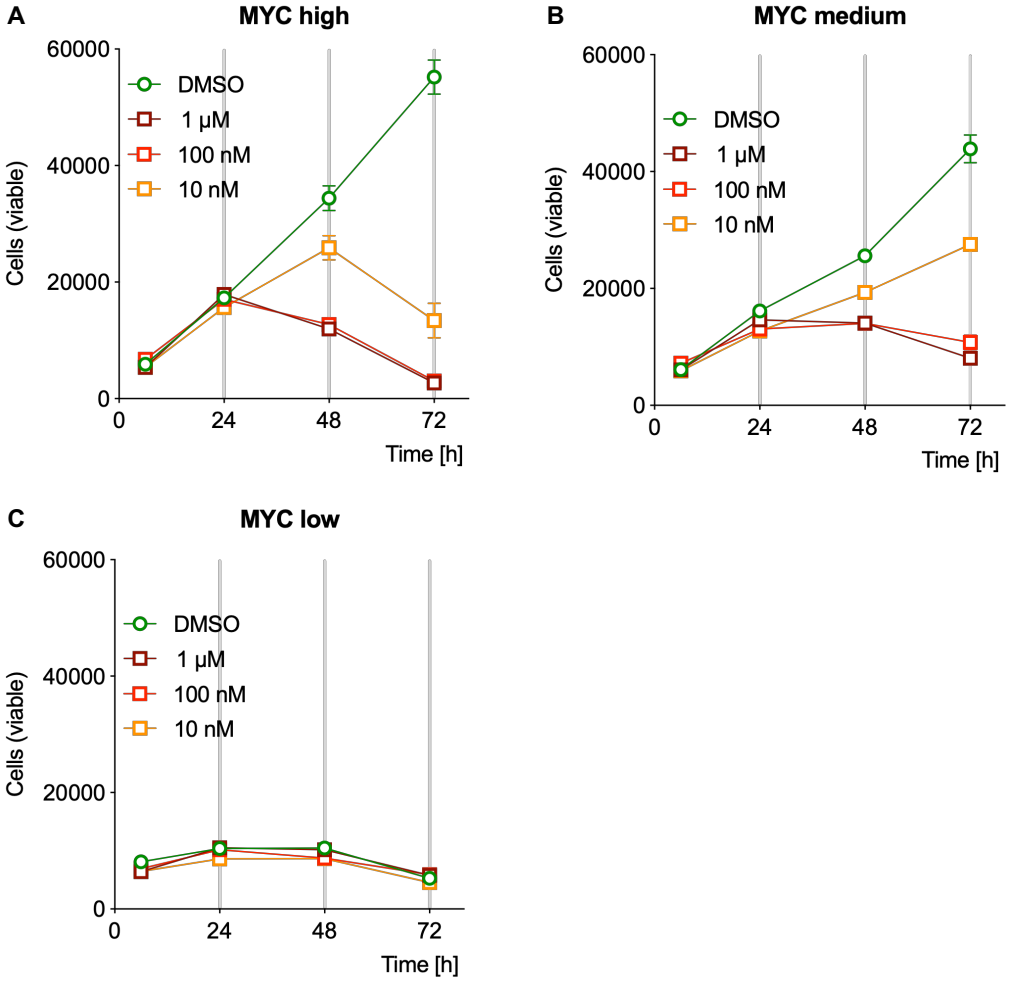

Figure 8-31: Cell numbers are strongly affected in MYC high and barely affected in MYC low.

[A] Quantification of viable cell numbers for MYC high. **[B]** Quantification of viable cell numbers for MYC medium. **[C]** Quantification of viable cells for MYC low.
(For all graphs: N = 2, error bars = SEM)

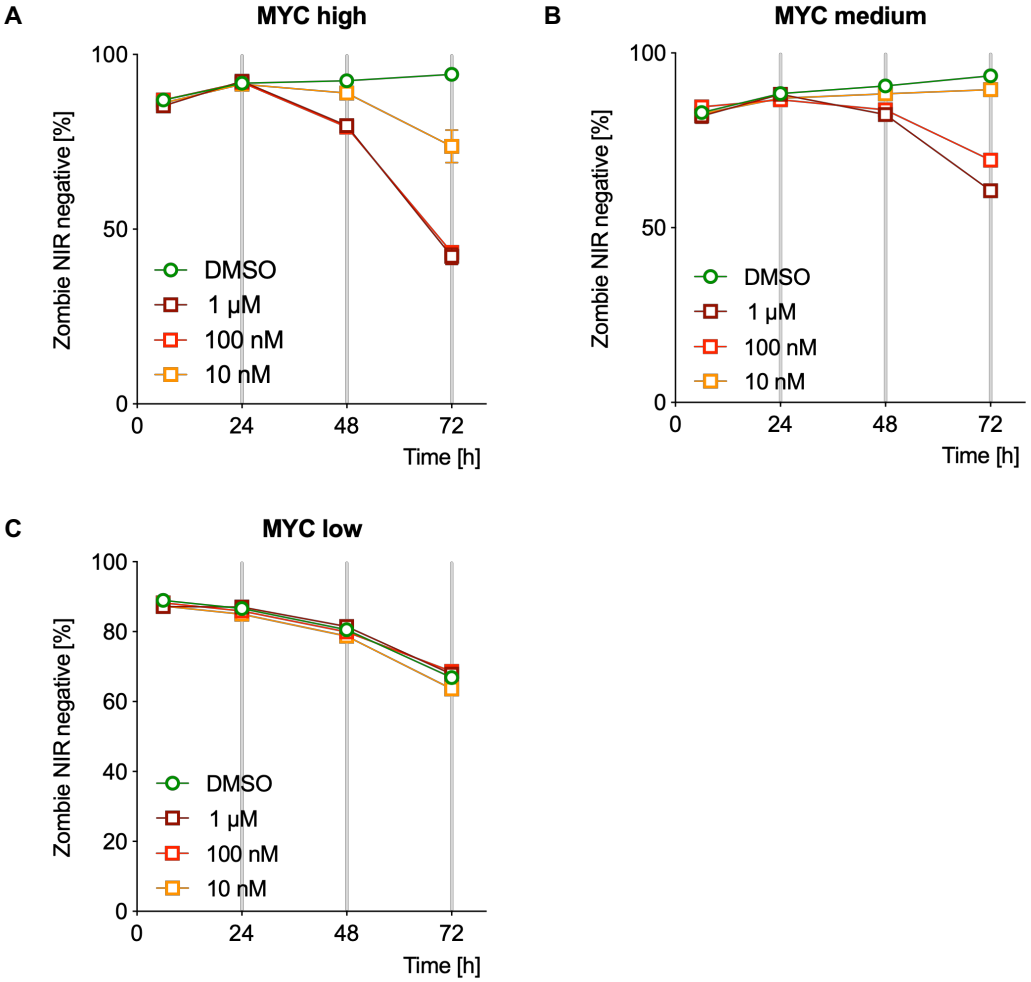

Figure 8-32: Cell viability is strongly affected in MYC high and barely affected in MYC low.

[A] Quantification of viability (Zombie NIR$^-$) for MYC high. **[B]** Quantification of viability (Zombie NIR$^-$) for MYC medium. **[C]** Quantification of viability (Zombie NIR$^-$) for MYC low.
(For all graphs: N = 2, error bars = SEM)

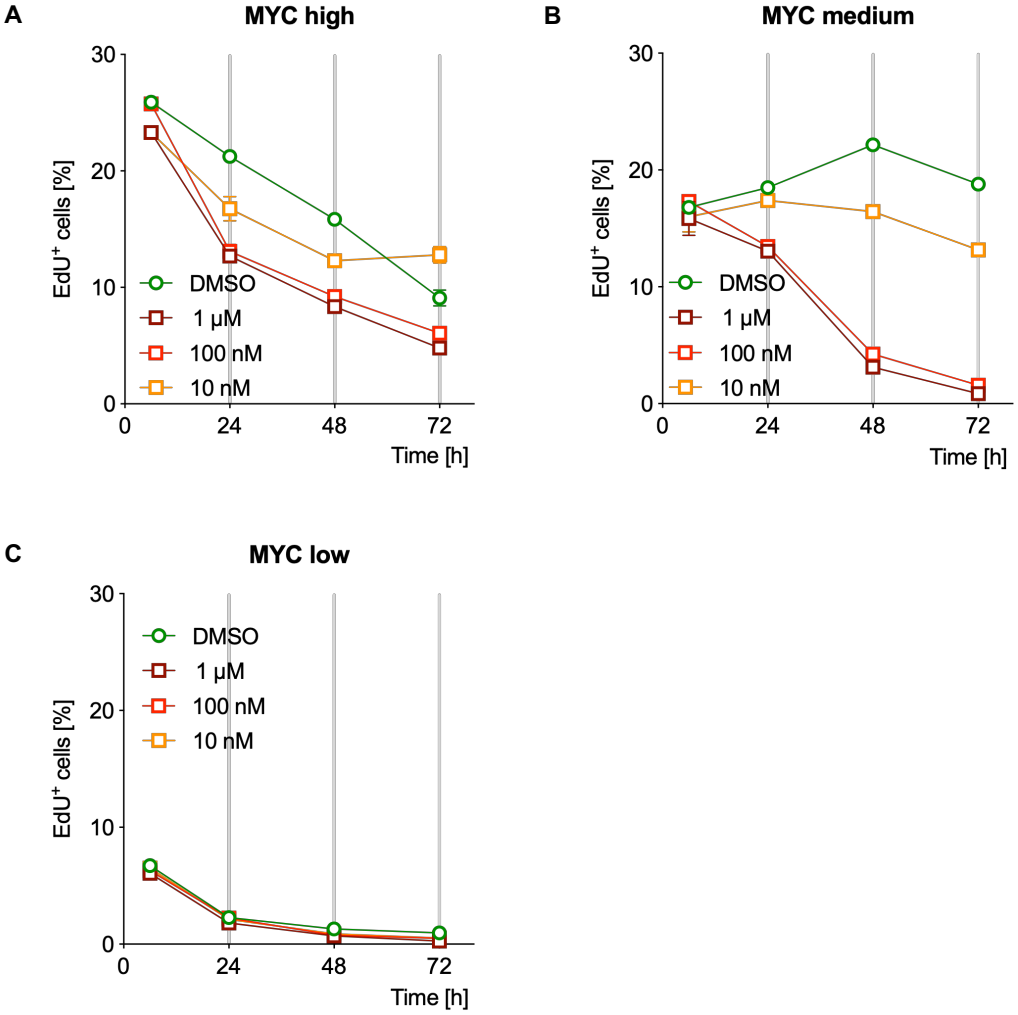

Figure 8-33: MYC high cells still undergo DNA synthesis upon NMTi.

[A] Quantification of DNA synthesis (EdU^+) for MYC high. **[B]** Quantification of DNA synthesis (EdU^+) for MYC medium. **[C]** Quantification of DNA synthesis (EdU^+) for MYC low.
(For all graphs: N = 2, error bars = SEM)

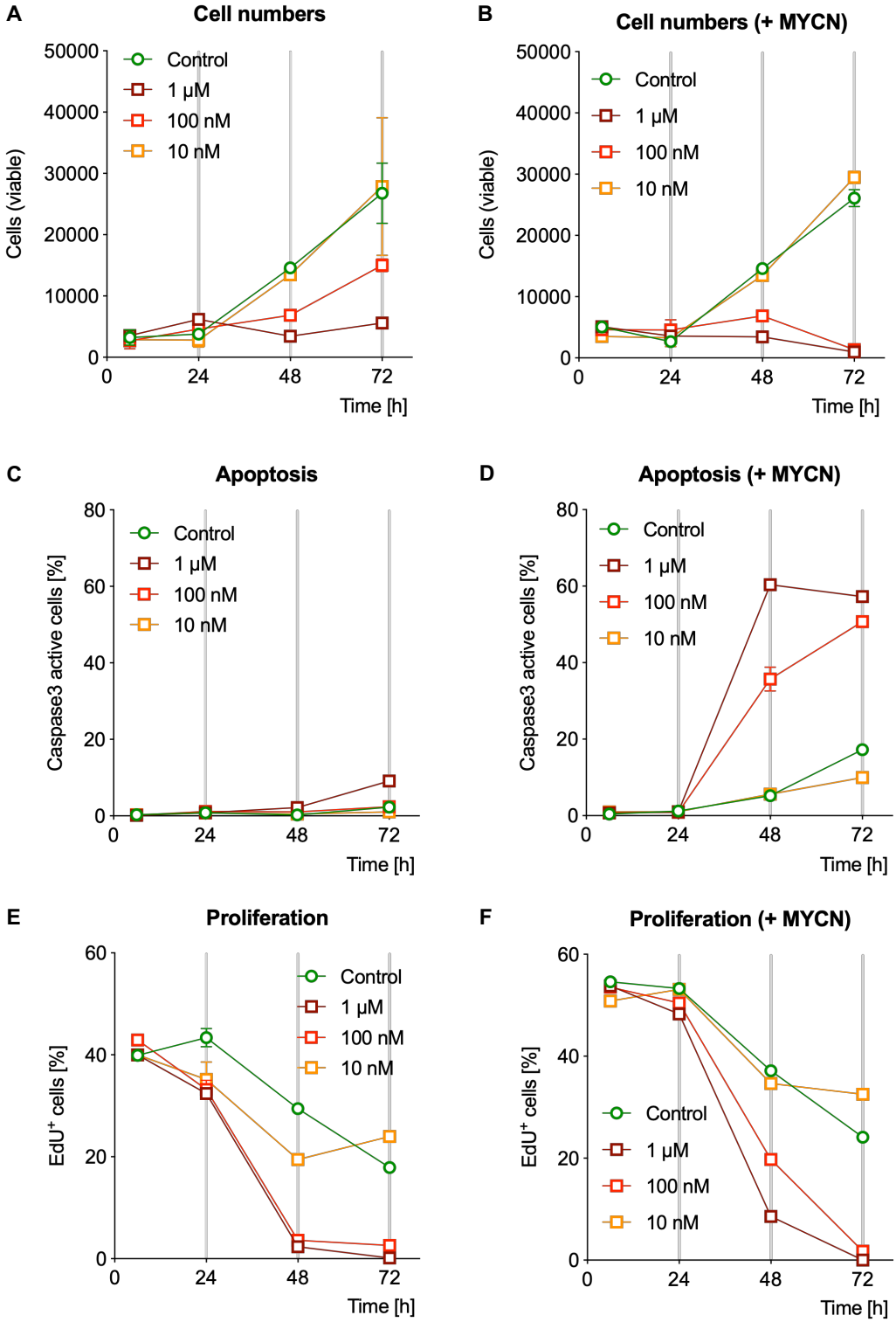

Figure 8-34: Quantifications of the MYCN-ER-Shep NMTi time line experiment.

[A] Quantification of viable cell numbers without MYCN induction. **[B]** Quantification of viable cell numbers with MYCN induction. **[C]** Quantification of DNA synthesis (EdU^+) without MYCN induction. **[D]** Quantification of DNA synthesis with MYCN induction. **[E]** Quantification of caspase3 activation without MYCN induction. **[F]** Quantification of caspase3 activation with MYCN induction.
(For all graphs: N = 2, error bars = SEM)

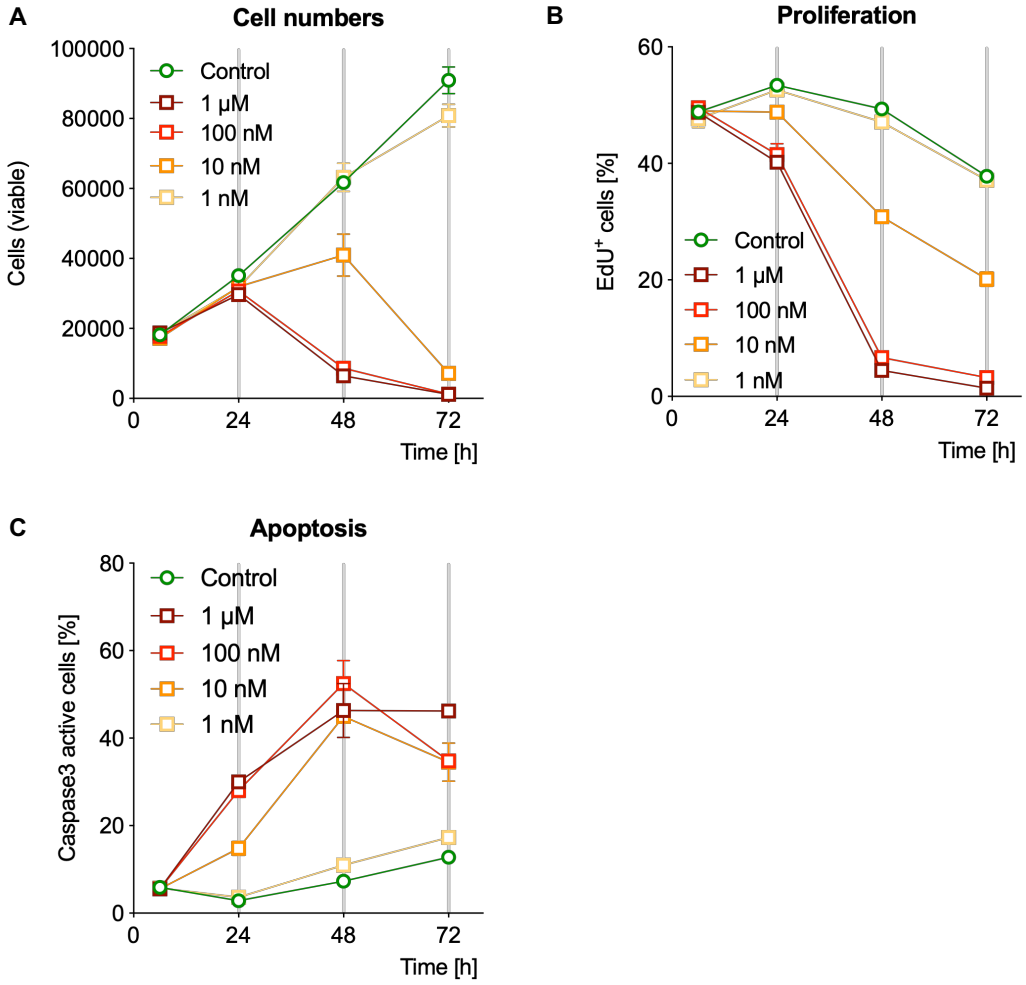

Figure 8-35: IMP1088 is highly lethal to the GCB DLBCL PDX LY11212, with c-Myc translocation.

[A] Quantification of viable cell numbers for LY11212. **[B]** Quantification of DNA synthesis (EdU+) for LY11212. **[C]** Quantification of caspase3 activation for LY11212. (For all graphs: N = 2, error bars = SEM)

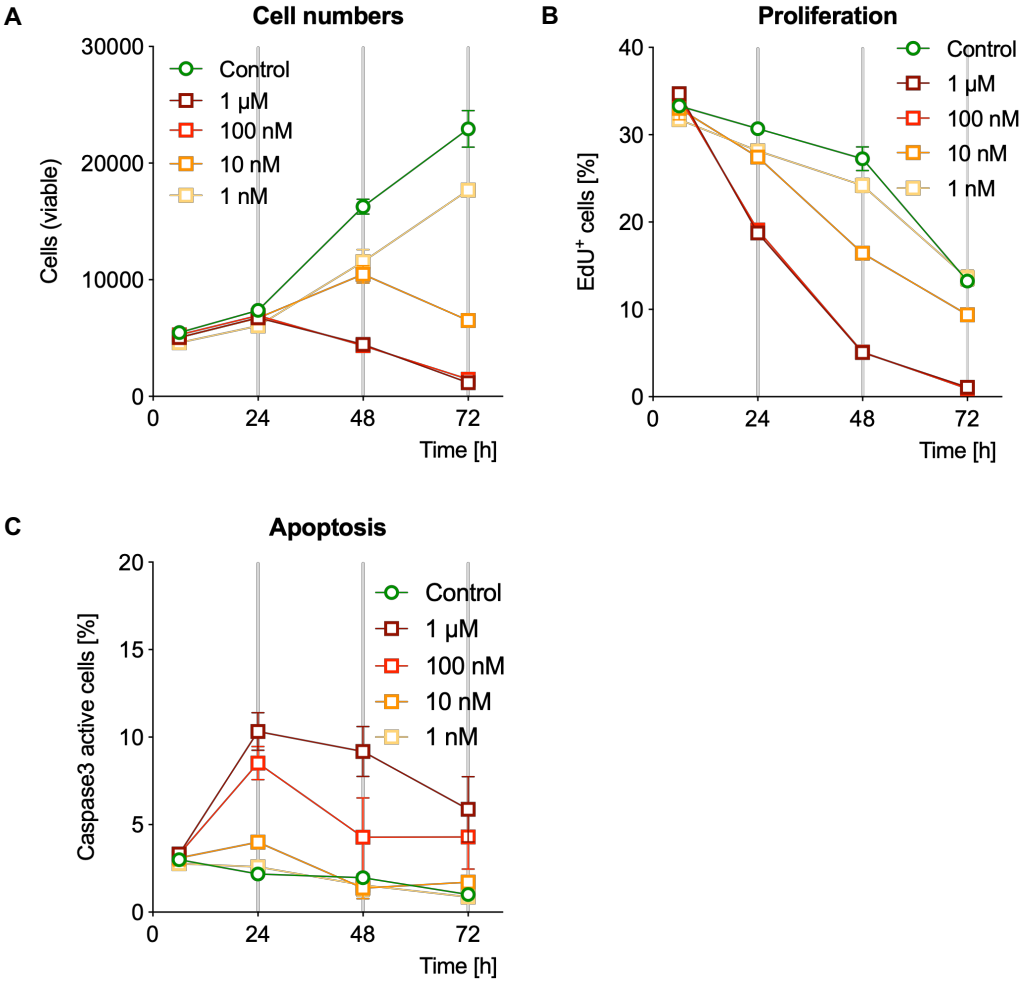

Figure 8-36: IMP1088 is highly lethal to the ABC DLBCL PDX LY12318, with c-Myc translocation.

[A] Quantification of viable cell numbers for LY12318. **[B]** Quantification of DNA synthesis (EdU+) for LY12318. **[C]** Quantification of caspase3 activation for LY12318. (For all graphs: N = 2, error bars = SEM)

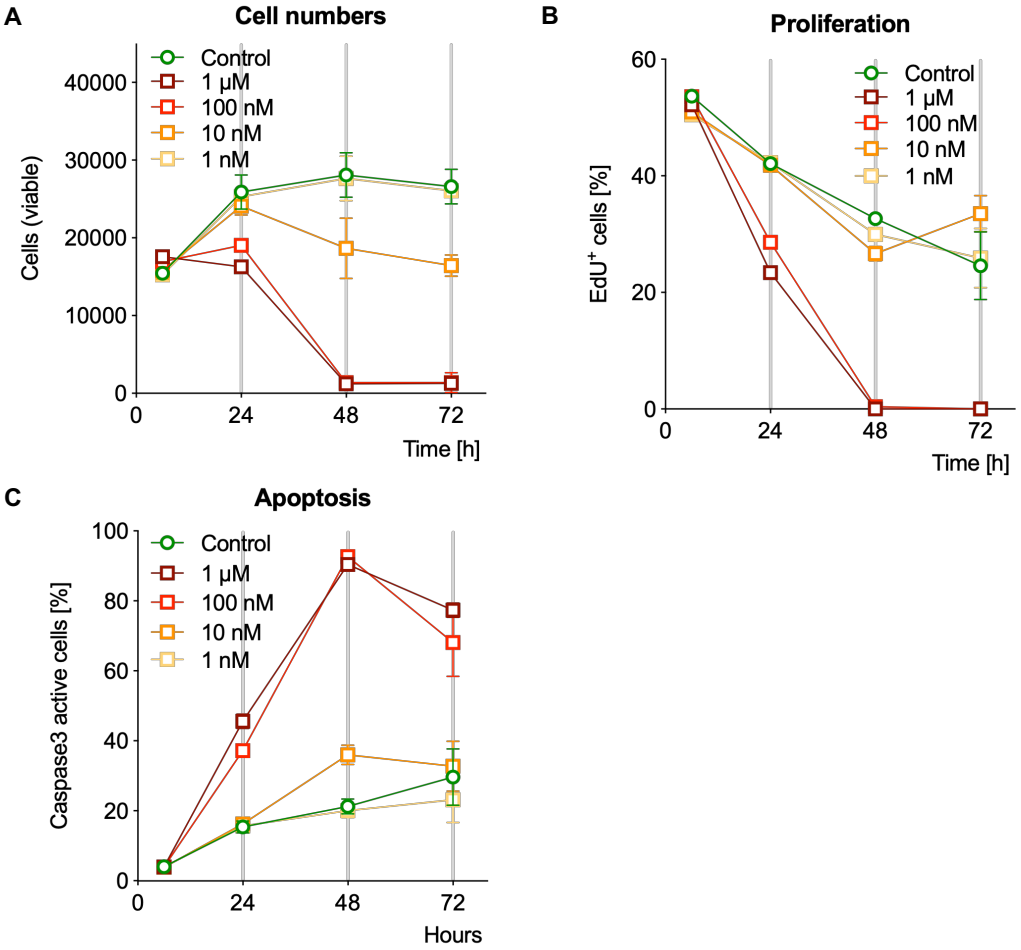

Figure 8-37: IMP1088 is highly lethal to the plasmablastic lymphoma PDX LY12657, with c-Myc translocation.

[A] Quantification of viable cell numbers for LY12657. **[B]** Quantification of DNA synthesis (EdU+) for LY12657. **[C]** Quantification of caspase3 activation for LY12657. (For all graphs: N = 2, error bars = SEM)

8.4 Appendix Chapter 5: Cell signalling is affected within minutes to hours of NMT inhibition in BL41, indicating a potential GOF.

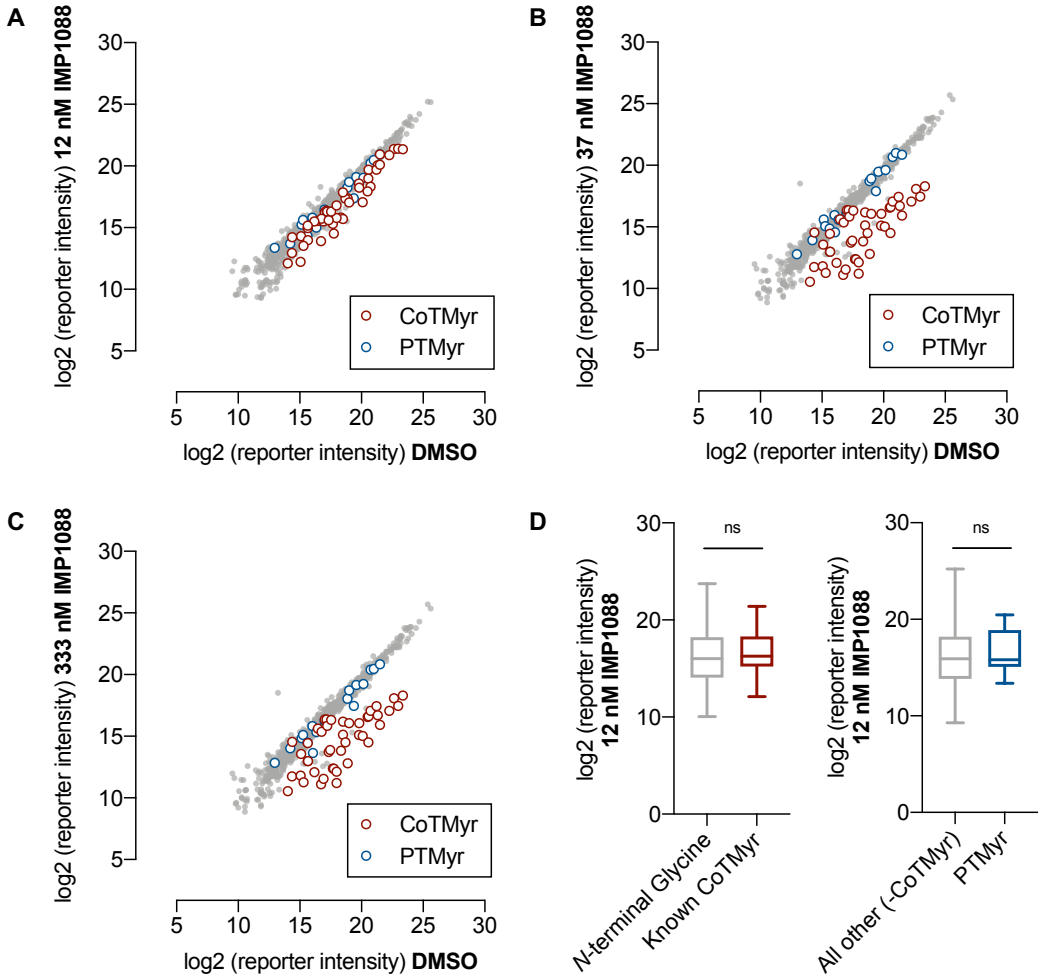

Figure 8-38: Concentration dependent effect on CoTMyr NMT substrates.

[A] 2D plot, comparing DMSO vs. the samples treated with 12 nM of IMP1088. **[B]** 2D plot, comparing DMSO vs. the samples treated with 37 nM of IMP1088. **[C]** 2D plot, comparing DMSO vs. the samples treated with 333 nM of IMP1088. **[D]** Left: Comparison of the effect of 12 nM IMP1088 on all previously identified CoTMyr substrates and proteins that have an *N*-terminal glycine. Right: Comparison of the effect of 12 nM IMP1088 on all previously identified PTMyr substrates against all other identified proteins.
(P-values were determined with Mann-Whitney test, error bars = minimum to maximum values)

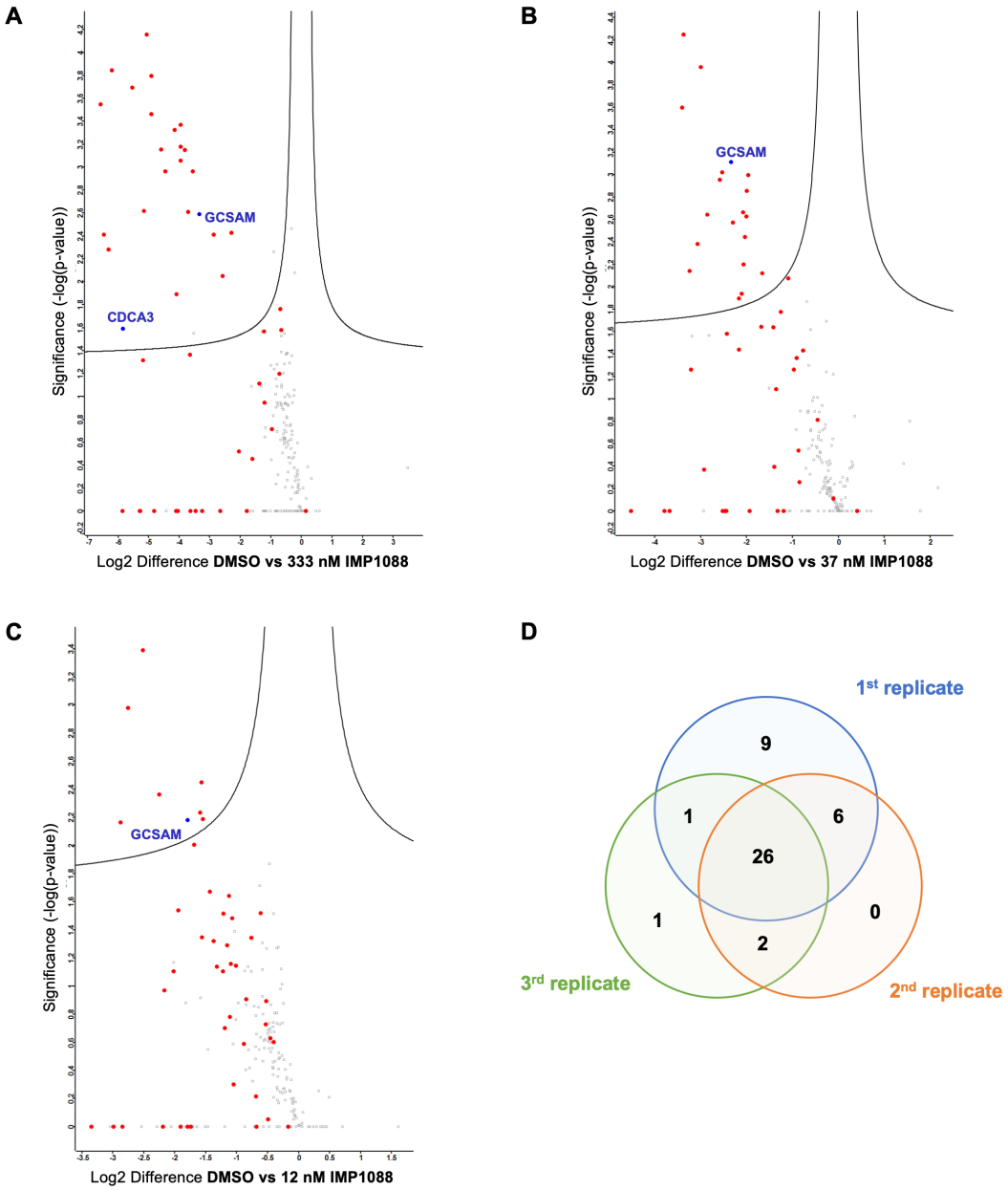

Figure 8-39: Enrichment of CoTMyr substrates across different conditions.

[A] Volcano plot showing the enrichment of known NMT substrates in the DMSO control vs 333 nM IMP1088. Two novel NMT substrates (GCSAM and CDCA3; blue) were also enriched in the DMSO treated sample. **[B]** Volcano plot showing the enrichment of known NMT substrates in the DMSO control vs 37 nM IMP1088. Two novel NMT substrates (GCSAM and CDCA3; blue) were also enriched in the DMSO treated sample. **[C]** Volcano plot showing the enrichment of known NMT substrates in the DMSO control vs 12 nM IMP1088. Two novel NMT substrates (GCSAM and CDCA3; blue) were also enriched in the DMSO treated sample. **[D]** Venn-Diagram showing the identification of known NMT substrates across the biological triplicates.

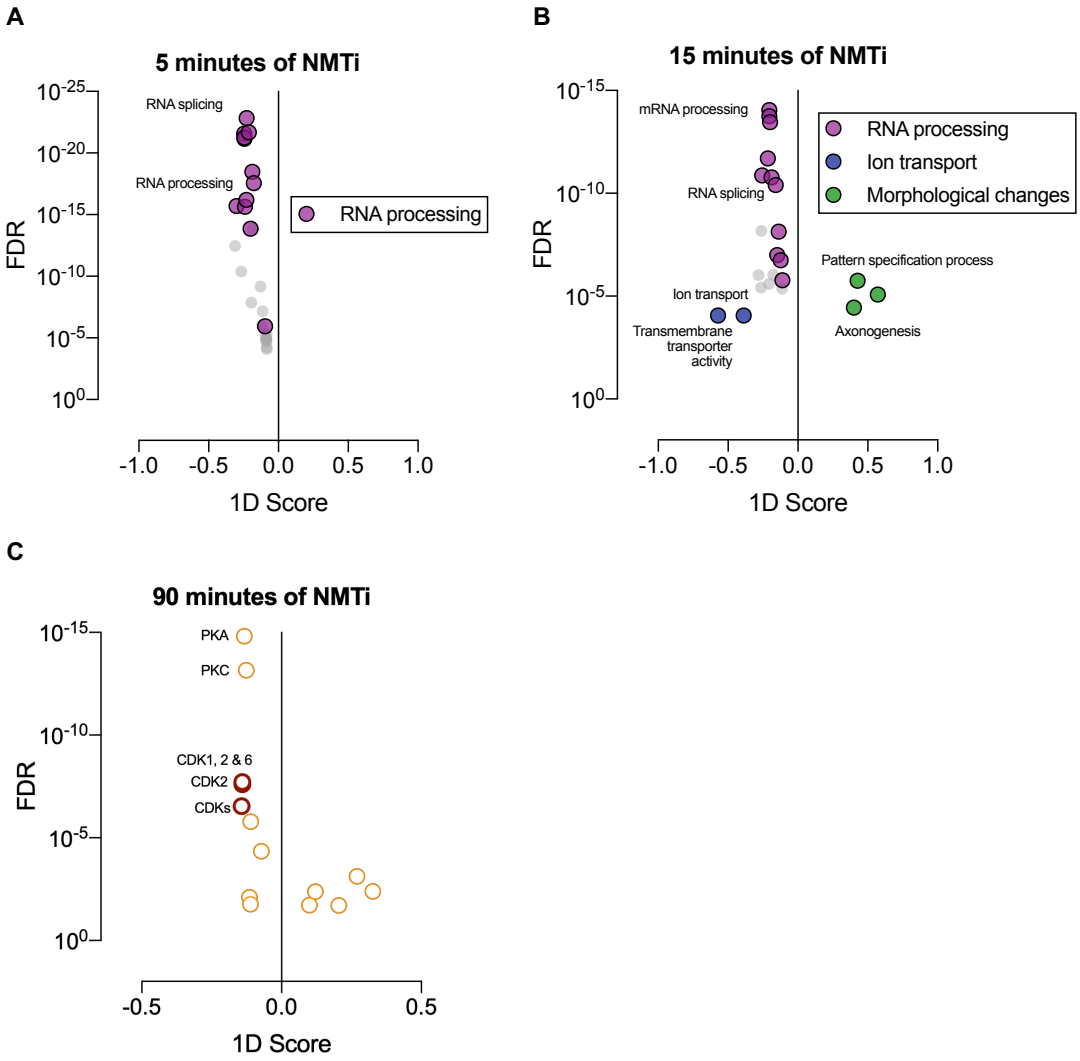

Figure 8-40: Phosphorylation is persistently altered on proteins involved in RNA processing and (putative) substrates of CDKs are strongly affected.

[A] 1D enrichment plot showing GOBP and GOMF enrichment of the phosphorylation changes at 5 minutes of NMT inhibition. **[B]** 1D enrichment plot showing GOBP and GOMF enrichment of the phosphorylation changes at 15 minutes of NMT inhibition. **[C]** 1D enrichment plot showing motif enrichment of the phosphorylation changes at 90 minutes of NMT inhibition.

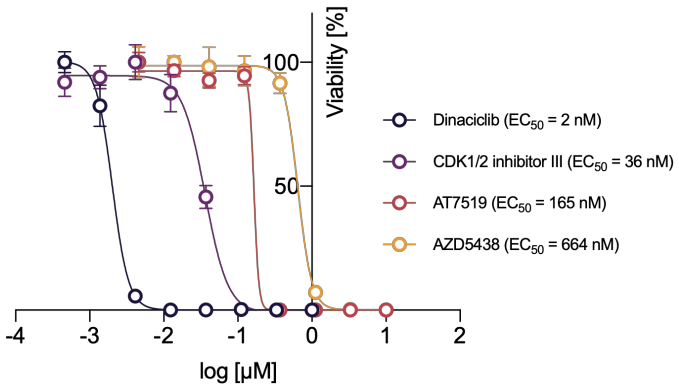

Figure 8-41: Growth inhibition curves of different pan CDK inhibitors in BL41.

Growth inhibition curves for BL41, treated with different CDK inhibitors. (For all graphs: N = 4, error bars = SEM)

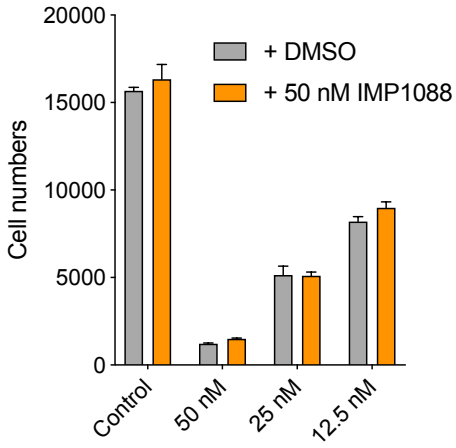

Figure 8-42: Cell numbers are unaffected by the addition of IMP1088 to CDK1/2 inhibitor III.

Quantification of viable cells ± 50 nM of IMP1088 (Error bars = SEM).

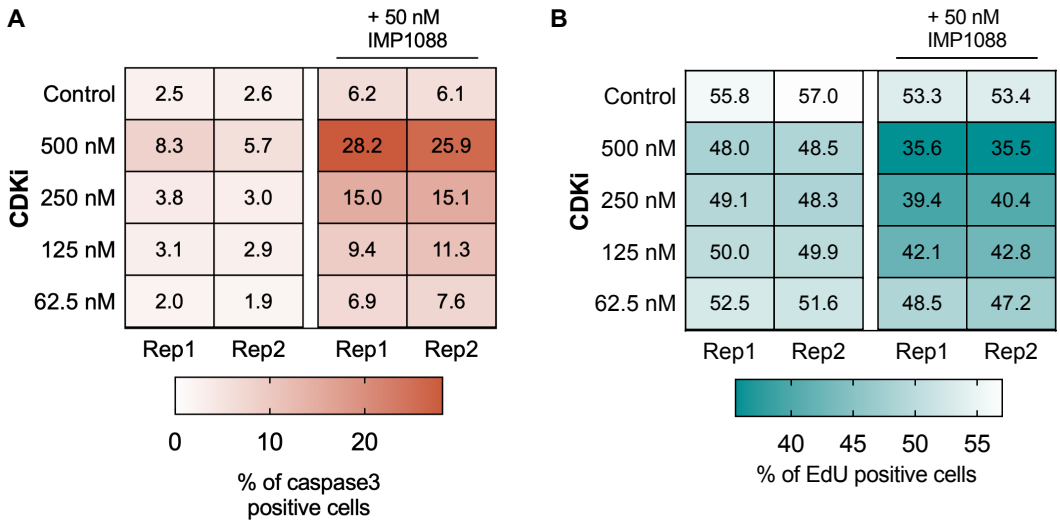

Figure 8-43: AZD5438 and IMP1088 synergise.

[A] Effect of adding 50 nM of IMP1088 for 24 hours to AZD5438 on DNA synthesis, measured by EdU incorporation. **[C]** Effect of adding 50 nM of IMP1088 for 24 hours to AZD5438 on apoptosis, measured by caspase 3 induction.

Table 8-3: Combination indices for the effects on apoptosis and proliferation with AZD5438.

	Apoptosis		Proliferation	
Concentration of AZD5438	Response Additivity	Bliss Independence	Response Additivity	Bliss Independence
500 nM + IMP1088	0.33	0.32	0.56	0.55
250 nM + IMP1088	0.35	0.35	0.68	0.66
125 nM + IMP1088	0.50	0.50	0.72	0.70
62.5 nM + IMP1088	0.63	0.62	0.92	0.90

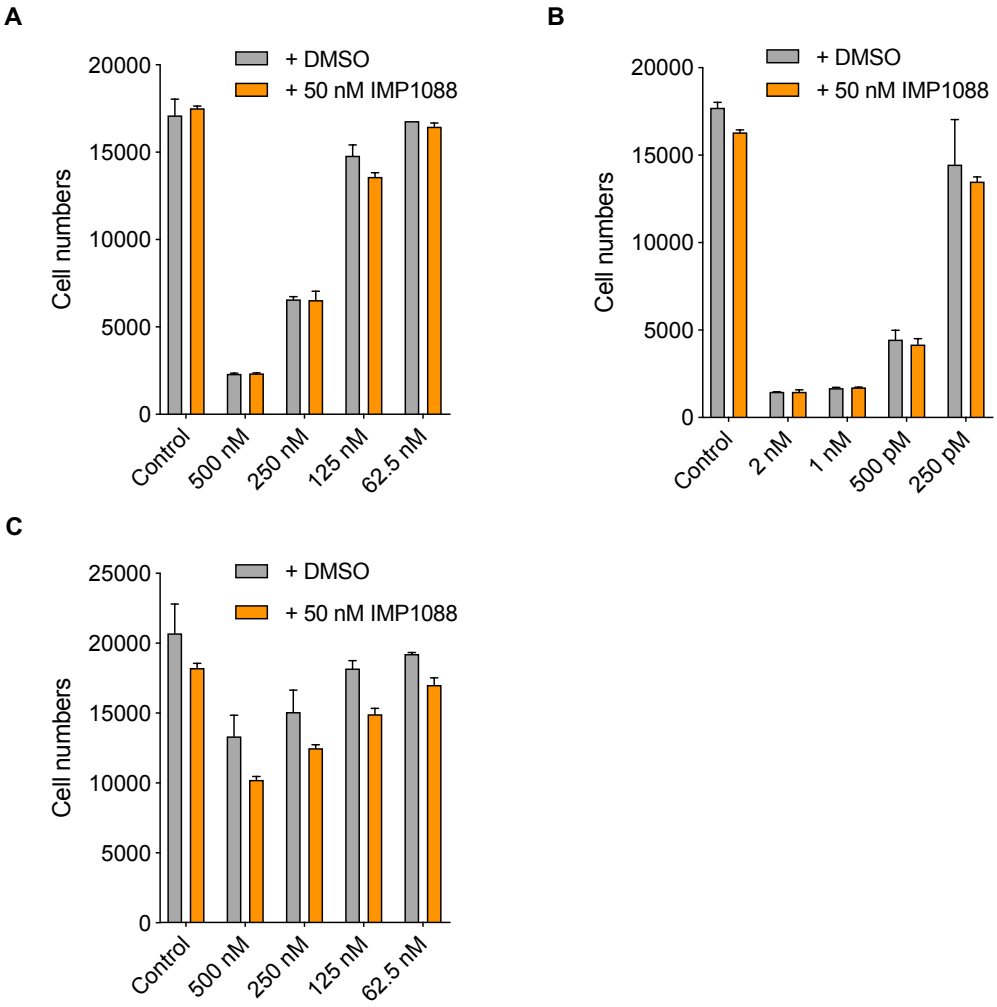

Figure 8-44: Cell numbers *per se* are not reduced within 24 hours of combined NMT and pan-CDK inhibition.

[A] Quantification of cell numbers of the combination study with AT7519. **[B]** Quantification of cell numbers of the combination study with Dinaciclib. **[C]** Quantifications of cell numbers of the combination study with AZD5438.

Reference List

Adams, J.M., Harris, A.W., Pinkert, C.A., Corcoran, L.M., Alexander, W.S., Cory, S., Palmiter, R.D., and Brinster, R.L. (1985). The c-myc oncogene driven by immunoglobulin enhancers induces lymphoid malignancy in transgenic mice. Nature *318*, 533-538.
Adams, M.N., Burgess, J.T., He, Y., Gately, K., Snell, C., Zhang, S.D., Hooper, J.D., Richard, D.J., and O'Byrne, K.J. (2017). Expression of CDCA3 Is a Prognostic Biomarker and Potential Therapeutic Target in Non-Small Cell Lung Cancer. J Thorac Oncol *12*, 1071-1084.
Alizadeh, A.A., Eisen, M.B., Davis, R.E., Ma, C., Lossos, I.S., Rosenwald, A., Boldrick, J.C., Sabet, H., Tran, T., Yu, X.*, et al.* (2000). Distinct types of diffuse large B-cell lymphoma identified by gene expression profiling. Nature *403*, 503-511.
Allemand, E., Hastings, M.L., Murray, M.V., Myers, M.P., and Krainer, A.R. (2007). Alternative splicing regulation by interaction of phosphatase PP2Cgamma with nucleic acid-binding protein YB-1. Nat Struct Mol Biol *14*, 630-638.
Amati, B., Brooks, M.W., Levy, N., Littlewood, T.D., Evan, G.I., and Land, H. (1993). Oncogenic activity of the c-Myc protein requires dimerization with Max. Cell *72*, 233-245.
An, X., Tiwari, A.K., Sun, Y., Ding, P.R., Ashby, C.R., Jr., and Chen, Z.S. (2010). BCR-ABL tyrosine kinase inhibitors in the treatment of Philadelphia chromosome positive chronic myeloid leukemia: a review. Leuk Res *34*, 1255-1268.
Anders, S., Pyl, P.T., and Huber, W. (2015). HTSeq--a Python framework to work with high-throughput sequencing data. Bioinformatics (Oxford, England) *31*, 166-169.
Anders, S., Reyes, A., and Huber, W. (2012). Detecting differential usage of exons from RNA-seq data. Genome Res *22*, 2008-2017.
Annibali, D., Whitfield, J.R., Favuzzi, E., Jauset, T., Serrano, E., Cuartas, I., Redondo-Campos, S., Folch, G., Gonzalez-Junca, A., Sodir, N.M.*, et al.* (2014). Myc inhibition is effective against glioma and reveals a role for Myc in proficient mitosis. Nat Commun *5*, 4632.
Argelaguet, R., Arnol, D., Bredikhin, D., Deloro, Y., Velten, B., Marioni, J.C., and Stegle, O. (2019). MOFA+: a probabilistic framework for comprehensive integration of structured single-cell data. bioRxiv, 837104.
Argelaguet, R., Velten, B., Arnol, D., Dietrich, S., Zenz, T., Marioni, J.C., Buettner, F., Huber, W., and Stegle, O. (2018). Multi-Omics Factor Analysis—a framework for unsupervised integration of multi-omics data sets. Molecular Systems Biology *14*, e8124.
Arvanitis, C., and Felsher, D.W. (2006). Conditional transgenic models define how MYC initiates and maintains tumorigenesis. Semin Cancer Biol *16*, 313-317.
Asghar, U., Witkiewicz, A.K., Turner, N.C., and Knudsen, E.S. (2015). The history and future of targeting cyclin-dependent kinases in cancer therapy. Nat Rev Drug Discov *14*, 130-146.
Bailey, M.H., Tokheim, C., Porta-Pardo, E., Sengupta, S., Bertrand, D., Weerasinghe, A., Colaprico, A., Wendl, M.C., Kim, J., Reardon, B.*, et al.* (2018). Comprehensive Characterization of Cancer Driver Genes and Mutations. Cell *173*, 371-385 e318.
Barretina, J., Caponigro, G., Stransky, N., Venkatesan, K., Margolin, A.A., Kim, S., Wilson, C.J., Lehar, J., Kryukov, G.V., Sonkin, D.*, et al.* (2012). The Cancer Cell Line Encyclopedia enables predictive modelling of anticancer drug sensitivity. Nature *483*, 603-607.
Basso, K., and Dalla-Favera, R. (2015). Germinal centres and B cell lymphomagenesis. Nat Rev Immunol *15*, 172-184.
Beaulieu, M.-E., Jauset, T., Massó-Vallés, D., Martínez-Martín, S., Rahl, P., Maltais, L., Zacarias-Fluck, M.F., Casacuberta-Serra, S., Serrano del Pozo, E., Fiore, C.*, et al.*

(2019). Intrinsic cell-penetrating activity propels Omomyc from proof of concept to viable anti-MYC therapy. Science Translational Medicine *11*, eaar5012.
Behan, F.M., Iorio, F., Picco, G., Goncalves, E., Beaver, C.M., Migliardi, G., Santos, R., Rao, Y., Sassi, F., Pinnelli, M.*, et al.* (2019). Prioritization of cancer therapeutic targets using CRISPR-Cas9 screens. Nature *568*, 511-516.
Bell, A.S., Mills, J.E., Williams, G.P., Brannigan, J.A., Wilkinson, A.J., Parkinson, T., Leatherbarrow, R.J., Tate, E.W., Holder, A.A., and Smith, D.F. (2012). Selective inhibitors of protozoan protein N-myristoyltransferases as starting points for tropical disease medicinal chemistry programs. PLoS Negl Trop Dis *6*, e1625.
Bell, A.S., Tate, E.W., Leatherbarrow, R.J., Hutton, J.A., and Brannigan, J.A. (2017). Preparation of pyrazole derivatives as inhibitors of N-myristoyl transferase (Imperial Innovations Limited, UK).
Bell, E., Lunec, J., and Tweddle, D. (2007). Cell Cycle Regulation Targets of MYCN Identified by Gene Expression Microarrays. Cell Cycle *6*, 1249-1256.
Ben-David, U., Siranosian, B., Ha, G., Tang, H., Oren, Y., Hinohara, K., Strathdee, C.A., Dempster, J., Lyons, N.J., Burns, R.*, et al.* (2018). Genetic and transcriptional evolution alters cancer cell line drug response. Nature *560*, 325-330.
Bennetzen, M.V., Larsen, D.H., Bunkenborg, J., Bartek, J., Lukas, J., and Andersen, J.S. (2010). Site-specific Phosphorylation Dynamics of the Nuclear Proteome during the DNA Damage Response. Molecular & Cellular Proteomics *9*, 1314-1323.
Bentley, D.L. (2014). Coupling mRNA processing with transcription in time and space. Nat Rev Genet *15*, 163-175.
Berg, M.G., Singh, L.N., Younis, I., Liu, Q., Pinto, A.M., Kaida, D., Zhang, Z., Cho, S., Sherrill-Mix, S., Wan, L.*, et al.* (2012). U1 snRNP determines mRNA length and regulates isoform expression. Cell *150*, 53-64.
Berman, H.M., Westbrook, J., Feng, Z., Gilliland, G., Bhat, T.N., Weissig, H., Shindyalov, I.N., and Bourne, P.E. (2000). The Protein Data Bank. Nucleic Acids Research *28*, 235-242.
Berndt, N., Hamilton, A.D., and Sebti, S.M. (2011). Targeting protein prenylation for cancer therapy. Nat Rev Cancer *11*, 775-791.
Beroukhim, R., Mermel, C.H., Porter, D., Wei, G., Raychaudhuri, S., Donovan, J., Barretina, J., Boehm, J.S., Dobson, J., Urashima, M.*, et al.* (2010). The landscape of somatic copy-number alteration across human cancers. Nature *463*, 899-905.
Berthiaume, L.G., and Beauchamp, E. (2017). Epigenetic silencing of NMT2. In PatentPak.
Berthiaume, L.G., Perinpanayagam, M.A., Yap, C., and Beauchamp, E. (2014). Synthetic lethality and the treatment of cancer. In PatentPak.
Bhandarkar, S.S., Bromberg, J., Carrillo, C., Selvakumar, P., Sharma, R.K., Perry, B.N., Govindarajan, B., Fried, L., Sohn, A., Reddy, K.*, et al.* (2008). Tris (dibenzylideneacetone) dipalladium, a N-myristoyltransferase-1 inhibitor, is effective against melanoma growth in vitro and in vivo. Clin Cancer Res *14*, 5743-5748.
Bhatnagar, R.S., Fütterer, K., Farazi, T.A., Korolev, S., Murray, C.L., Jackson-Machelski, E.J., Gokel, G.W., Gordon, J.I., and Waksman, G. (1998). Structure of N-myristoyltransferase with bound myristoylCoA and peptide substrate analogs. Nature Structural Biology *5*, 1091-1097.
Bielawska, A., Greenberg, M.S., Perry, D., Jayadev, S., Shayman, J.A., McKay, C., and Hannun, Y.A. (1996). (1S,2R)-D-erythro-2-(N-myristoylamino)-1-phenyl-1-propanol as an inhibitor of ceramidase. J Biol Chem *271*, 12646-12654.
Bishop, J.M. (1983). Cellular oncogenes and retroviruses. Annu Rev Biochem *52*, 301-354.
Blackwood, E., and Eisenman, R. (1991). Max: a helix-loop-helix zipper protein that forms a sequence-specific DNA-binding complex with Myc. Science *251*, 1211-1217.

Blanc, M., David, F., Abrami, L., Migliozzi, D., Armand, F., Burgi, J., and van der Goot, F.G. (2015). SwissPalm: Protein Palmitoylation database. F1000Res *4*, 261.
Blencowe, B.J., Baurén, G., Eldridge, A.G., Issner, R., Nickerson, J.A., Rosonina, E., and Sharp, P.A. (2000). The SRm160/300 splicing coactivator subunits. RNA (New York, NY) *6*, 111-120.
Bliss, C.I. (1939). THE TOXICITY OF POISONS APPLIED JOINTLY1. Annals of Applied Biology *26*, 585-615.
Boisvert, F.M., Ahmad, Y., Gierlinski, M., Charriere, F., Lamont, D., Scott, M., Barton, G., and Lamond, A.I. (2012). A quantitative spatial proteomics analysis of proteome turnover in human cells. Mol Cell Proteomics *11*, M111 011429.
Bolger, A.M., Lohse, M., and Usadel, B. (2014). Trimmomatic: a flexible trimmer for Illumina sequence data. Bioinformatics *30*, 2114-2120.
Bologna, G., Yvon, C., Duvaud, S., and Veuthey, A.L. (2004). N-Terminal myristoylation predictions by ensembles of neural networks. Proteomics *4*, 1626-1632.
Boss, D.S., Schwartz, G.K., Middleton, M.R., Amakye, D.D., Swaisland, H., Midgley, R.S., Ranson, M., Danson, S., Calvert, H., Plummer, R.*, et al.* (2010). Safety, tolerability, pharmacokinetics and pharmacodynamics of the oral cyclin-dependent kinase inhibitor AZD5438 when administered at intermittent and continuous dosing schedules in patients with advanced solid tumours. Ann Oncol *21*, 884-894.
Bouchard, C., Thieke, K., Maier, A., Saffrich, R., Hanley-Hyde, J., Ansorge, W., Reed, S., Sicinski, P., Bartek, J., and Eilers, M. (1999). Direct induction of cyclin D2 by Myc contributes to cell cycle progression and sequestration of p27. Embo j *18*, 5321-5333.
Boutin, J.A. (1997). Myristoylation. Cell Signal *9*, 15-35.
Bradner, J.E., Hnisz, D., and Young, R.A. (2017). Transcriptional Addiction in Cancer. Cell *168*, 629-643.
Brand, S., Norcross, N.R., Thompson, S., Harrison, J.R., Smith, V.C., Robinson, D.A., Torrie, L.S., McElroy, S.P., Hallyburton, I., Norval, S.*, et al.* (2014). Lead optimization of a pyrazole sulfonamide series of Trypanosoma brucei N-myristoyltransferase inhibitors: identification and evaluation of CNS penetrant compounds as potential treatments for stage 2 human African trypanosomiasis. J Med Chem *57*, 9855-9869.
Broncel, M., Serwa, R.A., Ciepla, P., Krause, E., Dallman, M.J., Magee, A.I., and Tate, E.W. (2015). Multifunctional reagents for quantitative proteome-wide analysis of protein modification in human cells and dynamic profiling of protein lipidation during vertebrate development. Angew Chem Int Ed Engl *54*, 5948-5951.
Burkitt, D. (1958). A sarcoma involving the jaws in african children. Br J Surg *46*, 218-223.
Burnaevskiy, N., Fox, T.G., Plymire, D.A., Ertelt, J.M., Weigele, B.A., Selyunin, A.S., Way, S.S., Patrie, S.M., and Alto, N.M. (2013). Proteolytic elimination of N-myristoyl modifications by the Shigella virulence factor IpaJ. Nature *496*, 106-109.
Burnaevskiy, N., Peng, T., Reddick, L.E., Hang, H.C., and Alto, N.M. (2015). Myristoylome profiling reveals a concerted mechanism of ARF GTPase deacylation by the bacterial protease IpaJ. Mol Cell *58*, 110-122.
Byth, K.F., Thomas, A., Hughes, G., Forder, C., McGregor, A., Geh, C., Oakes, S., Green, C., Walker, M., Newcombe, N.*, et al.* (2009). AZD5438, a potent oral inhibitor of cyclin-dependent kinases 1, 2, and 9, leads to pharmacodynamic changes and potent antitumor effects in human tumor xenografts. Mol Cancer Ther *8*, 1856-1866.
Cabezas-Wallscheid, N., Klimmeck, D., Hansson, J., Lipka, D.B., Reyes, A., Wang, Q., Weichenhan, D., Lier, A., von Paleske, L., Renders, S.*, et al.* (2014). Identification of regulatory networks in HSCs and their immediate progeny via integrated proteome, transcriptome, and DNA methylome analysis. Cell Stem Cell *15*, 507-522.
Calado, D.P., Sasaki, Y., Godinho, S.A., Pellerin, A., Kochert, K., Sleckman, B.P., de Alboran, I.M., Janz, M., Rodig, S., and Rajewsky, K. (2012). The cell-cycle regulator c-

Myc is essential for the formation and maintenance of germinal centers. Nat Immunol *13*, 1092-1100.
Cancer Cell Line Encyclopedia, C., and Genomics of Drug Sensitivity in Cancer, C. (2015). Pharmacogenomic agreement between two cancer cell line data sets. Nature *528*, 84-87.
Carow, B., Gao, Y., Coquet, J., Reilly, M., and Rottenberg, M.E. (2016). lck-Driven Cre Expression Alters T Cell Development in the Thymus and the Frequencies and Functions of Peripheral T Cell Subsets. J Immunol *197*, 2261-2268.
Castillo, J.J., Bibas, M., and Miranda, R.N. (2015). The biology and treatment of plasmablastic lymphoma. Blood *125*, 2323-2330.
Castrec, B., Dian, C., Ciccone, S., Ebert, C.L., Bienvenut, W.V., Le Caer, J.P., Steyaert, J.M., Giglione, C., and Meinnel, T. (2018). Structural and genomic decoding of human and plant myristoylomes reveals a definitive recognition pattern. Nat Chem Biol *14*, 671-679.
Chapuy, B., McKeown, M.R., Lin, C.Y., Monti, S., Roemer, M.G., Qi, J., Rahl, P.B., Sun, H.H., Yeda, K.T., Doench, J.G.*, et al.* (2013). Discovery and characterization of super-enhancer-associated dependencies in diffuse large B cell lymphoma. Cancer Cell *24*, 777-790.
Charron, J., Malynn, B.A., Fisher, P., Stewart, V., Jeannotte, L., Goff, S.P., Robertson, E.J., and Alt, F.W. (1992). Embryonic lethality in mice homozygous for a targeted disruption of the N-myc gene. Genes Dev *6*, 2248-2257.
Chavda, B., Arnott, J.A., and Planey, S.L. (2014). Targeting protein palmitoylation: selective inhibitors and implications in disease. Expert Opinion on Drug Discovery *9*, 1005-1019.
Chen, H., Liu, H., and Qing, G. (2018). Targeting oncogenic Myc as a strategy for cancer treatment. Signal Transduct Target Ther *3*, 5.
Chen, K., Koe, C.T., Xing, Z.B., Tian, X., Rossi, F., Wang, C., Tang, Q., Zong, W., Hong, W.J., Taneja, R.*, et al.* (2016). Arl2- and Msps-dependent microtubule growth governs asymmetric division. J Cell Biol *212*, 661-676.
Chida, T., Ando, M., Matsuki, T., Masu, Y., Nagaura, Y., Takano-Yamamoto, T., Tamura, S., and Kobayashi, T. (2013). N-Myristoylation is essential for protein phosphatases PPM1A and PPM1B to dephosphorylate their physiological substrates in cells. Biochem J *449*, 741-749.
Chipumuro, E., Marco, E., Christensen, C.L., Kwiatkowski, N., Zhang, T., Hatheway, C.M., Abraham, B.J., Sharma, B., Yeung, C., Altabef, A.*, et al.* (2014). CDK7 inhibition suppresses super-enhancer-linked oncogenic transcription in MYCN-driven cancer. Cell *159*, 1126-1139.
Chng, W.J., Huang, G.F., Chung, T.H., Ng, S.B., Gonzalez-Paz, N., Troska-Price, T., Mulligan, G., Chesi, M., Bergsagel, P.L., and Fonseca, R. (2011). Clinical and biological implications of MYC activation: a common difference between MGUS and newly diagnosed multiple myeloma. Leukemia *25*, 1026-1035.
Choo, J.R., and Lee, S.C. (2018). CDK4-6 inhibitors in breast cancer: current status and future development. Expert Opin Drug Metab Toxicol *14*, 1123-1138.
Ciriello, G., Miller, M.L., Aksoy, B.A., Senbabaoglu, Y., Schultz, N., and Sander, C. (2013). Emerging landscape of oncogenic signatures across human cancers. Nat Genet *45*, 1127-1133.
Clemons, M., Danson, S., and Howell, A. (2002). Tamoxifen ('Nolvadex'): a review. Cancer Treatment Reviews *28*, 165-180.
Cole, K.A., Huggins, J., Laquaglia, M., Hulderman, C.E., Russell, M.R., Bosse, K., Diskin, S.J., Attiyeh, E.F., Sennett, R., Norris, G.*, et al.* (2011). RNAi screen of the protein kinome identifies checkpoint kinase 1 (CHK1) as a therapeutic target in neuroblastoma. Proc Natl Acad Sci U S A *108*, 3336-3341.

Cole, M.D., and Cowling, V.H. (2008). Transcription-independent functions of MYC: regulation of translation and DNA replication. Nat Rev Mol Cell Biol *9*, 810-815.
Conacci-Sorrell, M., McFerrin, L., and Eisenman, R.N. (2014). An overview of MYC and its interactome. Cold Spring Harb Perspect Med *4*, a014357.
Consortium, T.U. (2019). UniProt: a worldwide hub of protein knowledge. Nucleic Acids Res *47*, D506-d515.
Coux, O., Tanaka, K., and Goldberg, A.L. (1996). Structure and functions of the 20S and 26S Proteasomes. Annu Rev Biochem *65*, 801-847.
Cowling, V.H., and Cole, M.D. (2007). The Myc transactivation domain promotes global phosphorylation of the RNA polymerase II carboxy-terminal domain independently of direct DNA binding. Mol Cell Biol *27*, 2059-2073.
Cowling, V.H., and Cole, M.D. (2010). Myc Regulation of mRNA Cap Methylation. Genes Cancer *1*, 576-579.
Cox, J., and Mann, M. (2008). MaxQuant enables high peptide identification rates, individualized p.p.b.-range mass accuracies and proteome-wide protein quantification. Nat Biotechnol *26*, 1367-1372.
Cox, J., and Mann, M. (2012). 1D and 2D annotation enrichment: a statistical method integrating quantitative proteomics with complementary high-throughput data. BMC Bioinformatics *13 Suppl 16*, S12.
Crosio, C., Fimia, G.M., Loury, R., Kimura, M., Okano, Y., Zhou, H., Sen, S., Allis, C.D., and Sassone-Corsi, P. (2002). Mitotic Phosphorylation of Histone H3: Spatio-Temporal Regulation by Mammalian Aurora Kinases. Molecular and Cellular Biology *22*, 874-885.
Dai, M.S., and Lu, H. (2008). Crosstalk between c-Myc and ribosome in ribosomal biogenesis and cancer. J Cell Biochem *105*, 670-677.
Dalla-Favera, R., Bregni, M., Erikson, J., Patterson, D., Gallo, R.C., and Croce, C.M. (1982). Human c-myc onc gene is located on the region of chromosome 8 that is translocated in Burkitt lymphoma cells. Proceedings of the National Academy of Sciences of the United States of America *79*, 7824-7827.
Dang, C.V. (2010). Rethinking the Warburg effect with Myc micromanaging glutamine metabolism. Cancer Res *70*, 859-862.
Dang, C.V. (2012). MYC on the path to cancer. Cell *149*, 22-35.
Dang, C.V. (2013). MYC, metabolism, cell growth, and tumorigenesis. Cold Spring Harb Perspect Med *3*.
Davda, D., El Azzouny, M.A., Tom, C.T.M.B., Hernandez, J.L., Majmudar, J.D., Kennedy, R.T., and Martin, B.R. (2013). Profiling Targets of the Irreversible Palmitoylation Inhibitor 2-Bromopalmitate. ACS Chemical Biology *8*, 1912-1917.
Davis, A.C., Wims, M., Spotts, G.D., Hann, S.R., and Bradley, A. (1993). A null c-myc mutation causes lethality before 10.5 days of gestation in homozygotes and reduced fertility in heterozygous female mice. Genes Dev *7*, 671-682.
de la Puente, P., Azab, F., Muz, B., Luderer, M., Arbiser, J., and Azab, A.K. (2016). Tris DBA palladium overcomes hypoxia-mediated drug resistance in multiple myeloma. Leuk Lymphoma *57*, 1677-1686.
De Silva, N.S., and Klein, U. (2015). Dynamics of B cells in germinal centres. Nat Rev Immunol *15*, 137-148.
Debets, M.F., van der Doelen, C.W.J., Rutjes, F.P.J.T., and van Delft, F.L. (2010). Azide: A Unique Dipole for Metal-Free Bioorthogonal Ligations. ChemBioChem *11*, 1168-1184.
Delgado, M.D., and Leon, J. (2010). Myc roles in hematopoiesis and leukemia. Genes Cancer *1*, 605-616.
Deng, L., Gao, X., Liu, B., He, X., Xu, J., Qiang, J., Wu, Q., and Liu, S. (2018). NMT1 inhibition modulates breast cancer progression through stress-triggered JNK pathway. Cell Death Dis *9*, 1143.
Devadas, B., Freeman, S.K., Zupec, M.E., Lu, H.-F., Nagarajan, S.R., Kishore, N.S., Lodge, J.K., Kuneman, D.W., McWherter, C.A., Vinjamoori, D.V.*, et al.* (1997). Design

and Synthesis of Novel Imidazole-Substituted Dipeptide Amides as Potent and Selective Inhibitors of Candida albicans MyristoylCoA:Protein N-Myristoyltransferase and Identification of Related Tripeptide Inhibitors with Mechanism-Based Antifungal Activity. Journal of Medicinal Chemistry *40*, 2609-2625.

Devadas, B., Zupec, M.E., Freeman, S.K., Brown, D.L., Nagarajan, S., Sikorski, J.A., McWherter, C.A., Getman, D.P., and Gordon, J.I. (1995). Design and Syntheses of Potent and Selective Dipeptide Inhibitors of Candida albicans Myristoyl-CoA:Protein N-Myristoyltransferase. Journal of Medicinal Chemistry *38*, 1837-1840.

Devany, E., Park, J.Y., Murphy, M.R., Zakusilo, G., Baquero, J., Zhang, X., Hoque, M., Tian, B., and Kleiman, F.E. (2016). Intronic cleavage and polyadenylation regulates gene expression during DNA damage response through U1 snRNA. Cell Discov *2*, 16013.

Diaz, B., Ostapoff, K.T., Toombs, J.E., Lo, J., Bonner, M.Y., Curatolo, A., Adsay, V., Brekken, R.A., and Arbiser, J.L. (2016). Tris DBA palladium is highly effective against growth and metastasis of pancreatic cancer in an orthotopic model. Oncotarget *7*, 51569-51580.

Dobin, A., Davis, C.A., Schlesinger, F., Drenkow, J., Zaleski, C., Jha, S., Batut, P., Chaisson, M., and Gingeras, T.R. (2013). STAR: ultrafast universal RNA-seq aligner. Bioinformatics *29*, 15-21.

Dolman, M.E., Poon, E., Ebus, M.E., den Hartog, I.J., van Noesel, C.J., Jamin, Y., Hallsworth, A., Robinson, S.P., Petrie, K., Sparidans, R.W.*, et al.* (2015). Cyclin-Dependent Kinase Inhibitor AT7519 as a Potential Drug for MYCN-Dependent Neuroblastoma. Clin Cancer Res *21*, 5100-5109.

Dominguez-Sola, D., Victora, G.D., Ying, C.Y., Phan, R.T., Saito, M., Nussenzweig, M.C., and Dalla-Favera, R. (2012). The proto-oncogene MYC is required for selection in the germinal center and cyclic reentry. Nat Immunol *13*, 1083-1091.

Dominguez-Sola, D., Ying, C.Y., Grandori, C., Ruggiero, L., Chen, B., Li, M., Galloway, D.A., Gu, W., Gautier, J., and Dalla-Favera, R. (2007). Non-transcriptional control of DNA replication by c-Myc. Nature *448*, 445-451.

Donaldson, J.G., and Jackson, C.L. (2011). ARF family G proteins and their regulators: roles in membrane transport, development and disease. Nat Rev Mol Cell Biol *12*, 362-375.

Doroshow, D.B., Eder, J.P., and LoRusso, P.M. (2017). BET inhibitors: a novel epigenetic approach. Ann Oncol *28*, 1776-1787.

Dowden, H., and Munro, J. (2019). Trends in clinical success rates and therapeutic focus. Nat Rev Drug Discov *18*, 495-496.

Drebin, J.A., Hartzell, S.W., Griffin, C., Campbell, M.J., and Niederhuber, J.E. (1995). Molecular cloning and chromosomal localization of the human homologue of a B-lymphocyte specific protein tyrosine kinase (blk). Oncogene *10*, 477-486.

Drew, Y. (2015). The development of PARP inhibitors in ovarian cancer: from bench to bedside. Br J Cancer *113 Suppl 1*, S3-9.

Ducker, C.E., Upson, J.J., French, K.J., and Smith, C.D. (2005). Two N-myristoyltransferase isozymes play unique roles in protein myristoylation, proliferation, and apoptosis. Mol Cancer Res *3*, 463-476.

Dyda, F., Klein, D.C., and Hickman, A.B. (2000). GCN5-related N-acetyltransferases: a structural overview. Annu Rev Biophys Biomol Struct *29*, 81-103.

Ebara, S., Naito, H., Nakazawa, K., Ishii, F., and Nakamura, M. (2005). FTR1335 is a novel synthetic inhibitor of Candida albicans N-myristoyltransferase with fungicidal activity. Biol Pharm Bull *28*, 591-595.

Ebiike, H., Masubuchi, M., Liu, P., Kawasaki, K.-i., Morikami, K., Sogabe, S., Hayase, M., Fujii, T., Sakata, K., Shindoh, H.*, et al.* (2002). Design and Synthesis of Novel Benzofurans as a New Class of Antifungal Agents Targeting Fungal N-Myristoyltransferase. Part 2. Bioorganic & Medicinal Chemistry *12*, 607-610.

Eischen, C.M., Weber, J.D., Roussel, M.F., Sherr, C.J., and Cleveland, J.L. (1999). Disruption of the ARF-Mdm2-p53 tumor suppressor pathway in Myc-induced lymphomagenesis. Genes Dev *13*, 2658-2669.
Elkon, R., Ugalde, A.P., and Agami, R. (2013). Alternative cleavage and polyadenylation: extent, regulation and function. Nat Rev Genet *14*, 496-506.
Elsey, J., Bubley, J.A., Zhu, L., Rao, S., Sasaki, M., Pollack, B.P., Yang, L., and Arbiser, J.L. (2019). Palladium based nanoparticles for the treatment of advanced melanoma. Sci Rep *9*, 3255.
End, D.W., Smets, G., Todd, A.V., Applegate, T.L., Fuery, C.J., Angibaud, P., Venet, M., Sanz, G., Poignet, H., Skrzat, S.*, et al.* (2001). Characterization of the Antitumor Effects of the Selective Farnesyl Protein Transferase Inhibitor R115777 in Vivo and in Vitro. Cancer Research *61*, 131-137.
Evan, G.I., Wyllie, A.H., Gilbert, C.S., Littlewood, T.D., Land, H., Brooks, M., Waters, C.M., Penn, L.Z., and Hancock, D.C. (1992). Induction of apoptosis in fibroblasts by c-myc protein. Cell *69*, 119-128.
Fabregat, A., Sidiropoulos, K., Viteri, G., Forner, O., Marin-Garcia, P., Arnau, V., D'Eustachio, P., Stein, L., and Hermjakob, H. (2017). Reactome pathway analysis: a high-performance in-memory approach. BMC Bioinformatics *18*, 142.
Fagnocchi, L., Cherubini, A., Hatsuda, H., Fasciani, A., Mazzoleni, S., Poli, V., Berno, V., Rossi, R.L., Reinbold, R., Endele, M.*, et al.* (2016). A Myc-driven self-reinforcing regulatory network maintains mouse embryonic stem cell identity. Nat Commun *7*, 11903.
Fagnocchi, L., and Zippo, A. (2017). Multiple Roles of MYC in Integrating Regulatory Networks of Pluripotent Stem Cells. Frontiers in Cell and Developmental Biology *5*.
Farrell, A.S., and Sears, R.C. (2014). MYC degradation. Cold Spring Harb Perspect Med *4*.
Fearon, E.R., and Vogelstein, B. (1990). A genetic model for colorectal tumorigenesis. Cell *61*, 759-767.
Felsted, R.L., Glover, C.J., and Hartman, K. (1995). Potential role of N-myristoyltransferase in cancer. J Natl Cancer Inst *87*, 1571-1573.
Ferrao, P.T., Bukczynska, E.P., Johnstone, R.W., and McArthur, G.A. (2012). Efficacy of CHK inhibitors as single agents in MYC-driven lymphoma cells. Oncogene *31*, 1661-1672.
Filippakopoulos, P., Qi, J., Picaud, S., Shen, Y., Smith, W.B., Fedorov, O., Morse, E.M., Keates, T., Hickman, T.T., Felletar, I.*, et al.* (2010). Selective inhibition of BET bromodomains. Nature *468*, 1067-1073.
Fong, P.C., Boss, D.S., Yap, T.A., Tutt, A., Wu, P., Mergui-Roelvink, M., Mortimer, P., Swaisland, H., Lau, A., O'Connor, M.J.*, et al.* (2009). Inhibition of Poly(ADP-Ribose) Polymerase in Tumors from BRCA Mutation Carriers. New England Journal of Medicine *361*, 123-134.
Foucquier, J., and Guedj, M. (2015). Analysis of drug combinations: current methodological landscape. Pharmacol Res Perspect *3*, e00149.
Frearson, J.A., Brand, S., McElroy, S.P., Cleghorn, L.A., Smid, O., Stojanovski, L., Price, H.P., Guther, M.L., Torrie, L.S., Robinson, D.A.*, et al.* (2010). N-myristoyltransferase inhibitors as new leads to treat sleeping sickness. Nature *464*, 728-732.
Frost, P., Moatamed, F., Hoang, B., Shi, Y., Gera, J., Yan, H., Frost, P., Gibbons, J., and Lichtenstein, A. (2004). In vivo antitumor effects of the mTOR inhibitor CCI-779 against human multiple myeloma cells in a xenograft model. Blood *104*, 4181-4187.
Gabay, M., Li, Y., and Felsher, D.W. (2014). MYC activation is a hallmark of cancer initiation and maintenance. Cold Spring Harb Perspect Med *4*.
Garcia-Cuellar, M.P., Fuller, E., Mathner, E., Breitinger, C., Hetzner, K., Zeitlmann, L., Borkhardt, A., and Slany, R.K. (2014). Efficacy of cyclin-dependent-kinase 9 inhibitors in a murine model of mixed-lineage leukemia. Leukemia *28*, 1427-1435.

Garnett, M.J., Edelman, E.J., Heidorn, S.J., Greenman, C.D., Dastur, A., Lau, K.W., Greninger, P., Thompson, I.R., Luo, X., Soares, J.*, et al.* (2012). Systematic identification of genomic markers of drug sensitivity in cancer cells. Nature *483*, 570-575.
Ghia, P., Scarfo, L., Pathiraja, K., Derosier, M., Small, K., and Patton, N. (2015). A Phase 3 Study to Evaluate the Efficacy and Safety of Dinaciclib Compared to Ofatumumab in Patients with Refractory Chronic Lymphocytic Leukemia. Blood *126*, 4171-4171.
Giang, D.K., and Cravatt, B.F. (1998). A second mammalian N-myristoyltransferase. J Biol Chem *273*, 6595-6598.
Globa, A.K., and Bamji, S.X. (2017). Protein palmitoylation in the development and plasticity of neuronal connections. Curr Opin Neurobiol *45*, 210-220.
Glover, C.J., Hartman, K.D., and Felsted, R.L. (1997). Human N-myristoyltransferase amino-terminal domain involved in targeting the enzyme to the ribosomal subcellular fraction. J Biol Chem *272*, 28680-28689.
Goel, S., DeCristo, M.J., McAllister, S.S., and Zhao, J.J. (2018). CDK4/6 Inhibition in Cancer: Beyond Cell Cycle Arrest. Trends Cell Biol *28*, 911-925.
Goldberg, J. (1998). Structural Basis for Activation of ARF GTPase: Mechanisms of Guanine Nucleotide Exchange and GTP–Myristoyl Switching. Cell *95*, 237-248.
Gomez-Roman, N., Grandori, C., Eisenman, R.N., and White, R.J. (2003). Direct activation of RNA polymerase III transcription by c-Myc. Nature *421*, 290-294.
Goncalves, V., Brannigan, J.A., Whalley, D., Ansell, K.H., Saxty, B., Holder, A.A., Wilkinson, A.J., Tate, E.W., and Leatherbarrow, R.J. (2012). Discovery of Plasmodium vivax N-myristoyltransferase inhibitors: screening, synthesis, and structural characterization of their binding mode. J Med Chem *55*, 3578-3582.
Goya Grocin, A., Serwa, R.A., Morales Sanfrutos, J., Ritzefeld, M., and Tate, E.W. (2019). Whole Proteome Profiling of N-Myristoyltransferase Activity and Inhibition Using Sortase A. Mol Cell Proteomics *18*, 115-126.
Grande, B.M., Gerhard, D.S., Jiang, A., Griner, N.B., Abramson, J.S., Alexander, T.B., Allen, H., Ayers, L.W., Bethony, J.M., Bhatia, K.*, et al.* (2019). Genome-wide discovery of somatic coding and non-coding mutations in pediatric endemic and sporadic Burkitt lymphoma. Blood, blood-2018-2009-871418.
Grandori, C., Gomez-Roman, N., Felton-Edkins, Z.A., Ngouenet, C., Galloway, D.A., Eisenman, R.N., and White, R.J. (2005). c-Myc binds to human ribosomal DNA and stimulates transcription of rRNA genes by RNA polymerase I. Nat Cell Biol *7*, 311-318.
Green, D.R. (2005). Apoptic Pathways: Ten Minutes to Dead. Cell *121*, 671-674.
Gregersen, L.H., Mitter, R., Ugalde, A.P., Nojima, T., Proudfoot, N.J., Agami, R., Stewart, A., and Svejstrup, J.Q. (2019). SCAF4 and SCAF8, mRNA Anti-Terminator Proteins. Cell.
Gregory, M.A., and Hann, S.R. (2000). c-Myc Proteolysis by the Ubiquitin-Proteasome Pathway: Stabilization of c-Myc in Burkitt's Lymphoma Cells. Molecular and Cellular Biology *20*, 2423-2435.
Gunaratne, R.S., Sajid, M., Ling, I.T., Tripathi, R., Pachebat, J.A., and Holder, A.A. (2000). Characterization of N-myristoyltransferase from Plasmodium falciparum. The Biochemical journal *348 Pt 2*, 459-463.
Haibe-Kains, B., El-Hachem, N., Birkbak, N.J., Jin, A.C., Beck, A.H., Aerts, H.J., and Quackenbush, J. (2013). Inconsistency in large pharmacogenomic studies. Nature *504*, 389-393.
Hanahan, D., and Weinberg, R.A. (2011). Hallmarks of cancer: the next generation. Cell *144*, 646-674.
Hart, L.S., Cunningham, J.T., Datta, T., Dey, S., Tameire, F., Lehman, S.L., Qiu, B., Zhang, H., Cerniglia, G., Bi, M.*, et al.* (2012). ER stress-mediated autophagy promotes Myc-dependent transformation and tumor growth. J Clin Invest *122*, 4621-4634.
Hart, T., Brown, K.R., Sircoulomb, F., Rottapel, R., and Moffat, J. (2014). Measuring error rates in genomic perturbation screens: gold standards for human functional genomics. Mol Syst Biol *10*, 733.

Hatton, K.S., Mahon, K., Chin, L., Chiu, F.C., Lee, H.W., Peng, D., Morgenbesser, S.D., Horner, J., and DePinho, R.A. (1996). Expression and activity of L-Myc in normal mouse development. Molecular and Cellular Biology *16*, 1794-1804.
Haverty, P.M., Lin, E., Tan, J., Yu, Y., Lam, B., Lianoglou, S., Neve, R.M., Martin, S., Settleman, J., Yauch, R.L.*, et al.* (2016). Reproducible pharmacogenomic profiling of cancer cell line panels. Nature *533*, 333-337.
Heal, W.P., Wright, M.H., Thinon, E., and Tate, E.W. (2011). Multifunctional protein labeling via enzymatic N-terminal tagging and elaboration by click chemistry. Nat Protoc *7*, 105-117.
Hermeking, H., and Eick, D. (1994). Mediation of c-Myc-induced apoptosis by p53. Science *265*, 2091-2093.
Hetz, C. (2012). The unfolded protein response: controlling cell fate decisions under ER stress and beyond. Nat Rev Mol Cell Biol *13*, 89-102.
Heyn, H., Vidal, E., Ferreira, H.J., Vizoso, M., Sayols, S., Gomez, A., Moran, S., Boque-Sastre, R., Guil, S., Martinez-Cardus, A.*, et al.* (2016). Epigenomic analysis detects aberrant super-enhancer DNA methylation in human cancer. Genome Biol *17*, 11.
Hill, K., Model, K., Ryan, M.T., Dietmeier, K., Wagner, R., and Pfanner, N. (1998). Tom40 forms a hydrophilic channel of the mitochondrial import pore for preproteins. Nature *395*, 516-521.
Honda, T., Soeda, S., Tsuda, K., Yamaguchi, C., Aoyama, K., Morinaga, T., Yuki, R., Nakayama, Y., Yamaguchi, N., and Yamaguchi, N. (2016). Protective role for lipid modifications of Src-family kinases against chromosome missegregation. Sci Rep *6*, 38751.
Hoque, M., Ji, Z., Zheng, D., Luo, W., Li, W., You, B., Park, J.Y., Yehia, G., and Tian, B. (2013). Analysis of alternative cleavage and polyadenylation by 3' region extraction and deep sequencing. Nat Methods *10*, 133-139.
Horiuchi, D., Kusdra, L., Huskey, N.E., Chandriani, S., Lenburg, M.E., Gonzalez-Angulo, A.M., Creasman, K.J., Bazarov, A.V., Smyth, J.W., Davis, S.E.*, et al.* (2012). MYC pathway activation in triple-negative breast cancer is synthetic lethal with CDK inhibition. J Exp Med *209*, 679-696.
Hornbeck, P.V., Zhang, B., Murray, B., Kornhauser, J.M., Latham, V., and Skrzypek, E. (2015). PhosphoSitePlus, 2014: mutations, PTMs and recalibrations. Nucleic Acids Res *43*, D512-520.
Hsu, T.Y., Simon, L.M., Neill, N.J., Marcotte, R., Sayad, A., Bland, C.S., Echeverria, G.V., Sun, T., Kurley, S.J., Tyagi, S.*, et al.* (2015). The spliceosome is a therapeutic vulnerability in MYC-driven cancer. Nature *525*, 384-388.
Hu, S., Marineau, J.J., Rajagopal, N., Hamman, K.B., Choi, Y.J., Schmidt, D.R., Ke, N., Johannessen, L., Bradley, M.J., Orlando, D.A.*, et al.* (2019). Discovery and characterization of SY-1365, a selective, covalent inhibitor of CDK7. Cancer Research, canres.0119.2019.
Huang, M., and Weiss, W.A. (2013). Neuroblastoma and MYCN. Cold Spring Harb Perspect Med *3*, a014415.
Humphrey, R.W., Brockway-Lunardi, L.M., Bonk, D.T., Dohoney, K.M., Doroshow, J.H., Meech, S.J., Ratain, M.J., Topalian, S.L., and Pardoll, D.M. (2011). Opportunities and challenges in the development of experimental drug combinations for cancer. J Natl Cancer Inst *103*, 1222-1226.
Iorio, F., Knijnenburg, T.A., Vis, D.J., Bignell, G.R., Menden, M.P., Schubert, M., Aben, N., Goncalves, E., Barthorpe, S., Lightfoot, H.*, et al.* (2016). A Landscape of Pharmacogenomic Interactions in Cancer. Cell *166*, 740-754.
Ise, W., Fujii, K., Shiroguchi, K., Ito, A., Kometani, K., Takeda, K., Kawakami, E., Yamashita, K., Suzuki, K., Okada, T.*, et al.* (2018). T Follicular Helper Cell-Germinal Center B Cell Interaction Strength Regulates Entry into Plasma Cell or Recycling Germinal Center Cell Fate. Immunity *48*, 702-715 e704.

Jiang, H., Zhang, X., Chen, X., Aramsangtienchai, P., Tong, Z., and Lin, H. (2018). Protein Lipidation: Occurrence, Mechanisms, Biological Functions, and Enabling Technologies. Chem Rev *118*, 919-988.
Jiang, X., Lu, X., McNamara, G., Liu, X., Cubedo, E., Sarosiek, K.A., Sanchez-Garcia, I., Helfman, D.M., and Lossos, I.S. (2010). HGAL, a germinal center specific protein, decreases lymphoma cell motility by modulation of the RhoA signaling pathway. Blood *116*, 5217-5227.
Jorda, R., Hendrychova, D., Voller, J., Reznickova, E., Gucky, T., and Krystof, V. (2018). How Selective Are Pharmacological Inhibitors of Cell-Cycle-Regulating Cyclin-Dependent Kinases? J Med Chem *61*, 9105-9120.
Kaida, D., Berg, M.G., Younis, I., Kasim, M., Singh, L.N., Wan, L., and Dreyfuss, G. (2010). U1 snRNP protects pre-mRNAs from premature cleavage and polyadenylation. Nature *468*, 664-668.
Kalkat, M., De Melo, J., Hickman, K.A., Lourenco, C., Redel, C., Resetca, D., Tamachi, A., Tu, W.B., and Penn, L.Z. (2017). MYC Deregulation in Primary Human Cancers. Genes (Basel) *8*.
Kallemeijn, W.W., Lueg, G.A., Faronato, M., Hadavizadeh, K., Goya Grocin, A., Song, O.R., Howell, M., Calado, D.P., and Tate, E.W. (2019). Validation and Invalidation of Chemical Probes for the Human N-myristoyltransferases. Cell Chem Biol.
Kanehisa, M., Furumichi, M., Tanabe, M., Sato, Y., and Morishima, K. (2016). KEGG: new perspectives on genomes, pathways, diseases and drugs. Nucleic Acids Research *45*, D353-D361.
Kang, J., Sergio, C.M., Sutherland, R.L., and Musgrove, E.A. (2014). Targeting cyclin-dependent kinase 1 (CDK1) but not CDK4/6 or CDK2 is selectively lethal to MYC-dependent human breast cancer cells. BMC Cancer *14*, 32.
Kaplan, J.H. (2002). Biochemistry of Na,K-ATPase. Annu Rev Biochem *71*, 511-535.
Kay, N.E., Sassoon, T., Secreto, C., Sinha, S., Shanafelt, T.D., Ghosh, A.K., and Arbiser, J.L. (2016). Tris (dibenzylideneacetone) dipalladium: a small-molecule palladium complex is effective in inducing apoptosis in chronic lymphocytic leukemia B-cells. Leuk Lymphoma *57*, 2409-2416.
Kim, S., Alsaidan, O.A., Goodwin, O., Li, Q., Sulejmani, E., Han, Z., Bai, A., Albers, T., Beharry, Z., Zheng, Y.G.G.*, et al.* (2017). Blocking myristoylation of Src inhibits its kinase activity and suppresses prostate cancer progression. Cancer Res.
Kimura, A., Kato, Y., and Hirano, H. (2012). N-myristoylation of the Rpt2 subunit regulates intracellular localization of the yeast 26S proteasome. Biochemistry *51*, 8856-8866.
Koegl, M., Zlatkine, P., Ley, S.C., Courtneidge, S.A., and Magee, A.I. (1994). Palmitoylation of multiple Src-family kinases at a homologous N-terminal motif. Biochemical Journal *303*, 749-753.
Koh, C.M., Bezzi, M., Low, D.H., Ang, W.X., Teo, S.X., Gay, F.P., Al-Haddawi, M., Tan, S.Y., Osato, M., Sabo, A.*, et al.* (2015). MYC regulates the core pre-mRNA splicing machinery as an essential step in lymphomagenesis. Nature *523*, 96-100.
Kortlever, R.M., Sodir, N.M., Wilson, C.H., Burkhart, D.L., Pellegrinet, L., Brown Swigart, L., Littlewood, T.D., and Evan, G.I. (2017). Myc Cooperates with Ras by Programming Inflammation and Immune Suppression. Cell *171*, 1301-1315 e1314.
Kudo, N., Perseghini, M., and Fu, G.C. (2006). A Versatile Method for Suzuki Cross-Coupling Reactions of Nitrogen Heterocycles. Angewandte Chemie International Edition *45*, 1282-1284.
Kukurba, K.R., and Montgomery, S.B. (2015). RNA Sequencing and Analysis. Cold Spring Harbor protocols *2015*, 951-969.
Kwiatkowski, N., Zhang, T., Rahl, P.B., Abraham, B.J., Reddy, J., Ficarro, S.B., Dastur, A., Amzallag, A., Ramaswamy, S., Tesar, B.*, et al.* (2014). Targeting transcription regulation in cancer with a covalent CDK7 inhibitor. Nature *511*, 616-620.

Lamb, J., Crawford, E.D., Peck, D., Modell, J.W., Blat, I.C., Wrobel, M.J., Lerner, J., Brunet, J.-P., Subramanian, A., Ross, K.N.*, et al.* (2006). The Connectivity Map: Using Gene-Expression Signatures to Connect Small Molecules, Genes, and Disease. Science *313*, 1929-1935.
Land, H., Parada, L.F., and Weinberg, R.A. (1983). Tumorigenic conversion of primary embryo fibroblasts requires at least two cooperating oncogenes. Nature *304*, 596-602.
Lanyon-Hogg, T., Faronato, M., Serwa, R.A., and Tate, E.W. (2017). Dynamic Protein Acylation: New Substrates, Mechanisms, and Drug Targets. Trends Biochem Sci *42*, 566-581.
Lawrence, M.S., Stojanov, P., Polak, P., Kryukov, G.V., Cibulskis, K., Sivachenko, A., Carter, S.L., Stewart, C., Mermel, C.H., Roberts, S.A.*, et al.* (2013). Mutational heterogeneity in cancer and the search for new cancer-associated genes. Nature *499*, 214-218.
Lee, D.H. (2017). Treatments for EGFR-mutant non-small cell lung cancer (NSCLC): The road to a success, paved with failures. Pharmacol Ther *174*, 1-21.
Lee, S.H., Singh, I., Tisdale, S., Abdel-Wahab, O., Leslie, C.S., and Mayr, C. (2018). Widespread intronic polyadenylation inactivates tumour suppressor genes in leukaemia. Nature *561*, 127-131.
Lee, Y., Yu, Y., Gunawardena, H., Xie, L., and Chen, X. (2012). BCLAF1 is a radiation-induced H2AX-interacting partner involved in cH2AX-mediated regulation of apoptosis and DNA repair. Cell Death and Disease *3*.
Lerner, E.C., Qian, Y., Blaskovich, M.A., Fossum, R.D., Vogt, A., Sun, J., Cox, A.D., Der, C.J., Hamilton, A.D., and Sebti, S.M. (1995). Ras CAAX peptidomimetic FTI-277 selectively blocks oncogenic Ras signaling by inducing cytoplasmic accumulation of inactive Ras-Raf complexes. J Biol Chem *270*, 26802-26806.
Li, B., and Dewey, C.N. (2011). RSEM: accurate transcript quantification from RNA-Seq data with or without a reference genome. BMC Bioinformatics *12*, 323.
Liang, J., Xu, Z.X., Ding, Z., Lu, Y., Yu, Q., Werle, K.D., Zhou, G., Park, Y.Y., Peng, G., Gambello, M.J.*, et al.* (2015). Myristoylation confers noncanonical AMPK functions in autophagy selectivity and mitochondrial surveillance. Nat Commun *6*, 7926.
Liberzon, A., Birger, C., Thorvaldsdottir, H., Ghandi, M., Mesirov, J.P., and Tamayo, P. (2015). The Molecular Signatures Database (MSigDB) hallmark gene set collection. Cell Syst *1*, 417-425.
Liberzon, A., Subramanian, A., Pinchback, R., Thorvaldsdóttir, H., Tamayo, P., and Mesirov, J.P. (2011). Molecular signatures database (MSigDB) 3.0. Bioinformatics *27*, 1739-1740.
Lim, S., and Kaldis, P. (2013). Cdks, cyclins and CKIs: roles beyond cell cycle regulation. Development *140*, 3079-3093.
Lim, S.G. (2016). Elucidating the roles of N-myristoyltranferase in cancers. In Department of Chemistry (Imperial College London).
Lin, C.Y., Loven, J., Rahl, P.B., Paranal, R.M., Burge, C.B., Bradner, J.E., Lee, T.I., and Young, R.A. (2012). Transcriptional amplification in tumor cells with elevated c-Myc. Cell *151*, 56-67.
Lin, R., Connolly, P.J., Huang, S., Wetter, S.K., Lu, Y., Murray, W.V., Emanuel, S.L., Gruninger, R.H., Fuentes-Pesquera, A.R., Rugg, C.A.*, et al.* (2005). 1-Acyl-1H-[1,2,4]triazole-3,5-diamine analogues as novel and potent anticancer cyclin-dependent kinase inhibitors: synthesis and evaluation of biological activities. J Med Chem *48*, 4208-4211.
Litichevskiy, L., Peckner, R., Abelin, J.G., Asiedu, J.K., Creech, A.L., Davis, J.F., Davison, D., Dunning, C.M., Egertson, J.D., Egri, S.*, et al.* (2018). A Library of Phosphoproteomic and Chromatin Signatures for Characterizing Cellular Responses to Drug Perturbations. Cell Syst *6*, 424-443 e427.

Liu, J., Xu, Y., Stoleru, D., and Salic, A. (2012). Imaging protein synthesis in cells and tissues with an alkyne analog of puromycin. Proc Natl Acad Sci U S A *109*, 413-418.
Liu, Y., Mi, Y., Mueller, T., Kreibich, S., Williams, E.G., Van Drogen, A., Borel, C., Frank, M., Germain, P.L., Bludau, I.*, et al.* (2019). Multi-omic measurements of heterogeneity in HeLa cells across laboratories. Nat Biotechnol *37*, 314-322.
Liu, Z., Yang, T., Li, X., Peng, T., Hang, H.C., and Li, X.D. (2015). Integrative chemical biology approaches for identification and characterization of "erasers" for fatty-acid-acylated lysine residues within proteins. Angew Chem Int Ed Engl *54*, 1149-1152.
Lodge, J.K., Jackson-Machelski, E., Toffaletti, D.L., Perfect, J.R., and Gordon, J.I. (1994). Targeted gene replacement demonstrates that myristoyl-CoA: protein N-myristoyltransferase is essential for viability of Cryptococcus neoformans. Proceedings of the National Academy of Sciences *91*, 12008-12012.
Lossos, I.S., Alizadeh, A.A., Rajapaksa, R., Tibshirani, R., and Levy, R. (2003). HGAL is a novel interleukin-4-inducible gene that strongly predicts survival in diffuse large B-cell lymphoma. Blood *101*, 433-440.
Love, C., Sun, Z., Jima, D., Li, G., Zhang, J., Miles, R., Richards, K.L., Dunphy, C.H., Choi, W.W., Srivastava, G.*, et al.* (2012). The genetic landscape of mutations in Burkitt lymphoma. Nat Genet *44*, 1321-1325.
Love, M.I., Huber, W., and Anders, S. (2014). Moderated estimation of fold change and dispersion for RNA-seq data with DESeq2. Genome Biol *15*, 550.
Loven, J., Hoke, H.A., Lin, C.Y., Lau, A., Orlando, D.A., Vakoc, C.R., Bradner, J.E., Lee, T.I., and Young, R.A. (2013). Selective inhibition of tumor oncogenes by disruption of super-enhancers. Cell *153*, 320-334.
MacDonald, B.T., Tamai, K., and He, X. (2009). Wnt/beta-catenin signaling: components, mechanisms, and diseases. Dev Cell *17*, 9-26.
Malumbres, M. (2014). Cyclin-dependent kinases. Genome biology *15*, 122-122.
Mammana A, H.J. (2019). bamsignals: Extract read count signals from bam files.
Manier, S., Huynh, D., Shen, Y.J., Zhou, J., Yusufzai, T., Salem, K.Z., Ebright, R.Y., Shi, J., Park, J., Glavey, S.V.*, et al.* (2017). Inhibiting the oncogenic translation program is an effective therapeutic strategy in multiple myeloma. Science Translational Medicine *9*, eaal2668.
Marshall, H.T., and Djamgoz, M.B.A. (2018). Immuno-Oncology: Emerging Targets and Combination Therapies. Front Oncol *8*, 315.
Martin, D.D., Beauchamp, E., and Berthiaume, L.G. (2011). Post-translational myristoylation: Fat matters in cellular life and death. Biochimie *93*, 18-31.
Martinez, A., Traverso, J.A., Valot, B., Ferro, M., Espagne, C., Ephritikhine, G., Zivy, M., Giglione, C., and Meinnel, T. (2008). Extent of N-terminal modifications in cytosolic proteins from eukaryotes. Proteomics *8*, 2809-2831.
Masubuchi, M., Ebiike, H., Kawasaki, K.-i., Sogabe, S., Morikami, K., Shiratori, Y., Tsujii, S., Fujii, T., Sakata, K., Hayase, M.*, et al.* (2003). Synthesis and biological activities of benzofuran antifungal agents targeting fungal N-myristoyltransferase. Bioorganic & Medicinal Chemistry *11*, 4463-4478.
Masubuchi, M., Kawasaki, K.-i., Ebiike, H., Ikeda, Y., Tsujii, S., Sogabe, S., Fujii, T., Sakata, K., Shiratori, Y., Aoki, Y.*, et al.* (2001). Design and Synthesis of Novel Benzofurans as a New Class of Antifungal Agents Targeting Fungal N-Myristoyltransferase. Part 1. Bioorganic & Medicinal Chemistry *11*, 1833-1837.
Mathieson, T., Franken, H., Kosinski, J., Kurzawa, N., Zinn, N., Sweetman, G., Poeckel, D., Ratnu, V.S., Schramm, M., Becher, I.*, et al.* (2018). Systematic analysis of protein turnover in primary cells. Nat Commun *9*, 689.
Maurer-Stroh, S., Eisenhaber, B., and Eisenhaber, F. (2002a). N-terminal N-myristoylation of proteins: prediction of substrate proteins from amino acid sequence11Edited by J. Thornton. Journal of Molecular Biology *317*, 541-557.

Maurer-Stroh, S., Eisenhaber, B., and Eisenhaber, F. (2002b). N-terminal N-myristoylation of proteins: refinement of the sequence motif and its taxon-specific differences11Edited by J. Thornton. Journal of Molecular Biology *317*, 523-540.
McIlhinney, R.A., Young, K., Egerton, M., Camble, R., White, A., and Soloviev, M. (1998). Characterization of human and rat brain myristoyl-CoA:protein N-myristoyltransferase: evidence for an alternative splice variant of the enzyme. The Biochemical journal *333 (Pt 3)*, 491-495.
McKeown, M.R., and Bradner, J.E. (2014). Therapeutic strategies to inhibit MYC. Cold Spring Harb Perspect Med *4*.
McMahon, S.B., Wood, M.A., and Cole, M.D. (2000). The essential cofactor TRRAP recruits the histone acetyltransferase hGCN5 to c-Myc. Mol Cell Biol *20*, 556-562.
Merico, D., Isserlin, R., Stueker, O., Emili, A., and Bader, G.D. (2010). Enrichment map: a network-based method for gene-set enrichment visualization and interpretation. PLoS One *5*, e13984.
Mertz, J.A., Conery, A.R., Bryant, B.M., Sandy, P., Balasubramanian, S., Mele, D.A., Bergeron, L., and Sims III, R.J. (2011). Targeting MYC dependence in cancer by inhibiting BET bromodomains. Proceedings of the National Academy of Sciences *108*, 16669-16674.
Meyer, N., and Penn, L.Z. (2008). Reflecting on 25 years with MYC. Nat Rev Cancer *8*, 976-990.
Meyers, R.M., Bryan, J.G., McFarland, J.M., Weir, B.A., Sizemore, A.E., Xu, H., Dharia, N.V., Montgomery, P.G., Cowley, G.S., Pantel, S.*, et al.* (2017). Computational correction of copy number effect improves specificity of CRISPR-Cas9 essentiality screens in cancer cells. Nat Genet *49*, 1779-1784.
Mikulasova, A., Ashby, C.C., Tytarenko, R.G., Bauer, M., Mavrommatis, K., Wardell, C.P., Trotter, M., Deshpande, S., Stephens, O.W., Tian, E.*, et al.* (2017). MYC Rearrangements in Multiple Myeloma Are Complex, Can Involve More Than Five Different Chromosomes, and Correlate with Increased Expression of MYC and a Distinct Downstream Gene Expression Pattern. Blood *130*, 65-65.
Mousnier, A., Bell, A.S., Swieboda, D.P., Morales-Sanfrutos, J., Pérez-Dorado, I., Brannigan, J.A., Newman, J., Ritzefeld, M., Hutton, J.A., Guedán, A.*, et al.* (2018). Fragment-derived inhibitors of human N-myristoyltransferase block capsid assembly and replication of the common cold virus. Nature Chemistry.
Murga, M., Campaner, S., Lopez-Contreras, A.J., Toledo, L.I., Soria, R., Montana, M.F., Artista, L., Schleker, T., Guerra, C., Garcia, E.*, et al.* (2011). Exploiting oncogene-induced replicative stress for the selective killing of Myc-driven tumors. Nat Struct Mol Biol *18*, 1331-1335.
Murphy, D.J., Junttila, M.R., Pouyet, L., Karnezis, A., Shchors, K., Bui, D.A., Brown-Swigart, L., Johnson, L., and Evan, G.I. (2008). Distinct thresholds govern Myc's biological output in vivo. Cancer Cell *14*, 447-457.
Nakagawa, M., Koyanagi, M., Tanabe, K., Takahashi, K., Ichisaka, T., Aoi, T., Okita, K., Mochiduki, Y., Takizawa, N., and Yamanaka, S. (2008). Generation of induced pluripotent stem cells without Myc from mouse and human fibroblasts. Nat Biotechnol *26*, 101-106.
Nie, Z., Hu, G., Wei, G., Cui, K., Yamane, A., Resch, W., Wang, R., Green, D.R., Tessarollo, L., Casellas, R.*, et al.* (2012). c-Myc is a universal amplifier of expressed genes in lymphocytes and embryonic stem cells. Cell *151*, 68-79.
Nishimura, D. (2001). BioCarta. Biotech Software & Internet Report *2*, 117-120.
O'Reilly, D., Dienstbier, M., Cowley, S.A., Vazquez, P., Drozdz, M., Taylor, S., James, W.S., and Murphy, S. (2013). Differentially expressed, variant U1 snRNAs regulate gene expression in human cells. Genome Res *23*, 281-291.
Obeng, E.A., Chappell, R.J., Seiler, M., Chen, M.C., Campagna, D.R., Schmidt, P.J., Schneider, R.K., Lord, A.M., Wang, L., Gambe, R.G.*, et al.* (2016). Physiologic

Expression of Sf3b1(K700E) Causes Impaired Erythropoiesis, Aberrant Splicing, and Sensitivity to Therapeutic Spliceosome Modulation. Cancer Cell *30*, 404-417.
Oiseth, S.J., and Aziz, M.S. (2017). Cancer immunotherapy: a brief review of the history, possibilities, and challenges ahead. Journal of Cancer Metastasis and Treatment *3*.
Olson, C.M., Jiang, B., Erb, M.A., Liang, Y., Doctor, Z.M., Zhang, Z., Zhang, T., Kwiatkowski, N., Boukhali, M., Green, J.L.*, et al.* (2018). Pharmacological perturbation of CDK9 using selective CDK9 inhibition or degradation. Nat Chem Biol *14*, 163-170.
Ott, G., Rosenwald, A., and Campo, E. (2013). Understanding MYC-driven aggressive B-cell lymphomas: pathogenesis and classification. Blood *122*, 3884-3891.
Pajic, A., Spitkovsky, D., Christoph, B., Kempkes, B., Schuhmacher, M., Staege, M.S., Brielmeier, M., Ellwart, J., Kohlhuber, F., Bornkamm, G.W.*, et al.* (2000). Cell cycle activation by c-myc in a Burkitt lymphoma model cell line. International Journal of Cancer *87*, 787-793.
Palmer, A.C., and Sorger, P.K. (2017). Combination Cancer Therapy Can Confer Benefit via Patient-to-Patient Variability without Drug Additivity or Synergy. Cell *171*, 1678-1691 e1613.
Palsuledesai, C.C., and Distefano, M.D. (2015). Protein prenylation: enzymes, therapeutics, and biotechnology applications. ACS Chem Biol *10*, 51-62.
Pan, C., Olsen, J.V., Daub, H., and Mann, M. (2009). Global effects of kinase inhibitors on signaling networks revealed by quantitative phosphoproteomics. Mol Cell Proteomics *8*, 2796-2808.
Park, M.H., and Hong, J.T. (2016). Roles of NF-κB in Cancer and Inflammatory Diseases and Their Therapeutic Approaches. Cells *5*, 15.
Parrish, A.B., Freel, C.D., and Kornbluth, S. (2013). Cellular mechanisms controlling caspase activation and function. Cold Spring Harb Perspect Biol *5*.
Parry, D., Guzi, T., Shanahan, F., Davis, N., Prabhavalkar, D., Wiswell, D., Seghezzi, W., Paruch, K., Dwyer, M.P., Doll, R.*, et al.* (2010). Dinaciclib (SCH 727965), a Novel and Potent Cyclin-Dependent Kinase Inhibitor. Molecular Cancer Therapeutics *9*, 2344-2353.
Patel, H., Periyasamy, M., Sava, G.P., Bondke, A., Slafer, B.W., Kroll, S.H.B., Barbazanges, M., Starkey, R., Ottaviani, S., Harrod, A.*, et al.* (2018a). ICEC0942, an Orally Bioavailable Selective Inhibitor of CDK7 for Cancer Treatment. Mol Cancer Ther *17*, 1156-1166.
Patel, H., Periyasamy, M., Sava, G.P., Bondke, A., Slafer, B.W., Kroll, S.H.B., Barbazanges, M., Starkey, R., Ottaviani, S., Harrod, A.*, et al.* (2018b). ICEC0942, an Orally Bioavailable Selective Inhibitor of CDK7 for Cancer Treatment. Molecular Cancer Therapeutics *17*, 1156-1166.
Patterson, S.E., Liu, R., Statz, C.M., Durkin, D., Lakshminarayana, A., and Mockus, S.M. (2016). The clinical trial landscape in oncology and connectivity of somatic mutational profiles to targeted therapies. Hum Genomics *10*, 4.
Patwardhan, P., and Resh, M.D. (2010). Myristoylation and membrane binding regulate c-Src stability and kinase activity. Mol Cell Biol *30*, 4094-4107.
Paul, F., Arkin, Y., Giladi, A., Jaitin, D.A., Kenigsberg, E., Keren-Shaul, H., Winter, D., Lara-Astiaso, D., Gury, M., Weiner, A.*, et al.* (2015). Transcriptional Heterogeneity and Lineage Commitment in Myeloid Progenitors. Cell *163*, 1663-1677.
Payne, G.S., Bishop, J.M., and Varmus, H.E. (1982). Multiple arrangements of viral DNA and an activated host oncogene in bursal lymphomas. Nature *295*, 209-214.
Perez-Roger, I., Kim, S.H., Griffiths, B., Sewing, A., and Land, H. (1999). Cyclins D1 and D2 mediate myc-induced proliferation via sequestration of p27(Kip1) and p21(Cip1). Embo j *18*, 5310-5320.
Pervaiz, M., Mishra, P., and Gunther, S. (2018). Bromodomain Drug Discovery - the Past, the Present, and the Future. Chem Rec *18*, 1808-1817.

Petri, S., Grimmler, M., Over, S., Fischer, U., and Gruss, O.J. (2007). Dephosphorylation of survival motor neurons (SMN) by PPM1G/PP2Cgamma governs Cajal body localization and stability of the SMN complex. J Cell Biol *179*, 451-465.
Poli, V., Fagnocchi, L., Fasciani, A., Cherubini, A., Mazzoleni, S., Ferrillo, S., Miluzio, A., Gaudioso, G., Vaira, V., Turdo, A.*, et al.* (2018). MYC-driven epigenetic reprogramming favors the onset of tumorigenesis by inducing a stem cell-like state. Nat Commun *9*, 1024.
Price, H.P., Menon, M.R., Panethymitaki, C., Goulding, D., McKean, P.G., and Smith, D.F. (2003). Myristoyl-CoA:protein N-myristoyltransferase, an essential enzyme and potential drug target in kinetoplastid parasites. J Biol Chem *278*, 7206-7214.
Rahl, P.B., Lin, C.Y., Seila, A.C., Flynn, R.A., McCuine, S., Burge, C.B., Sharp, P.A., and Young, R.A. (2010). c-Myc regulates transcriptional pause release. Cell *141*, 432-445.
Rajala, R.V., Datla, R.S., Carlsen, S.A., Anderson, D.H., Qi, Z., Wang, J.H., and Sharma, R.K. (2001). Phosphorylation of human N-myristoyltransferase by N-myristoylated SRC family tyrosine kinase members. Biochem Biophys Res Commun *288*, 233-239.
Rakhra, K., Bachireddy, P., Zabuawala, T., Zeiser, R., Xu, L., Kopelman, A., Fan, A.C., Yang, Q., Braunstein, L., Crosby, E.*, et al.* (2010). CD4(+) T cells contribute to the remodeling of the microenvironment required for sustained tumor regression upon oncogene inactivation. Cancer Cell *18*, 485-498.
Rampoldi, F., Bonrouhi, M., Boehm, M.E., Lehmann, W.D., Popovic, Z.V., Kaden, S., Federico, G., Brunk, F., Grone, H.J., and Porubsky, S. (2015). Immunosuppression and Aberrant T Cell Development in the Absence of N-Myristoylation. J Immunol *195*, 4228-4243.
Rampoldi, F., Brunk, F., Bonrouhi, M., Federico, G., Krunic, D., Porubsky, S., Gröne, H.-J., and Popovic, Z.V. (2017). Deficiency of N-myristoylation reveals calcineurin activity as regulator of IFN-γ-producing γδ T cells. Journal of Leukocyte Biology, jlb.1A0616-0264R.
Reddy, A., Zhang, J., Davis, N.S., Moffitt, A.B., Love, C.L., Waldrop, A., Leppa, S., Pasanen, A., Meriranta, L., Karjalainen-Lindsberg, M.L.*, et al.* (2017). Genetic and Functional Drivers of Diffuse Large B Cell Lymphoma. Cell *171*, 481-494 e415.
Reimand, J., Isserlin, R., Voisin, V., Kucera, M., Tannus-Lopes, C., Rostamianfar, A., Wadi, L., Meyer, M., Wong, J., Xu, C.*, et al.* (2019). Pathway enrichment analysis and visualization of omics data using g:Profiler, GSEA, Cytoscape and EnrichmentMap. Nat Protoc *14*, 482-517.
Reimand, J., Kull, M., Peterson, H., Hansen, J., and Vilo, J. (2007). g:Profiler--a web-based toolset for functional profiling of gene lists from large-scale experiments. Nucleic acids research *35*, W193-W200.
Resh, M.D. (1999). Fatty acylation of proteins: new insights into membrane targeting of myristoylated and palmitoylated proteins. Biochimica et Biophysica Acta (BBA) - Molecular Cell Research *1451*, 1-16.
Resh, M.D. (2006). Trafficking and signaling by fatty-acylated and prenylated proteins. Nat Chem Biol *2*, 584-590.
Resh, M.D. (2012). Targeting protein lipidation in disease. Trends Mol Med *18*, 206-214.
Resh, M.D. (2017). Palmitoylation of proteins in cancer. Biochemical Society Transactions *45*, 409-416.
Rickert, R.C. (2013). New insights into pre-BCR and BCR signalling with relevance to B cell malignancies. Nat Rev Immunol *13*, 578-591.
Rickman, D.S., Schulte, J.H., and Eilers, M. (2018). The Expanding World of N-MYC–Driven Tumors. Cancer Discovery *8*, 150-163.
Riedell, P.A., and Smith, S.M. (2018). Double hit and double expressors in lymphoma: Definition and treatment. Cancer *124*, 4622-4632.
Riley, N.M., and Coon, J.J. (2016). Phosphoproteomics in the Age of Rapid and Deep Proteome Profiling. Anal Chem *88*, 74-94.

Rocque, W.J., McWherter, C.A., Wood, D.C., and Gordon, J.I. (1993). A comparative analysis of the kinetic mechanism and peptide substrate specificity of human and Saccharomyces cerevisiae myristoyl-CoA:protein N-myristoyltransferase. J Biol Chem *268*, 9964-9971.
Rodgers, U.R., Lanyon-Hogg, T., Masumoto, N., Ritzefeld, M., Burke, R., Blagg, J., Magee, A.I., and Tate, E.W. (2016). Characterization of Hedgehog Acyltransferase Inhibitors Identifies a Small Molecule Probe for Hedgehog Signaling by Cancer Cells. ACS Chem Biol *11*, 3256-3262.
Rogers, S., Wells, R., and Rechsteiner, M. (1986). Amino acid sequences common to rapidly degraded proteins: the PEST hypothesis. Science *234*, 364-368.
Romero-Camarero, I., Jiang, X., Natkunam, Y., Lu, X., Vicente-Duenas, C., Gonzalez-Herrero, I., Flores, T., Garcia, J.L., McNamara, G., Kunder, C.*, et al.* (2013). Germinal centre protein HGAL promotes lymphoid hyperplasia and amyloidosis via BCR-mediated Syk activation. Nat Commun *4*, 1338.
Rose, A.S., Bradley, A.R., Valasatava, Y., Duarte, J.M., Prlic, A., and Rose, P.W. (2018). NGL viewer: web-based molecular graphics for large complexes. Bioinformatics *34*, 3755-3758.
Rudnick, D.A., McWherter, C.A., Rocque, W.J., Lennon, P.J., Getman, D.P., and Gordon, J.I. (1991). Kinetic and structural evidence for a sequential ordered Bi Bi mechanism of catalysis by Saccharomyces cerevisiae myristoyl-CoA:protein N-myristoyltransferase. J Biol Chem *266*, 9732-9739.
Sabo, A., Kress, T.R., Pelizzola, M., de Pretis, S., Gorski, M.M., Tesi, A., Morelli, M.J., Bora, P., Doni, M., Verrecchia, A.*, et al.* (2014). Selective transcriptional regulation by Myc in cellular growth control and lymphomagenesis. Nature *511*, 488-492.
Sanchez-Vega, F., Mina, M., Armenia, J., Chatila, W.K., Luna, A., La, K.C., Dimitriadoy, S., Liu, D.L., Kantheti, H.S., Saghafinia, S.*, et al.* (2018). Oncogenic Signaling Pathways in The Cancer Genome Atlas. Cell *173*, 321-337 e310.
Santo, L., Vallet, S., Hideshima, T., Cirstea, D., Ikeda, H., Pozzi, S., Patel, K., Okawa, Y., Gorgun, G., Perrone, G.*, et al.* (2010). AT7519, A novel small molecule multi-cyclin-dependent kinase inhibitor, induces apoptosis in multiple myeloma via GSK-3beta activation and RNA polymerase II inhibition. Oncogene *29*, 2325-2336.
Santoni-Rugiu, E., Falck, J., Mailand, N., Bartek, J., and Lukas, J. (2000). Involvement of Myc activity in a G(1)/S-promoting mechanism parallel to the pRb/E2F pathway. Molecular and cellular biology *20*, 3497-3509.
Schaub, F.X., Dhankani, V., Berger, A.C., Trivedi, M., Richardson, A.B., Shaw, R., Zhao, W., Zhang, X., Ventura, A., Liu, Y.*, et al.* (2018). Pan-cancer Alterations of the MYC Oncogene and Its Proximal Network across the Cancer Genome Atlas. Cell Syst *6*, 282-300 e282.
Schick, M., Habringer, S., Nilsson, J.A., and Keller, U. (2017). Pathogenesis and therapeutic targeting of aberrant MYC expression in haematological cancers. Br J Haematol *179*, 724-738.
Schlott, A.C., Mayclin, S., Reers, A.R., Coburn-Flynn, O., Bell, A.S., Green, J., Knuepfer, E., Charter, D., Bonnert, R., Campo, B.*, et al.* (2019). Structure-Guided Identification of Resistance Breaking Antimalarial N-Myristoyltransferase Inhibitors. Cell Chemical Biology.
Schmitz, R., Ceribelli, M., Pittaluga, S., Wright, G., and Staudt, L.M. (2014). Oncogenic mechanisms in Burkitt lymphoma. Cold Spring Harb Perspect Med *4*.
Schmitz, R., Young, R.M., Ceribelli, M., Jhavar, S., Xiao, W., Zhang, M., Wright, G., Shaffer, A.L., Hodson, D.J., Buras, E.*, et al.* (2012). Burkitt lymphoma pathogenesis and therapeutic targets from structural and functional genomics. Nature *490*, 116-120.
Schwanhausser, B., Busse, D., Li, N., Dittmar, G., Schuchhardt, J., Wolf, J., Chen, W., and Selbach, M. (2011). Global quantification of mammalian gene expression control. Nature *473*, 337-342.

Seiler, M., Peng, S., Agrawal, A.A., Palacino, J., Teng, T., Zhu, P., Smith, P.G., Cancer Genome Atlas Research, N., Buonamici, S., and Yu, L. (2018a). Somatic Mutational Landscape of Splicing Factor Genes and Their Functional Consequences across 33 Cancer Types. Cell Rep *23*, 282-296 e284.
Seiler, M., Yoshimi, A., Darman, R., Chan, B., Keaney, G., Thomas, M., Agrawal, A.A., Caleb, B., Csibi, A., Sean, E.*, et al.* (2018b). H3B-8800, an orally available small-molecule splicing modulator, induces lethality in spliceosome-mutant cancers. Nat Med *24*, 497-504.
Selvakumar, P., Lakshmikuttyamma, A., Shrivastav, A., Das, S.B., Dimmock, J.R., and Sharma, R.K. (2007). Potential role of N-myristoyltransferase in cancer. Prog Lipid Res *46*, 1-36.
Shannon, P., Markiel, A., Ozier, O., Baliga, N.S., Wang, J.T., Ramage, D., Amin, N., Schwikowski, B., and Ideker, T. (2003). Cytoscape: a software environment for integrated models of biomolecular interaction networks. Genome Res *13*, 2498-2504.
Sharer, J.D., Shern, J.F., Van Valkenburgh, H., Wallace, D.C., and Kahn, R.A. (2002). ARL2 and BART enter mitochondria and bind the adenine nucleotide transporter. Mol Biol Cell *13*, 71-83.
Sharma, K., D'Souza, R.C., Tyanova, S., Schaab, C., Wisniewski, J.R., Cox, J., and Mann, M. (2014). Ultradeep human phosphoproteome reveals a distinct regulatory nature of Tyr and Ser/Thr-based signaling. Cell Rep *8*, 1583-1594.
Shen, S., Park, J.W., Lu, Z.X., Lin, L., Henry, M.D., Wu, Y.N., Zhou, Q., and Xing, Y. (2014). rMATS: robust and flexible detection of differential alternative splicing from replicate RNA-Seq data. Proc Natl Acad Sci U S A *111*, E5593-5601.
Sheng, C., Xu, H., Wang, W., Cao, Y., Dong, G., Wang, S., Che, X., Ji, H., Miao, Z., Yao, J.*, et al.* (2010). Design, synthesis and antifungal activity of isosteric analogues of benzoheterocyclic N-myristoyltransferase inhibitors. Eur J Med Chem *45*, 3531-3540.
Shi, J., Gao, W., and Shao, F. (2017). Pyroptosis: Gasdermin-Mediated Programmed Necrotic Cell Death. Trends Biochem Sci *42*, 245-254.
Shi, W., Liao, Y., Willis, S.N., Taubenheim, N., Inouye, M., Tarlinton, D.M., Smyth, G.K., Hodgkin, P.D., Nutt, S.L., and Corcoran, L.M. (2015). Transcriptional profiling of mouse B cell terminal differentiation defines a signature for antibody-secreting plasma cells. Nat Immunol *16*, 663-673.
Shi, Y., Glynn, J., Guilbert, L., Cotter, T., Bissonnette, R., and Green, D. (1992). Role for c-myc in activation-induced apoptotic cell death in T cell hybridomas. Science *257*, 212-214.
Siegel, R.L., Miller, K.D., and Jemal, A. (2019). Cancer statistics, 2019. CA Cancer J Clin *69*, 7-34.
Singh, I., Lee, S.H., Sperling, A.S., Samur, M.K., Tai, Y.T., Fulciniti, M., Munshi, N.C., Mayr, C., and Leslie, C.S. (2018). Widespread intronic polyadenylation diversifies immune cell transcriptomes. Nat Commun *9*, 1716.
Slinker, B.K. (1998). The Statistics of Synergism. Journal of Molecular and Cellular Cardiology *30*, 723-731.
Smith, G., Carey, F.A., Beattie, J., Wilkie, M.J., Lightfoot, T.J., Coxhead, J., Garner, R.C., Steele, R.J., and Wolf, C.R. (2002). Mutations in APC, Kirsten-ras, and p53--alternative genetic pathways to colorectal cancer. Proc Natl Acad Sci U S A *99*, 9433-9438.
Sodir, N.M., and Evan, G.I. (2011). Finding cancer's weakest link. Oncotarget *2*, 1307-1313.
Song, M., Bode, A.M., Dong, Z., and Lee, M.H. (2019). AKT as a Therapeutic Target for Cancer. Cancer Res *79*, 1019-1031.
Sosman, J.A., Kim, K.B., Schuchter, L., Gonzalez, R., Pavlick, A.C., Weber, J.S., McArthur, G.A., Hutson, T.E., Moschos, S.J., Flaherty, K.T.*, et al.* (2012). Survival in BRAF V600-mutant advanced melanoma treated with vemurafenib. N Engl J Med *366*, 707-714.

Soucek, L., and Evan, G.I. (2010). The ups and downs of Myc biology. Curr Opin Genet Dev *20*, 91-95.
Soucek, L., Helmer-Citterich, M., Sacco, A., Jucker, R., Cesareni, G., and Nasi, S. (1998). Design and properties of a Myc derivative that efficiently homodimerizes. Oncogene *17*, 2463-2472.
Soucek, L., Nasi, S., and Evan, G.I. (2004). Omomyc expression in skin prevents Myc-induced papillomatosis. Cell Death Differ *11*, 1038-1045.
Soucek, L., Whitfield, J., Martins, C.P., Finch, A.J., Murphy, D.J., Sodir, N.M., Karnezis, A.N., Swigart, L.B., Nasi, S., and Evan, G.I. (2008). Modelling Myc inhibition as a cancer therapy. Nature *455*, 679-683.
Sridhar, S.S., Seymour, L., and Shepherd, F.A. (2003). Inhibitors of epidermal-growth-factor receptors: a review of clinical research with a focus on non-small-cell lung cancer. The Lancet Oncology *4*, 397-406.
Stevenson, F.T., Bursten, S.L., Fanton, C., Locksley, R.M., and Lovett, D.H. (1993). The 31-kDa precursor of interleukin 1 alpha is myristoylated on specific lysines within the 16-kDa N-terminal propiece. Proceedings of the National Academy of Sciences of the United States of America *90*, 7245-7249.
Stine, Z.E., Walton, Z.E., Altman, B.J., Hsieh, A.L., and Dang, C.V. (2015). MYC, Metabolism, and Cancer. Cancer Discovery *5*, 1024-1039.
Storck, E.M., Morales-Sanfrutos, J., Serwa, R.A., Panyain, N., Lanyon-Hogg, T., Tolmachova, T., Ventimiglia, L.N., Martin-Serrano, J., Seabra, M.C., Wojciak-Stothard, B.*, et al.* (2019). Dual chemical probes enable quantitative system-wide analysis of protein prenylation and prenylation dynamics. Nat Chem *11*, 552-561.
Storck, E.M., Serwa, R.M., and Tate, E.W. (2013). Chemical proteomics: a powerful tool for exploring protein lipidation. Biochemical Society Transactions *41*, 56-61.
Strasser, A., Harris, A.W., Bath, M.L., and Cory, S. (1990). Novel primitive lymphoid tumours induced in transgenic mice by cooperation between myc and bcl-2. Nature *348*, 331-333.
Subramanian, A., Narayan, R., Corsello, S.M., Peck, D.D., Natoli, T.E., Lu, X., Gould, J., Davis, J.F., Tubelli, A.A., Asiedu, J.K.*, et al.* (2017). A Next Generation Connectivity Map: L1000 Platform and the First 1,000,000 Profiles. Cell *171*, 1437-1452 e1417.
Subramanian, A., Tamayo, P., Mootha, V.K., Mukherjee, S., Ebert, B.L., Gillette, M.A., Paulovich, A., Pomeroy, S.L., Golub, T.R., Lander, E.S.*, et al.* (2005). Gene set enrichment analysis: a knowledge-based approach for interpreting genome-wide expression profiles. Proc Natl Acad Sci U S A *102*, 15545-15550.
Tabaczar, S., Czogalla, A., Podkalicka, J., Biernatowska, A., and Sikorski, A.F. (2017). Protein palmitoylation: Palmitoyltransferases and their specificity. Experimental Biology and Medicine *242*, 1150-1157.
Tacke, R., Tohyama, M., Ogawa, S., and Manley, J.L. (1998). Human Tra2 Proteins Are Sequence-Specific Activators of Pre-mRNA Splicing. Cell *93*, 139-148.
Taha, M.O., Qandil, A.M., Al-Haraznah, T., Khalaf, R.A., Zalloum, H., and Al-Bakri, A.G. (2011). Discovery of new antifungal leads via pharmacophore modeling and QSAR analysis of fungal N-myristoyl transferase inhibitors followed by in silico screening. Chem Biol Drug Des *78*, 391-407.
Takahashi, K., Tanabe, K., Ohnuki, M., Narita, M., Ichisaka, T., Tomoda, K., and Yamanaka, S. (2007). Induction of pluripotent stem cells from adult human fibroblasts by defined factors. Cell *131*, 861-872.
Tameire, F., Verginadis, II, Leli, N.M., Polte, C., Conn, C.S., Ojha, R., Salas Salinas, C., Chinga, F., Monroy, A.M., Fu, W.*, et al.* (2019). ATF4 couples MYC-dependent translational activity to bioenergetic demands during tumour progression. Nat Cell Biol *21*, 889-899.
Tang, J., Pearce, L., O'Donnell-Tormey, J., and Hubbard-Lucey, V.M. (2018). Trends in the global immuno-oncology landscape. Nat Rev Drug Discov.

Taplin, M.E., and Balk, S.P. (2004). Androgen receptor: a key molecule in the progression of prostate cancer to hormone independence. J Cell Biochem *91*, 483-490.
Tate, E.W. (2008). Recent advances in chemical proteomics: exploring the post-translational proteome. Journal of chemical biology *1*, 17-26.
Tavana, O., Li, D., Dai, C., Lopez, G., Banerjee, D., Kon, N., Chen, C., Califano, A., Yamashiro, D.J., Sun, H.*, et al.* (2016). HAUSP deubiquitinates and stabilizes N-Myc in neuroblastoma. Nat Med *22*, 1180-1186.
Team, R.C. (2014). R: A language and environment for statistical computing. R Foundation for Statistical Computing.
Thinon, E. (2013). Chemical tools to validate N-myristoyltransferase as a new target in cancer therapy. In Department of Chemistry (Imperial College London).
Thinon, E., Morales-Sanfrutos, J., Mann, D.J., and Tate, E.W. (2016). N-myristoyltransferase inhibition induces ER-stress, cell cycle arrest and apoptosis in cancer cells. ACS Chem Biol *11*, 2165-2176.
Thinon, E., Serwa, R.A., Broncel, M., Brannigan, J.A., Brassat, U., Wright, M.H., Heal, W.P., Wilkinson, A.J., Mann, D.J., and Tate, E.W. (2014). Global profiling of co- and post-translationally N-myristoylated proteomes in human cells. Nat Commun *5*, 4919.
Thul, P.J., Akesson, L., Wiking, M., Mahdessian, D., Geladaki, A., Ait Blal, H., Alm, T., Asplund, A., Bjork, L., Breckels, L.M.*, et al.* (2017). A subcellular map of the human proteome. Science *356*.
Timms, R.T., Zhang, Z., Rhee, D.Y., Harper, J.W., Koren, I., and Elledge, S.J. (2019). A glycine-specific N-degron pathway mediates the quality control of protein N-myristoylation. Science *365*, eaaw4912.
Ting, L., Rad, R., Gygi, S.P., and Haas, W. (2011). MS3 eliminates ratio distortion in isobaric multiplexed quantitative proteomics. Nat Methods *8*, 937-940.
Trumpp, A., Refaeli, Y., Oskarsson, T., Gasser, S., Murphy, M., Martin, G.R., and Bishop, J.M. (2001). c-Myc regulates mammalian body size by controlling cell number but not cell size. Nature *414*, 768-773.
Tsherniak, A., Vazquez, F., Montgomery, P.G., Weir, B.A., Kryukov, G., Cowley, G.S., Gill, S., Harrington, W.F., Pantel, S., Krill-Burger, J.M.*, et al.* (2017). Defining a Cancer Dependency Map. Cell *170*, 564-576 e516.
Tsimberidou, A.M., Chandhasin, C., and Kurzrock, R. (2010). Farnesyltransferase inhibitors: where are we now? Expert Opin Investig Drugs *19*, 1569-1580.
Tyanova, S., Temu, T., Sinitcyn, P., Carlson, A., Hein, M.Y., Geiger, T., Mann, M., and Cox, J. (2016). The Perseus computational platform for comprehensive analysis of (prote)omics data. Nat Methods *13*, 731-740.
Uchida, F., Uzawa, K., Kasamatsu, A., Takatori, H., Sakamoto, Y., Ogawara, K., Shiiba, M., Tanzawa, H., and Bukawa, H. (2012). Overexpression of cell cycle regulator CDCA3 promotes oral cancer progression by enhancing cell proliferation with prevention of G1 phase arrest. BMC Cancer *12*, 321.
Uhlen, M., Fagerberg, L., Hallström, B.M., Lindskog, C., Oksvold, P., Mardinoglu, A., Sivertsson, Å., Kampf, C., Sjöstedt, E., Asplund, A.*, et al.* (2015). Tissue-based map of the human proteome. Science *347*, 1260419.
Uhlen, M., Zhang, C., Lee, S., Sjöstedt, E., Fagerberg, L., Bidkhori, G., Benfeitas, R., Arif, M., Liu, Z., Edfors, F.*, et al.* (2017). A pathology atlas of the human cancer transcriptome. Science *357*, eaan2507.
Ushmorov, A., Hogarty, M.D., Liu, X., Knauss, H., Debatin, K.M., and Beltinger, C. (2008). N-myc augments death and attenuates protective effects of Bcl-2 in trophically stressed neuroblastoma cells. Oncogene *27*, 3424-3434.
Utsumi, T., Matsuzaki, K., Kiwado, A., Tanikawa, A., Kikkawa, Y., Hosokawa, T., Otsuka, A., Iuchi, Y., Kobuchi, H., and Moriya, K. (2018). Identification and characterization of protein N-myristoylation occurring on four human mitochondrial proteins, SAMM50, TOMM40, MIC19, and MIC25. PLoS One *13*, e0206355.

Valentjin, L.J., Koppen, A., van Asperen, R., Root, H.A., Haneveld, F., and Versteeg, R. (2005). Inhibition of a New Differentiation Pathway in Neuroblastoma by Copy Number Defects of N-myc, Cdc42, and nm23 Genes. Cancer Res *65*, 3136-3145.
Vervoorts, J., Luscher-Firzlaff, J., and Luscher, B. (2006). The ins and outs of MYC regulation by posttranslational mechanisms. J Biol Chem *281*, 34725-34729.
Victora, G.D., and Nussenzweig, M.C. (2012). Germinal centers. Annu Rev Immunol *30*, 429-457.
Vis, D.J., Bombardelli, L., Lightfoot, H., Iorio, F., Garnett, M.J., and Wessels, L.F. (2016). Multilevel models improve precision and speed of IC50 estimates. Pharmacogenomics *17*, 691-700.
Vo, B.T., Wolf, E., Kawauchi, D., Gebhardt, A., Rehg, J.E., Finkelstein, D., Walz, S., Murphy, B.L., Youn, Y.H., Han, Y.G*., et al.* (2016). The Interaction of Myc with Miz1 Defines Medulloblastoma Subgroup Identity. Cancer Cell *29*, 5-16.
Wacker, S.A., Houghtaling, B.R., Elemento, O., and Kapoor, T.M. (2012). Using transcriptome sequencing to identify mechanisms of drug action and resistance. Nature Chemical Biology *8*, 235-237.
Wagner, A.J., Kokontis, J.M., and Hay, N. (1994). Myc-mediated apoptosis requires wild-type p53 in a manner independent of cell cycle arrest and the ability of p53 to induce p21waf1/cip1. Genes Dev *8*, 2817-2830.
Walz, S., Lorenzin, F., Morton, J., Wiese, K.E., von Eyss, B., Herold, S., Rycak, L., Dumay-Odelot, H., Karim, S., Bartkuhn, M*., et al.* (2014). Activation and repression by oncogenic MYC shape tumour-specific gene expression profiles. Nature *511*, 483-487.
Wang, M., and Casey, P.J. (2016). Protein prenylation: unique fats make their mark on biology. Nat Rev Mol Cell Biol *17*, 110-122.
Wang, T., Birsoy, K., Hughes, N.W., Krupczak, K.M., Post, Y., Wei, J.J., Lander, E.S., and Sabatini, D.M. (2015a). Identification and characterization of essential genes in the human genome. Science *350*.
Wang, T., Wei, J.J., Sabatini, D.M., and Lander, E.S. (2014). Genetic Screens in Human Cells Using the CRISPR-Cas9 System. Science *343*, 80-84.
Wang, Y., Zhang, T., Kwiatkowski, N., Abraham, B.J., Lee, T.I., Xie, S., Yuzugullu, H., Von, T., Li, H., Lin, Z*., et al.* (2015b). CDK7-dependent transcriptional addiction in triple-negative breast cancer. Cell *163*, 174-186.
Wanzel, M., Herold, S., and Eilers, M. (2003). Transcriptional repression by Myc. Trends in Cell Biology *13*, 146-150.
Wardell, C.P., Begum, D., Dahir, N., Johnson, D.C., Davies, F.E., and Morgan, G.J. (2013). MYC Translocations In Multiple Myeloma Involve Recruitment Of Enhancer Elements Resulting In Over-Expression and Decreased Overall Survival. Blood *122*, 274-274.
Weinberg, R.A., McWherter, C.A., Freeman, S.K., Wood, D.C., Gordon, J.I., and Lee, S.C. (1995). Genetic studies reveal that myristoylCoA:protein N-myristoyltransferase is an essential enzyme in Candida albicans. Molecular Microbiology *16*, 241-250.
Wen, Z., Jin, K., Shen, Y., Yang, Z., Li, Y., Wu, B., Tian, L., Shoor, S., Roche, N.E., Goronzy, J.J*., et al.* (2019). N-myristoyltransferase deficiency impairs activation of kinase AMPK and promotes synovial tissue inflammation. Nat Immunol *20*, 313-325.
Whittaker, S.R., Mallinger, A., Workman, P., and Clarke, P.A. (2017). Inhibitors of cyclin-dependent kinases as cancer therapeutics. Pharmacol Ther *173*, 83-105.
Will, C.L., Urlaub, H., Achsel, T., Gentzel, M., Wilm, M., and Luhrmann, R. (2002a). Characterization of novel SF3b and 17S U2 snRNP proteins, including a human Prp5p homologue and an SF3b DEAD-box protein. Embo j *21*, 4978-4988.
Will, C.L., Urlaub, H., Achsel, T., Gentzel, M., Wilm, M., and Lührmann, R. (2002b). Characterization of novel SF3b and 17S U2 snRNP proteins, including a human Prp5p homologue and an SF3b DEAD-box protein. The EMBO Journal *21*, 4978-4988.

Williamson, L., Saponaro, M., Boeing, S., East, P., Mitter, R., Kantidakis, T., Kelly, G.P., Lobley, A., Walker, J., Spencer-Dene, B.*, et al.* (2017). UV Irradiation Induces a Non-coding RNA that Functionally Opposes the Protein Encoded by the Same Gene. Cell *168*, 843-855 e813.
Willyard, C. (2018). New human gene tally reignites debate. Nature *558*, 354-355.
Wilson, A., Murphy, M.J., Oskarsson, T., Kaloulis, K., Bettess, M.D., Oser, G.M., Pasche, A.C., Knabenhans, C., Macdonald, H.R., and Trumpp, A. (2004). c-Myc controls the balance between hematopoietic stem cell self-renewal and differentiation. Genes Dev *18*, 2747-2763.
Wise, D.R., DeBerardinis, R.J., Mancuso, A., Sayed, N., Zhang, X.Y., Pfeiffer, H.K., Nissim, I., Daikhin, E., Yudkoff, M., McMahon, S.B.*, et al.* (2008). Myc regulates a transcriptional program that stimulates mitochondrial glutaminolysis and leads to glutamine addiction. Proc Natl Acad Sci U S A *105*, 18782-18787.
Wise, D.R., and Thompson, C.B. (2010). Glutamine addiction: a new therapeutic target in cancer. Trends in biochemical sciences *35*, 427-433.
Wojcechowskyj, J.A., Didigu, C.A., Lee, J.Y., Parrish, N.F., Sinha, R., Hahn, B.H., Bushman, F.D., Jensen, S.T., Seeholzer, S.H., and Doms, R.W. (2013). Quantitative phosphoproteomics reveals extensive cellular reprogramming during HIV-1 entry. Cell Host Microbe *13*, 613-623.
Wright, M.H., Clough, B., Rackham, M.D., Rangachari, K., Brannigan, J.A., Grainger, M., Moss, D.K., Bottrill, A.R., Heal, W.P., Broncel, M.*, et al.* (2014). Validation of N-myristoyltransferase as an antimalarial drug target using an integrated chemical biology approach. Nat Chem *6*, 112-121.
Wright, M.H., Heal, W.P., Mann, D.J., and Tate, E.W. (2010). Protein myristoylation in health and disease. J Chem Biol *3*, 19-35.
Wright, M.H., Paape, D., Storck, E.M., Serwa, R.A., Smith, D.F., and Tate, E.W. (2015). Global analysis of protein N-myristoylation and exploration of N-myristoyltransferase as a drug target in the neglected human pathogen Leishmania donovani. Chem Biol *22*, 342-354.
Xie, H., Tang, C.H., Song, J.H., Mancuso, A., Del Valle, J.R., Cao, J., Xiang, Y., Dang, C.V., Lan, R., Sanchez, D.J.*, et al.* (2018). IRE1alpha RNase-dependent lipid homeostasis promotes survival in Myc-transformed cancers. J Clin Invest *128*, 1300-1316.
Xu, J., Chen, Y., and Olopade, O.I. (2010). MYC and Breast Cancer. Genes Cancer *1*, 629-640.
Yamazaki, K., Kaneko, Y., Suwa, K., Ebara, S., Nakazawa, K., and Yasuno, K. (2005). Synthesis of potent and selective inhibitors of Candida albicans N-myristoyltransferase based on the benzothiazole structure. Bioorg Med Chem *13*, 2509-2522.
Yang, S.H., Shrivastav, A., Kosinski, C., Sharma, R.K., Chen, M.H., Berthiaume, L.G., Peters, L.L., Chuang, P.T., Young, S.G., and Bergo, M.O. (2005). N-myristoyltransferase 1 is essential in early mouse development. J Biol Chem *280*, 18990-18995.
Yang, W., Soares, J., Greninger, P., Edelman, E.J., Lightfoot, H., Forbes, S., Bindal, N., Beare, D., Smith, J.A., Thompson, I.R.*, et al.* (2013). Genomics of Drug Sensitivity in Cancer (GDSC): a resource for therapeutic biomarker discovery in cancer cells. Nucleic Acids Res *41*, D955-961.
Yin, X., Giap, C., Lazo, J.S., and Prochownik, E.V. (2003). Low molecular weight inhibitors of Myc-Max interaction and function. Oncogene *22*, 6151-6159.
Yorikawa, C., Shibata, H., Waguri, S., Hatta, K., Horii, M., Katoh, K., Kobayashi, T., Uchiyama, Y., and Maki, M. (2005). Human CHMP6, a myristoylated ESCRT-III protein, interacts directly with an ESCRT-II component EAP20 and regulates endosomal cargo sorting. The Biochemical journal *387*, 17-26.
Yu, C., Niu, X., Jin, F., Liu, Z., Jin, C., and Lai, L. (2016). Structure-based Inhibitor Design for the Intrinsically Disordered Protein c-Myc. Sci Rep *6*, 22298.

Yu, K., Toral-Barza, L., Discafani, C., Zhang, W.G., Skotnicki, J., Frost, P., and Gibbons, J.J. (2001). mTOR, a novel target in breast cancer: the effect of CCI-779, an mTOR inhibitor, in preclinical models of breast cancer. Endocr Relat Cancer *8*, 249-258.
Yue, M., Jiang, J., Gao, P., Liu, H., and Qing, G. (2017). Oncogenic MYC Activates a Feedforward Regulatory Loop Promoting Essential Amino Acid Metabolism and Tumorigenesis. Cell Rep *21*, 3819-3832.
Zack, T.I., Schumacher, S.E., Carter, S.L., Cherniack, A.D., Saksena, G., Tabak, B., Lawrence, M.S., Zhsng, C.Z., Wala, J., Mermel, C.H.*, et al.* (2013). Pan-cancer patterns of somatic copy number alteration. Nat Genet *45*, 1134-1140.
Zha, J., Weiler, S., Oh, K.J., Wei, M.C., and Korsmeyer, S.J. (2000). Posttranslational N-Myristoylation of BID as a Molecular Switch for Targeting Mitochondria and Apoptosis. Science *290*, 1761-1765.
Zhang, W., Lu, Y., Li, X., Zhang, J., Zheng, L., Zhang, W., Lin, C., Lin, W., and Li, X. (2018). CDCA3 promotes cell proliferation by activating the NF-kappaB/cyclin D1 signaling pathway in colorectal cancer. Biochem Biophys Res Commun *500*, 196-203.
Zhang, X., Choi, P.S., Francis, J.M., Imielinski, M., Watanabe, H., Cherniack, A.D., and Meyerson, M. (2016). Identification of focally amplified lineage-specific super-enhancers in human epithelial cancers. Nat Genet *48*, 176-182.
Zhao, N., Cao, J., Xu, L., Tang, Q., Dobrolecki, L.E., Lv, X., Talukdar, M., Lu, Y., Wang, X., Hu, D.Z.*, et al.* (2018). Pharmacological targeting of MYC-regulated IRE1/XBP1 pathway suppresses MYC-driven breast cancer. J Clin Invest *128*, 1283-1299.
Zheng, Q., Hou, J., Zhou, Y., Li, Z., and Cao, X. (2017). The RNA helicase DDX46 inhibits innate immunity by entrapping m6A-demethylated antiviral transcripts in the nucleus. Nat Immunol.
Zhou, Q., Derti, A., Ruddy, D., Rakiec, D., Kao, I., Lira, M., Gibaja, V., Chan, H., Yang, Y., Min, J.*, et al.* (2015). A chemical genetics approach for the functional assessment of novel cancer genes. Cancer Res *75*, 1949-1958.
Zhu, B., He, Q., Xiang, J., Qi, F., Cai, H., Mao, J., Zhang, C., Zhang, Q., Li, H., Lu, L.*, et al.* (2017). Quantitative Phosphoproteomic Analysis Reveals Key Mechanisms of Cellular Proliferation in Liver Cancer Cells. Sci Rep *7*, 10908.
Zhu, F., Xie, N., Jiang, Z., Li, G., Ma, L., and Tong, T. (2018). The Cellular Senescence-Inhibited Gene Is Essential for PPM1A Myristoylation To Modulate Transforming Growth Factor beta Signaling. Mol Cell Biol *38*.
Zirath, H., Frenzel, A., Oliynyk, G., Segerstrom, L., Westermark, U.K., Larsson, K., Munksgaard Persson, M., Hultenby, K., Lehtio, J., Einvik, C.*, et al.* (2013). MYC inhibition induces metabolic changes leading to accumulation of lipid droplets in tumor cells. Proc Natl Acad Sci U S A *110*, 10258-10263.
Zuber, J., Shi, J., Wang, E., Rappaport, A.R., Herrmann, H., Sison, E.A., Magoon, D., Qi, J., Blatt, K., Wunderlich, M.*, et al.* (2011). RNAi screen identifies Brd4 as a therapeutic target in acute myeloid leukaemia. Nature *478*, 524-528.